BEHAVIOUR OF CRITICAL REGIONS OF CONCRETE SLABS UNDER IMPULSIVE LOADING

A THESIS SUBMITTED TO THE

COUNCIL FOR NATIONAL ACADEMIC AWARDS (CNAA)

FOR THE

MASTER OF PHILOSOPHY DEGREE

BY

JOHNNY TANG B.Sc

SCHOOL OF CIVIL ENGINEERING

MIDDLESEX POLYTECHNIC, MIDDLESEX

FEBRUARY 1988

ABSTRACT

BEHAVIOUR OF CRITICAL REGIONS OF CONCRETE SLABS UNDER IMPULSIVE LOADING

J. TANG

An attempt has been made to analyse the local failure of reinforced concrete slabs subjected to soft missile impact by using three-dimensional dynamic finite element analysis in which provision is made for the simulation of impact loads, plasticity and cracking of concrete. An assessment is made for perforation and scabbing.

Two existing three-dimensional finite element programs are used to carry out the analysis. The program NONSAP is modified to include a four-parameter concrete model based on Ottosen's failure criterion. The reinforcement and concrete are modelled simultaneously by assuming they act as a composite material. Concrete cracking is modelled based on the smeared crack concept. The Newmark direct integration scheme is used to carry out the iteration process.

A three-dimensional non-linear dynamic finite element package, MARC is used for comparison. In this analysis the parabolic Mohr-Coulomb yield criterion is adopted to model the concrete while the failure of the reinforcement is predicted using the Von Mises yield criterion. Cracking criteria used by MARC is based on the smeared crack concept. Again the Newmark direction integration scheme is adopted in this analysis.

Two reinforced concrete slabs tested by UKAEA have been examined using the above computer packages and the analytical results are compared with each other and with those of the experiment. Despite slight deviations, the analytical results are in reasonable agreement with those given by experiment.

ACKNOWLEDGEMENTS

The author wishes to express his gratitude to Dr. Y. Bangash for his supervision and support throughout the research. He is also grateful to Dr. S. Chakarvarty for his useful advice on computing.

The author would like to thank Mr. A. Neilson of UKAEA, Winfrith for providing all input data and experimental results. His helpful discussion on data input is especially acknowledged.

The author also wishes to thank Mr. P. Brown for reading the manuscript and his valuable advice on the graph plotting.

Finally, the author wishes to thank Mr. R. Chandwani, Managing Director of Zentech Consultants, for providing the MARC package, computer and other facilities, without which the research would not have been possible.

CONTENTS

		Page
ABSTRACT		1
ACKNOWLEDGEMENTS		2
CONTENTS		3
NOTATION		7
CHAPTER 1 -	STATE-OF-THE-ART	
	1.1 General	9
	1.2 Experimental Investigations	15
	1.3 Theoretical Investigations	25
	1.4 Empirical Formulae	41
	1.5 Scope of Research	44
CHAPTER 2 -	MODELLING OF CONCRETE BEHAVIOUR	
	2.1 General Introduction	47
	2.2 Impact on Concrete	47
	2.3 Failure Criterion in NONSAP	48
	2.4 Reinforced Concrete in NONSAP	53
	2.5 Concrete Cracking Model in NONSAP	56
	2.5.1 Transformation	61
	2.6 Failure Criterion in MARC	63
	2.6.1 Mohr-Coulomb Model	63
	2.7 Concrete Cracking Model in MARC Analysis	67
	2.7.1 Concrete Non-linear Behaviour Under Compression	67

2.7.2 Concrete Non-linear Behaviour Under Tension 67

2.7.3 The Effect of Reinforment 67

2.7.4 Smeared Crack Constitutive Modelling 68

2.7.5 Stress and Strain Calculation With Cracking 69

2.7.6 Iterative Procedure and Convergence Testing 69

CHAPTER 3 - FINITE ELEMENT ANALYSIS

3.1 General Finite Element Formulation 71

3.1.1 Shape Function 71

3.1.2 Displacement Functions 73

3.1.3 Strain Displacement Relationship Derivative Transformation and The Jacobian matrix 73

3.1.4 Stress Calculation and The Element Stiffness Matrix 75

3.2 Elasto-plasticity 76

3.2.1 Marc plasticity Solution Procedures And Algorithms 77

3.3 Dynamic Analysis 77

3.3.1 Mass Matrix 78

3.3.2 Numerical Damping 79

CHAPTER 4 - EXPERIMENTAL TEST RESULTS ON CONCRETE SLABS

4.1 Concrete Slabs Subjected to Impact 82

4.2 Experimental Investigations of Reinforced Concrete Slabs 83

4.2.1 Experimental Equipment 83

4.2.2 Concrete Target 84

4.2.3 Load from Deformable missiles 85

4.2.4 Target Response 85

CHAPTER 5 - IMPACT ANALYSIS

5.1 General Introduction 113

5.2 Input for Analyses 113

5.2.1 Geometry 113

5.2.2 Material properties 113

5.2.3 Load-time History 114

5.3 Method of Analysis in NONSAP 114

5.4 Finite Element Model in NONSAP 116

5.5 method of Analysis in MARC 116

5.6 Finite Element Model in MARC 118

CHAPTER 6 - COMPUTER PROGRAMS-NONSAP AND MARC

6.1 Program Description of NONSAP and Modification Procedures 124

6.2 Three-dimension Concrete Model - Main Subroutine (RCRK3D) 127

6.3 Program Description of MARC 131

CHAPTER 7 - ANALYSIS OF RESULTS

7.1 General Introduction 133

7.2 Modal Analysis 133

7.3 NONSAP Results 134

7.4 MARC Results 135

7.5 Comparison of NONSAP and MARC 136

7.6 Comparison of NONSAP, MARC and Experimental Results 137

CHAPTER 8 - CONCULSIONS AND FUTURE RECOMMENDATIONS

8.1 Conculsions 194

8.2 Future Rcommendations 195

REFERENCES 196

APPENDIX A - STRESS INVARIANTS AND CALCULATION OF OTTOSON FAILURE CRITERION FOR NONSAP SUBROUTINE, CONMOD 213

APPENDIX B - CALCULATION OF NUMERICAL DAMPING FACTOR AND INCREMENTAL TIME STEP FOR MARC 217

APPENDIX C - CALCULATION OF INPUT PARAMETERS FOR MOHR-COULUMB FAILURE CRITERION FOR MARC 218

APPENDIX D - LISTING OF NONSAP SUBROUTINES 219

APPENDIX E - LISTING OF MARC USER SUBROUTINES 230

NOTATION

$[\ ], \{\}$	denotes matrices
A,B	material parameters of Ottosen model
A_c	area of concrete
A_s	area of reinforcement
[a]	nodal acceleration matrix
b	aggregate interlocking factor
C	cohesion
[Cd]	damping matrix
[D]	material matrix
$[D_e]$	elastic material matrix
$[D_{ep}]$	elasto-plastic material matrix
E	composite tangent modulus for concrete and reinforcement
E_c	tangent modulus of concrete
E_s	tangent modulus of reinforcement
F	interpolation function
fc	uniaxial compressive strength of concrete
ft	uniaxial allowable tensile stress of concrete
G	shear modulus
H	material hardening factor
I_1, J_2, J_3	stress invariants
[J]	Jacobian matrix
K_1	size factor parameter in Ottosen model
K_2	shape factor parameter in Ottosen model
[K]	element stiffness matrix
[M]	mass matrix
[R]	external force matrix
r,s,t	curviliean coordinates
S_T	element deformation variable matrix
SF	shear relation factor
$[T_A], [T_B]$	transformation matrices

ts	time step increment
U,V,W	displacements in global system
[v]	nodal velocity matrix
X,Y,Z	nodal coordinates in global system
[z]	nodal displacement matrix
*	crack direction
σ_i	stress components at point i
ε_i	strain components at point i
σ_i^*	stress components in crack directions at point i
ε_i^*	strain components in crack directions at point i
σ_0	initial stress
ε_0	initial strain
σ_o	octahedral normal stress
τ_o	octahedral shear stress
$d\sigma_i$	incremental stress components at point i
$d\varepsilon_i$	incremental strain components at point i
μ_{com}	composite Poisson's ratio for concrete and reinforcement
ρ	density of material
ρ_c	density of concrete
η, ζ	cohesion constants
θ	angle of similarity
ϕ	angle of friction
ν	numerical damping factor
ω	eigen frequency

CHAPTER 1

STATE OF THE ART
MISSILE IMPACT ON CONCRETE - A LITERATURE SURVEY

1.1 General

Within the last decade, there has been a great deal of investigation into the impact of aircraft and missiles on structures [1 - 140] particularly in the nuclear industry. Although it was mentioned by Broman et al. [1] that if the likelihood of occurrence of certain impactive and impulsive loads is small enough, the loads do not have to be considered in the structural design basis, structural failure in the nuclear industry is a consequence that cannot be allowed.

Many organisations have been conducting experiments on the effects of missile impact on structures. Even in the 1950's, a few individuals showed particular interest in the properties of materials subject to loading [5, 15].

From December 19th, 1979 to June 12th, 1980, four full scale experiments on the response of reinforced concrete containment walls to impact and penetration by postulated turbine produced missiles were conducted at approximately six week intervals. In their papers [41, 42], Woodfin and Sliter describe the deviation of the test matrix and the method of conducting the experiments as well as the modelling process. They showed that predictions using the modified NDRC penetration formula were moderately conservative, agreeing with measured values, to within about 30%. Perforation and scabbing predictions were much less accurate but were conservative Impact of a sharp with a sharp missile attitude caused significantly more severe back face cracking than impact of a blunt attitude. These results were substantiated by [2].

The perforation of reinforced concrete slabs by rigid missiles was

studied experimentally in Germany [46, 47, 48]. It started with 13 perforation tests of concrete slabs where steel cylinder missiles fell from a height of about 47m at a speed of about 28.5 m/s. The geometry and disposion of the slab, the form and diameter of the nose and the weight of the slabs after impact were compared to the application of the Petry formula. Then the investigation continued on with reinforced concrete slabs of dimension 5m x 5m x 40-50cm. These are impacted by steel missiles weighted from 160-227 kg, the heaviest being 305mm diameter and 103cm long, which were fixed from a projectile gun. Different missiles were tried on various types of slab with their speed increasing from 77 to 160 m/s. Penetration and perforation were studied. Results were predicted tried by means of finite element computation assuming an elastic-plastic constitutive law for concrete but unfortunately, no distinct conclusion could be drawn from the comparisons.

Some models of proposed prestressed concrete containment structures for a sodium cooled fast breeder reactor have been constructed and tested by Davidson and Bradbury [49]. These models were partly filled with water and loaded internally by detonating explosive charges. Prior to the tests, the model was analysed by an axisymmetric dynamic relaxation computer program. The correlation of computer and test results is discussed in [49]. The behaviour of structures in which loads and deflections do not have a given relationship with each other was considered. The computer program also analysed the models with the loads being applied dynamically as time dependent quantities.

Highly deformable missile impacting reinforced concrete slabs have been tested at Meppen in Germany, with the intention of applying them to structures which could be subject to the treatment of aircraft impact load. Comparative computational investigations have been carried out by Nachtsheim and Stangenberg [55, 108, 109] using a dynamic nonlinear physical method. Most of the parameter variations examined at Meppen were between bending and shearing capacity. Deformations are distinctly influenced by varying the bending and shearing reinforcement, and thus the amount of the total displacements is also influenced too. This corresponds with

different degrees of damage and crack formation in the experiment. In the range of ultimate slab resistance the results generally show a high sensitivity with respect to the load conditions and they are strongly influenced by the impact velocity as well as the projectile deformation behaviour. In the experiments, the structural behaviour of test slabs demonstrates a greater sensitivity to altering thickness than to variations of equivalent amounts of reinforcement.

The incorporation of tensile and notch impact bend tests with an experimentally validated fracture mechanics concept has been performed by Kussmaul [56]. He presents a fracture concept for practical use which is based on a correlation between of notch impact energy and the fracture mechanics characteristic quantities for crack limitation and instability.

Impact tests for steel fibre reinforced concrete slabs with liner have been carried out by Stangenberg and Buttmann [99]. The results of these dynamic tests, performed by a drop hammer facility, shoeed that steel fibre reinforced concrete is an excellent material for impact resistant structures The reasons for this are that steel fibres are more ductile, the maximum and residual deformations are diminished and the local penetration and spalling damages are considerably restricted.

Romander and Hiter [177] present the experimental results of twenty-five impact tests on 1/11 scale models of reinforced concrete walls using postulated turbine missiles. This work suggested that the predictions of the NDRC and CEA-EDF perforation formulae are overly conservative.

Missiles may be either external, for example aircraft and tornado generated missiles, or internal, such as turbine missiles and plant generated missiles. Both have been fully discussed in the literature [2, 22, 23, 64, 69, 86, 88, 103, 107, 117, 118, 122, 150, 162, 164, 165, 167, 171, 172, 173]. Missiles can also be divided into hard missiles or soft missile. Brandes [11] speaks of soft missile impact when a deformable projectile strikes a reinforced concrete structural member when plastic deformation of the

projectile absorbs the kinetic energy. On the other hand, Riera [57] classifies missiles as soft, intermediate or hard, by using the total reaction function which has parameters of missile velocity and velocity of propagation of a longitudinal and compressive wave.

There are two types of effect that can be produced when a missile impacts on a concrete slab. The overall structural response is commonly evaluated in terms of the flexural reactions and the shear behaviour. In his definitions, Degen [58] puts up the following terminology for the local effects:-

- Penetration is the depth to which a projectile enters a massive concrete target without passing through it. The concrete is assumed not to scab on the back face, thus penetration depth is independent of the thickness of the target.

- Perforation thickness is used specifically when the projectile just passes completely through the slab. That is, the exit velocity of the projectile after it passes through the slab is zero.

- Scabbing consists of the ejection of pieces of concrete from the back of the slab opposite to the impact area, thus leaving a back crater after the impact.

- Spalling is the ejection of pieces of concrete from the front face region surrounding the area of impact, thus leaving a front crater.

- Ricochet is the rebound of the projectile according to an angle of incidence different from the normal.

Quite a great deal of work [4, 6, 7, 16, 17, 27, 35, 36, 44, 59-63, 65, 67, 68, 71-74, 76-79, 88, 103, 111, 106, 122, 123, 126, 147] has been done on the structural response of structures subject to impact loading. In their report, Linderman et al. [59] pointed out that if the interface function is experimentally determined and the target structure is modelled mathematically then conventional numerical techniques can be used to predict the structural response. If the interface function is not known, as in most cases,

a rational method involving an energy balance technique is used to estimate the structural response, as demonstrated in [59]. The impact may be either elastic or plastic, depending on whether or not significant energy losses are sustained during impact. These losses are associated with inelastic deformations, local damage in the impact zone, etc. In their definitions, plastic impact is characterised by the missile remaining in contact with the target subsequent to impact. Elastic impact is characterised by missile and target remaining in contact for a very short period of time and then disengageing due to elastic interface restoring forces.

Riera [60] conducted the force-time relationship assuming an ideal plastic impact of a Boeing 707 on a rigid wall. This was based on the assumptions that the aircraft will crash only at the cross-section next to the target, and this buckling load on the cross-section decelerates the remaining uncrushed portion. This is assumed to behave rigidly so that the total force experienced by the rigid target thus equals to the sum of the buckling load and the force required to fully decelerate the mass of impinging cross-section. The valuation of this large commercial plane impacted onto a prestressed concrete dome was carried out using the maximum response curve and the system was considered to be elastic undamped and of one-degree-of-freedom.

Soon after, new work [61] was performed to extend the work carried out by Riera [60]. In this new article, Yang and Godfrey completed three major aspects.

- A consistent mass finite element approach for slab vibration analysis, which is not limited to simply supported boundary conditions, was employed to find a more realistic maximum response of rectangular slabs.

- A finite element plate bending analysis of rectangular slabs with arbitrary boundary conditions was used in order to achieve a more economic design.

- A numerical method of solution, which combines the advantages of direct integrations, the static finite difference approach

and vibration analysis using the first-order ordinary differential equations describing rotationally symmetric shells subject to "non-systematic" load, was employed to analyse the impact on various possible critical positions of the containment vessel. A velocity of 103 m/s was again used for a large commercial plane (Boeing 720).

It is worthwhile noting the differences between impact load and impulse load as defined by Broman et al. [74]. Impact load is defined as the input of a finite amount of kinetic load transient, which is determined by the inertial and stiffness properties of the missile and target structure Impulse load is also a load transient, but it is determined by an external source and it is not dependent upon target inertial and stiffness properties. Impulse loads are generally force but not energy limited. In their definitions [75], soft impact is a process with irreversible deformation and the process does not take place instantaneously. The total kinetic energy of the system is changed during the impact process, which follows the laws of motion and energy, while hard impact is a process with no irreversible deformation. The process takes place instantaneously and the total kinetic energy of the system is not changed during the impact process which also follows the laws of motion and energy. It is also pointed out that when striking a barrier, a missile or missile component produces a hard "impact" if missile deformation, barrier penetration and barrier shear plug movement are relatively small compared to barrier structural deformation or barrier external kinetic energy. However, if either missile deformation, barrier penetration or basic shear plug movement is relatively large compared to barrier structural deformation or barrier external kinetic energy, the impact is considered "soft".

Kennedy [111] describes simplified procedures for determining both the local impact effects and the overall barrier wall behaviour when subject to hard missile impact with emphasis on missile velocities between 30.5 and 457.2 m/s. Reviews have also been made on the various empirical procedures commonly used for determining depth, perforation thickness and scabbing thickness. Design

recommendations to prevent detrimental local wall damage are presented. It is pointed out that both missile deformability and target deformability reduce the energy available to penetrate the target wall and thus reduce the depth of penetration, perforation thickness and scabbing thickness.

A hypothesis of a general model for the evaluation of changes due to local effects including penetration and spalling of reinforced concrete barriers subject to impact of deformable tornado generated missiles was presented by McMahon et al. [155]. In their paper, methods to analyse the impact of non-deformable missile were also presented.

Later, a different concrete model has been developed to investigate the problem of concrete wall perforation by rigid missiles (see Jamet et al. [159]) and the results were checked with those from the simple case of a rigid missile perforating a concrete slab.

1.2 Experimental Investigations

Scale model tests of turbine missile impact into concrete panels were carried out by Mechugh, Seaman and Gupta [2]. In their report, 25 impact tests were performed on a 1/11 scale of reinforced concrete walls. Irregularly shaped masses were used, typical of postulated turbine missiles, with speeds from 39.6 m/s to 213.4 m/s. These struck the target in piercing, blunt and glancing blow orientations. Apart from determining the threshold velocity at which postulated turbine missiles perforate reinforced concrete walls, comparisons between test data and the predictions of the NDRC and CEA-EDF perforation formulae were performed. It was concluded that these two formulae were conservative in predicting the perforation of reinforced concrete targets.

By using apparatus for high speed loading driven by compressed air, Takeda and Tachikawa [3] were able to show the influence of loading rate upon inelastic deformation and fracture of concrete and reinforced concrete members loaded in high rates of application, These experiments showed that there was an increase in concrete strength in these cases and that the rate of increment is larger in

tensile tests than compressive tests.

Goldstein, Berriaud and Labrot [4] shown that the overall behaviour of the building is easily calculated when the applied force as a function of time is known. Two calculation examples were used for demonstration. On the other hand, the local perforation is much more difficult and experimental work is necessary. In the report, a series of perforation tests on concrete plates by cylinderical missiles with flat noses were presented.

Both analytical and experimental investigations were carried out by Kameswara Rao and Prasad [6]. The analytical methods used the modal analysis and energy methods. In modal analysis, the free-vibration equation is solved by replacing the applied impulse with suitable initial conditions. The solution is obtained by assuming a linear combination of an infinite sequence of eigen-vectors.Iin the energy method, the beam-foundation system is considered to be subject to forced vibrations and the forcing function has been obtained using Herz's law of impact. In this impact investigation into loads on beams on elastic foundations, good agreement was found between the analytical and experimental results. The suitability of modal analysis and energy methods to impact problems was also demonstrated.

In experimental investigations, Davies [7] discovered that, for elastic conditions, an impulsively applied load would double the deflections compared to the same load applied statically in the case of reinforced concrete structures. He also showed that when a weight is dropped from increasing heights, the dynamic effect increase such that when the drop height is 40 times greater than the static deflection,the dynamic deflections are 10 times greater than the static deflections.

Rezansoff, Jirsa and Breen [8] tested 19 reinforced concrete beams containing lapped splices in a constant moment region under loading and compared the behaviour with that under static loading. A weight of 1180 kg was dropped onto the beams. Failure was achieved by a single-impact load, incrementally increasing impact loads, repeated undirectional impact loads at fixed levels, or repeated

undirectional impact loads at fixed levels.

Reinhardt [10] suggests that although analytical methods are quite advanced, they cannot predict all kinds of structural behaviour and so for highly complex loading cases, model or full scale experimental investigations are still necessary.

Brandes [11] points out that experimental investigations in the past years have indicated that deformation velocity, from impact and impulsive loading influences the mechanical behaviour and that this affect should not be disregarded. Behaviour of the critical regions of reinforced concrete and integration of this behaviour into theoretical-numerical analysis has not yet been applied to problems concerning hard missile impact.

In his definition, Eikl [12] states that soft impact occurs if the kinetic energy of the striking body is mainly transformed into recoverable deformation energy of the striking body or is dissipated mainly without participation of the struck body. On the other hand, hard impact occurs if the kinetic energy is completely transmitted to the resting body, which may be deformed or destroyed.

In their report, Hughes and Speirs [13] describe 80 transverse impact tests on pin-ended reinforced concrete beams and 12 tests on simply supported reinforced concrete beams. The impact was from a relatively rigid moving missile striking the beams in mid-span.

In his investigations, Bathe [14] analysed experimental data obtained at the Building Research station. These data reported the behaviour of prestressed and ordinary reinforced concrete beams under impact loading of a blow from a freely falling hammer with weight of the same order as that of the test beam. This hammer struck a simply supported test specimen of rectangular section at mid-span. This showed how the development of failure under impact loading compared with that under static loading, and how far the effect of any modifications in the mode of failure may be detrimental to structural security. Both single and repeated blow impacts were performed to test the impact resistance of the beams.

In order to compare the load-deflection and cracking response

characteristics of abeam, under static and impact loads, 1/8th scale reinforced microconcrete beams on a simply supported span under static and impact load from a 360mm long steel rod of 1.78kg weight were considered by Watson and Ang [16]. A minimum force of 191kN was applied for a maximum duration of 158ms. They found out that impact loads induced large shear forces and local damage near the impact zone and produced higher mode deformation than that produced by a static load.

Another impact experiment was carried out on model scale reinforced microconcrete beam-column frames by Watson and Ang [17]. In that experiment, the impact load was applied at the beam mid-span and transient measurements of impact force and deformation of the frame were obtained. The residual load carrying capacity was also determined by subsequent slow reloading of the impact damaged frames in mid-span.

A continuing project of impact tests has been carried out at Imperial College [18,19,20]. The impact is caused by a dropped rigid mass at low approach velocities of 10 m/s. The impact is of the hard type and the targets concerned include prestressed concrete slabs and shallow reinforced concrete domes. Perry et al. [19] divided concrete loads into 5 classes:-

- Static loads and quasi-static impact loads (velocities 0-10 m/s)
- Accidental impact loads caused by dropped objects (velocities 0-40 m/s)
- Aircraft impact (velocities 200-300 m/s)
- Ballistic impact (velocities 1,000 m/s)
- nuclear blast

These authors also suggested that a generally accepted model is not available particularly for tensile behaviour [20].

A series of experiments on model reinforced concrete slabs subject to falling projectiles was carried out by Burgess and Cambell-Allen

[21]. Flexural and shear failures under normal loading to the surface were identified together with the location and proportion of reinforcement necessary for the two modes to occur simultaneously. In this case the impact resistance of the slab would be optimised with respect to the amount of steel used in a given section thickness. By experiment, they showed that increasing the thickness of a slab without altering the reinforcement layout was not a satisfactory method of improving the impact resistance, Furthermore it was found that normal impact was the most damaging to the slab.

Full-scale testing of tornado-generated missiles on targets of reinforced concrete panels, concrete block walls and chain link fence was carried out by the Sandia Laboratory under contract with the Energy Research and Development Administration, Hanford Engineering and Developing Laboratory and Electric Power Research Institute [22]. These tests determined the adequacy of specific current designs, the effectiveness of tornado-missile barrier systems to resist penetration, and the threshold velocity that will cause incipient spalling to be generated on the back face of the panels subject to impact over a range of missile velocities. Stephenson concluded that

- ERDA facilities tested are conservative in design.
- Chain link fence can be an effective barrier for light weight tornado-missile protection and
- ERDI test results show that a minimum of 24 inches of reinforced concrete is sufficient to prevent back face scabbing from normal impact of postulated tornado missiles.

At the same time, a generator-scale reinforced concrete barrier missile test was carried out by Jankov et al. [23] to investigate the resistance of reinforced concrete panels to impact from an assortment of missiles. There were 40 tests (firings) in total using 22 barriers of 3 designs. Most of these barriers were impacted more than once, the first shot frequently being a probe of the scabbing threshold condition and the second shot having a velocity great enough to cause enterprise damage. Within the range

of validity, it was concluded that the threshold velocity varies inversely with the square root of the mass of the missile assuming all other quantities remain constant.For missiles that neither buckle nor crush, the scabbing threshold velocity increases with a decrease in the ratio of missile wall thickness / diameter (2t/D). A further increase in this threshold velocity results from nose crushing or buckling, and buckling of the entire missile due to excessive L/D and L/radius of gyration. If the material of the missile yields or disintegrates during impact, the scabbing threshold velocity increases.

In their papers Stephenson and Sliter [24] describe a test program in which reinforced concrete panels were impacted by poles, pipes and rods propelled by a rocket sledge. The work was sponsored by the Electric Power Research Institute in cooperation with the United States Energy Research and Development Administration to generate full-scale data for use in designing nuclear facilities against postulated impacts from tornado debris. Scabbing velocity of reinforced concrete walls was determined.

Both experimental and theoretical analyses were investigated on the behaviour of reinforced concrete slabs subject to deformed projectiles in the research program on reactor safety, initiated by the Ministry of Research and Technology of the Federal Republic of Germany. In the program Jonas and Ridiger [25] used non-linear constitutive relations between the bending moments and curvatures to solve numerically the equations of geometric linear plate theory. On the assumption of a cracked tension area, the internal plate forces and the stiffness matrices were calculated by numerical integration over the plate thickness, resulting in the instantaneous deformation of the plate.

Since 1974, C.E.A. and E.D.F. in France have developed a large program with the aim of working out a means of computation that is reliable enough to predict the behaviour of reinforced concrete walls under missile impacts. However, as pointed out by Berriaud et al. [26,94], in the cases when hard missiles are involved only empirical ballistic formulae are currently used. Despite various formulae and experimental results being available describing impacts

of hard missiles on concrete walls, it was not possible to estimate damage with sufficient reliability.

In an experimental and computational study to obtain the constitutional relations for determining the response of reinforced concrete walls to impacts from postulated tornado missiles, Gupta and Seaman [27] used an axisymmetric finite difference wave propagation computer program. Crushing, cratering, spalling, radial cracking, and shear failure along the surface of a plug or core of concrete extending through the wall were considered.

The behaviour of reactor structures under impact loading is being studied experimentally and theoretically under a formal technical collaboration agreement covering the exchange of data on experimental and theoretical studies and the implementation of co-ordinated and experimental programs in the missile impact fields between the United Kingdom and West Germany [28,29,35,55]. Present interest in Germany, originating from the aircraft crash load case, is largely focussed on the study of effects of deformable missiles with impact velocities between 200 m/s and 300 m/s. The work in the United Kingdom Atomic Energy Establishment covers both rigid and deformable missiles. The overall dimensions of the targets in Meppen, Germany were 6.5 x 6 x 0.7m with a gross weight of 70t. The targets Winfrith, United Kingdom were geometrically similar but were 1/4 the size of the Meppen targets. These tests will provide information on the validity of the scaling rules used. The U.K. test results will also give guidance on the impact velocities to be used in the German large scale tests. As the results are presented, the two organisations are able to confirm that the modelling techniques employed provide good representations of the overall prototype behaviour.

From the program of experiments on impact of missiles with reinforced concrete structures undertaken by the Safety and Reliability Directorate and the Atomic Energy Establishment Winfrith, Barr et al. [30] used computer code predictions to compare with experimental results obtained from the impact tests. They suggested three useful approaches for the designer or safety analyst of nuclear reactor structures (1) Use empirical formulae for

'first cut' approximate calculations. (2) Use 'exact' calculational models, preferably incorporated in available structural analysis computer codes, (3) Model testing facilities for full scale testing are only feasible for some missiles.

Some impact tests with metal targets were also carried out at the Atomic Energy Establishment Winfrith aimed at validating computer codes for the recalculation of target response [31]. Drop tests were used to obtain impact velocities up to 25 m/s while a missile launcher powered by compressed air was used for impact velocities approaching 250 m/s. Both finite element and finite difference computer codes were used to compare with results from the impact results. Preliminary calculations indicated that even at impact velocities below 20 m/s, strain rate effects have a significant effect on the response of mild steel target panels. Reductions of more than 20% in the peak deflection have been indicated for the target panels used in these tests.

In their paper, Anderson et al. [32] discuss the use of fibre-reinforced concrete materials to resist projectile impact. In their project, the resistance of fibre-reinforced concretes, suitable for sprayed concrete application, was examined. Specimens 450mm square and of various thickness were prepared with different mix proportions. These were cured and then impacted centrally with a 7.62mm copper-sheathed hardened steel projectile of mass 9.6-9.9g travelling at approximately 800 m/s. Target damage was quantified and correlated to the fibre concrete parameters. Instrumentation and high speed photography were used to investigate the failure mechanisms.

Since the conference of the 4th. SMIRT, new tests have been performed in France by the CEA concerning the local behaviour (penetration and perforation) of reinforced concrete slabs and walls under hard missile impact concentrating on the quantity and situation of reinforcement and the age of the concrete [53].

In order to determine experimentally and theoretically the ultimate bearing capacity of reinforced concrete slabs under impact loading, Gonas et al. [35] carried out the investigations to determine the

impact load/time characteristics for the impact of strongly deformable missiles onto quasi-rigid reinforced concrete structures. This determined the kinetic ultimate bearing capacity of reinforced concrete slabs subject to impact of strongly deformable missiles.

In order to investigate at which mode failure occures with respect to elastic design, 20 reinforced concrete slabs have been tested under the same impact loading [37]. Different rates of bending reinforcement were fixed to the slabs. Dulac and Giraud [37] conclude that there is no risk of shearing failure even though the slabs have no shear reinforcement. It is also possible to significantly reduce the bending reinforcement by up to 50% without provoking large deformations or plastic hinge and mechanism failure.

An analysis on the local effects of concrete and steel barriers subject to tornado generated missiles has been presented by Healey [103]. He states that, in general, missile damage can be attributed to a combination of localised effects and overall structural response of the barrier. Hence, apart from the preliminary missile chacteristics (e.g. weight, velocity, overall configuration, nose shape and material properties) and barrier data (e.g. thickness, the relative masses of the missile and barriers), the rigidity and support condition of the frame and deformation in the missile itself must be considered. This study, concentrates on the important practical case where the predominant damage mechanisms are the local effects induced by the action of a rigid non-deforming missile on a barrier. A residual velocity relationship for evaluating the performance of composite multi-layer barriers is also analysed.

In his investigation of crashworthiness of concrete structures subject to impact or explosion, Taketa [104] concludes that in order to improve the crashworthiness of reinforced concrete structures, the characteristics of response of the structures under impact or explosion should be taken into consideration. The primary and secondary responses generated in reinforced concrete structures subject to impact or explosion are governed by the mechanical properties of structural materials in structures influenced by rate

effects. Many responses are ionduced by rate effects which cause multi-fracture modes of failure of reinforced concrete structures under impact or explosion.

In his analysis, Attalla [112] made an attempt to study the behaviour of reinforced concrete structures under missile impact loading. The local deformation in all directions, including the wall thickness, the plasticity and the stress waves at and surrounding the impact point, were taken into account.

Bartley and Davies [118] used built-in reinforced concrete slabs to study local effects from aircraft impact loading by yield line analysis. They pointed out that the minimum information which is required to investigate the effect of an aircraft impact should include :- (a) the mass of the aircraft; (b) the impact velocity; (c) the variation of contact area between the aircraft and the containment building during impact; (d) the variation of impact force with time; (e) the deformation chacteristics of the containment structure, most suitably in the form of a force displacement curve and (f) the effects of high rates of strain on the structural material.

Perhaps the most aircraft crash tests have been performed at the NASA Langley Research Center in the United States. In the International Conference of Structural Impact and Crashworthiness in July 1984, Thomson [140] announced that they had crashed up to 29 military aircrafts with a variation of impact angle up to 45 degrees. Films were taken inside and outside the aircraft in order to study the deformability of the aircraft but the main concern was focussed on the safety of the pilots. No work was performed to investigate the failure criterion of the target.

In their investigation, Chiapetta and Costello [153] developed representative design orientated loading data for reinforced concrete wall panels subject to automobile impact considering the deformability of both the vehicle and structure. A one-dimensional model was used to calculate impact force-time histories on rigid walls due to head-on impact and a three-dimensional lump-mass vehicle model was used to predict the effect of various impact

angles in one plane.

Several other researchers have carried out work on the impact of soft missiles. In his work, Porter [154] gives a full analysis of a situation liable to produce metal fragments or blasts consisting of three inter-related considerations. They are force and character of the fragments, or blast wave integrity of the target and the effectiveness of protective barriers. In the paper, he also attempted to highlight some of the technical considerations involved in the overall safety assessment of a plate which could, under accident conditions, be subject to missile or destructive shock form.

1.3 Theoretical Investigations

A numerical analysis of missile impact problems was carried out by Chita et al. [38] using the multi-purpose finite element code ADINA. The dynamic elasto-plastic responses of projectile and target plates after impact were solved as a function of time by the direct integration method and calculated results were compared with experimental ones obtained from impact tests on with carbon steel plates used for primary containment vessels using rocket propelled projectiles of stainless steel. The comparison showed that the method of calculation is capable of solving for impact behaviour, presuming that the target plate deforms and undergoes thickness reduction in a ductile manner due to contact effects with the projectile. Details of the test have been described in reference [39] This presents a new formula for evaluation of critical energy for steel plate integrity applicable to cylindrical, semi-spherical and conical nosed missiles. The series of tests performed, indicated that the target fracture mode and critical fracture energy required, differ significantly differ from each other in relation to the missile's nose shape (cylindrical missiles). Results for semi-spherical missiles mostly agree with values predicted by the empirical equations generally used. Subsequently these authors have produced a paper [40] using non-linear dynamic analysis to simulate

these impacts.

A theoretical and experimental study of perforated uniform thickness concrete slabs with a triangular layout of holes was performed by Harrop and Abdul-Wahab [45]. The theoretical analysis is an extension of earlier work [175] on perforation of plates and includes the effect of tensile reinforcement on the flexural behaviour of concrete slabs. Results support the analysis, which may provide a practical method of design for the containment of nuclear reactor pressure vessels.

In an other paper, Gupta and Seamen [50] describe an experimental and computational study undertaken to determine the local response of reinforced concrete walls subject to impact from postulated tornado and other missiles. The study involved laboratory-scale missile impacts, experiments to characterise concrete, computational model development and two-dimensional simulation of missile impact. Impact experiments using rods and pipes on small reinforced concrete walls showed crushing, cratering, spalling, radial cracking and plug formation. The mechanisms governing the material response appear to be crush, shear and tensile fracture. State triaxial and dynamic plate impact experiments were used to determine the material properties of which dynamic strength was higher than static. A constitutive model was developed for concrete compaction, Mohr-Coulomb yield, and tensile operation following tensile strain accumulation.

In the case of low velocity impact of a simple model, this was developed by Limberger [51] for the determination of energy dissipation of thin plates being perforated by hard missiles. Having compared the predicted energy of missiles having passed through a target with test results using plates made of wood-chip, he concluded that for a projectile with a large diameter relative to the thickness of the target, it is shown that the energy absorption of the plate is essentially influenced by the fracture type.

A foundation of stress-strain criterion for the mechanical design of fast breeder reactor structures have been developed by Albertini and Montagnani [54] to deal with the constitutive laws of materials in

dynamics. These structures must be capable of bearing extreme dynamic loading conditions and the reference decribes the experimental determination of dynamic mechanical properties of materials in end-of-life conditions with respect to the damaging process.

In the 8th SMIRT, Ohnuma et al. [81] presented a series of test results and theoretical analyses on the response of reinforced and precast beams due to impacting stress waves, bending waves, shear waves, penetration and deflection. They concluded that reinforced concrete beams can take impact load fairly well.

The structural response of a spherical shell under the impact of an aircraft has been investigated by Hammel [62, 63]. By using an idealization of a linear mass-spring-dashpot combination, which can easily be treated in computational method, he showed that impact force on plates is influenced by the elasticity of the plate whereas the impact force on shells is unchanged by the elasticity of the shell. The impact force of a deformable aircraft on an elastic shell is more influenced by the aircraft model considered than by the elastic displacement of the shell.

Connor et al. [64] have used a computer program for performing dynamic three-dimensional finite element analysis assuming non-linear material properties, for reinforced and prestressed concrete structures to study global response. This analyses treated the missile as a spring index system, employing a tri-linear material model, and modelling the concrete target with a 20 node isoparametric element employing fifteen symmetrically distributed integration points.

Habip [65] presents a general survey of methods of design and analysis on the structural effects of extreme dynamic loads. He carries out an analysis of a linear oscillator subject to blast pause and shows that the pressure-impulse contour, a curve relating the peak pressure and the impulse necessary for a specific peak displacement, is a practical representation of a dynamic damage threshold or failure boundary. This separates the pressure-impulse plate into the region of damage of continuous systems exhibiting

several physical different modes of damage due to dynamic loading. He points out that for short duration loads, the peak pressure amplitude is relatively unimportant and only the impulse is significant as a critical damage factor while the reverse applies for the long duration loads. For loads of moderate duration, both amplitude and impulse are significant.

A rigid plastic theory has been developed by Florence [66] as a preliminary structural design aid for missile-plate impact problems. In his method, he uses a clamped circular slabs of reinforced concrete. The loading is by means of a rectangular pulse uniformly distributed over a central circular area. This method is potentially useful where structural modes higher than the fundamental plastic mode are excited. In this case the equivalent single-degree-of-freedom or resistance-function method is too approximate. The suggested method concerned with the analysis of a soft crushable missile under impulsive loading.

The overall behaviour of reinforced concrete structures subject to impact of deformable missiles has also been evaluated by a method of analysis [67] based on approximating the structure-missile system by a two degree-of-freedom model - the missile and structure. The impact is simulated by applying an impulse on the two degree-of-freedom system. A step-by-step numerical time integration scheme (Central Difference formulation) is used. The time history of the displacement and velocities of both the missile and structure are obtained.

The analysis of the impact of a slow-flying Boeing 707 and the impact of a fast-flying military Phantom have been performed by Zimmermann et al. [68]. This studied the influence of material non-linear behaviour on the response of a reinforced reactor building and on equipment response. The material model assumed for the concrete accounts for a non-linear stress-strain equation including isotropic hardening, multi-axial cracking and crushing. The reinforcement model accounts for an elasto-plastic stress-strain relationship coupled with kinetic hardening. Three-dimensional non-linear finite element analysis results are presented for both the impact of Boeing 707 and a Phantom on a reactor building.

Vertical impacts onto the top of the reactor dome are analysed for both Boeing flying at 103 m/s and the Phantom, flying at 215 m/s. The results indicate that the impact of a Boeing 707 induces only moderate damage: some concrete cracking, no crushing and no steel yielding. Failure limitation is of the bending type In the Plantom analysis, a punching shear failure type tends to appear first, followed by a bending failure.

In their paper, McMahon et al. [69] point out that although some analytical procedures have been suggested to evaluate the barrier response due to tornado missile impact, none has been adequately compared with available test data. They examined a reported analytical procedure in the light of available test data however their investigation was restricted to the impact effects of steel-pipe and wooden missiles.

Concerning the potential danger associated with larger tornado-tossed projectiles, for example passenger vehicles, Labra [70] has investigated the dynamic response of a 19mm thick steel panel struck by a 210 km/h wind-tossed 1800 kg vehicle. A reinforced concrete barrier model was also set up. In his finite element computer program, the dynamic analysis is performed by either the modal analysis or direct integration. The computer program includes (a) dynamic analysis capability (b) elasto-plastic phenomena including work hardening effects (c) two and three-dimensional finite element library and (d) non-linear large displacement capability.

A finite element method has been presented to analyse the effects of impulsive loading, for example the air-blast-induced ground shock of shallow based flat roofed reinforced concrete structures, by Ghaboussi et al. [71] who have adopted a finite element analysis based on Timoshenko beam theory. Material properties are defined in terms of non-linear stress-strain relations in each of several layers through the thickness of the element. Elastic ideally plastic constitutive properties for plain concrete are present in terms of shear-stress / normal stress variables and elastic strain-hardening constitutive properties are assumed for steel. Nodal degrees-of-freedom induced are transverse and axial

displacements and flexural and shear rotations. In their conclusions, they stated that on the basis of favourable comparison with previously published beam-column data, the elastic, ideally-plastic model of concrete properties in conjunction with the finite element model presented is adequate to represent behaviour under combined flexure and thrust.

The shock behaviour of reinforced concrete structural systems has been studied by Zerna and Stangenberg [72]. They focus on the overall dynamic response of reinforced concrete structures subject to impact and impulse loads. The problems of concrete cracking, plasticity, membrane compression, large deformation effects, damping, special mass-inertia effects, filtering effects influencing the transmission of vibrations and material strength increase due to high strain rates have been dealt with. Reference is made to the overall dynamic response behaviour and to the behaviour of strain transmission in the main direction of a reinforced concrete structure. Typical aspects of the non-local response behaviour of reinforced concrete structures due to impact and impulsive loads are presented. An introduction is also given to special problems arising from this situation, and some representative examples taken from practical cases are presented for illustration.

Douglas and Bingham [73] point out that in order to determine the mechanical behaviour of a material during impact, it is necessary to determine, for each impact velocity, the stress-strain relationship and the wave velocity-strain relationship in order to evaluate the intensity function.

A mass-spring model, force-time solution and energy balance solution have been used by Rotz [76] to evaluate the structural response of structures subject to tornado missile impact accountint for both elastic and plastic effects. It is mentioned that a conservative estimate of structural response can be obtained by firstly determining the response of the impacted structural element and then applying its reaction forces to the supporting structure. The predicted structural response enables assessment of the structural design adequacy in terms of strain energy capacity, deformation limits,stability and structural rigidity.

Bokor [77] attempted to investigate some of the grey area, between a massive large impact area, moderate velocity missiles which produce substantial local target deformation and the likely introduction of high bending stresses in the target as a whole, and high velocity small impact area missiles. He stated that one can combine empirical penetration formulae with beam vibration theory to obtain results which do not contradict reasonable expectations.

A simple crash model has been proposed by Jonker [78] to analyse the transient torsional response of a clamped and a free hole circular cylinder due to tangential components of the impact loads. By choosing a suitable shape of the pulse, measurements of the transient torsional response are shown to be in good agreement with the calculated response. The effects of travelling velocity and pulse shape are investigated as well as the transfer of kinetic energy in the rotor to vibrational energy of torsion in the casing. An elementary one-dimensional wave equation is derived from the Poch-Hammer-Chree theory using a perturbation technique.

In a paper by Buyukozturk and Connor [79] current research status is presented for the multi-dimensional non-linear analysis of reinforced concrete subject to impulsive load conditions. Strategy for the solution of non-linear dynamic equations is discussed and a description of the development of the model for material behaviour is given. Further research needs and interests for the development of improved analysis capabilities are also indicated.

In their analysis and design recommendation, Broman et al. [80] suggest an equivalent single-degree-of-freedom system to represent the multi-degree-of-freedom system for impulsive loads. They also point out that in the case of structures subject to impulsive forces, plastic deformation may occur at some intermediate point simply because there has not been sufficient time for the stress wave to reach the actual boundary prior to the yield of the material.

Current numerical capabilities for solving the scenario with rigid missiles using Lagrangian Finite Element and Finite Difference methods have been discussed by Dubois et al. [95]. They show that

current advanced numerical methods give reasonable answers to impact-penetration problems provided that realistic models are used for material properties, penetration mechanics and boundary conditions.

An interface force-time history and barrier failure mechanism is developed in [98] to evaluate the local damage of a reinforced concrete barrier impacted by a non-deformable missile. The procedure for predicting missile penetration is based on a triangular interface force-time history derived from time history measurement of smaller missile impacts.

Reviews have been given by Haldar [100, 101] on turbine missile problems. In paper [100], some of the critical parameters related to this problem have been identified and their probability characteristics have been discussed. A probability methodology to estimate the damage potential of turbine missiles is also developed. In the other paper [101], a review of local effects on concrete structures during missile impact is given. Probability methodology is also proposed to consider the uncertainty in the damage-predicting equations.

Davis [102] also attempts to review the whole spectrum of impact studies, comment upon the experiments which have been performed and describe some of the techniques used for the analysis of structural behaviour. Experimental programs, empirical formulae and penetration theories of concrete structures under impact and impulsive loading are reviewed.

In order to study the fracture of concrete under impact loading, Zielinski [105] sets up a model for the behaviour and fracture of plain concrete under impact tensile loading. It is stated that the behaviour of concrete under impact tensile loading is governed by more extensive simultaneous cracking of the material and fracturing tougher zone than in the case of static loading.

In a further paper, Davis [110] outlines a typical analysis which was executed as a precursor to an experiment on determining the damaging effects from the impact of soft missiles on reinforced

concrete structures. It describes a finite difference computer program analysing barrier performance under impact loading. It also describes techniques which have been used or are in the process of development to facilitate the assessment of missile load functions, the design of barriers and the study of the response.

Concrete cracking is a phenomenon that has to be considered with a certain amount of care when dealing with both local effects and overall structural failure because it initiates both of these events. Unfortunately only a mimimal amount of work has been performed on these aspects in which the problem of missile impact on concrete containment has been dealt with [3, 114, 115, 116, 134, 135, 137, 174].

In their paper, McGeorge and Sivec Jr. [113] discussed an analysis procedure for the detailed evaluation of cracking in large reinforced concrete structures and components. Analyses performed for an actual unlined reinforced concrete containment structure using this procedure were discussed and results were presented. Discussion also brought into consideration recently developed finite element based procedures for the determination of cracking in the reinforced concrete drywell structure of a typical P.W.R. reactor building subject to operational and environmental loadings.

A simple crack model for reinforced concrete has been implemented by Reynen et al. [114] who have attempted to study the behaviour of reinforced concrete structures under impulsive loadings. In their paper, the more recent developments of the computer program SLOOFDYN are addressed and in particular application of the element SEMLOOF to reinforced concrete accounting for dead weight, prestressing and cracking. The model for concrete cracking in SLOOFDYN is based on the concept of zero tensile strength of concrete.

A limit state analysis of a prestressed concrete containment vessel for P.W.R. has been presented by Bangash [115]. In his work, equilibrium equations for spherical domes have been derived. A computer program LIMIT has also been developed to examine the vessel under internal and external loads, and loads caused by aircraft crashes. Together with perforation and scabbing, cracking

conditions are also assessed. In an other paper [116], this author discusses elastic, inelastic and cracking conditions of containment vessels under extreme loads with emphasis on problems associated with the structure. The three-dimensional finite element analysis and limit state analysis were used to design such vessels and these analysis cater for service, overload and dynamic cracking of the structures.

In May 1984, the NDRC equations for penetration and back face scabbing thickness were reevaluated using presently available test results. In their paper, Haldar and Hussein [166] used a non-dimensional impact factor to improve the predictability of these equations. Penetration depths are estimated using NDRC, statistical NDRC and the proposed Haldar equations. It is found that the Haldar equations can predict the penetration depth reasonably well for all types of missiles while the NDRC equations only showed good results with bullet type missiles.

In a paper presented at the 8th SMIRT 1985 [182], Maurel et al. verified that reinforcement necessary to prevent perforation, that had been predicted by approximate methods for dimensioning the slabs, was sufficient. In their three-dimensional finite element model, the Drucker Prager criterion was used for concrete while Von Mises criterion was used for steel. Failure criteria such as perforation, scabbing and cracking were, however, not investigated.

A procedure by which reinforced concrete structures such as slabs and shells may be designed to retain the required structural integrity after an aircraft impact has been outlined by Rice and Bahar [119]. The reaction time relationship for a deformable aircraft impacting on a rigid wall is derived.

Analyses have been performed by Sharpe, Kamal and Scanlan [121] to determine the effects of the impact of an aircraft on the critical portions of the reactor building of a nuclear plant located in Germany. The perforation and penetration equations relative to reinforced concrete walls and roofs are reviewed and the applicable ballistic formulae are examined.

In their papers, Kamil et al. [122, 123] identified the major aspects of the aircraft impact problem and spotlighted the most relevant topics for future investigations. The emphasis was on modelling techniques, influence of non-linear behaviour and the importance of damping in the dynamic structural response analysis for aircraft loading. Results are presented for brief studies involving response of linear and non-linear simple systems to short duration impulsive loadings from aircraft impact types. For non-linear ranges, the required ductility ratios for a typical aircraft impact loading were compared against available ductility ratios for typical wall and slab panels.

Schmidt et al. [124] carried out an initial investigation into defining important features that would allow soft shell-hardcore design to successfully sustain a postulated aircraft impact In their investigation, the frame of the aircraft was assumed to crush progressively from the nose towards the tail as it impacted the wall and crushing was assumed to occur only at the point of wall contact.

Studies on local and global response of reactor buildings using aircraft impact load cases were carried out by Kaiser et al. [125]. In thier paper, the local behaviour of the crushed and plasticly deformed area of the structure was investigated by means of a model which considers the anisotropic properties of the structure.

Investigations on aircraft impact have also been made by Fuzier et al. [126], Carlton and Bedi [127, 132] and Kotulla and Hansson [128]. Fuzier carried out elastic analysis for an aircraft impact at the top of the dome of a reacto. Analysis was performed using the MARC program assuming an ultimate limit design without cracking limitation with special consideration of the reinforcement of the reactor structure. Carlton and Bedi applied a finite difference program to the theoretical study of the effects of an aircraft striking reinforced concrete slab with special emphasis on the proportion of reinforcement and the thickness of concrete. Kotulla and Hansson, on the other hand, analysed the impact of an aircraft crashing on underground ducts with protective slabs in reactor buildings. They also discussed and compared different types of

idealization for dynamic analysis.

Recommendations have been made by Danisch and Graubner [129] for the design of reinforced concrete structures against the induced vibrations of short time impact, such as aircraft impact, as follows :- (a) to consider no resonance amplification phenomena and to assume that, in the case of overstressing the structures, they will behave in a ductile fashion; (b) to make a simplified analysis with the peak acceleration of the force-time histories without calculating the fundamental frequency of the structure; (c) to calculate the elasto-plastic response only for those cases where additional reinforcement resulting from the above mentioned method is uneconomical.

Ree and Hock [130]have performed analysis with PISCES-2DL on a containment vessel, with different concrete thicknesses, and on a flat slab subject to impact of an airplane The reinforcement of the concrete has been taken into account in their analysis. They conclude that reinforcement plays a significant role in the analysis and keeps the concrete together after failure.

Lazzeri et al. [131] analyse the consequences of aircraft impact on a nuclear power structure with particular reference to (a) analysis of large structures up to medium high frequencies, (b) local analysis of concrete, (c) analysis of ductile components and (d) analysis of fragile equipment.

Shell structures have been dealt with by several authors [133, 134, 135] concerning the impact of an aircraft. Filho et al. [133] attempted to design the reinforced concrete shell of a nuclear reactor for aircraft impact, including checking of penetration, scabbing and back face spalling, by using a non-linear dynamic analysis. Grutzen and Reynen [134] addressed the highly non-linear problem of aircraft impact on reinforced concrete shell structures including cracking of concrete in the tensile regime, crushing of concrete in the compressive regime and plasticity of the reinforcement. Rebora et al. [135] examined a thin-wall reinforced concrete shell consisting of a cylinder and a sphere for a non-symmetric loading involving the interaction of membrane and

bending behaviour. A dynamic non-linear analysis was performed for a load case which represented impact of an airplane on the external shield building of a nuclear power plant.

Another two-dimensional explicit finite element analysis has been used by Puttonen [136] to solve the dynamic structure and flow problem in order to make an estimate of the sufficient thickness of the containment building capable of withstanding an aircraft impact. The load-time function used simulated the impact of a military aircraft with a weight of 20 tons and velocity of 200 m/s.

In the 7th SMIRT 1983, a few papers [137, 138, 139] presented three-dimensional finite element analyses to analyse the aircraft impact problem. Bauer et al. [137] carried out an analysis of reinforced concrete structures subjected to aircraft impact loading using the full three-dimensional Lagrange code DYSMASIL. This simulated the impact and penetration process with inherent considerations of the interaction between impacting projectile and target within the scope of non-linear effects. The local failure of concrete and the plastic deformaton of reinforcement were considered. Buchhardt et al. [138] attempted to close the gaps between the findings of experimental and analytical analysis of reinforced concrete structures under impact of an airplane. In their calculation, the finite element code ADINA was applied. Also a full three-dimensional dynamic non-linear numerical analysis on aircraft was performed by Marti et al. [139]. In their analysis,concrete was modelled as an elasto-plastic solid with limited tensile strength and a criterion to detect crushing. The elasto-plastic behaviour was represented in some cases with a simple bilinear law, while in others, a smooth non-linear hardening curve was used. An elasto-plastic law was used for describing the reinforcing bars but the compressional, bending and shear strength of the bars were neglected.

Stangenberg [142] carried out a non-linear dynamic analysis of reinforced concrete structures composed of beams and plates under the impact of an aircraft. The finite propagation velocities of bending and shear waves were taken into account by numerical integration using finite time and space intervals. Dynamic analysis

was presented assuming realistic laws governing the material behaviour of reinforced concrete. A mathematical-mechanical model was used to model loads from jet forces, external blast and deformable aircraft mass.

A safety investigation was undertaken by Degen et al. [145] to assess the effect of a large commercial airplane crashing perpendicularly onto the surface of a spherical reactor building dome. Based on safety considerations, the various solutions were discussed from the viewpoint of penetration, cracking and collapse modes of failure. The performed investigations include :-

- Calculation of the failure load following the yield theory.
- Calculation of the sectional forces using the linear-elastic shell theory and subsequent design by the ultimate strength method.
- Calculation of failure load, establishing the failure mechanism and distribution of sectional forces using the plastic shell theory, and
- Calculation using a three-dimensional isoparametric finite element program with plastic capabilities which include the collapse load, the failure mechanism and the distribution of sectional forces.

One of the very few investigations into the effects of varying reinforcement levels in reinforced concrete structures subjected to aircraft impact was carried out by Zerna et al. [146]. Their paper deals with optimization of reinforcement for resisting impact forces resulting from an aircraft crash. Reinforcements with high tensile bars and tensile cables are considered.

In his paper, Meder [147] calculates the response of elasto-plastic single-degree-of-freedom systems subjected to an aircraft impact pulse. The the results were compared with simple pulse models and presented in the usual form of design charts.

In the nuclear industry, when considering the design of concrete

containments for aircraft impact, Schnellenbach and Stangenberg [148] point out that, in order to withstand high impact forces, reinforcing steel of high strength is used. In their analysis large deformations, cracking of concrete, plasticity and changed-bond properties between steel and concrete have been taken into consideration.

After determining aforce-time relationship assuming an ideal plastic impact on a rigid wall for a Boeing 707, Riera [149] discussed the overall problem of nuclear power plant safety after an accidental impact of an aircraft in relation to its structural analysis and design. The available solutions for the resulting structural dynamic problem and the present practice to evaluate floor response /spectrum were also reviewed.

Stevenson [150] summarizes the international extreme load design requirements. The specific loads considered include earthquake, tornado, airplane crash, detonation and high energy system rupture. He also identifies five national centres for extreme load criteria development: Canada, Great Britian, United States, USSR and West Germany. France and Japan are also prominent as independent centres of exterme load criteria development.

Soft missile modelling has been used by both Hornyk [151] and Stoykovich [152]. Hornyk uses the principle of conservation of energy and momentum as well as common engineering assumptions to derive an analytical model to describe the perpendicular impact of deformable missiles on yielding walls with ideal plastic behaviour while Stoykovich represents his viscoelastic models by the Voigt model and the Maxwell model as missiles impacting on elastic and rigid targets.

Local failure of reinforced concrete under hard missile impact loading has been studied by Brown et al. [158] by using theoretical modelling of the local response. A computer code using explicit integration and the Lagrangian finite difference formulation of the equation of motion has been written to serve as a vehicle for the assessment of specific constitutive models of concrete.

Twisdale et al. [164] developed a methodology to simulate the initial release conditions and subsequent motion of objects transported by tornadoes. In their paper, they presented a model they had developed to simulate rigid body dynamics in turbulent tornado injection fields. A simulation study of missile injection was also performed to determine a conservative range for the assumed horizontal force.

The probability of a tornado missile hitting a target has been studied by Goodman and Koch [165]. It is shown that the tornado missile transportation is a diffusion Markovian process. The Green's function method is applied for the elimination of the probability of a unit target area.

In the 1960s, Watwood Jr. [168] used a finite element method to predict the crack behaviour of concrete. The procedure consisted of computing the strain energy for two slightly different crack lengths and employing numerical differentiation to determine the strain energy release rate.

In 1980, Hopkirk et al. [167] used a three-dimensional program which uses explicit time integration to predict the impact effects of concrete. The program allows large displacements and strains as well as arbitrary constitutive and contact laws with simple elasto-plasticity combined with Von Mises and Mohr-Coulomb associated and non-associated yield criteria built in as standard.

A three-dimensional dynamic finite element analysis of concrete containment vessels under impact of soft missiles has been developed by Bangash [172], who attempts to carry out non-linear and cracking analyses of the vessels and to compare results using aircraft impact loading functions. A percentage of reinforcement necessary to prevent perforation is also computed for various characteristic loads.

1.4 Empirical Formulae

A number of empirical formulae have been developed to describe the impactive penetration and perforation processes. Examples are the Petry, BRL, ACE, NDRC, BETH and CEA-EDF formulae [30, 84, 90-93, 101, 102, 107, 141, 166, 171, 173, 174], in which empirical relations are based on experiments conducted using high velocity, low mass and small diameter projectiles. However they are valid only within the range of variables for which experimental data is available. Most of these formulae have been developed with a certain degree of conservation due to the complication of the impact process and the complexity of the material behaviour under impact loading.

In their paper, Chang, Burdette and Barnett [81] deal with historical aspects of the Petry formula for missile penetration. They point out that the Petry formula and the modified Petry formula are essentially simplifications of the original Poncelet formula and, except for some additional data for concrete, it appears that these formulae contribute little new information in the understanding and development of penetration equations.

Five years later, Chang [82] developed two semianalytical formulae for concrete scabbing and perforation for concrete barriers subject to impact by cylinderical solid steel missiles. These two formulae are unit consistent and they provide a rational way to determine a safety margin factor according to a selected confidence level.

In his papers [83, 85, 86], Kar presents empirical formulae to determine local effects, for example penetration depth, the thickness for prevention of perforation and scabbing of concrete and steel barriers subject to missile impact. Proecedures are also given for determining the design load for overall effects. For concrete barriers, the proposed formulae take into consideration not only the shape, size and velocities of missiles, but also their material properties and those of the targets. The weight of the missile and its impact velocity are also ancluded. Aggregate sizes are also shown to have effects on the thickness necessary to prevent perforation and back face spalling. For steel barriers, the formula considers the material property of the barrier, energy-absorbing

capacity of the barrier material, weight, material properties, nose shape, general shape and size of the projectile, and impact velocity. Recommendations are also made for the determination of residual velocity after perforation of a steel barrier.

Recommendations have also been made by Kar [86] on the available barrier ductility during impact by aircrafts and tornado generated missiles. Tentative suggestions have also been made for the elevated elastic strain. It is recommended in the paper that flexural design for missile and aircraft impact be performed by considering elastic behaviour with limited local plasticity. A method is also presented [87] for determining the penetration into barrier concrete structures with assumptions that the impact is normal and the earth material overlying the concrete structures is either rock or clay. This earth material can be uniform or layered and the water table can vary. The residual velocity of the missile after penetration of the overburden material is then used to determine local effects.

Another method has also been developed by Kar [88] to determine the contact pressure at the interface between the missile and the target, and the velocity and acceleration time-histories of the missile. In his paper, he also gives a method to obtain the design load due to impact by tornado generated missiles. This deals with hard missile impact on concrete walls and it is shown the the velocity-time history of an impacting missile can be determined from the principles governing the collision of an elastic body with a relatively rigid target. By obtaining the deceleration of the missile, he also presents a simple method to determine the load-time history [89] for the most critical tornado generated pipe missiles.

In his paper, Sliter [90] mentioned that, because of the complex nature of the local impact response of reinforced concrete, detailed analysis by means of computational mechanics are not yet developed enough for application in the design for nuclear power facilities and other structures for local impact effects. Therefore, designers need to rely on empirical formulae. Local effects on reinforced concrete such as perforation, scabbing and penetration of concrete as observed in 145 recent tests, have been used to assess the NDRC, CEA-ED, Bechtel and Stone and Webster formulae and the range of impact parameters over which the relations are applicable has been

considered.

Some works [58, 91-93, 166] have also been carried out to analyse the existing NDRC formulae. Haldar et al. [91, 92] re-evaluated the NDRC equation to estimate penetration depth by using presently available test data on missiles similar to those expected in nuclear power plants The NDRC equation is also statistical and a new relationship is proposed to estimate the penetration depth by introducing a dimensional factor.

It has also been pointed out by Tulacz and Smith [107] that scabbing may be produced when a stress wave arising from the impact of the missile on the target is transmitted through the structure and reflected from the back face. They also give stages of the design assessment of a missile problem as follows :-

- Identify potential source
- Quantify missile properties
- Identify possible targets
- Assess damage to targets
- Consider likelihood of an overall event sequence
- From judgement, regard design acceptability

It is concluded that the NDRC formulae are currently available for predicting penetration, perforation and scabbing depths in concrete. Relatively few results for realistic irregular shaped missiles have been presented. It is recommended that further work to demonstrate the validity of the correlations for realistic missiles might be useful. Currently available information suggests that irregularly shaped missiles have a smaller penetration depth than the equivalent mass cylindrical missiles.

New penetration, perforation and scabbing formulae have been derived by Hughes [113] for use in the design of reinforced concrete barriers to withstandthe impact of hard missiles. This is done by using dimensional analysis together with physical theories for the various impact processes. This leads to impact formulae with unknown coefficients which are then determined by an analysis of the

available test data. The analysis indicated that some recently proposed impact formulae are not safe from the point of view of barrier design because the test data used for their derivation was affected by global movement of the barriers which reduced the measured local damage.

Less than half a year later, Walter and Wolde-Tinsae [171] presented a series of improved empirical methods for the prediction of perforation of reinforced concrete barriers by missiles produced by turbine fracture. Data from recent turbine missile tests and existing empirical methods of perforation damage analysis were collected and compared. They produced a more accurate prediction of the occurence of perforation of reinforced concrete barriers by missiles typical to those that might be found at nuclear power generating facilities.

In their paper of December 1984, Gopalakrishna and Wolde-Tinsae [176] used the Monte Carlo method and Advanced First Order Second Moment methods for the evaluation of damage probabilities. Empirical formulae have been selected from all existing turbine missile test data from the United States and elsewhere, and uncertainty in the predictions have been incorporated in the assessment of damage probability of concrete and steel barriers.

1.5 Scope of Research

The literature survey indicates the complexities associated with impact and impulsive loads. A comprehensive limit state design is needed for both the nuclear industry and air force defence departments and designers should be given well-proven formulae to deal with impact problems. This research takes one step in that direction. A dynamic non-linear finite element analysis is needed for both reinforced and prestressed concrete under missile impact. A great deal of research is also needed for the simulation of non-linear material properties. In order to optimize the solution cost and time in the equation system, automatic selection of variable time steps and variable load steps is necessary in dynamic analysis. A great deal of research is also needed into reliable time integration schemes for dynamics time-domain analyses.

A three-dimensional concrete cracking criterion under missile impact is a very highly complex phenomenon in both local and global areas. The influence on the remaining elastic state of the structure and on the deformation characteristics of missile target system are additional problems to be looked at in detail.

Not a great deal of investigation has been carried out into the reinforcement and concrete grading of the target structure in response to missile impact. Again a great deal of research is needed on both of these parameters to give a true understanding of the material behaviour under missile impact. There is very little correlation between dynamic finite element analysis results and the corresponding experimental results on slabs.

Although some work has been done on the prediction of penetration, perforation,spalling and back face scabbing of reinforced concrete targets under both soft and hard missile impacts, a tremendous amount of work is still vitally required for three-dimensional prediction of local failure of reinforced concrete under impact of both soft and hard missiles.

The current research is concerned with the effective use of three-dimensional dynamic finite element analysis in which a provision is made for the simulation of impact loads, plasticity, perforation, scabbing, and cracking of concrete. Two existing three-dimensional finite element programs are used to carry out the analysis. The program NONSAP is modified to include a three-dimensional four-parameter concrete model based on the Ottosen failure criterion [187-189]. A reinforced concrete model based on a composite model developed by Isenberg and Adham [190] is used to model the reinforcement / concrete. Newmark direct integration is used to perform the solution process.

A three-dimensional non-linear dynamic finite element package, MARC is used as for comparison. In this analysis, the parabolic Mohr-Coulomb yield criterion is adopted to model concrete while the failure of reinforcement is predicted using the Von Mises yield criterion. Again the Newmark direct integration scheme is adopted in this analysis. Cracking criteria used by MARC is based on the smeared crack concept.

Two reinforced concrete slabs tested at UKAEA, Winfrith have been examined using the above analyses. Load time functions provided by UKAEA were treated as the major input. Two slabs were idealized using the finite element mesh generator MENTAT, a pre- and post-processor associated with MARC.

CHAPTER 2

MODELLING OF CONCRETE BEHAVIOUR

2.1 General Introduction

Under normal static loading, it is the limiting tensile strain which determines the strength of concrete. The local break down in bond between the cement and the aggregate can also cause local concrete cracking. In a three-dimensional cracking criterion, a crack is assumed to occur in a plane normal to the offending principal stress. When the principal stress exceeds its limiting value, the concrete is assumed to crack.

It is assumed that when a crack is formed, there will be no tensile stresses across the crack. The stiffness of the material is also reduced to a very low value in that direction. If there is an increase in loading, further cracks may occur perpendicularly to the first crack. Although cracks may occur in a direction normal to previous directions, opposite faces of the crack(s) may interlock-the degree of this depends upon the texture of the cracked surfaces and the constraints on the surfaces not allowing them to move apart. Aggregate interlocking assists the transfer of shear force across crack surfaces.

The crushing of concrete can occur when concrete strain reaches an ultimate value between 0.003-0.0035. In the current research, Ottoson and Mohr-Coulomb models are used to create failure envelopes.

2.2 Impact on Concrete

The impact load, when compared with the static load, produces sharp differences in the magnitude of a stress and the material resisting properties of concrete. This includes ductility reduction in areas

of stress concentration and ultimate strength.

In his impact tests, Spath [5] was able to show that the compressive strength of the concrete increases with the application of load. He also found out that the average ratio of dynamic to static compressive strength at the highest rate of loading was almost 1.84

On the other hand, from impact tests on concrete beams, Billig [15] pointed out that for very high rates of strain, the dynamic strength could be 60-80% greater than the ultimate static strength. From his investigation, he also concluded that the proportion of vertical reinforcement appears to be almost as important in developing impact resistance as that of the longitudinal reinforcement. Beams without stirrup reinforcement possessed little impact resistance and failure in shear for cases where failure under static loading occured in bending. Under impact conditions, transverse reinforcement fulfilled an important role in developing the maximum resistance of a reinforced beam, which could not be determined from the result of static tests. He also found out that the use of overlapping spirals of steel as a secondary reinforcement can increase the impact strength of slabs by as much as 3 times.

It is vital to point out that impact strength is more closely related to tensile strength than to compressive strength and also that impact strength is greater for coarse aggregate of greater angularity and surface roughness. Due to the insufficient bond between coarse aggregates and mortar, concrete made with gravel coarse aggregates has a low impact strength.It is also worth noting that both a small maximum size of aggregate and aggregates with a low modulus of elasticity and low Poisson's ratio improve the impact resistance of concrete significantly but the use of fine sand usually leads to a slightly lower impact strength.

2.3 Failure Criterion in NONSAP

The Ottosen Model [187, 188, 190], which is a four-parameter failure criterion model containing all three stress invariants, is applied in NONSAP to analyse the elasto-plastic and plastic behaviour of concrete. This model corresponds to a smooth convex failure surface

with curve meridians open in the negative direction of the hydrostatic axis. The trace in the deviatoric plane changes from nearly triangular to more circular shape with increasing hydrostatic pressure. It is especially developed for cases with short-term loading.

If we consider proportional loading, a one-to-one relationship exists between stresses and strains, and a failure criterion for an isotropic material in a homogeneous stress state can be expressed in terms of the three stress invariants. The failure criterion can be expressed as

$$f(\sigma_1, \sigma_2, \sigma_3) = 0 \qquad (2.1)$$

in which σ_1, σ_2 and σ_3 are the principal stresses that occur symmetrically. (For stress invariants and the application of the failure criterion function to elasto-plastic situations see Appendix A)

The octahedral normal stress, σ_o and shear stress, τ_o are related to the preceding invariants by

$$\sigma_o = I_1 / 3 \quad \text{and} \quad \tau_o = 2 J_2 / 3 \qquad (2.2)$$

where I_1 and J_2 are defined in Appendix A.

Using Fig. (2.1), the invariants defined in Appendix A give a simple geometrical interpretation surface in a cartesian coordinate system with symmetry properties of the failure surface. For this purpose, any point P (σ_1, σ_2, σ_3), in the stress space is described by the coordinates (x,y,θ) in which x is the projection on the unit vector $\bar{v} = (1, 1, 1) / 3^{1/2}$ on the hydrostatic axis, and (y, θ) are polar coordinates in the deviatoric plane which is orthogonal to (1,1,1).

$x = |\overline{ON}| = I_1 / 3^{1/2}$; $y = |\overline{NP}| = \sqrt{2J_2}$; and $\text{Cos}3\theta = J$

Equation (2.1) can be expressed as

$$f\ (I_1\ ,\ J_2\ ,\ \mathrm{Cos}3\theta\ ) = 0 \qquad (2.3)$$

Now, if A and B = material parameters

fc = uniaxial compressive cylinder strength of concrete

(fc > 0)

La = a function of $\mathrm{Cos}3\theta$

= La($\mathrm{Cos}3\theta$) > 0

$$\text{then } f(I_1,\ J_2,\ \mathrm{Cos}3\theta\ ) = \frac{A\ J_2}{fc^2} + \frac{La\ J_2^{1/2}}{fc} + \frac{B\ I_1}{fc} - 1 = 0 \qquad (2.4)$$

Values of $f\ (I_1\ ,\ J_2\ ,\ \mathrm{Cos}3\theta\ ) < 0$ correspond to stress states inside the failure surface.

For A > 0, B > 0, it can be seen that the meridians are curved, smooth and convex, and the surface does not intersect the negative hydrostatic axis.

From Equation (2.4)

$$\frac{J_2^{1/2}}{fc} = \frac{1}{2A}\left[-La + \sqrt{La^2 - 4A\left(B\left[\frac{I_1}{fc}\right] - 1\right)}\right] \qquad (2.5)$$

When q = 1 / La ($\mathrm{Cos}3\theta$) Equation (2.4) described a smooth convex curve in the polar coordinates (q, θ) and the trace of a failure surface in the deviatoric plane is given by Equation (2.5), which is also smooth and convex. When approaching the convex of the failure surface, corresponding to hydrostatic tension, $J_2^{1/2}$ goes to 0 will lead to

$$\frac{J_2^{1/2}}{fc} \text{ goes to } \frac{1}{La}\left[1 - \left(\frac{BI_1}{fc}\right)\right] \quad \text{i.e. } \frac{pt}{pc} \text{ goes to } \frac{Lac}{Lat} \text{ for } J_2^{1/2} \text{ becomes 0} \tag{2.6}$$

if pc = point P in compression

pt = point P in tension

Lac = La (-1) is the compressive meridian

Lat = La (1) is the tensile meridian

As Lac/Lat is inside the range of 0.54-0.58 Equation (2.6) indicates a nearly triangular shape of the trace in the deviatoric plane for stresses, Furthermore, Equation (2.5) implies pt/pc becomes 1 for I_1 as minus infinitive, i.e. for very high compressive stresses, the trace in the deviatoric plane becomes nearly circular. It was found that the function, La = LaCos3θ , could be adequately represented as

$$La = K_1 \text{ Cos}\left[\frac{1}{3}\text{Cos}^{-1}(K_2 \text{ Cos}3\theta)\right] \quad \text{for Cos}3\theta \text{ (> or =) } 0 \tag{2.7}$$

$$La = K_1 \text{ Cos}\left[\frac{\pi}{3} - \frac{1}{3}\text{Cos}^{-1}(-K_2 \text{ Cos}3\theta)\right] \quad \text{for Cos}3\theta < 0 \tag{2.8}$$

which K_1 is a size factor parameter

K_2 is a shape factor parameter

and (0 < or =) K_2 (< or = 1)

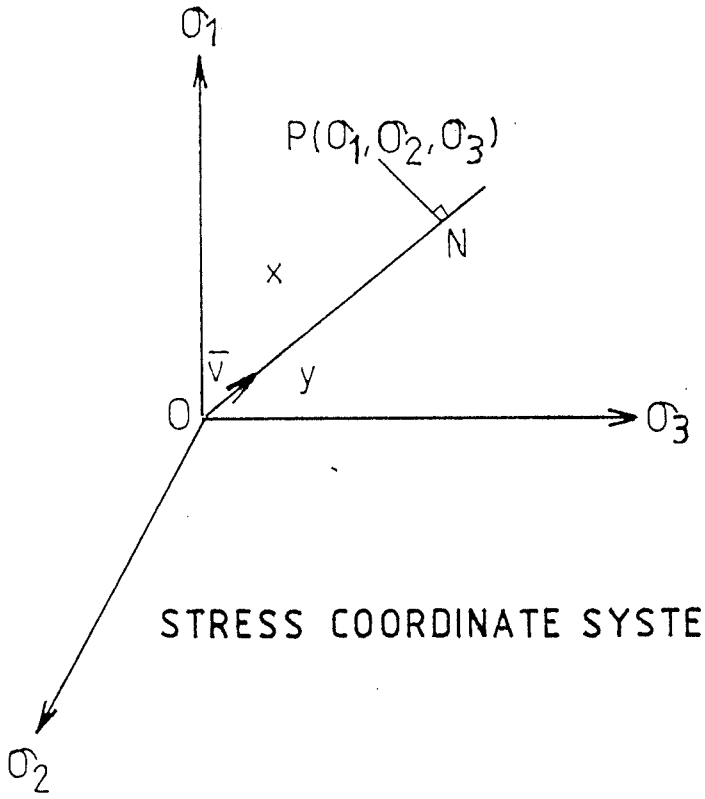

STRESS COORDINATE SYSTEM

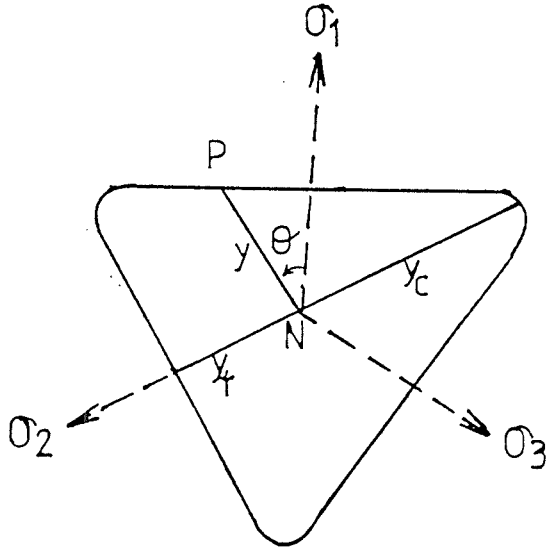

DEVIATORIC PLANE

Fig. 2.1 OTTOSON FAILURE SURFACE

2.4 Reinforced Concrete in NONSAP

The model used for the reinforced concrete target in this research is based on the composite model developed by Isenberg and Adham [190]. This model takes into consideration the properties of the reinforcing steel, non-linearity of the stress-strain relationship due to inelasticity of concrete and steel, and cracking.

In this model the properties of the composite material are specified within each element with respect to the principal direction of orthotropy. These directions of stress are kept constant up to the point of cracking. When cracking occurs, the principal orthotropic axes may be rotated relative to the global axes. However if cracking occurs in the element, the principal directions of orthotropy in that element are assumed to be fixed parallel and perpendicular to the orientation of the first crack.

If $[d\sigma]$ and $[d\varepsilon]$ are respectively the incremental stresses and strains in the global coordinates system, we have

$$[d\sigma] = [D]\,[d\varepsilon] \tag{2.9}$$

For the orthotropic directions, we have

$$[d\sigma]_o = [D]_o\,[d\varepsilon]_o \tag{2.10}$$

If $[T_A]$ and $[T_B]$ are transformation matrices, we can write

$$[d\sigma]_o = [T_B]\,[d\sigma] \tag{2.11}$$

and

$$[d\varepsilon]_o = [T_A]\,[d\varepsilon] \tag{2.12}$$

Now from the above equations,

$$[d\sigma] = [T_B]^{-1} [D]_o [T_A] [d\varepsilon] \tag{2.13}$$

and [D] is defined by:

$$[D] = [T_B]^{-1} [D]_o [T_A] \tag{2.14}$$

Assuming that the principal direction of incremental stress and strain coincide, it can be shown that

$$[T_B]^{-1} = [T_A]^T \tag{2.15}$$

where $[T_A]^T$ denodes the transpose of the matrix T_A

We therefore have:

$$[D] = [T_A]^T [D]_o [T_A] \tag{2.16}$$

Now

$$[D]_o = \begin{bmatrix} \mathbf{AA}\begin{bmatrix} E_1 & BB(E_1\,E_2)^{1/2} & BB(E_1\,E_3)^{1/2} \\ BB(E_1\,E_2)^{1/2} & E_2 & BB(E_2\,E_3)^{1/2} \\ BB(E_1\,E_3)^{1/2} & BB(E_2\,E_3)^{1/2} & E_3 \end{bmatrix} & \begin{matrix} 0 & 0 & 0 \\ 0 & 0 & 0 \\ 0 & 0 & 0 \end{matrix} \\ \begin{matrix} 0 & 0 & 0 \\ 0 & 0 & 0 \\ 0 & 0 & 0 \end{matrix} & \begin{matrix} G_{12} & 0 & 0 \\ 0 & G_{13} & 0 \\ 0 & 0 & G_{23} \end{matrix} \end{bmatrix} \tag{2.17}$$

where

$$AA = \frac{(1 - \mu_{com})}{(1 + \mu_{com})(1 - 2\mu_{com})} \tag{2.18}$$

$$BB = \frac{\mu_{com}}{(1 - \mu_{com})} \tag{2.19}$$

$$G_{ij} = 0.25 \left[AA(E_i + E_j) - 2\ AA\ BB\ (E_i E_j)^{1/2} \right] \tag{2.20}$$

$$E_i = b\ E_{ci}\ A_{ci} + E_{si}\ A_{si} \tag{2.21}$$

where

μ_{com} is the composite Poisson's ratio for concrete and reinforcement

G_{ij} are the shear moduli for i,j = 1, 2, 3

E_i are the composite Young's moduli for concrete and reinforcement

E_{ci} and E_{si} are the Young's moduli for concrete and reinforcement respectively

A_{ci} and A_{si} are respectively the relative areas of concrete and reinforcement projected upon the ith orthotropic face

b is the aggregate interlocking factor = 1

2.5 Concrete Cracking Model in NONSAP

A smeared concrete model is incorporated in NONSAP to deal with cracking behaviour. In this the cracked concrete is assumed to remain in continuum. It is assumed also that the crack criterion is based on the concept of changing the material properties and allowing for the effects of cracking by redistributing the stresses to the surrounding material. Here the maximum principal stress and strain criteria are used to define the cracks. When a principal stress in any direction exceeds the allowable limiting tensile strength, a crack forms perpendicularly to the principal stress direction. Thus for cracking

$$\sigma_i \ (> \text{or} =) \ ft$$

where σ_i is the principal stress (i = 1,2,3)

ft is the allowable limiting tensile stress

On further loading, some cracks may be formed at some angle to the first crack. It is assumed that further cracks are allowed in orthogonal direction, to the first crack.

Concrete in tension, up to the point of cracking, is assumed as a linear elastic material which becomes orthotropic as soon as a crack occurs. It is assumed that the direct tensile stress cannot be supported in the direction normal to crack$_j$ when it first occurs. Moreover the material matrix in this direction is reduced. It is also assumed that there is no inter-relation between this and other directions. However the material parallel to the crack is still capable of carrying stresses which are given by the new material constitutive relationship. A crack is assumed to close when the stress normal to the crack is compressive and also it is less than the strain at which the crack is opened.

As derived by Bangash [155, 156] and Admah [157], for uncracked concrete, we have the constitutive relationship assumed as:-

$$[d\sigma] = [D]\,[d\varepsilon] \tag{2.22}$$

where

$$[D] = \begin{bmatrix} D_{11} & D_{12} & D_{13} & 0 & 0 & 0 \\ D_{21} & D_{22} & D_{23} & 0 & 0 & 0 \\ D_{31} & D_{32} & D_{33} & 0 & 0 & 0 \\ 0 & 0 & 0 & D_{44} & 0 & 0 \\ 0 & 0 & 0 & 0 & D_{55} & 0 \\ 0 & 0 & 0 & 0 & 0 & D_{66} \end{bmatrix} \tag{2.23}$$

Where

$$D_{11} = (1 - \mu_{c23}\,\mu_{c32})\,E_{c1}\,/BF$$

$$D_{12} = (\mu_{c12} - \mu_{c13}\,\mu_{c32})\,E_{c2}\,/BF$$

$$D_{13} = (\mu_{c13} + \mu_{c12}\,\mu_{c23})\,E_{c3}\,/BF$$

$$D_{21} = (\mu_{c21} + \mu_{c23}\,\mu_{c31})\,E_{c1}\,/BF$$

$$D_{22} = (1 - \mu_{c13}\,\mu_{c31})\,E_{c2}\,/BF$$

$$D_{23} = (\mu_{c23} + \mu_{c13}\,\mu_{c32})\,E_{c3}\,/BF$$

$$D_{31} = (\mu_{c31} + \mu_{c21}\,\mu_{c32})\,E_{c1}\,/BF$$

$$D_{32} = (\mu_{c32} + \mu_{c31}\,\mu_{c12})\,E_{c2}\,/BF$$

$$D_{33} = (1 - \mu_{c12}\,\mu_{c21})\,E_{c3}\,/BF$$

$$D_{44} = [E_{c1}\,/2(1 + \mu_{c12}) + E_{c2}\,/2(1 + \mu_{c21})]\,/2$$

$$D_{55} = [E_{c2}\,/2(1 + \mu_{c23}) + E_{c3}\,/2(1 + \mu_{c32})]\,/2$$

$$D_{66} = [E_{c3}\,/2(1 + \mu_{c31}) + E_{c1}\,/2(1 + \mu_{c13})]\,/2$$

and

$$BF = 1 - \mu_{c12}\,\mu_{c21} - \mu_{c13}\,\mu_{c31} - \mu_{c23}\,\mu_{c32} - \mu_{c12}\,\mu_{c23}\,\mu_{c31} - \mu_{c21}\,\mu_{c13}\,\mu_{c32}$$

where

[D] is the material matrix of the concrete

μ_c is the density of the concrete

E_{ci} are the Young's moduli of concrete

Once cracking occurs, orthotropic conditions are introduced and the incremental constitutive relations are written in the cracked material direction. The total normal stress across the crack is reduced to zero and shear terms are introduced to account for any aggregate interlock.

If we define

$d\sigma$ as the incremental stress

$d\varepsilon$ as the increment strain

* denote the crack direction

SF as the shear relation factor, (assuming full shear stress develops along the crack)

= 1.0 for closed cracks

= 0.5 for open cracks

G as the shear modulus of uncracked concrete

Then:

$$\sigma^*_{xy} = SF\ G\ \varepsilon^*_{xy}$$

$$\sigma^*_{yz} = SF\ G\ \varepsilon^*_{yz}$$

$$\sigma^*_{zx} = SF\ G\ \varepsilon^*_{zx}$$

thus with cracking, from Equations (2.22) and (2.23)

$$d\sigma_x^* = D_{11}\, d\varepsilon_x^* + D_{12}\, d\varepsilon_y^* + D_{13}\, d\varepsilon_z^* \tag{2.24}$$

$$d\sigma_y^* = D_{21}\, d\varepsilon_x^* + D_{22}\, d\varepsilon_y^* + D_{23}\, d\varepsilon_z^* \tag{2.25}$$

$$d\sigma_z^* = D_{31}\, d\varepsilon_x^* + D_{32}\, d\varepsilon_y^* + D_{33}\, d\varepsilon_z^* \tag{2.26}$$

$$d\sigma_{xy}^* = D_{44}\, d\varepsilon_{xy}^* \tag{2.27}$$

$$d\sigma_{yz}^* = D_{55}\, d\varepsilon_{yz}^* \tag{2.28}$$

$$d\sigma_{zx}^* = D_{66}\, d\varepsilon_{zx}^* \tag{2.29}$$

Consider an element having 1, 2 or 3 cracks as in Fig. 2.2. For only one crack in cracking direction "1", the concrete offers no resistance in this direction.

In this case

$$d\sigma_x^* = 0 \quad \text{i.e.}$$

$$d\varepsilon_x^* = \frac{-D_{12}}{D_{11}}\, d\varepsilon_y^* - \frac{D_{13}}{D_{11}}\, d\varepsilon_z^* \tag{2.30}$$

Substituting Equation (2.30) into Equations (2.25) to (2.29):

$$d\sigma_y^* = \left(D_{22} - \frac{D_{12}\, D_{21}}{D_{11}}\right) d\varepsilon_y^* + \left(D_{23} - \frac{D_{21}\, D_{13}}{D_{11}}\right) d\varepsilon_z^* \tag{2.31}$$

$$d\sigma_z^* = \left(D_{32} - \frac{D_{31}\, D_{12}}{D_{11}}\right) d\varepsilon_y^* + \left(D_{33} - \frac{D_{31}\, D_{13}}{D_{11}}\right) d\varepsilon_z^* \tag{2.32}$$

$$d\sigma^*_{xy} = SF\ D_{44}\ d\varepsilon^*_{xy} \tag{2.33}$$

$$d\sigma^*_{yz} = SF\ D_{55}\ d\varepsilon^*_{yz} \tag{2.34}$$

$$d\sigma^*_{zx} = SF\ D_{66}\ d\varepsilon^*_{zx} \tag{2.35}$$

If the concrete cracks in the 2 directions "1" and "2"

$$d\sigma^*_x = 0 = D_{11}\ d\varepsilon^*_x + D_{12}\ d\varepsilon^*_y + D_{13}\ d\varepsilon^*_z \tag{2.36}$$

$$d\sigma^*_y = 0 = D_{21}\ d\varepsilon^*_x + D_{22}\ d\varepsilon^*_y + D_{23}\ d\varepsilon^*_z \tag{2.37}$$

thus we have

$$d\varepsilon^*_x = \left(\frac{D_{13}\ D_{22} - D_{12}\ D_{23}}{D_{21}\ D_{12} - D_{11}\ D_{22}} \right) d\varepsilon^*_z \tag{2.38}$$

$$d\varepsilon^*_y = \left(\frac{D_{23}\ D_{11} - D_{21}\ D_{31}}{D_{21}\ D_{12} - D_{11}\ D_{22}} \right) d\varepsilon^*_z \tag{2.39}$$

$$d\sigma^*_z = \left[D_{33} - D_{31} \left(\frac{D_{13}\ D_{22} - D_{12}\ D_{23}}{D_{11}\ D_{22} - D_{21}\ D_{12}} \right) - D_{32} \left(\frac{D_{11}\ D_{23} - D_{21}\ D_{31}}{D_{11}\ D_{22} - D_{21}\ D_{12}} \right) \right] d\varepsilon^*_z \tag{2.40}$$

$$d\sigma_{xy}^{*} = SF\ D_{44}\ d\varepsilon_{xy}^{*} \tag{2.41}$$

$$d\sigma_{yz}^{*} = SF\ D_{55}\ d\varepsilon_{yz}^{*} \tag{2.42}$$

$$d\sigma_{zx}^{*} = SF\ D_{66}\ d\varepsilon_{zx}^{*} \tag{2.43}$$

For cracks in "2" and "3" directions and "1" and "3" directions the above procedures are applied in a similar way. If 3 cracks occur in directions "1", "2" and "3", the material matrix becomes zero and concrete at this point carries no shear.

Hence $[D]^{*} = [0]$

2.5.1 Transformation

Since [D] in Equation (2.23) refers to a local crack coordinate system, it is necessary to transform back to a global coordinate system for the calculation of stiffness matrix. If TA and TB are the stress and strain transformation matrices, we have the relationships

$$[d\sigma]^{*} = [T_A]\ [d\sigma] \tag{2.44}$$

and

$$[d\varepsilon]^{*} = [T_B]\ [d\varepsilon] \tag{2.45}$$

then we have

$$[d\sigma] = [T_A]^{-1}\ [d\sigma]^{*} \tag{2.46}$$

and

$$[d\varepsilon] = [T_B]^{-1}\ [d\varepsilon]^{*} \tag{2.47}$$

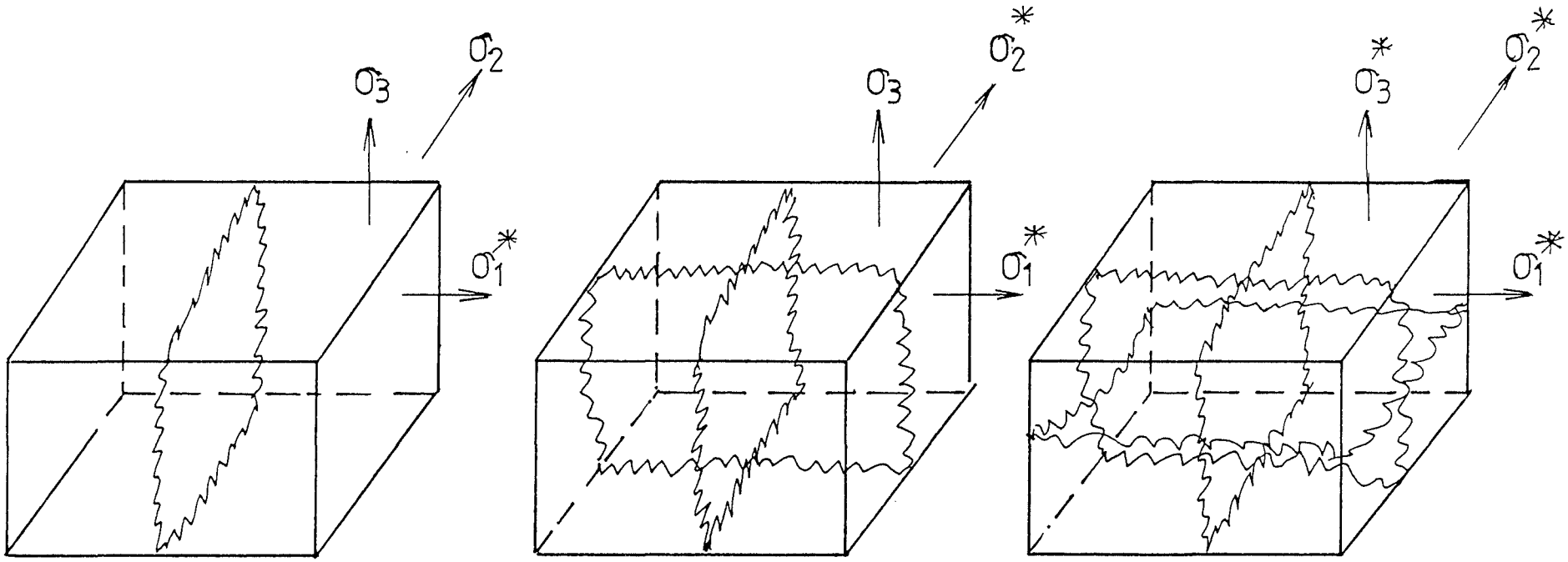

Fig. 2.2 CRACK DIRECTIONS IN ELEMENT

2.6 Failure Criterion in MARC

The Mohr-Coulomb failure criterion and concrete cracking model adopted by MARC are presented in this section. They are based on the MARC Finite Element System developed by MARC Analysis Research Corporation [192]

2.6.1 Mohr-Coulomb Model

In MARC analyses the Mohr-Coulomb yield criterion is applied to the concrete model while the reinforcement yield is represented by the Von Mises yield surface. A parabolic Mohr-Coulomb criterion is used for the concrete behaviour in which the hydrostatic dependence is generalized to give a yield envelope, which is parabolic in the case of plane strain (see Fig. 2.3)

The failure function is given by:-

$$f = (3 J_2 ; 3^{1/2} \xi fc I_1)^{1/2} - fc = 0 \qquad (2.48)$$

I_1 and J_1 are the invariants of stress tensor

η, ξ are cohesion constants

ϕ is the angle of friction of concrete

fc is the compressive strength of concrete

and constant ξ is related to fc and η as defined for the linear Mohr-Coulomb criterion by:

$$\xi fc = \eta / 3^{1/2}$$

where

$$\frac{3\eta}{(1-3\eta^2)^{1/2}} = \text{Sin}\,\phi \qquad (2.49)$$

and hence ζ can be related to the cohesion by

$$\zeta = \frac{\eta}{[3\ (3C^2 - \eta^2)]^{1/2}} \qquad (2.50)$$

where

$$C = \frac{fc}{3\ (1 - 12\eta^2)^{1/2}}$$

For calculation of the constant ζ see Appendix C

The kinematic hardening rule is applied in the analyses. It is assumed that under this rule, the Von Mises yield surface does not change in size or shape, but the centre of the yield surface can move in stress space. This condition is illustrated in Fig. 2.4.

The loading path for a uniaxial test in such conditions is shown in Fig. 2.5. This implies that the specimen is loaded as follows:- from stress free point 0 to initial yield point "a", "b" (loading), "c"(unloading), "b"(reloading), "d"(loading), "e" and "f"(unloading). In isotropic hardening, stress at "a" equals to the initial yield stress σ_x, and stress at "b" and "d" are higher than σ_x because of work hardening. On unloading the stress state can either remain elastic (point "c") or reach a subsequent yield point (point "e"). Under the kinematic hardening rule, the reverse occurs at a level $\theta_e = (\sigma_d - 2\sigma_x)$.

Elastic, elasto-plastic and plastic situations are included in the analyses. The plasticity computations are based on incremental plasticity theory using Prantl-Reuss stress-strain relations in a normality flow rule. The elasto-plastic material model allows for dissipation of energy. The plastic work is assumed to be irrecoverable and the model used also requires an incremental formulation. These conditions cause the elasto-plastic problem to be non-linear and the final solution to be path independent.

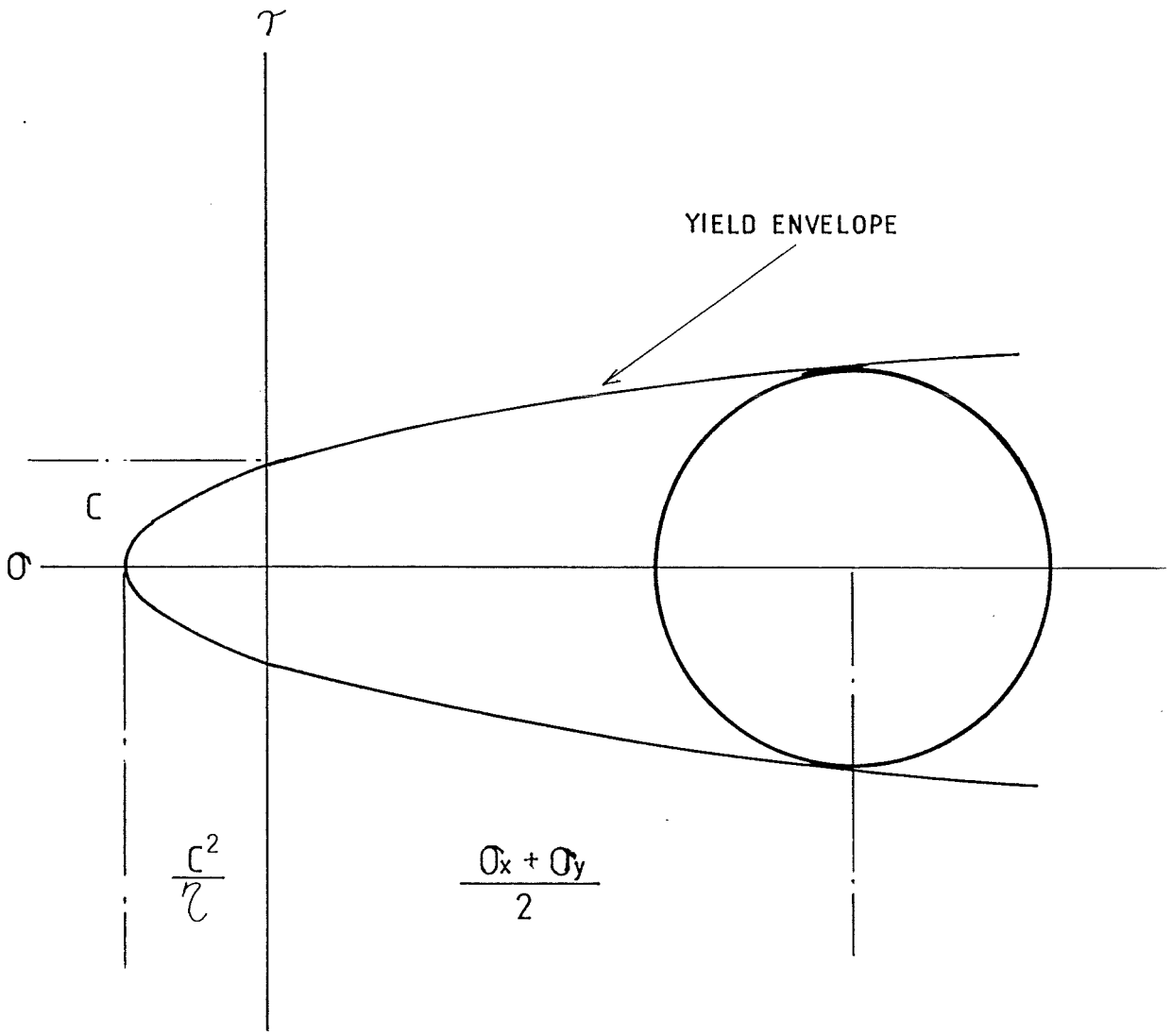

Fig. 2.3 PARABOLIC MOHR-COULOMB FAILURE SURFACE

REF. [192]

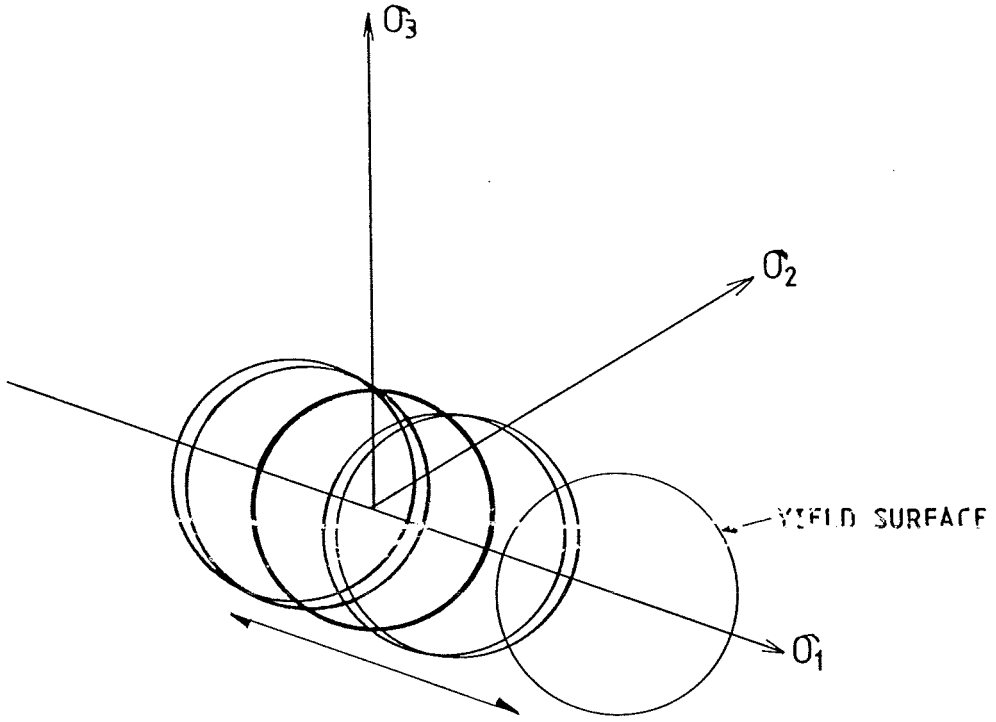

Fig. 2.4 VON MISES YIELD SURFACE

REF. [192]

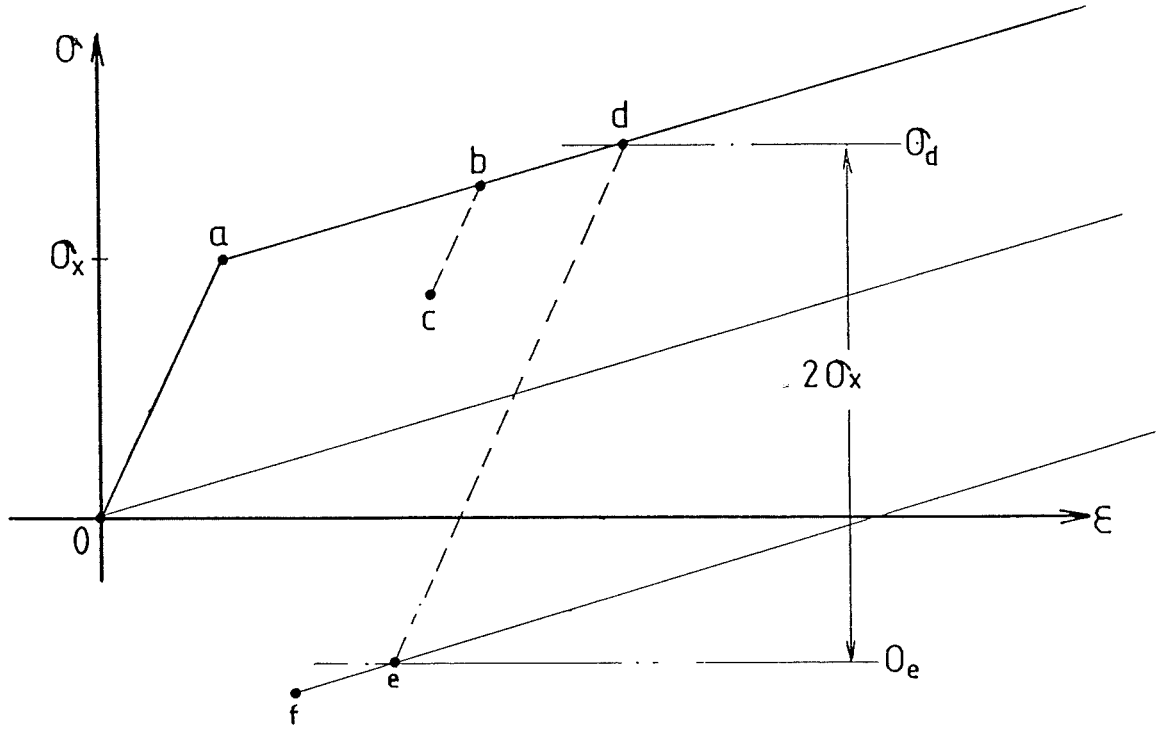

Fig. 2.5 LOADING PATH

REF. [192]

2.7 Concrete Cracking Model in MARC Analysis

2.7.1 Concrete Non-linear Behaviour Under Compression

Complex non-linearilities will take place if concrete is subjected to high enough compressive stress. Micro cracking and internal friction sliding are normally caused by these non-linear phenomena. The Mohr-Coulomb model, which is used for the MARC analyses, has been developed on the basis of plastic flow theories. The Mohr-Coulomb yield is quite suitable for this application since the deviatoric failure stress in concrete depends on the hydrostatic pressure.

2.7.2 Concrete Non-linear Behaviour Under Tension

In MARC it is assumed that if the tensile stress of concrete exceeds the maximum value of principal tensile stress, small cracks will form which will eventually join to form large cracks in the whole model. Crack growth is a brittle process and it is assumed that as soon as the crack has formed, the strength perpendicular to the crack becomes zero. It is assumed that plain concrete shows stable crack growth and a certain amount of ductility exists in concrete cracking. The stress perpendicular to the crack does not become zero immediately. Instead, it decreases gradually as a function of the opening, and hence the ductility is simulated. However for most calculations, it is assumed that the stress becomes zero immediately and satisfactory results can still be obtained [191]. This is due to the fact that crack propagation is made stable by reinforcement which appears in open cracks.

2.7.3 The Effects of Reinforcement

Apart from the behaviour of reinforcement, MARC also takes into account the pull-out effect which occurs when a high tensile stress exists in the reinforced concrete to cause cracking. In MARC the effect of tension stiffening is modelled together with a bond model for the pull-out effect.

2.7.4 Smeared Crack Constitutive Modelling

Cracking is also introduced in the MARC finite element analysis by assuming for cracks occurring in three directions. The cracking option is accessed through the CONSTITUTIVE option. The critical cracking stress, the modular of the linear strain softening behaviour, and the strain at which crushing occurs are necessary for input to the CRACKING option. Material properties such as Young's modulus and Poisson's ratio, are entered using the PROPERTY option.

In MARC a crack is considered to develop in a material perpendicular to the direction of the maximum stress as soon as the maximum principal stress in the material exceeds the ultimate tensile stress of the material. It is assumed that after an initial crack has formed, a second crack may form perpendicular to the first one. In the same way, a third crack may form perpendicular to the first two.

Once a crack is open, the applied loading may be reversed and the crack may close. When a crack is closed, an assumption is made that the crack has regained its full compressive stress and therefor its full load carrying capability. The shear stresses are considered to transmitted over the crack surface with respect to a reduced shear modulus.

Yield stress may occur in compression if the yield stress in that integration point exceeds the yield input. If the stress level continues to increase, crushing will eventually take place. In this case the material loses all its load carrying capacity at the integration point. The crushing surface is considered to have the same shape as the yield surface.

It is assumed that, in this smeared crack model, cracks form at the integration point of a specific element. A preferred crack direction can occur in an element with a particular volume. It is also assumed that once cracks have developed, plasticity and crushing may still occur.

The cracking strain, which indicates the opening of a discrete crack, is then defined as the difference between material strains

and element strains. The material strain indicates the strain of the model. It contains elastic and plastic components in general. Once cracks have developed, it is assumed that the material strains are no longer equal to the element strains.

2.7.5 Stress and Strain Calculation with Cracking

In MARC analysis, there are four different situations to be considered in the stress and strain calculation regarding cracking.

- If no cracks are present at a certain point during an increment, the standard plasticity relations will be applied.

- If there is any crack during the current increment and it is still open at the end of that increment, the change in crack must be calculated.

- If there are cracks that open or reopen during an increment, the stresses normal to the crack will be set to zero. A tension softening behaviour is also required to be specified in the crack directions.

- If there are cracks close during an increment, the crack strains are set to zero.

2.7.6 Iterative Procedure and Convergence Testing

In the MARC analysis, Newton Raphson iteration is used. It is assumed that the last obtained solution will always be used as a starting point for an iteration. In the cracking routines, an estimated strain increment will be used in the first assembly. Perfect healing will also be assumed if a crack has opened in the current increment and closed during the iteration. However no healing will be given if a crack has opened in the previous increment and closed during the current iteration. The crack direction will only be stored permanently if there is no healing. The general iteration procedure is as follows:-

(a) New increments of stresses are added to previous stresses as:-

$$[d\sigma_i^*] = [D]\,[d\varepsilon]$$

$$\sigma_i^* = \sigma_{i-1} + d\sigma_i^*$$

(b) Stresses existing normal to cracks or crushing stress σ_{CR} are released from the new stresses σ_i^* using:-

$$\sigma_i^R = \sigma_i^* - \sigma_{CR}$$

where σ_i^R are the released stresses

(c) Stress that cannot be supported or resisted will be computed as

$$\sigma_R = \sigma_i - \sigma_i^R = \sigma_i - \sigma_i^* + \sigma_{CR}$$

The rest of the procedure is the same as given in the general formulation under NONSAP in Section 2.

CHAPTER 3

FINITE ELEMENT ANALYSIS

3.1 General Finite Element Formulation

Isoparametric elements have been used throughout the whole of this analysis, and the displacement interpolation functions are assumed to be the same as the shape interpolation functions. Therefore the number of displacement coordinates must equal the number of shape function coordinates.

In NONSAP analyses, 20-noded isoparametric brick elements are used while in the MARC analyses, 20-noded, isoparametric brick elements and 20-noded rebar elements are used. For full details of the analyses see CHAPTER 5 - Impact Analysis.

3.1.1 Shape Function

The shape of these isoparametric elements is expressed in terms of interpolation functions and its nodal coordinates in the global system can be expressed as:-

$$X = \sum_{i=1}^{n} F_i(r,s,t)X_i \qquad (3.1)$$

$$Y = \sum_{i=1}^{n} F_i(r,s,t)Y_i \qquad (3.2)$$

$$Z = \sum_{i=1}^{n} F_i(r,s,t)Z_i \qquad (3.3)$$

where $F_i(r,s,t)$, $i = 1$ to n, are the interpolation functions in the curvilinear coordinates r, s, and t. X, Y, Z are the global coordinates and X_i, Y_i and Z_i are the local coordinates. (See Fig. 3.1)

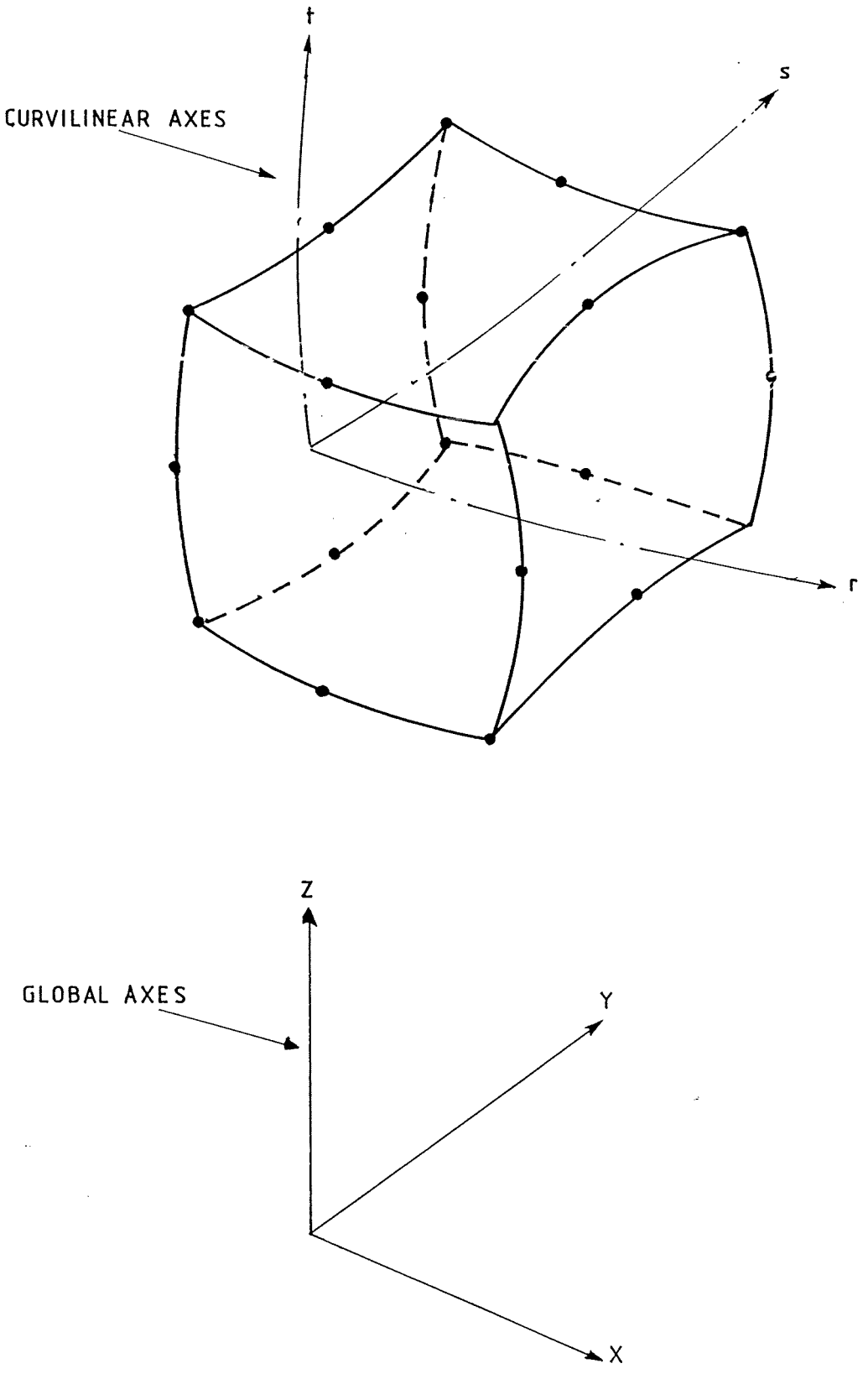

Fig. 3.1 20-NODED SOLID ELEMENT

3.1.2 Displacement Functions

In the same way as the global coordinate development, if the displacement functions for the solid element are U, V and W, where U, V and W are the displacements in the global X, Y and Z-directions respectively. The displacement functions are expressed as:-

$$U = \sum_{i=1}^{n} F_i(r,s,t)U_i \tag{3.4}$$

$$V = \sum_{i=1}^{n} F_i(r,s,t)V_i \tag{3.5}$$

$$W = \sum_{i=1}^{n} F_i(r,s,t)W_i \tag{3.6}$$

where U_i, V_i and W_i are the nodal displacements in the X, Y and Z directions at node i.

3.1.3 Strain-Displacement Relationship, Derivative Transformation and The Jacobian Matrix

If the total strain field $[\varepsilon_T]$ is given by

$$[\varepsilon_T] = [\varepsilon_x, \varepsilon_y, \varepsilon_z, \varepsilon_{xy}, \varepsilon_{yz}, \varepsilon_{zx}] \tag{3.7}$$

the strain displacement relation can be expressed as:-

$$[\varepsilon_T] = [T_B][S_T] \tag{3.8}$$

where the element deformation variable matrix,

$$[S_T] = [U_1V_1W_1, U_2V_2W_2, \ldots\ldots U_iV_iW_i, \ldots\ldots U_nV_nW_n] \tag{3.9}$$

And the transformation matrix, $[T_g]$ and the Jacobian matrix, $[J]$ are defined as:-

$$[T_{Bi}(r,s,t)] = \begin{bmatrix} \frac{dF_i}{dX} & 0 & 0 \\ 0 & \frac{dF_i}{dY} & 0 \\ 0 & 0 & \frac{dF_i}{dZ} \\ \frac{dF_i}{dY} & \frac{dF_i}{dX} & 0 \\ 0 & \frac{dF_i}{dZ} & \frac{dF_i}{dY} \\ \frac{dF_i}{dZ} & 0 & \frac{dF_i}{dX} \end{bmatrix} \qquad (3.10)$$

$$[J] = \begin{bmatrix} \frac{dX}{dr} & \frac{dY}{dr} & \frac{dZ}{dr} \\ \frac{dX}{ds} & \frac{dY}{ds} & \frac{dZ}{ds} \\ \frac{dX}{dt} & \frac{dY}{dt} & \frac{dZ}{dt} \end{bmatrix} \qquad (3.11)$$

3.1.4 Stress Calculation and The Element Stiffness Matrix

The stress at any point within the element

$$[\sigma] = [D]\,[\{\varepsilon\} - \{\varepsilon_0\}] + [\sigma_0] \tag{3.12}$$

in which

$$[\sigma_{6x1}] = [\sigma_x, \sigma_y, \sigma_z, \sigma_{xy}, \sigma_{yz}, \sigma_{zx},] \tag{3.13}$$

$$[\varepsilon_{0_{6x1}}] = [\varepsilon_{x0}, \varepsilon_{y0}, \varepsilon_{z0}, 0, 0, 0] \tag{3.14}$$

Here σ_0 and ε_0 are the initial stresses and strains. From the constitutive relationship for stress and strain, we have

$$[\sigma] = [D]\,[\varepsilon] \tag{3.15}$$

but with the initial stresses and strains involved Equation (3.15) becomes

$$[\sigma] = [D]\,[\{\varepsilon\} - \{\varepsilon_0\}] + [\sigma_0] \tag{3.16}$$

Now by the principle of virtual work, considering imposing a virtual displacement of U_v on the element, the internal work done "Uw" by the stresses is made equal to the external work by the applied loads. We have

$$Uw = \int_v [\varepsilon]^T [\sigma] dV = \int_v [U_v]^T [T_B(r,s,t)]^T [\sigma] dV \qquad (3.17)$$

Applying the external work done, the element stiffness matrix becomes:-

$$[K] = \int_{-1}^{+1}\int_{-1}^{+1}\int_{-1}^{+1} [T_B(r,s,t)]^T [D] [T_B(r,s,t)] \, detJ \, dr \, ds \, dt \qquad (3.18)$$

where detJ is the determinant of the Jacobian matrix of Equation (3.11)

3.2 Elasto-plasticity

When the impact force is great enough to cause the concrete to pass its elastic limit, plasticity will occur, but before the plasticity stage is reached, the material enters an elasto-plastic stage. Elasto-plastic behaviour is characterized by an initial elastic material response, after which a plastic deformation is superimposed when a certain level of stress is reached. Plastic deformation is taken as irreversible on unloading and is incompressible in nature. The onset of plastic deformation is then governed by a yield criterion and post-yield deformation normally takes place at a largely reduced material stiffness. The situation is complicated by the fact that different classes of materials exhibit different elasto-plastic characteristics.

The famous Prantl-Reuss normality flow rule is applied to both the NONSAP and MARC analyses and the elasto-plastic matrix is given by a standard formulation as:-

$$[D_{ep}] = [D_e] - \frac{[D_e]\left[\frac{df}{d\sigma_{ij}}\right]\left[\frac{df}{d\sigma_{ij}}\right]^T[D_e]}{H + \left[\frac{df}{d\sigma_{ij}}\right]^T[D_e]\left[\frac{df}{d\sigma_{ij}}\right]} \qquad (3.19)$$

where $[D_e]$ is the elastic material matrix

$[D_{ep}]$ is the elasto-plastic material matrix and

H is the material hardening factor

3.2.1 MARC Plasticity Solution Procedures and Algorithms

The following plasticity solution procedures and algorithms are based on reference [192]. Based on the incremental strain prediction, a mid-increment state is found for each integration point and this prediction is based on the strain increment for the preceding increment. The elasto-plastic response is established by using the mean normal method which calculates a secant stiffness at each increment. Recycle will only take place if the displacement at the end of the increment does not satisfy the chosen tolerance. During recycling the strains recovered from the previous iterations are now used as estimated strains for the stiffness evaluation.

3.3 Dynamic Analysis

Unlike the other loadings, impact loads due to missiles affect not only the modelling but also the layout of the finite element analysis. The constitutive laws could include strain-rate dependency of the material properties and provisions for large deformations, slide lines and re-zoning.

As mentioned by Cook [183], a structural problem has to be considered dynamically when the induced frequency is more than 1/3 of the lowest natural frequency of vibration of the structure. If the forces are time dependent, the problem becomes dynamic and the inertia, velocity and acceleration must be taken into consideration.

In the impact load case, which has one distinct time maximum only, hysteresis damping, damping due to friction and energy migration to the surrounding matter can be neglected and hence is not taken into account in the finite element analysis.

The equation of motion is written as:-

$$[M]\,[a] + [K]\,[z] = [R] \tag{3.20}$$

where [M] is the mass matrix

[K] is the stiffness matrix

[R] is the external force matrix

[a] is the nodal acceleration matrix

[z] is the nodal displacement matrix

In the first approximation it can be assumed that this equation is valid over a finite domain dts, hence Equation (3.20) can be written as:-

$$[M]\,d[a] + [K]\,d[z] = d[R] \tag{3.21}$$

By introducing a recurrance algorithm, for Newmark integration we have

$$\left\{4[M]/dts^2 + [K]\right\} d[z] = d[R] + \left\{4[M]/dts\right\}[V]^n + 2[M][V]^n \tag{3.22}$$

where [v] is the nodal velocity matrix

dts is the time step increment

In this procedure the incremental dynamic equilibrium equations are satisfied approximately. Hence the error in each increment will accumulate and the solution may degenerate. Newmark integration is an implicit operator, the stiffness matrix is present in the operator matrix so the non-linearity of the matrix requires a reassembly and solution of the operator matrix for every time step.

3.3.1 Mass Matrix

A consistent mass matrix is used in both the NONSAP and MARC analyses. A consistent mass matrix which has the same bandwidth as the stiffness matrix has been recommended by Zienkiewicz [184], Owen and Hinton [185] and Holland and Bell [186]. The equation gives:-

$$[M] = \int [F]^T \rho [F]\, dV \tag{3.23}$$

[F] is the interpolation function matrix

ρ is the density of the material

3.3.2 Numerical Damping

In the MARC analysis, numerical damping is used to damp out the modes which are excited during the transient analysis because of the value of the time step.

The idea is based on the structural damping model. The excitation frequency is exchanged by the time step frequency. If the time step is ts then the damping matrix is

$$[Cd] = \gamma \; ts \; [K]/\pi \tag{3.24}$$

In the time domain, at node i

$$ts_i = 2\pi/\omega i \tag{3.25}$$

where γ is the numerical damping factor

ωi is the eigen frequency for mode i

With this damping matrix Equation (3.22) becomes

$$\left\{4[M]/dts^2 + 2[Cd]/dts + [K]\right\} d[z] = d[R] + \left\{4[M]/dts + 2[Cd]\right\} [V]^n + 2[M][V]^n \tag{3.26}$$

The procedures for the material matrix [D] and cracking criteria in CHAPTER 2 are then linked at this stage with the dynamic analysis. The procedures can be shown in the following flowcharts (Tables 3.2a and 3.2b)

Table 3.2a Dynamic Finite Element Calculation Procedures

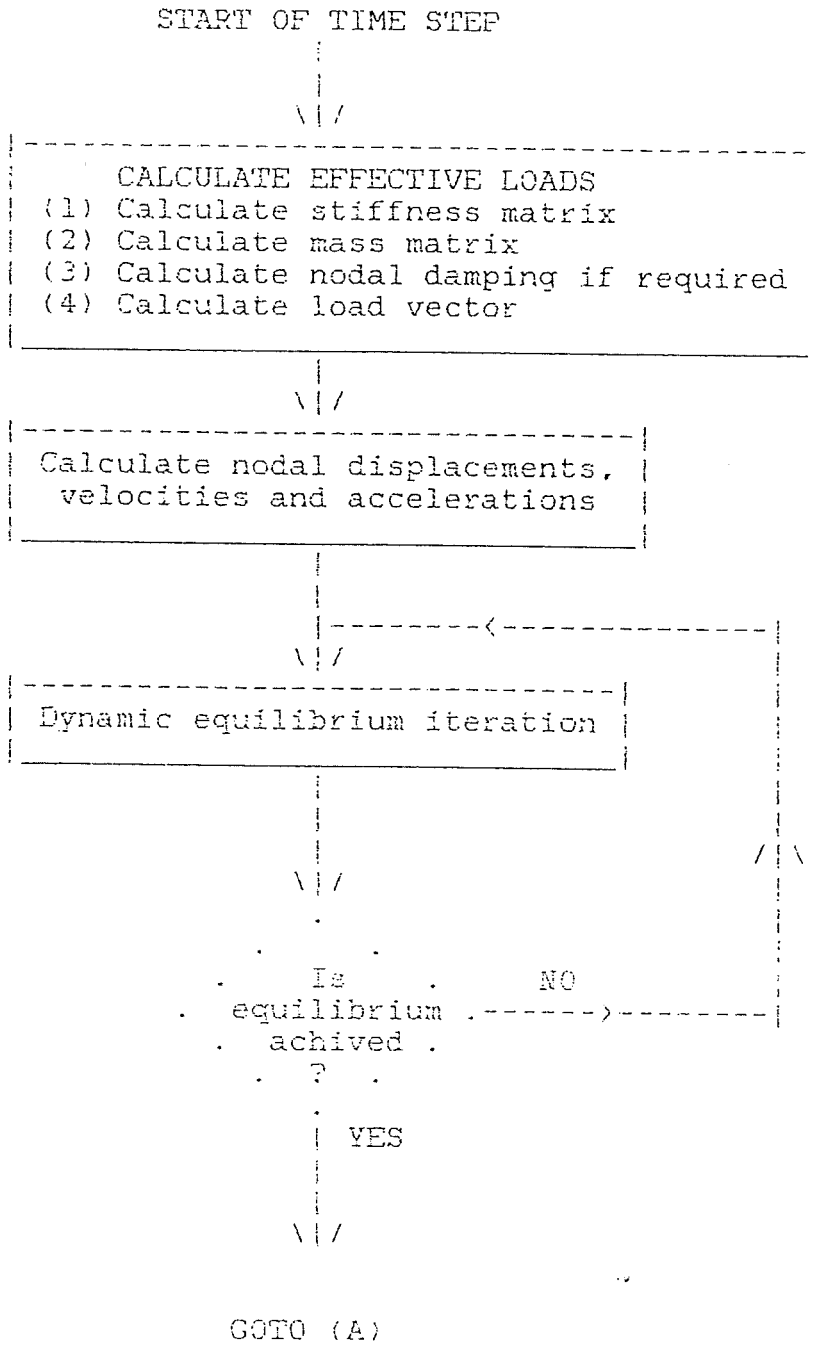

Table 3.2b Dynamic Finite Element Calculation Procedures (Con't)

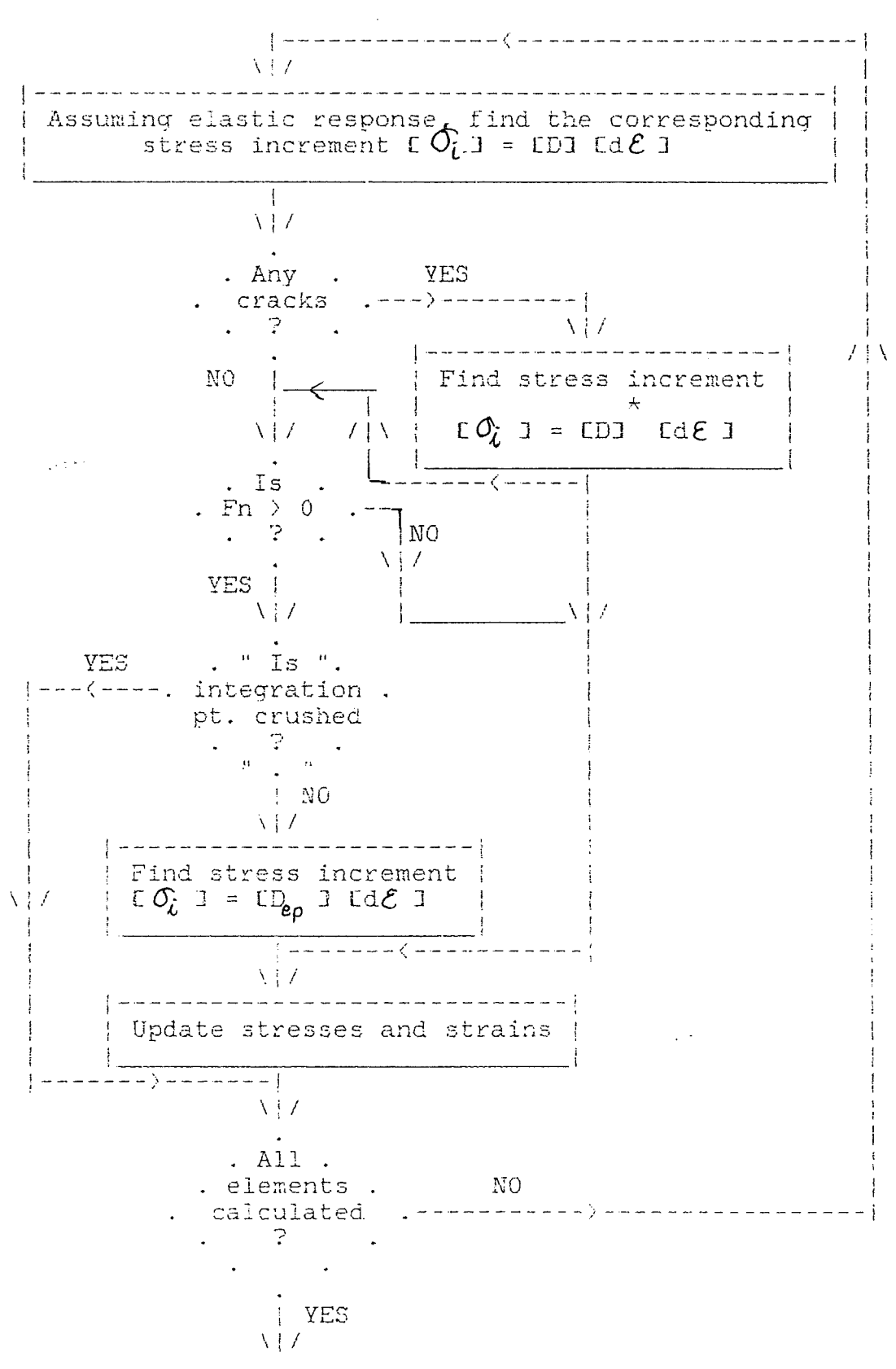

CHAPTER 4

EXPERIMENTAL TEST RESULTS ON CONCRETE SLABS

4.1 Concrete Slabs Subjected to Impact - A General Introduction

When a reinforced concrete slab is subjected to a missile impact, one or a more of the following phenomena can occur

(a) no damage
(b) cracking
(c) penetration
(d) perforation
(e) spalling
(f) scabbing

Fig. 4.1 shows the general missile impact phenomena for concrete targets. The target damage characteristics can also be defined in detail on the lines shown in Fig. 4.2

Perforation is treated as full penetration.The missile passes through the target with or without exit velocity. In some cases, flexural or shear failure may occur if the strain energy capacity of the slab does not exceed the kinetic input to the slab by the missile impact. Normally, with very low velocities, the missile will bounce off after striking the target without causing any local damage. As the velocity increases, cracks may form at the front face of the target and this may be followed by pieces of concrete being spalled off the front face of the target. A crater which normally extends over a substantially larger cross-sectional area of the missile may be formed at this stage. Sometimes cracking occurs at back face even without spalling taking place. If the velocity continues to increase, penetration will take place to depths beyond the crater depth, and a penetration hole will be formed with a diameter only slightly larger than the missile diameter. The missile will stick to the target instead of rebounding if the penetration depth increases. If even higher velocity is induced, cracking of concrete on the back face will then be followed by scabbing, which is the peeling off of pieces of concrete from the

back face. The zone of scabbing is normally much wider but not as deep as the crater at the front face. The penetration depth will increase drastically, once scabbing begins. Penetration will occur if there is a further increase in velocity.

If the missile diameter is large compared to the target thickness, only a small amount of impact energy is needed for local damage to take place. However if there is no perforation during the impact, most of the kinetic energy will be converted to strain energy.

Above a certain velocity, a truncated cone shaped shear plug will be formed. The plug will be displaced more and more for increasing velocity. It is shown experimentally [28, 30] that the reinforcement in the concrete slab does help preventing the slab from being perforated completely.

4.2 Experimental Investigations of Reinforced Concrete Slabs

The experiments mentioned in this chapter have been carried out at United Kingdom Energy Authority (UKAEA), Winfrith. These experimental results are also confirmed by Kraftwerke Union in Germany.

4.2.1 Experimental Equipment

To achieve impact velocity up to 300 m/s with missiles of a given weight, a compressed air launcher has been constructed as in Fig. 4.3. Firing of primary and secondary missiles are remotely controlled. The launcher has a 150mm bore barrel which projects missiles with an energy up to 1MJ. Over 100 signal channel pairs are used to feed transient data to recording equiment. The basic support structure in a corridor 2.4m wide with 750mm thick walls. Two horizontal steel I-beams with connecting plates are bolted to the concrete walls using a total number of 50 embedded wall bolts. In this way the impact loads are transported easily to the wall by shear forces created on these bolts. Some experiments use an alternative system, which has massive concrete blocks weighing 35 tonne which are supported on the building wall. In order to handle the target and supported structure, a 5 tonne railed hoist is used.

Up to five high speed (3038 m/s) cameras are used which monitor missile velocity, the zone of impact and the overall target behaviour. The impact velocity is measured by timing the interruption of 10 light beams across the missile flight path. A multi-channel timer gives these intervals directly. A number of points from the target and supporting structure displacements are measured. Two types of transducer are employed: a commercial type using deflection, and a potentiometer type developed by UKAEA, Winfrith. The transient load transmitted by the target, such as given in Fig. 4.4, has been measured using load cells of chain gauged steel cylinders. The load of the deformable missile can therefore be measured. Fig. 4.3b shows a soft missile in aluminium alloy. The steel impact anvil in Fig. 4.3a supported by a piezo-electric load cell is used. The transient data are normally recorded on one or two high speed (78 mm/s, 8Hz band width) tape recorders of 42 channel each. A 1 KHz standard is recorded on both tapes and films to standardize timing. Fig. 4.5 shows a collapsing steel tube missile type 11, which was used for tests M126 and M289 which are analysed in the current research.

4.2.2 Concrete Target

Recent impact experiments have shown good coorespondence in a scale of 1:5.6 to a prototype concrete slab subjected to a deformable missile load.

Two target slabs (B16 and B26) are chosen as typical examples from the test results of M126 and M289 as shown in Figs. 4.6 and 4.7. The details of panel instrumentation are given in Figs. 4.8. and 4.9. The results of tests M126 and M289 are given in Tables 4.1 and 4.2 respectively. This data is used as input in the computer analyses.

In these chosen square slab targets, 12 load cells were fixed at one edge of target B16 (test M126) and 3 were fixed at one edge of target, B26 (test M289). 8 displacement transducers were located at the centre of both of the targets. For the location details see Figs. 4.8 and 4.9. The load cells were fixed to a concrete abutment weighing some 37 tonnes, and the abutment was connected to a building structure, weighing some thousands of tonnes, through intervening layers of sandbags.

4.2.3 Load from Deformable Missiles

A number of experiments have been conducted in which missiles have been released at various velocities ranging from 170 m/s to 247 m/s. Load cells were used to measure the load imposed by the target onto the abutment during the impact process. Loading functions were measured in all the tests. A typical load-time function graph is given in Fig. 4.10.

4.2.4 Target Response

The target slabs shown in Figs. 4.6 and 4.7 have already been described above. Transducers were attached to the rear of the targets. Displacement-time graphs for test M126 and M289 are given in Figs. 4.11 to 4.22. Figs. 4.23 and 4.24 show the deformed missiles after tests of M216 and M289 following impact loads and velocities.

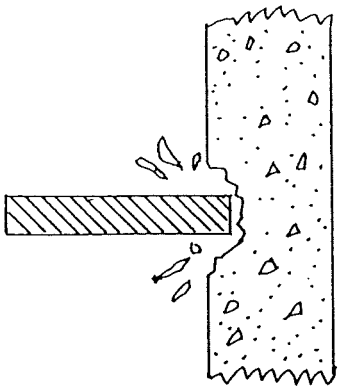

PENETRATION AND SPALLING

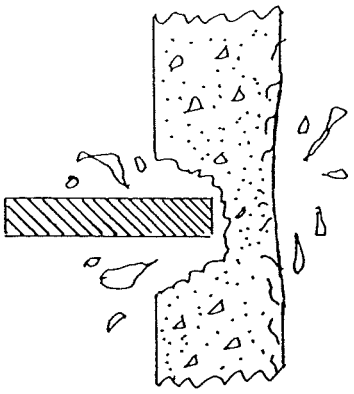

SPALLING AND SCABBING

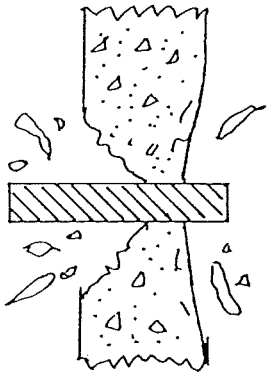

PERFORATION

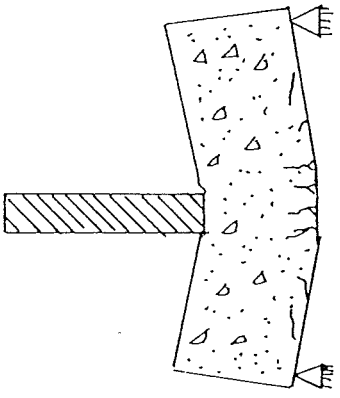

OVERALL TARGET RESPONSE

Fig. 4.1 MISSILE IMPACT PHENOMENA

REF. [111]

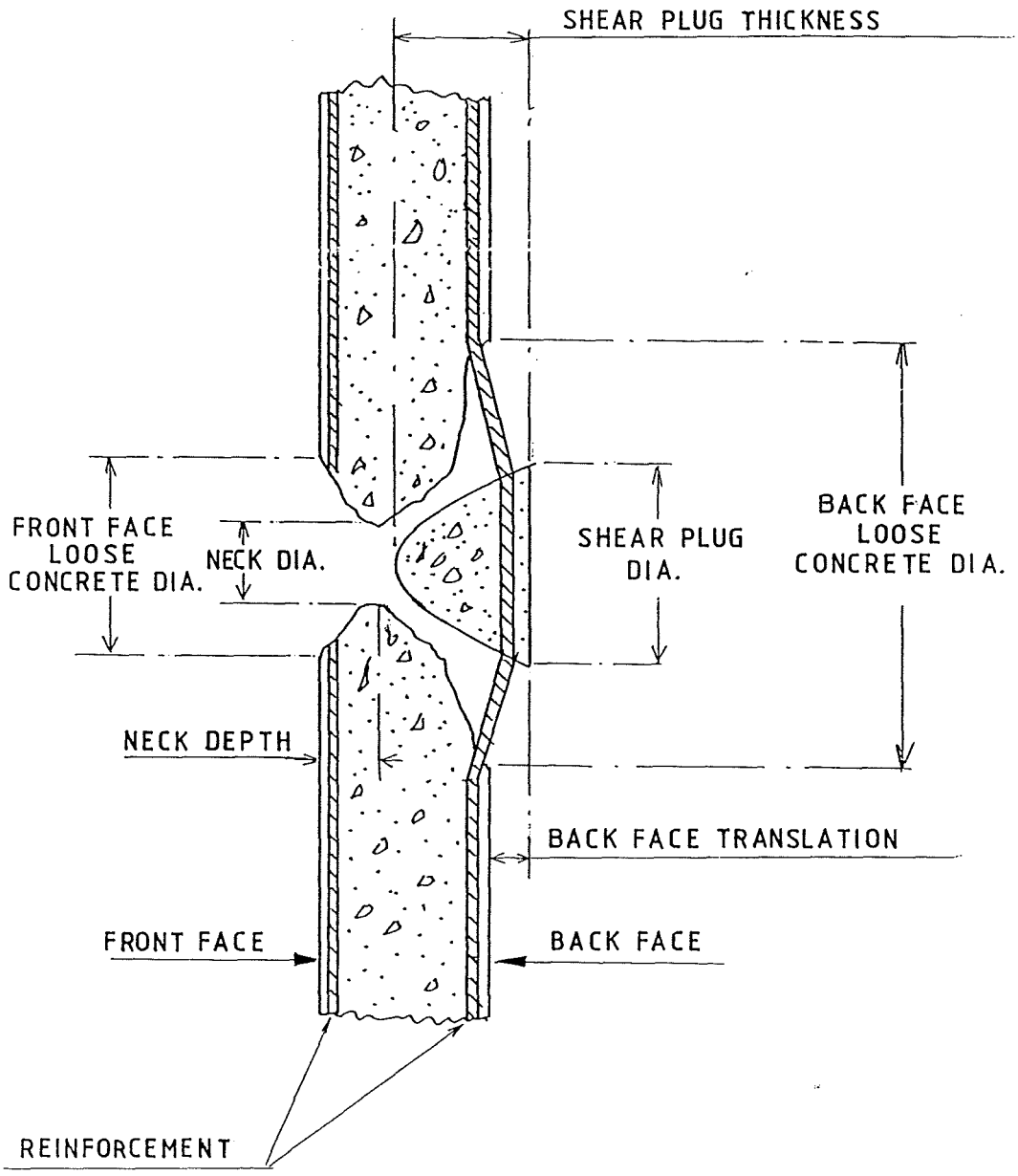

Fig. 4.2 DAMAGE CHARACTERISTICS OF A TARGET

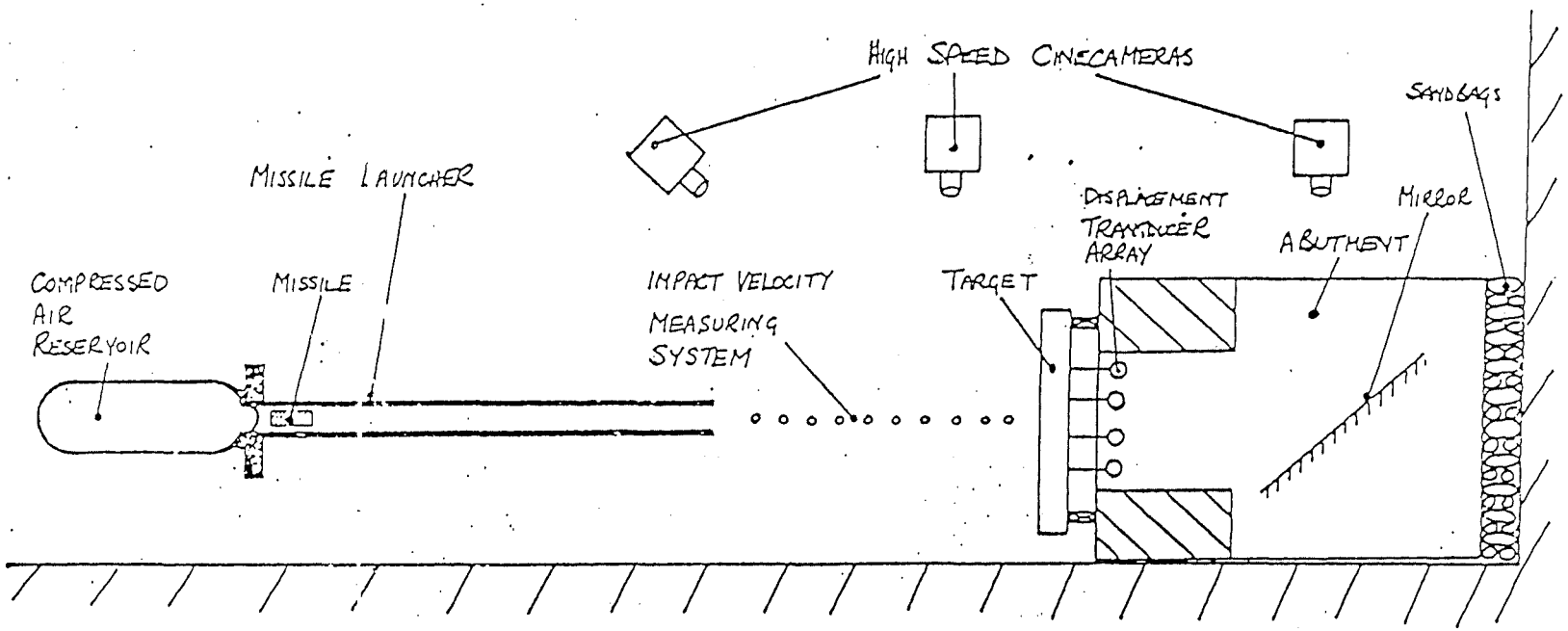

Fig. 4.3 SCHMATIC OF MISSIL LAUNCHER LABORATORY

(WITH COMPLEMENT OF UKAEA, WINFRITH) REF. [28-31]

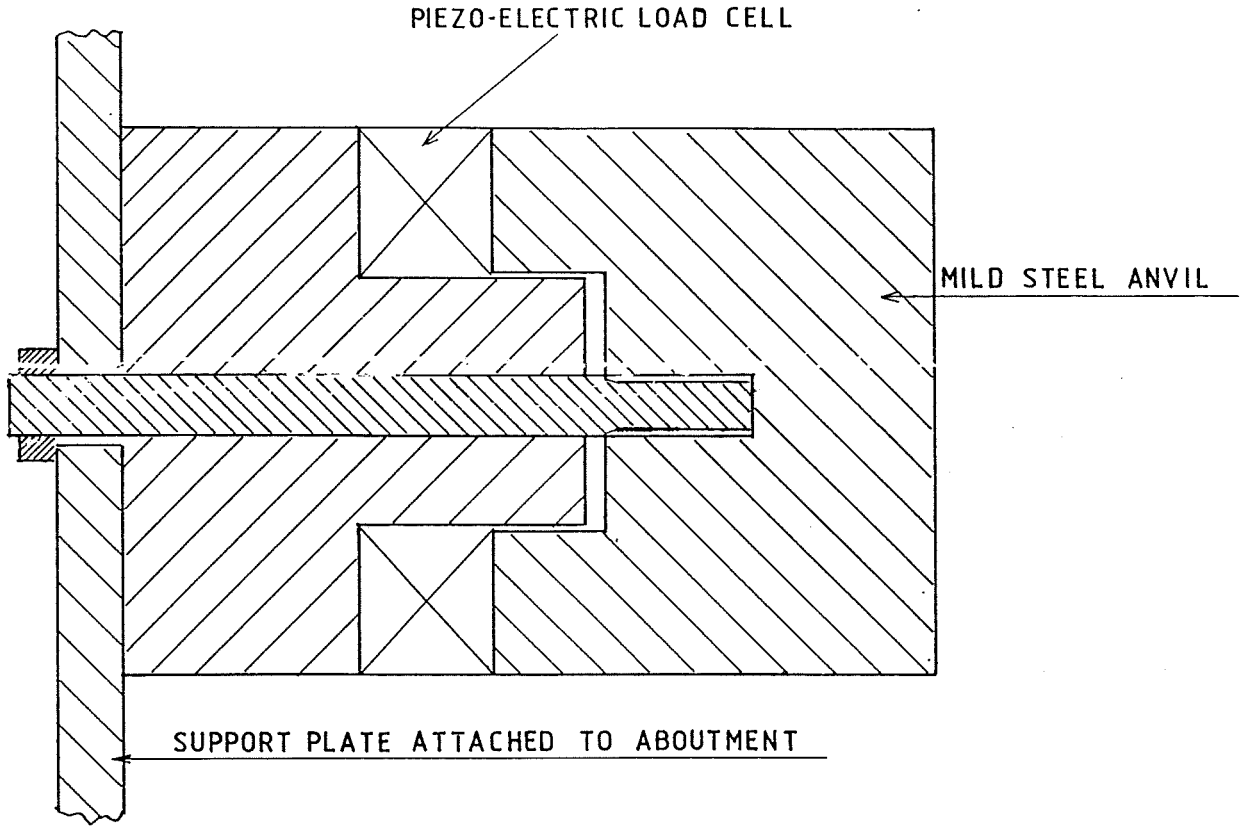

Fig. 4.3a STEEL ANVIL AND LOAD CELL FOR MEASURING IMPOSED LOADS OF SOFT MISSILES

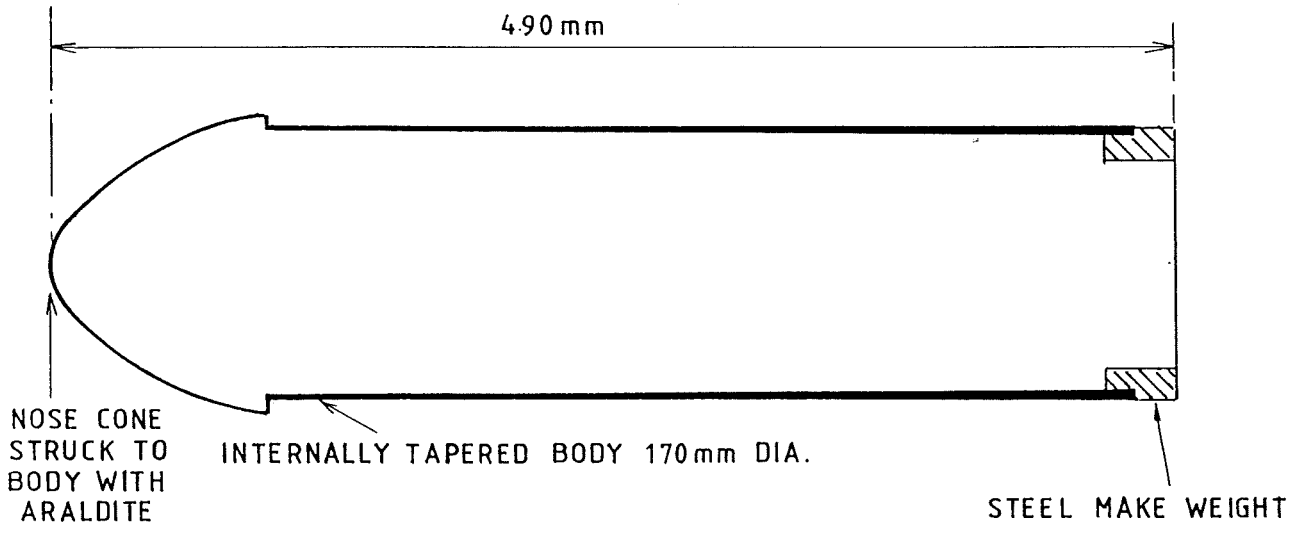

Fig. 4.3b SOFT MISSILE IN ALUMINIUM ALLOY

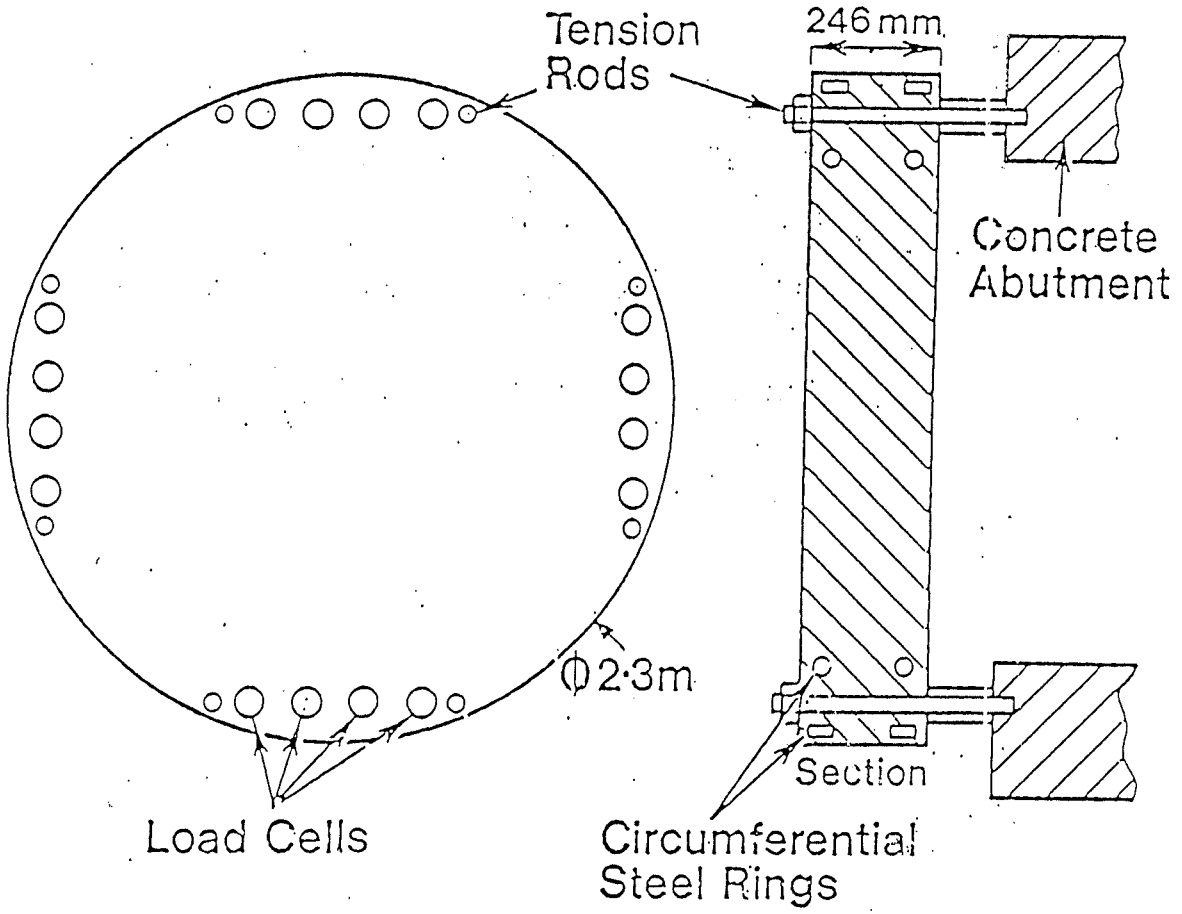

Fig. 4.4 SCHEMATIC OF A CIRCULAR CONCRETE TARGET

(WITH COMPLEMENT OF UKAEA, WINFRITH) REF. [28-31]

NOTE:- ALL DIMENSIONS IN MM

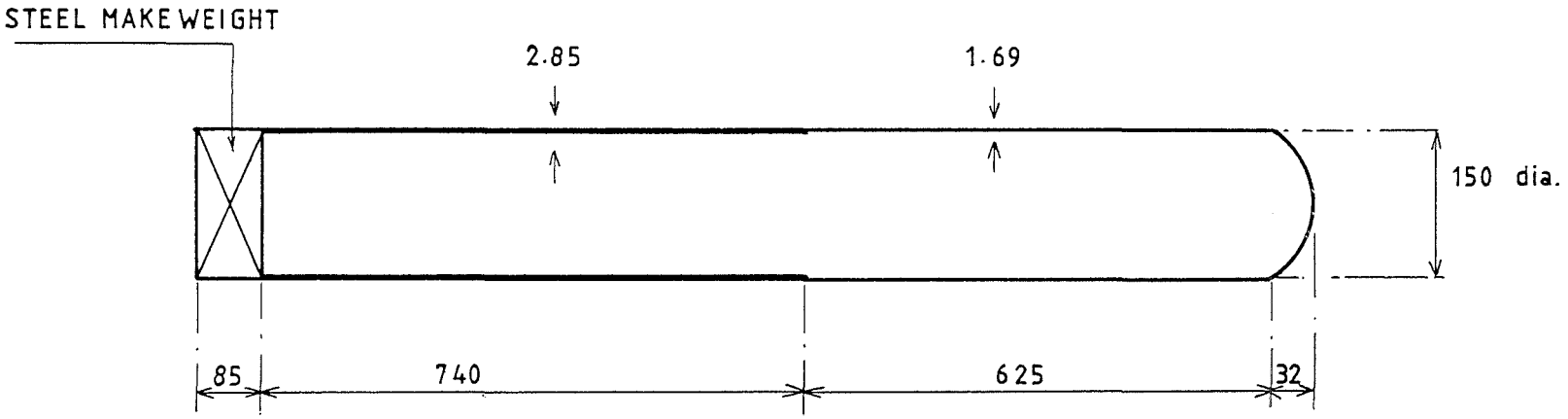

Fig. 4.5 DIMENSIONS OF SOFT MISSILES TYPE 12-USED FOR TESTS M126 AND M289

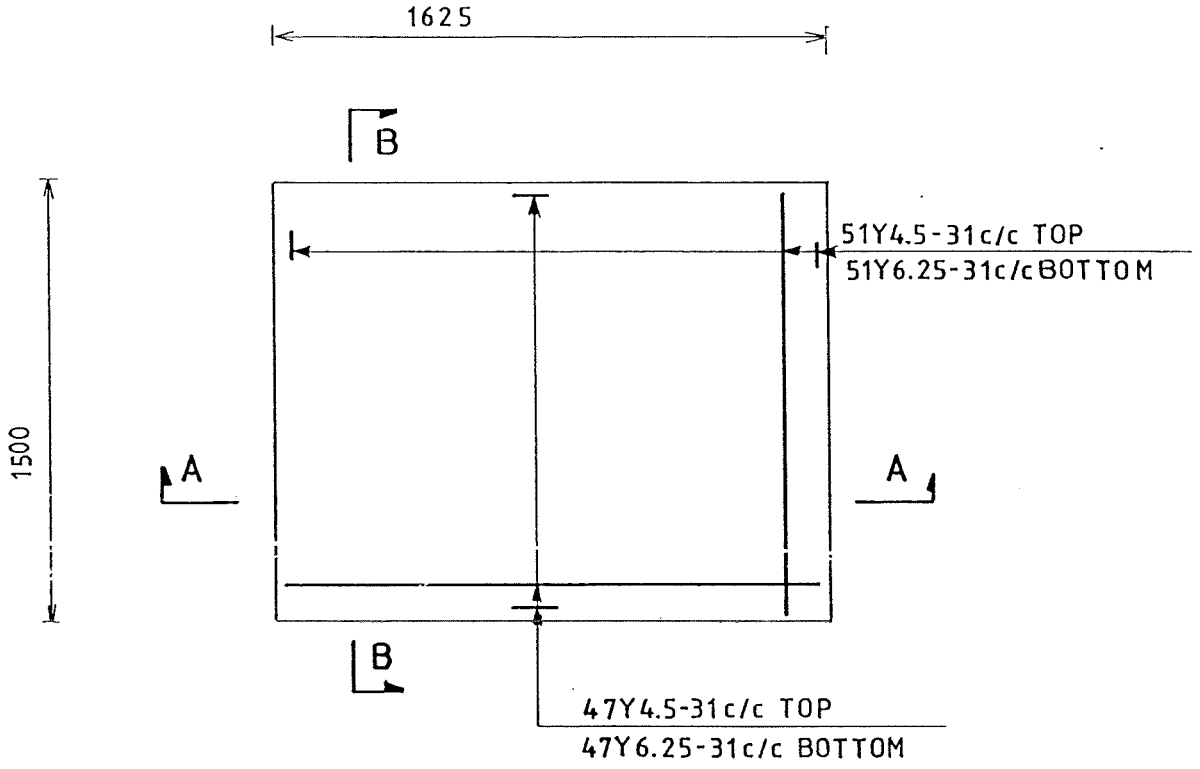

PLAN

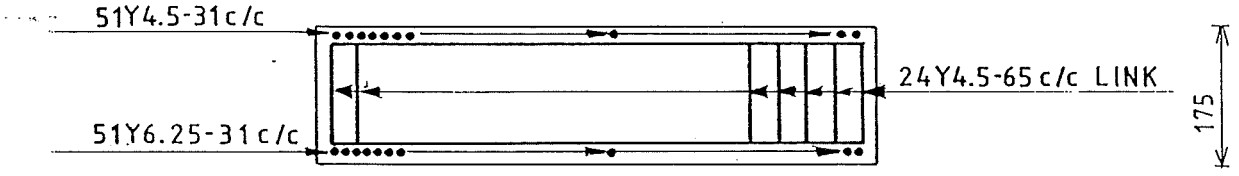

SECTION AA

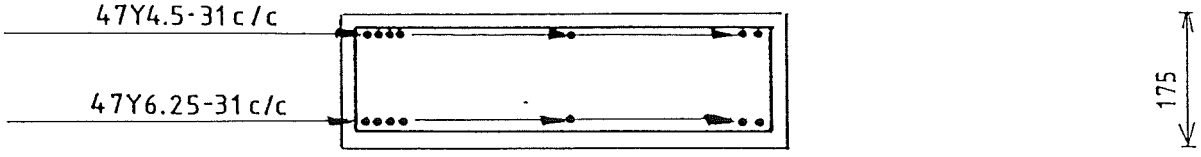

SECTION BB

NOTE:- All DIMENSIONS IN MM

Fig.4.6 R.C. DETAIL OF TARGET SLAB B16

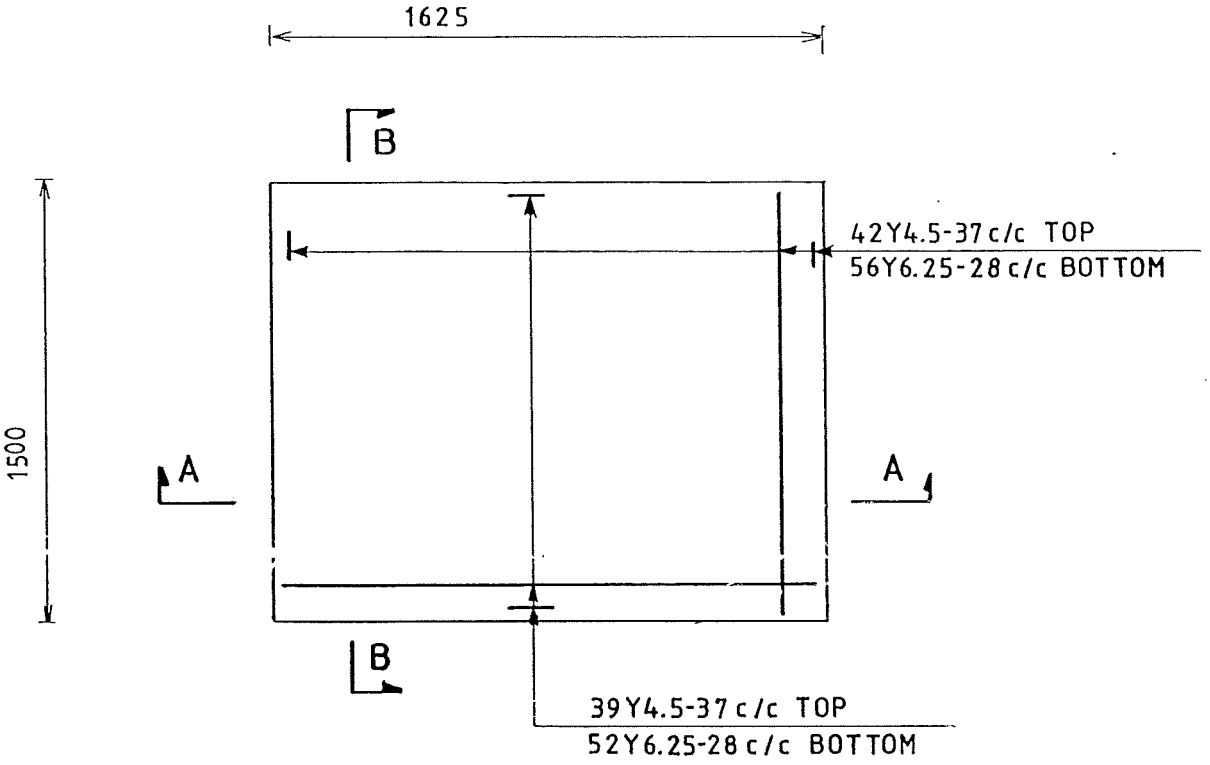

PLAN

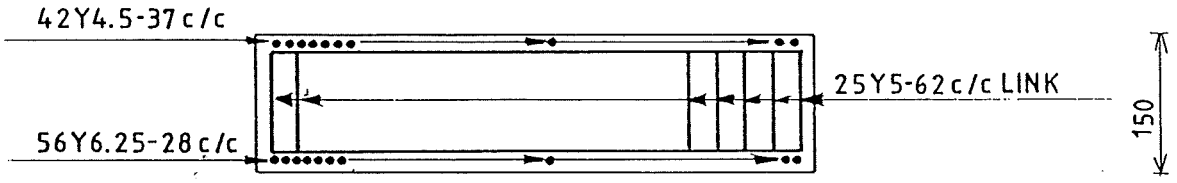

SECTION AA

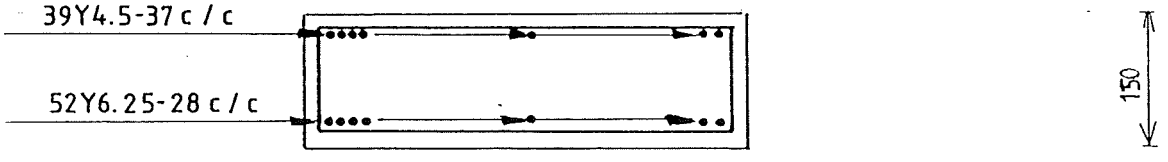

SECTION BB

NOTE:- All DIMENSIONS IN MM

Fig. 4.7 R.C. DETAIL OF TARGET SLAB B26

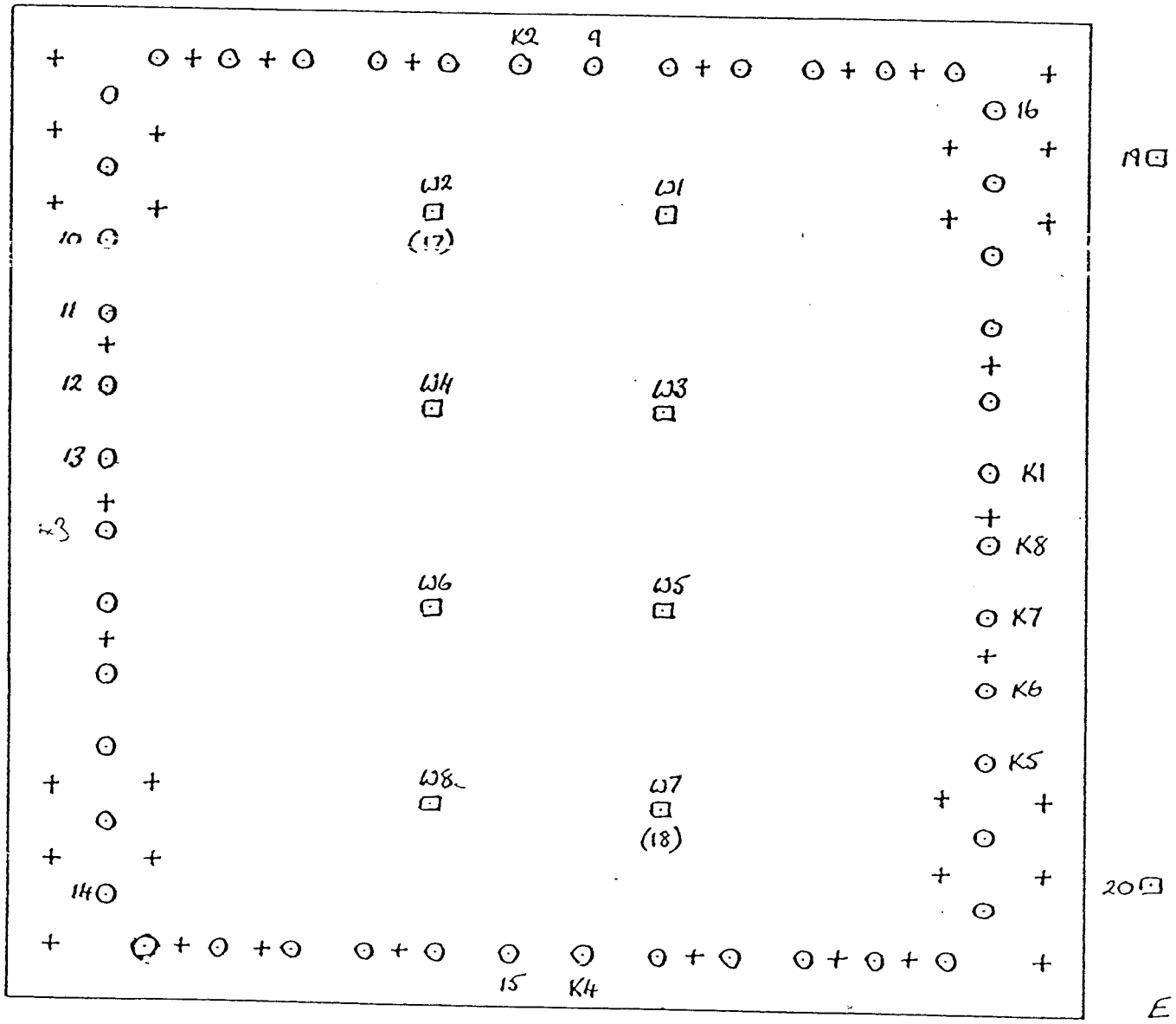

○ LOAD CELLS □ DISPLACEMENT TRANSDUCERS

\+ TIE RODS

LOCATIONS 17, 18 ARE ON THE FRONT (IMPACT) FACE OF THE PANEL

LOCATIONS 19 - 22 MEASURE ABUTMENT DISPLACEMENTS

Fig. 4.8 INSTRUMENTATION OF TARGET B16

(WITH COMPLEMENT OF UKAEA, WINFRITH)

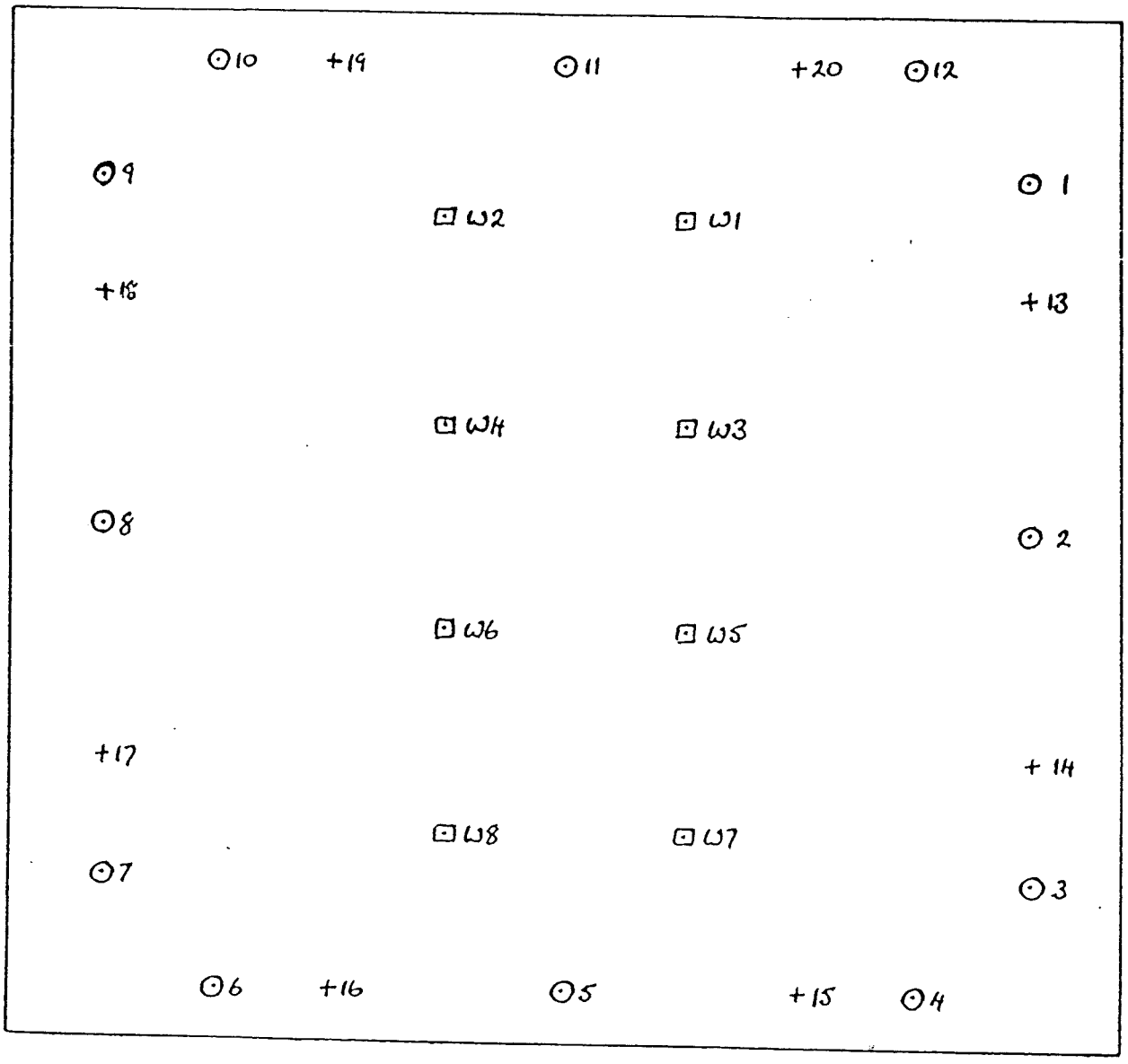

⊙ Load Cells ⊡ Displacement Transducers
\+ Tie Rods

Fig. 4.9 INSTRUMENTATION OF TARGET B26

(WITH COMPLEMENT OF UKAEA, WINFRITH)

EXPERIMENT, FILE NO. 1 M118 002 010880 00 3 CL

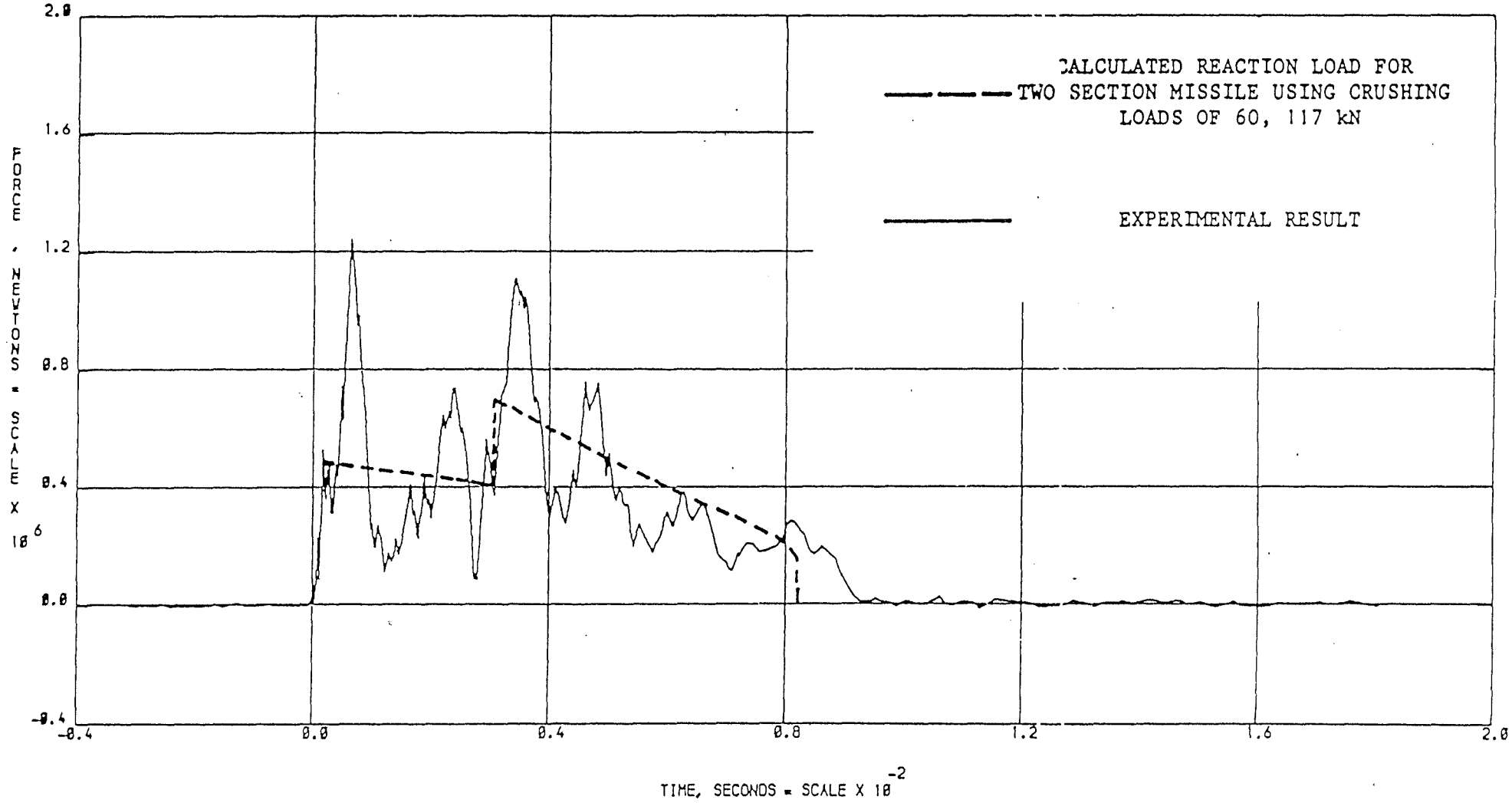

Fig. 4.10 LOAD-TIME FUNCTION FOR TYPE 11 MISSILE LOAD AT 236 M/S IMPACT
(WITH COMPLEMENT OF UKAEA, WINFRITH)

EXPERIMENT, FILE NO. 1 M126 007 171180 02 '1

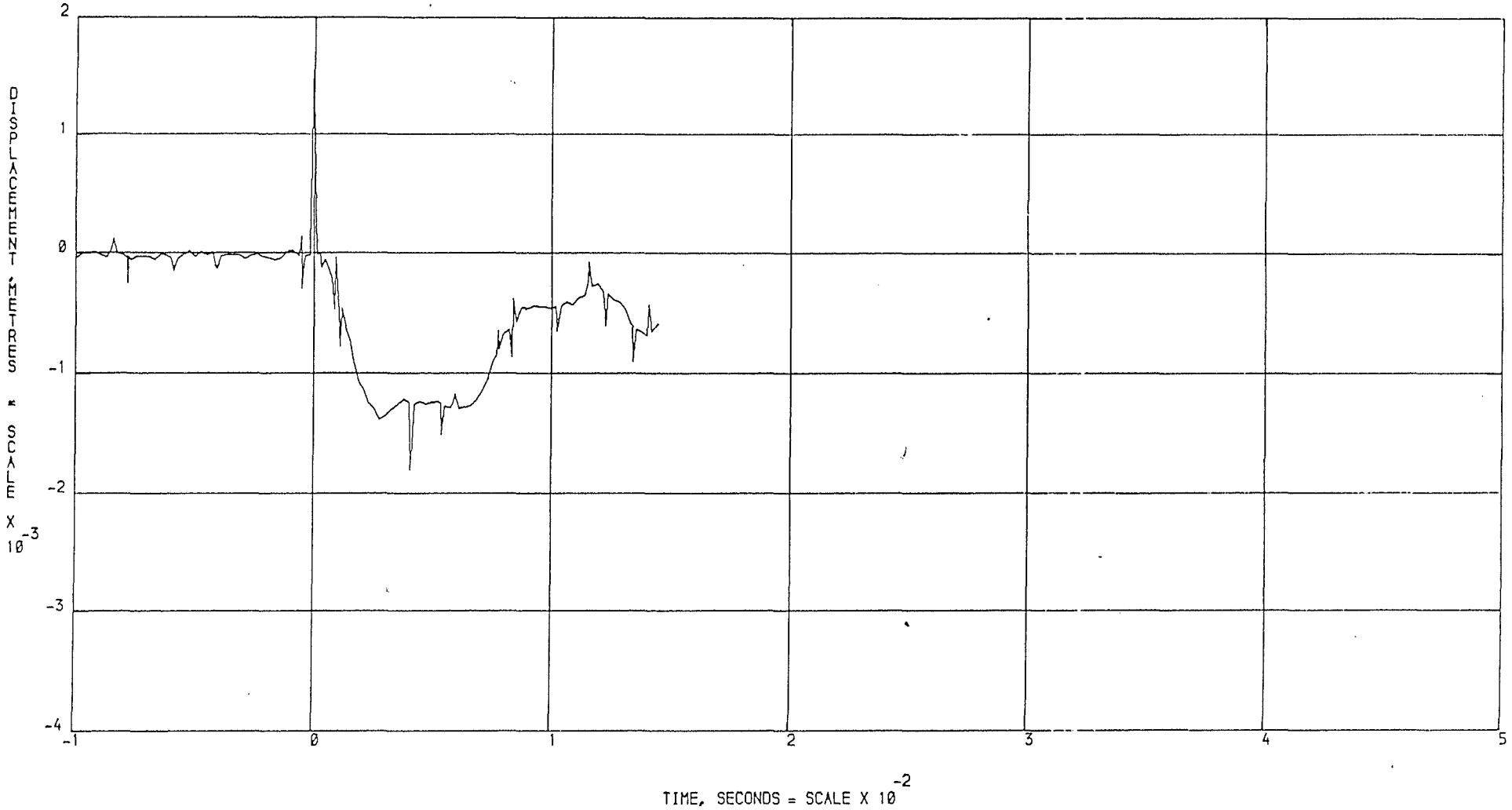

Fig. 4.11 DISPLACEMENTS AT LOCATION W1

(WITH COMPLEMENT OF UKAEA, WINFRITH)

MISSILE IMPACT TEST M126

EXPERIMENT, FILE NO. 1 M126 Ø07 171180 Ø2 W2

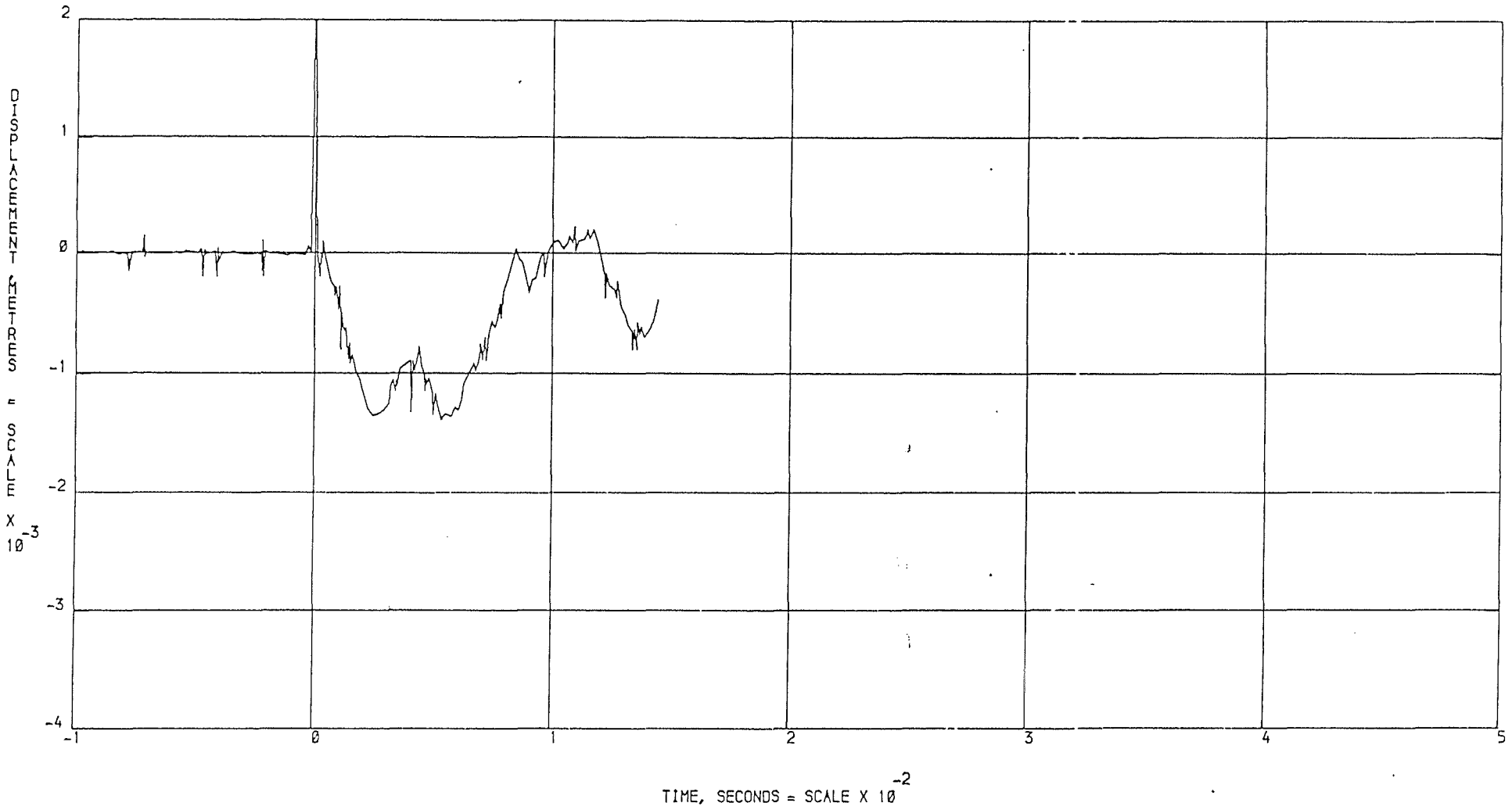

Fig. 4.12 DISPLACEMENTS AT LOCATION W2

(WITH COMPLEMENT OF UKAEA, WINFRITH) MISSILE IMPACT TEST M126

EXPERIMENT, FILE NO. 1 M126 007 171180 02 W3

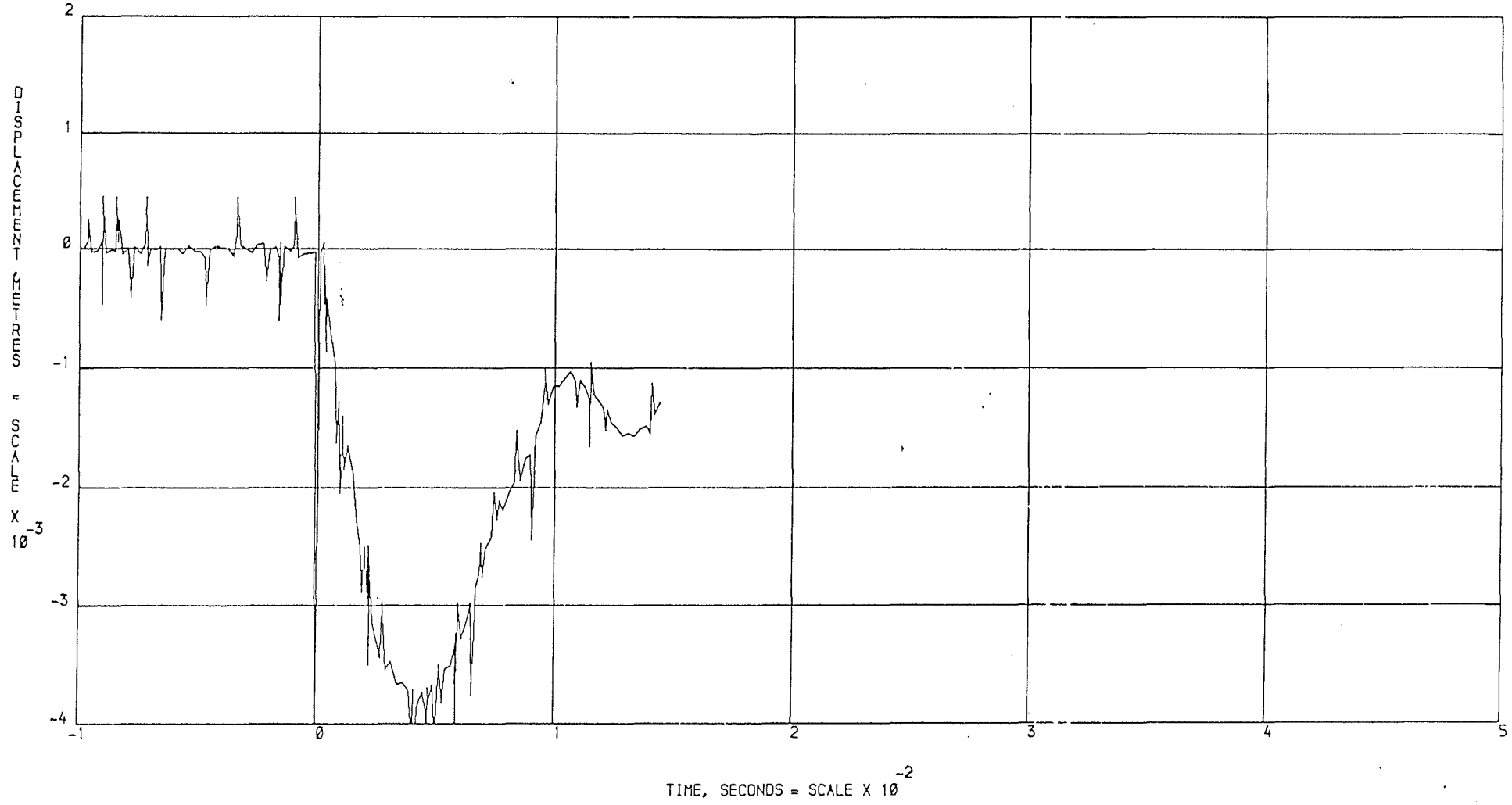

Fig. 4.13 DISPLACEMENTS AT LOCATION W3

(WITH COMPLEMENT OF UKAEA, WINFRITH) MISSILE IMPACT TEST M126

EXPERIMENT, FILE NO. 1 M126 Ø07 171180 Ø2 W4

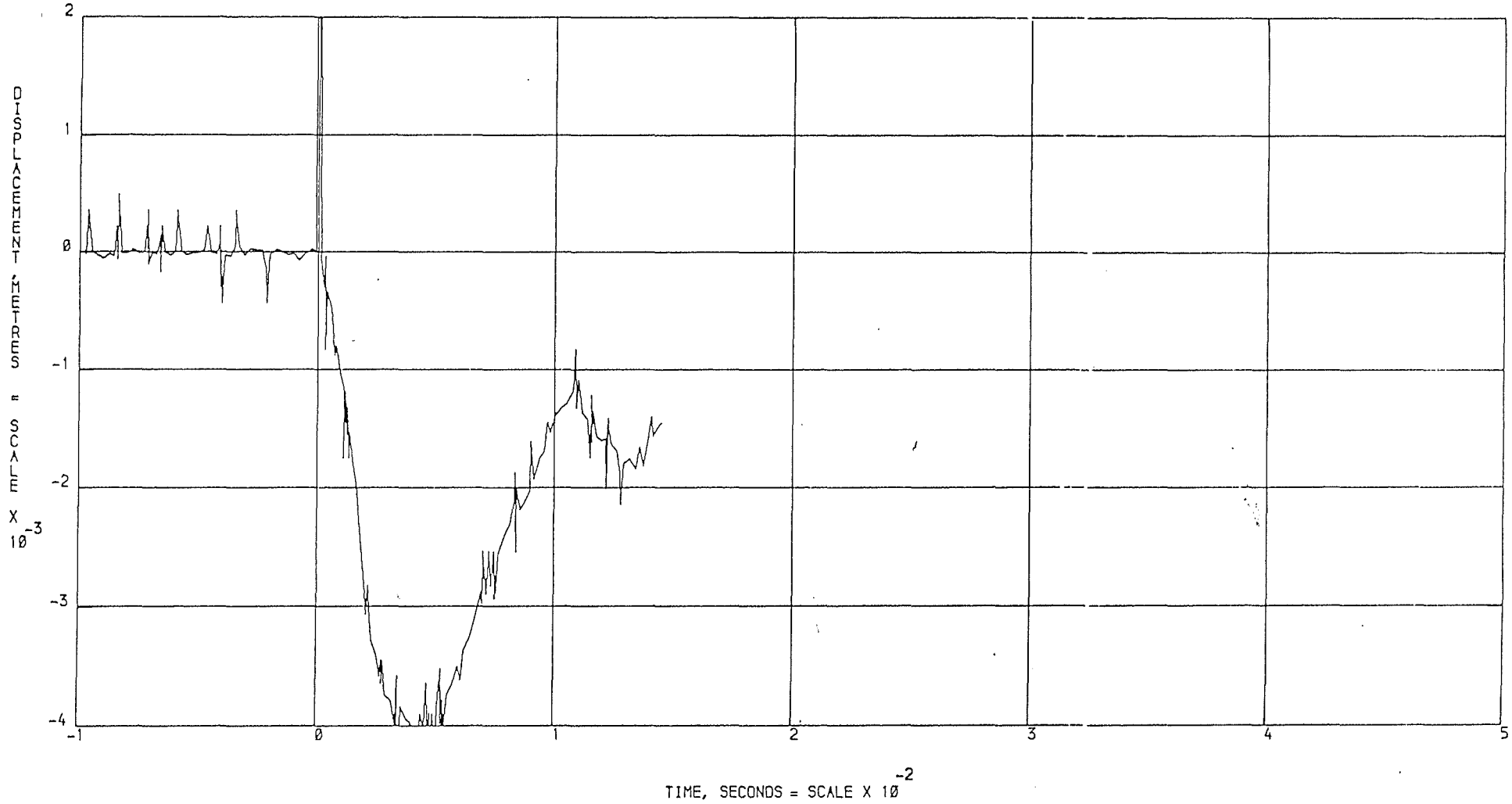

Fig. 4.14 DISPLACEMENTS AT LOCATION W4

(WITH COMPLEMENT OF UKAEA, WINFRITH) MISSILE IMPACT TEST M126

EXPERIMENT, FILE NO. 1 M126 007 171180 02 W5

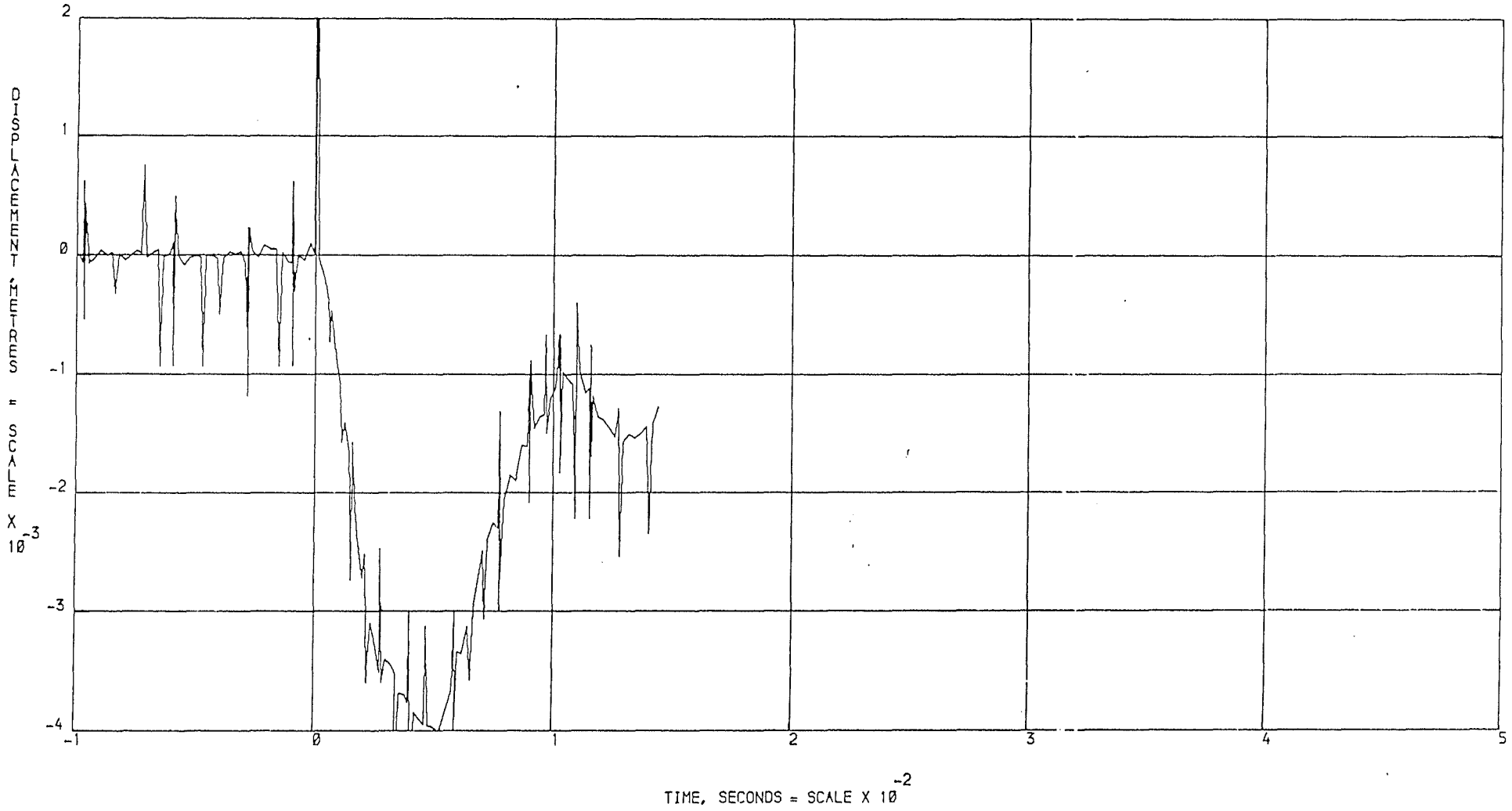

Fig. 4.15 DISPLACEMENTS AT LOCATION W5

(WITH COMPLEMENT OF UKAEA, WINFRITH) M'SSILE IMPACT TEST M126

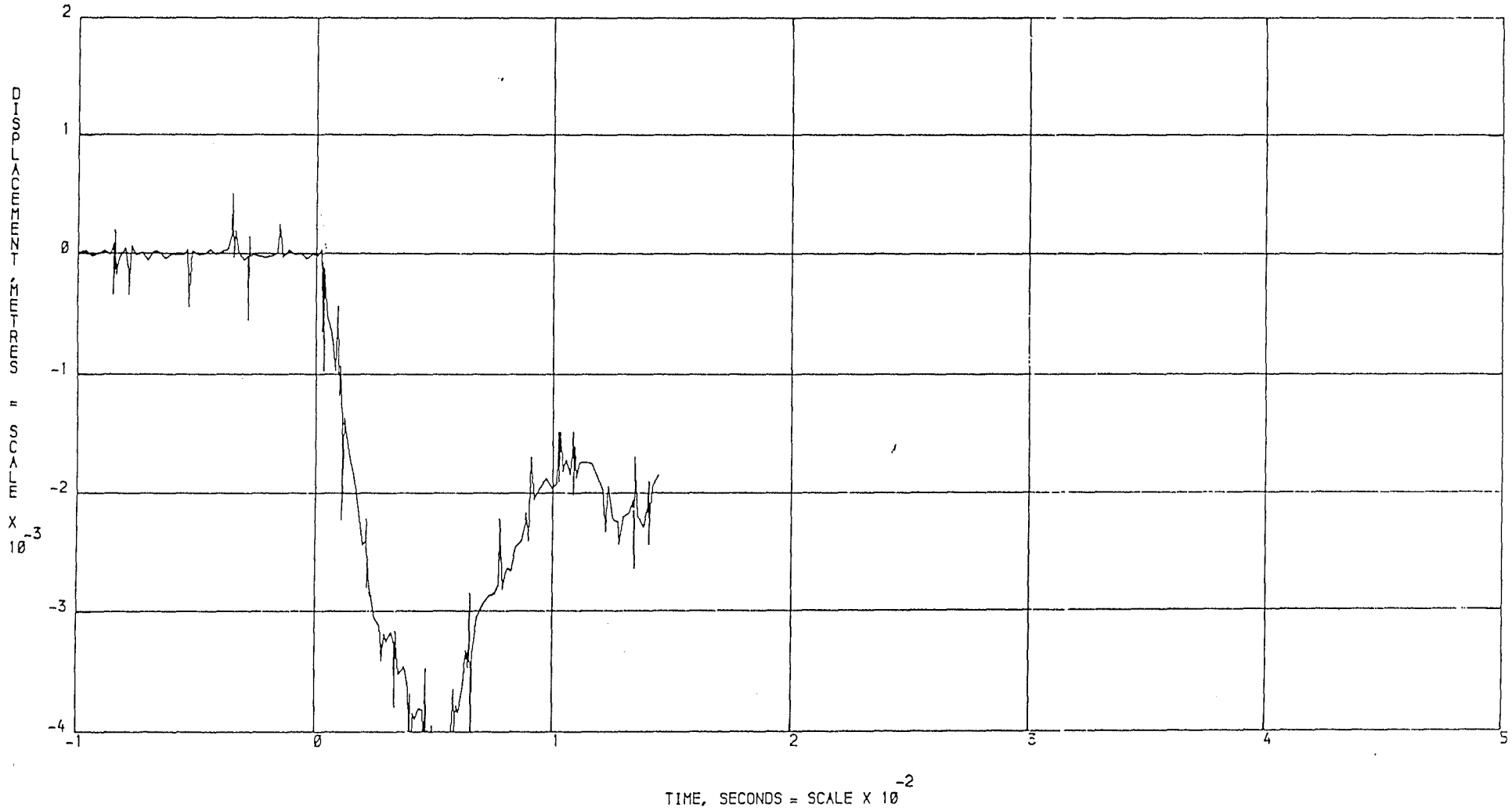

Fig. 4.16 DISPLACEMENTS AT LOCATION W6

(WITH COMPLEMENT OF UKAEA, WINFRITH) MISSILE IMPACT TEST M126

EXPERIMENT, FILE NO. 1 M126 007 171180 6? W7

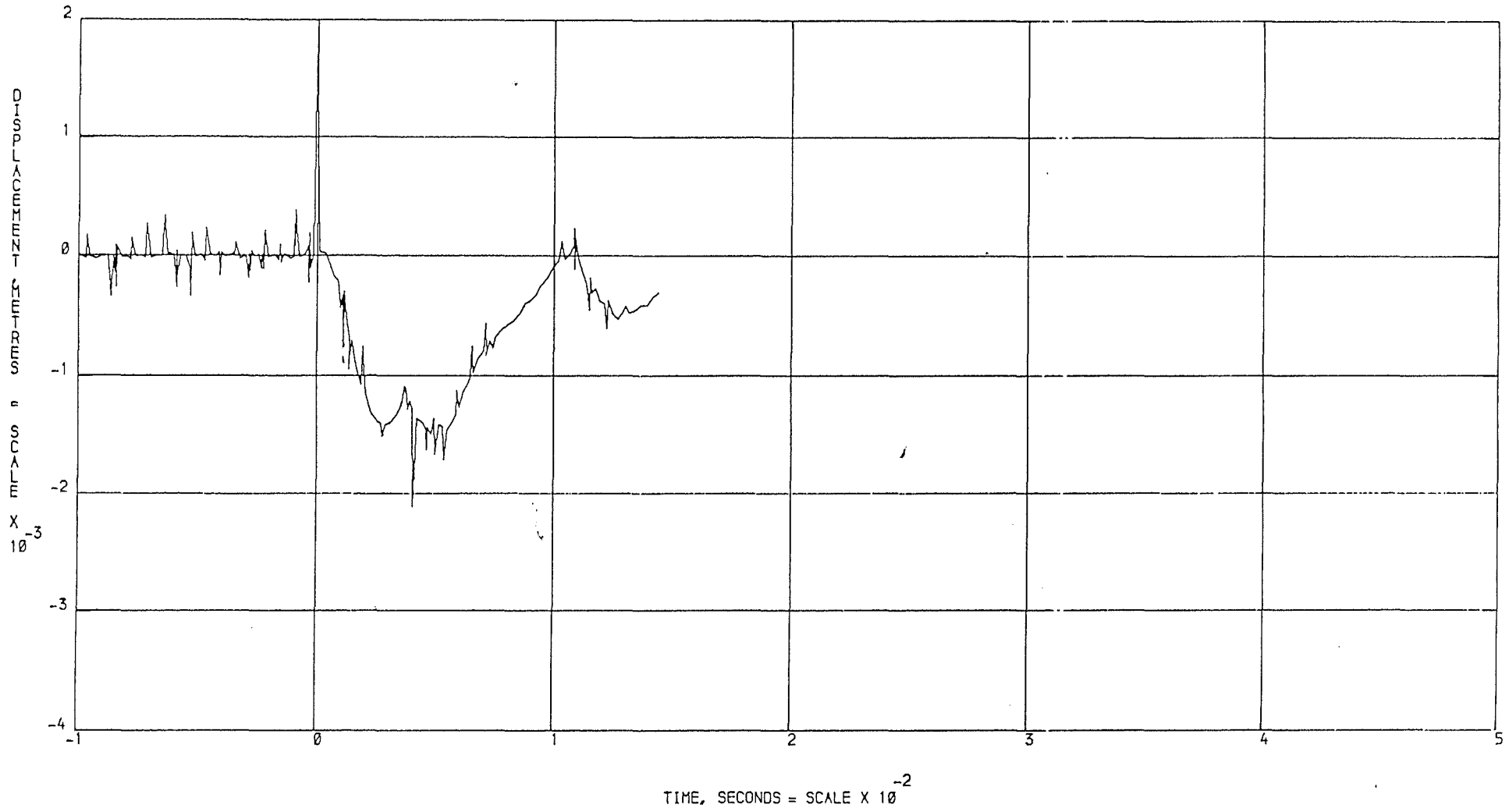

Fig. 4.17 DISPLACEMENTS AT LOCATION W7

(WITH COMPLEMENT OF UKAEA, WINFRITH) MISSILE IMPACT TEST M126

EXPERIMENT, FILE NO. 1 M126 007 17118\ 02 W8

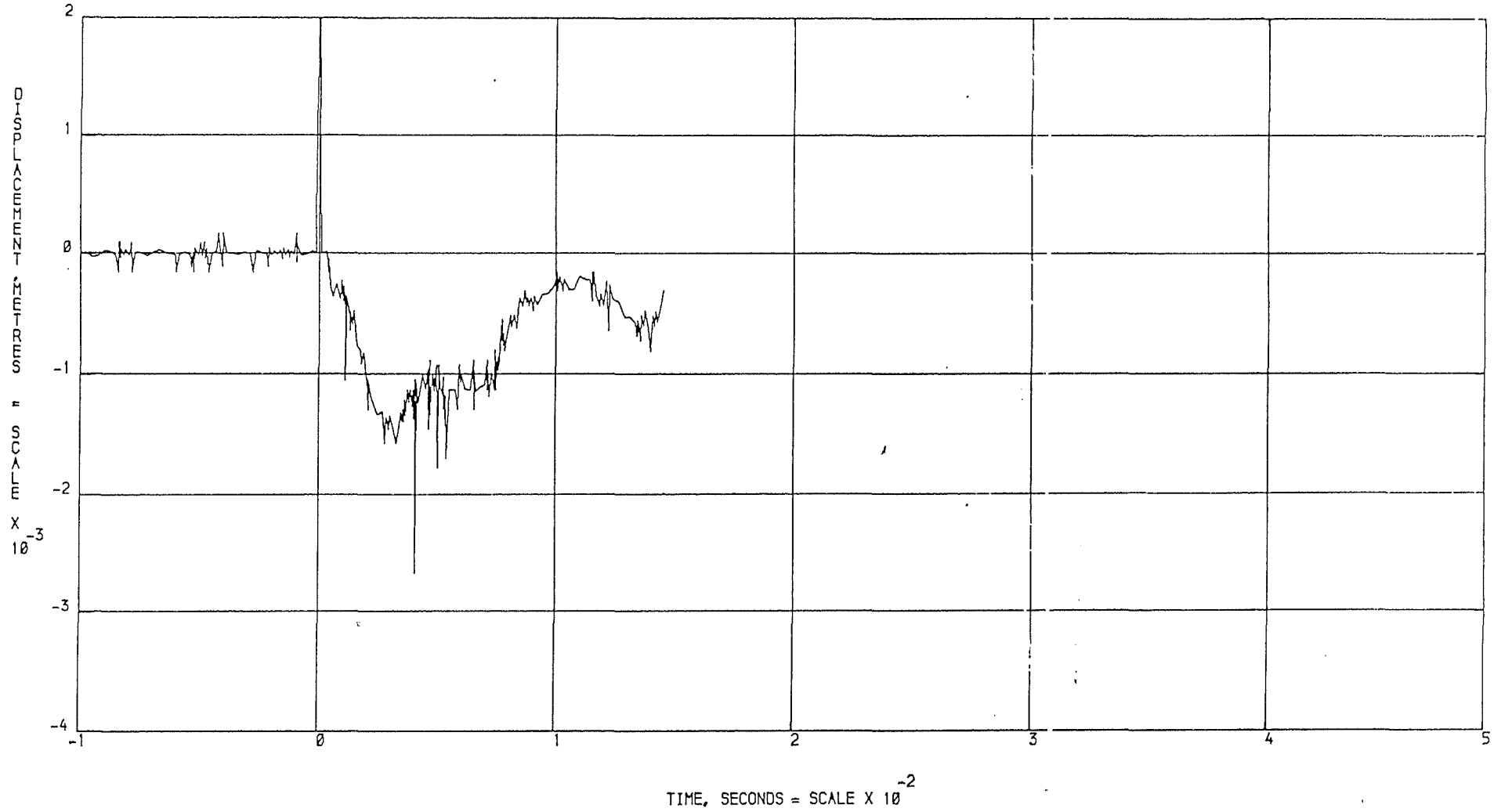

Fig. 4.18 DISPLACEMENTS AT LOCATION W8

(WITH COMPLEMENT OF UKAEA, WINFRITH) MISSILE IMPACT TEST M126

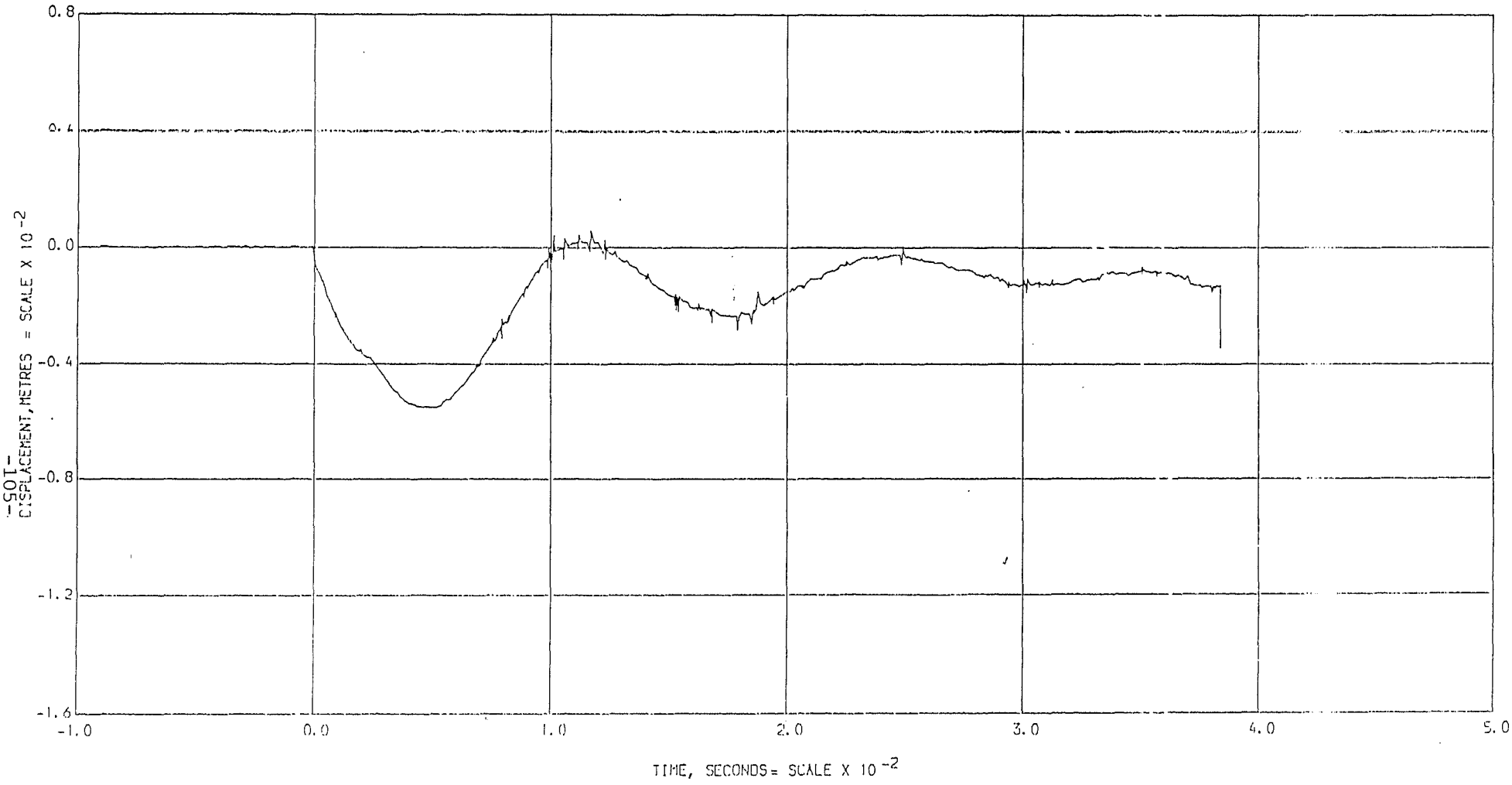

MISSILE IMPACT TEST M289

Fig. 4.19 DISPLACEMENTS AT LOCATION W1

(WITH COMPLEMENT OF UKAEA, WINFRITH)

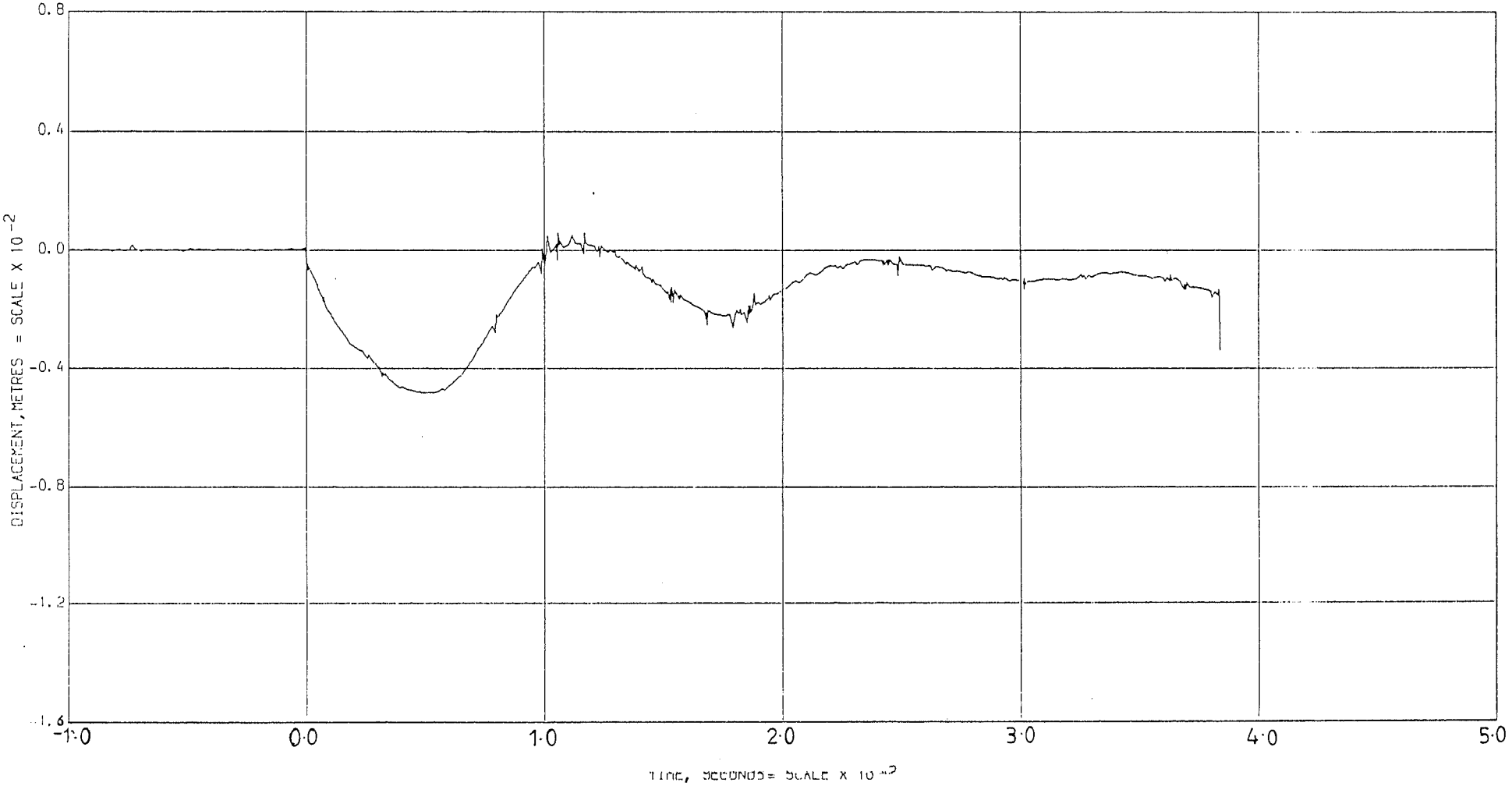

Fig.4.20 DISPLACEMENTS AT LOCATION W2

MISSILE IMPACT TEST M289

(WITH COMPLEMENT OF UKAEA, WINFRITH)

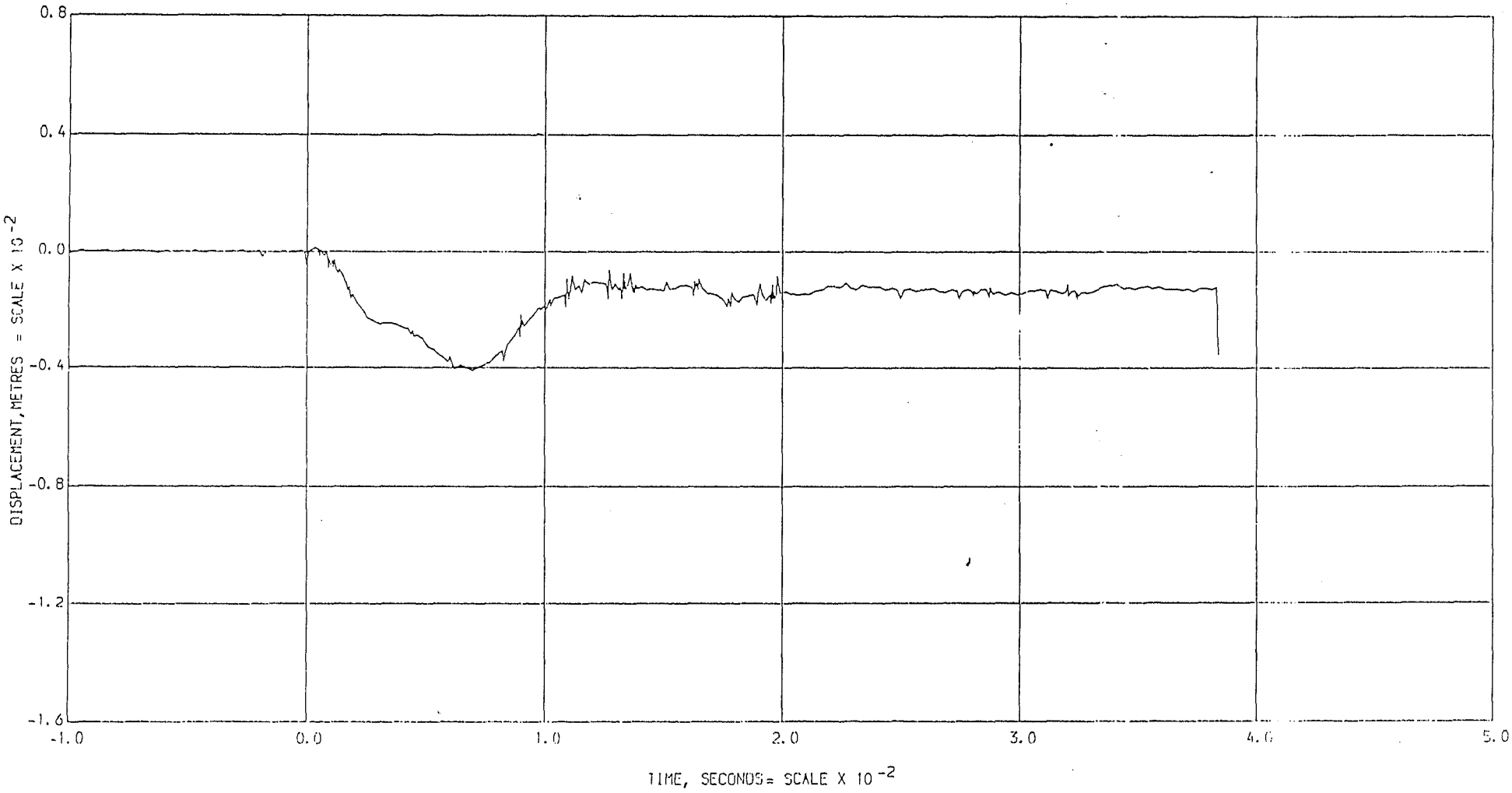

Fig. 4.21 DISPLACEMENT AT LOCATION W7

MISSILE IMPACT TEST M289

(WITH COMPLEMENT OF UKAEA, WINFRITH)

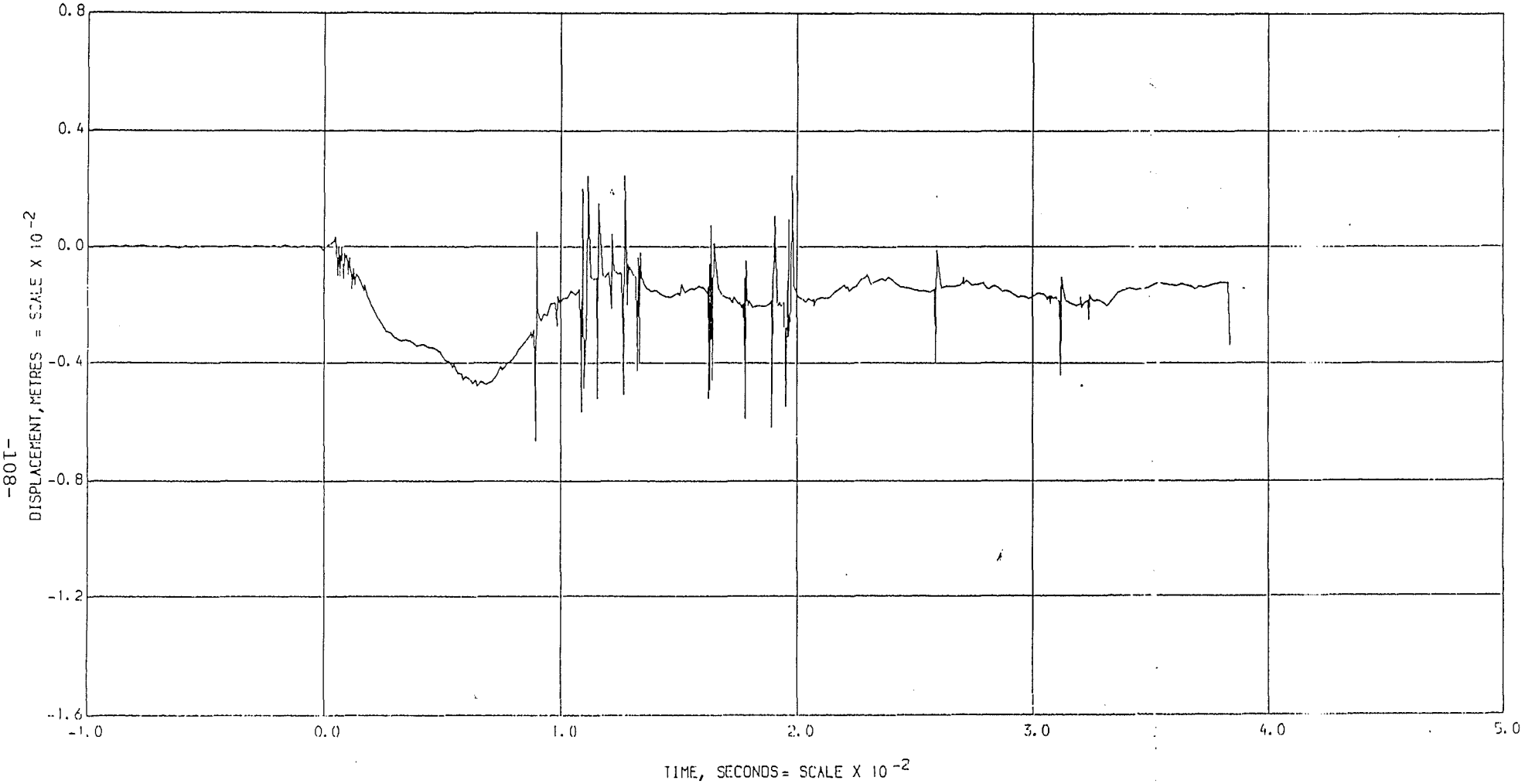

Fig. 4.22 DISPLACEMENS AT LOCATION W8

MISSILE IMPACT TEST M289

(WITH COMPLEMENT OF UKAEA, WINFRITH)

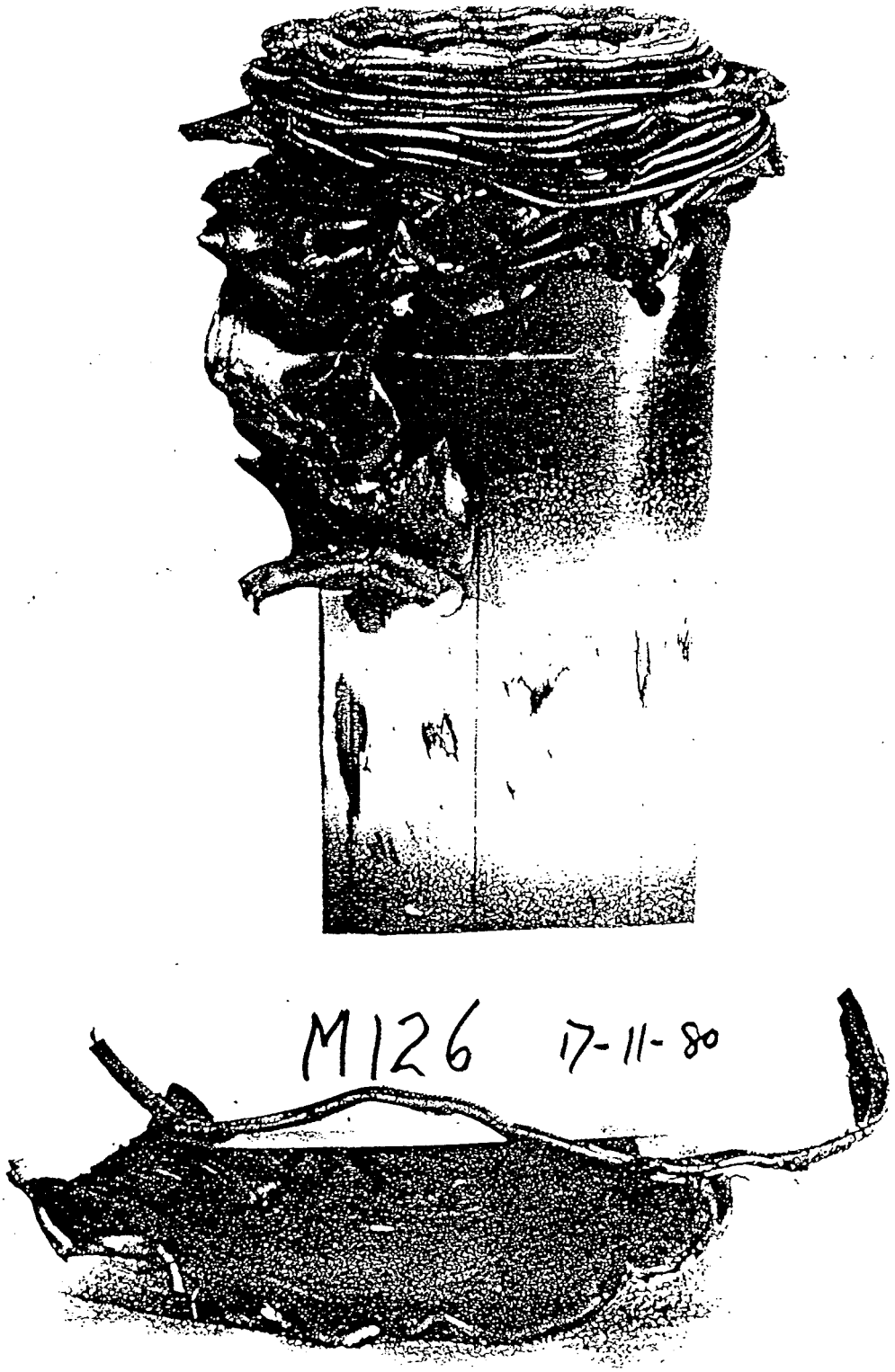

Fig. 4.23 TYPE 11 MISSILE AFTER IMPACT ON TARGET B16 AT 237 M/S

(WITH COMPLEMENT OF UKAEA, WINFRITH)

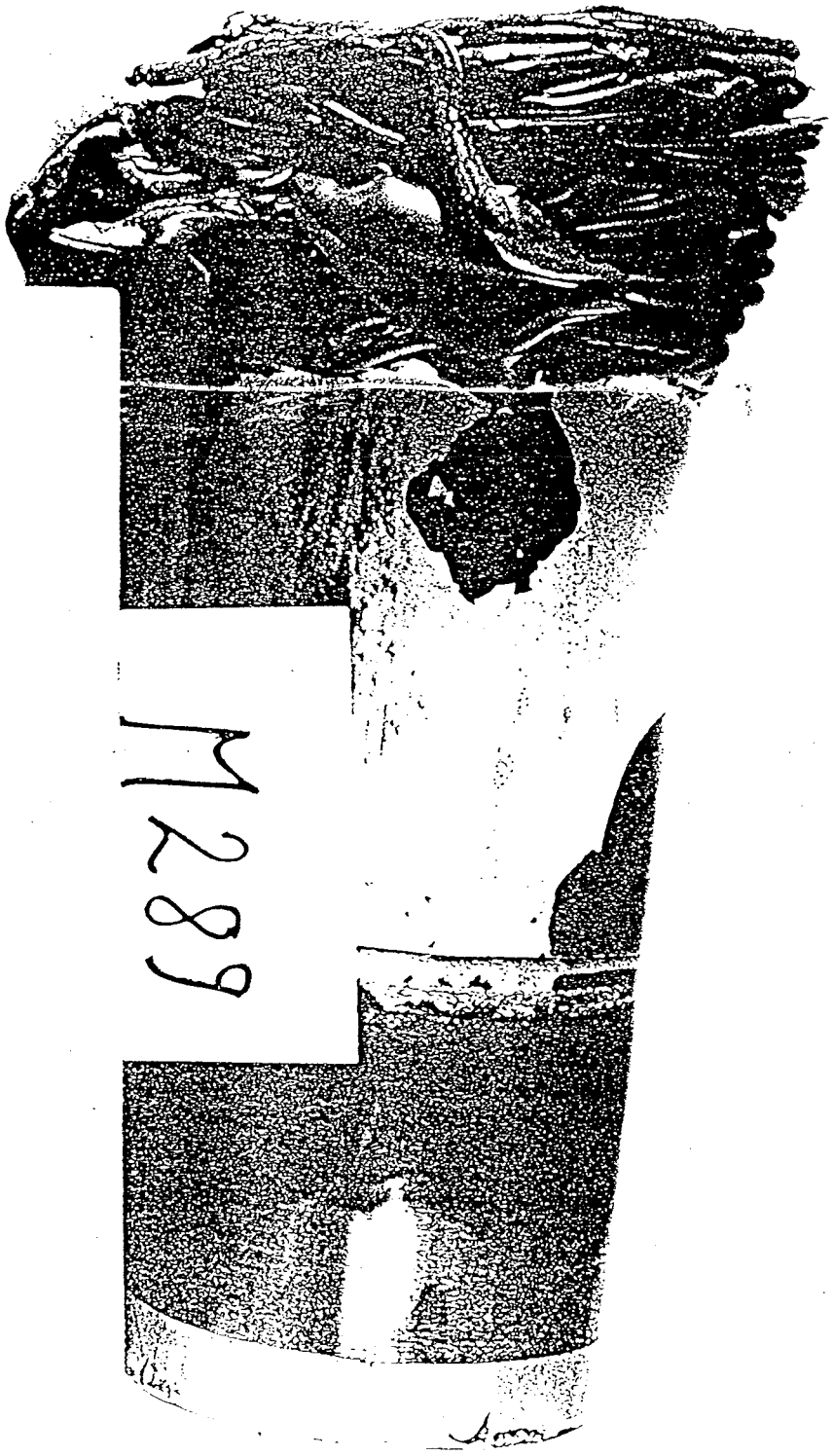

Fig. 4.24 TYPE 11 MISSILE AFTER IMPACT ON TARGET B26 AT 240 M/S

(WITH COMPLEMENT OF UKAEA, WINFRITH)

Not for Publication (Commercial)

Results of test no. M126

Missile : Collapsing steel tube type 11($\frac{1}{4}$)

Impact velocity : 237 m/s

Target : Type 16($\frac{1}{4}$) no bending reinforcement — 1.625 x 1.5 x 0.175 m
shear reinforcement — ϕ4.5 impact face, ϕ6.25 rear face on 31 mm pitch
ϕ4.5 mm 0.37% of plan area in central region

Concrete strength measurements :

'Lok-test' measurements (post test) indicate ucs 24.6 ± 3.2 MPa

Age, days	28 days	
152 mm cubes	34.4 MPa	std.dev. 2.0 MPa
75 mm cubes	32.0	2.6
75 x 75 x 300 mm beams	3.0	0.4
Brazilian	2.5	0.3
ϕ 152 x 300 mm cylinders	33.7	2.0

Panel age at date of test — 28 days

Damage to panel :

Front (impact) face — maximum penetration 20 mm
reinforcement exposed over area ϕ 180 mm

Rear face — light cracking within a region side ~300 mm
radial cracking from corners of this region
no scabbing

Final undamaged length of missile 355 mm (total length 440 mm)

TABLE 4.1 RESULTS OF TEST M126

(WITH COMPLEMENT OF UKAEA, WINFRITH)

Not for Publication (Commercial)

Results of test no. M289

Missile : type 11($\frac{1}{4}$), mass 15.6 kg

Impact velocity : 240 m/s

Target : B26($\frac{1}{4}$)/2 1500 x 1625 x 150mm
bending reinforcement Φ4.5/Φ6.25mm @ 37/28mm front/rear
shear reinforcement Φ5.0 @ 62mm

Concrete strength measurements :

LOK-test measurements (post test) indicate ucs = 41.0 ± 3.8 MPa

Age, days 35

152 mm cubes	45.1 ± 1.6 MPa
75 mm cubes	61.3 ± 2.9 MPa
75 x 75 x 300 mm beams	3.8 ± 0.4 MPa
Brazilian	3.8 ± 0.9 MPa
Φ 152 x 300 mm cylinders	37.0 ± 4.7 MPa

Panel age at date of test 36 days

Damage to panel :

Front (impact) face: shear cone formed and displaced ∿70mm
5 rebars broken
entry hole diameter 260mm

Rear face: concrete cover scabbed to diameter 650mm
8 rebars broken
maximum heave ∿50mm

Residual length of missile 290mm (undamaged) 420mm (total)

TABLE 4.2 RESULTS OF TEST M289

(WITH COMPLEMENT OF UKAEA, WINFRITH)

CHAPTER 5

IMPACT ANALYSIS

5.1 General Introduction

Elastic, elasto-plastic and crack analyses have been performed for two slab models, B16 and B26. All the slab geometries, material properties and input load-time histories were provided by UKAEA, Winfrith. Both the NONSAP and MARC programs were used to carry out the analyses. The results are compared with each other and with experiment.

5.2 Input for Analyses

The model geometries, material properties and load-time history are described in this section.

5.2.1 Geometry

The geometries of the two test slabs are illustrated in Figs. 4.6 and 4.7. These two reinforced concrete slabs are of the same length and breadth (1625mm x 1500mm). Different thicknesses are chosen in order to compare the damage effects. The thickness of B16 is 175mm and the thickness of B26 is 150mm. These two slabs are reinforced top and bottom with bending reinforcement. Shear reinforcement was also introduced.

5.2.2 Material Properties

The reinforcement and concrete properties are listed in Tables 4.1 and 4.2. The Young's moduli and Poisson's ratios of concrete and

reinforcement were used in material matrices. In NONSAP, the reinforced concrete slabs were modelled by three-dimensional composite elements. The area of the reinforcement and concrete in directions X, Y and Z are included for the material matrix.

5.2.3 Load-time History

Time domain analysis has been used for this highly non-linear impact problem. Load-time histories were used as input in the dynamic analyses as shown in Fig. 4.10.

5.3 Method of Analysis in NONSAP

A three-dimensional non-linear finite element program, NONSAP has been used to carry out the analyses. Since NONSAP was written on an IBM computer, it was converted to run on a DEC VAX computer. It was then modified so as to be able to solve this highly non-linear dynamic problem.

A three-dimensional, four parameter concrete model based on the Ottosen failure criterion was used to represent the concrete behaviour. (For details of the Ottosen model, see Section 2.2). The effects of the reinforcement were taken care of by considering the reinforced concrete as a composite material. (See Section 2.3 - Reinforced Concrete). A reinforced concrete model, which combines all these properies, has been written in Fortran 77 subroutines and these were linked with the main program. (See Section 6.2 for description of subroutines).

Cracking effects were also taken into account. Cracks in three-directions were calculated based on criterion adopted in Section 2.5. Elastic, elasto-plastic and plastic situations have been included in both analyses.

In the dynamic analysis, a time domain approach was used. The Newmark time integration method (with Alpha = 1/2, Beta = 1/4) and a consistent mass matrix were used.No damping was included for the reasons given earlier

The time step increment used in these analyses was 0.000155 seconds and a total number of 60 time steps were needed. This gives a total impact time of 0.0093 seconds which was required for both analyses.

The force generated from the impact between the missile and the target was applied equally at the centre corner of the model slabs. In this case force was applied equally to 5 nodes (16, 23, 24, 32 and 33) for one slab. Apexes from the load-time function curve were chosen as input points. A total of 5 points were chosen. A linear relationship is assumed between any 2 points. All forces were applied in the vertical direction.

The major input data includes:-

1. Density of the reinforced concrete
2. Young's moduli of concrete and reinforcement
3. Tensile and compressive strengths of concrete
4. Poisson's ratios of concrete and composite material
5. Areas of concrete and reinforcement in the three coordinate directions
6. Yield stress of reinforcement
7. Volume fractions of concrete and reinforcement
8. Crushing strain of concrete

In each analysis, nodal displacements, velocities and accelerations were calculated in each time step. Output from critical time steps were printed out. Six stress components, σ_{xx}, σ_{yy}, σ_{zz}, σ_{xy} σ_{yz} and σ_{zx} were calculated from the integrations. Direction cosines for the cracks were also calculated and printed out from the integration.

5.4 Finite Element Model in NONSAP

The finite element models used are illustrated in Figs. 5.1-5.5. By symmetry, only one-quarter of the slab needs to be modelled. The element used is a 20-noded, isoparametric, three-dimensional brick with 8 corner nodes and 12 edge mid-point nodes. This element has 8 Gaussian integration points. A total of 36 elements and 315 nodes have been generated for each reinforced concrete model. The models were designed in such a way that most of the elements were situated at the impact and damage areas where most of the cracks were believed to initiate.

The MARC finite element pre-processor, MENTAT was used to generate the meshes. The connectivities had to be rearranged to fit into the input requirement of NONSAP since MARC and NONSAP have different connectivity definitions.

Three degrees of freedom were assumed at each node, X, Y, and Z displacements. A total of 854 degrees of freedom were in each Model. As the model is one-quarter of the actual slab, one edge of the model was suppressed in the X-direction and the other edge was suppressed in the Y-direction. The two free edges were simply supported in the Z-direction.

5.5 Method of Analysis in MARC

The three-dimensional non-linear dynamic finite element program, MARC has been used to process the results in order to compare with NONSAP. This analysis was carried out on a micro VAX computer.

The parabolic Mohr-Coulomb failure criterion was used to model the concrete behaviour while the Von Mises yield condition was assumed for the steel behaviour. (See Section 2.6, Failure Criterion in MARC). Concrete cracking and crushing have been considered based on the ultimate tensile stress and the crushing strain of concrete. (See Section 2.7, Concrete Cracking Model in MARC analysis).

Elastic, elasto-plastic and plastic situations were included in the analysis. The elasto-plastic analysis was based on the incremental plasticity theory of Prandtl-Reuss stress-strain relations on flow rule.

In the dynamic analysis, the Newmark direct integration method (with Alpha = 1/2, Beta = 1/4) was applied. A modal analysis was first carried out to find out the critical natural frequencies and mode shapes of the models so that the higher frequencies could be damped out. Based on the selected frequency, the time step size and numerical damping factor could be calculated. For calculation of time step size and numerical damping factor see Appendix B The time step size and the total transient time are specified through the DYNAMIC CHANGE option in MARC.

The force was applied in the same way as in the NONSAP analysis but input was made via the user subroutine, FORCDT. In this subroutine, time dependent load is calculated based on the amount of transient time at that moment. (For details see user subroutine FORCDT in Section 6.3)

In each analysis nodal displacements, velocities and accelerations were calculated for each time step. Tresca, Mises, Mean Normal and six components of stress and strain were calculated for each integration point. Principal stresses and strains, direction cosines, plastic strains and crack strains were also calculated and printed out from the integration points together with six stress and strain components in each of these three-dimensional brick elements. Nodal forces and nodal reactions were calculated and printed for each node. The stresses and strains are output along the rebar axes for the rebar elements. The major input data includes:-

1. Densities of concrete reinforcement
2. Young's moduli of concrete and steel
3. Tensile and compressive strengths of concrete
4. Poisson's ratios of concrete and reinforcement
5. Yield stress of reinforcement
6. Constant Zeta (ζ) for Parabolic Mohr-Coulomb failure criterion
7. Crushing strain of concrete
8. Numerical damping factor, γ

5.6 Finite Element Model in MARC

In order to make an easy comparison with NONSAP, the coordinate geometries and element and node numbers were not changed between the NONSAP and MARC analyses.

Two types of elements have been chosen for the MARC analysis. Three-dimensional 20-noded brick elements, (type 21), have been used to represent the concrete. Each edge of this isoparametric element forms a parabola, so that 8 nodes define the corner of the element and a further 12 nodes define the position of the "mid-point" of each edge. This element has 27 Gaussian integration points located in three layers within the element. There are 3 global coordinates in the X, Y and Z-directions and there are 3 global degrees of freedom, U, V and W. There are 6 components of stress and strain.

The reinforcement is represented by the rebar element, (type 23). This element is an isoparametric, three-dimensional empty block which contains reinforcing bars running in patterns designed by the user through user subroutine, REBAR. These elements are used in conjunction with 20-noded brick elements, (type 21) which represent the concrete. The combination of these two elements approximate the reinforced concrete behaviour. As in the brick elements, each edge of this isoparametric element forms a parabola, so that 8 nodes define the corner of the element and a further 12 nodes define the position of the "mid-point" of each edge. The rebar elements are integrated using a numerical scheme based on Gauss quadrature. Each layer contains 9 integration points. In each of these elements there are 5 layers and a total of 45 integration points. For input details see Section 6.4, User Subroutines for MARC Analysis.

As in the NONSAP analysis, the models were generated by MENTAT, the MARC finite element pre-processor. There are 3 global degrees of freedom, U, V and W in each node of these rebar elements. There are 36 x 20-noded solid elements in total and 36 rebar elements in each model. There are 315 nodes and a total of 854 degrees of freedom in each model.

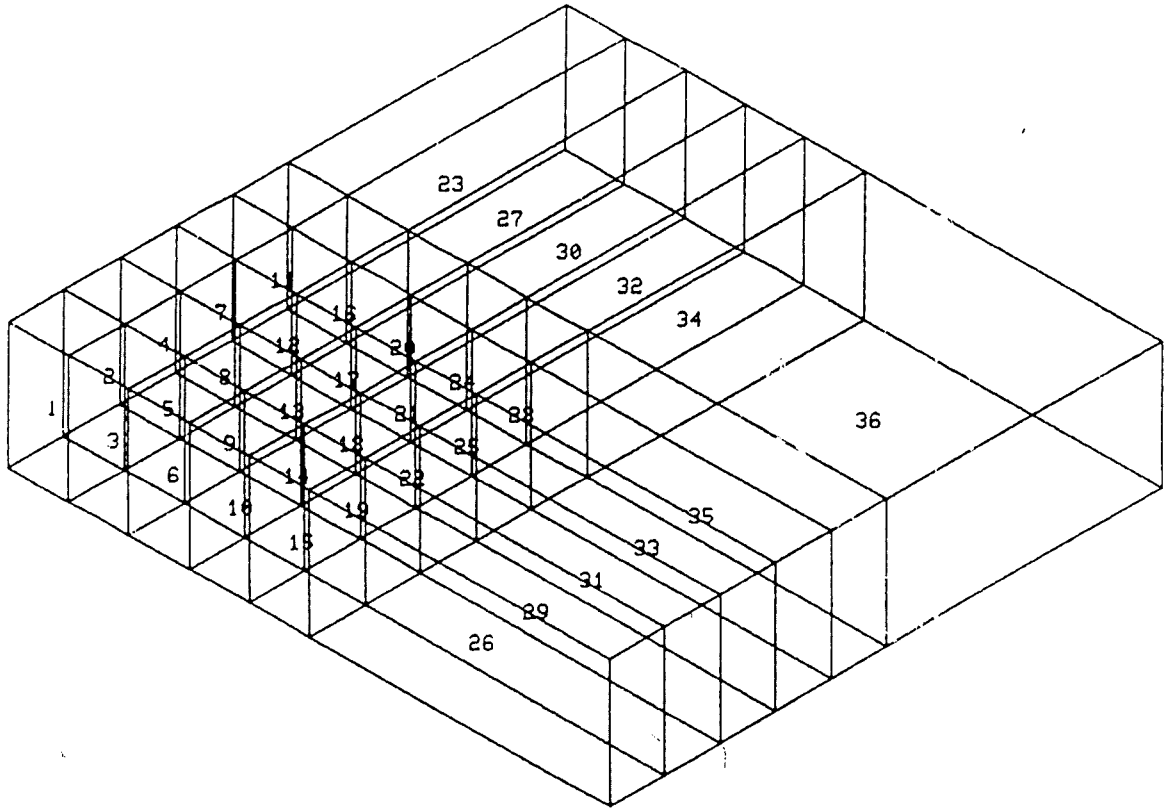

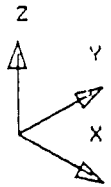

FIG. 5.1 MODEL OF 1/4 OF THE SLAB SHOWING ELEMENT NUMBERS

ORTHO V.P. 1.0000 -1.000 1.0000

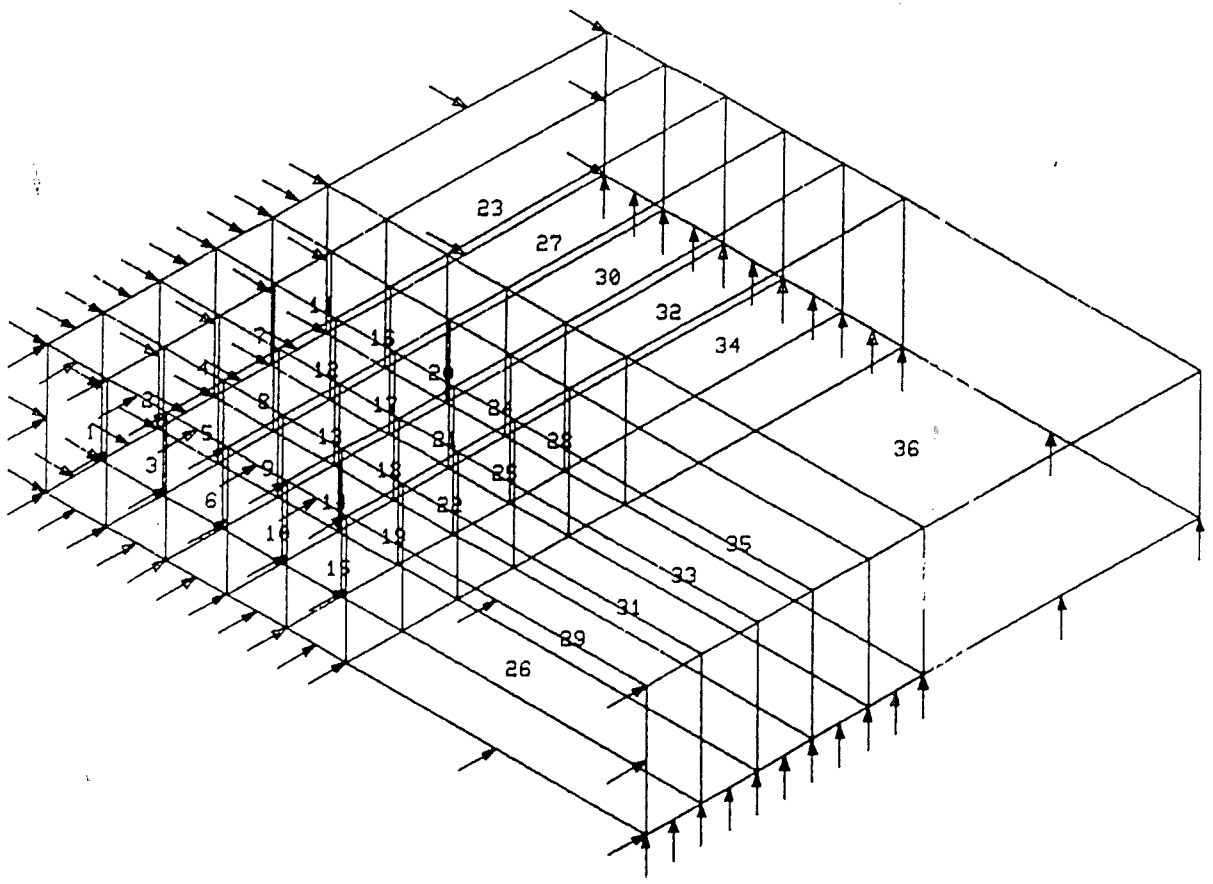

FIG. 5.2 MODEL OF 1/4 OF THE SLAB SHOWING SUPPORT CONDITION

ORTHO V.P. 1.0000 -1.000 1.0000

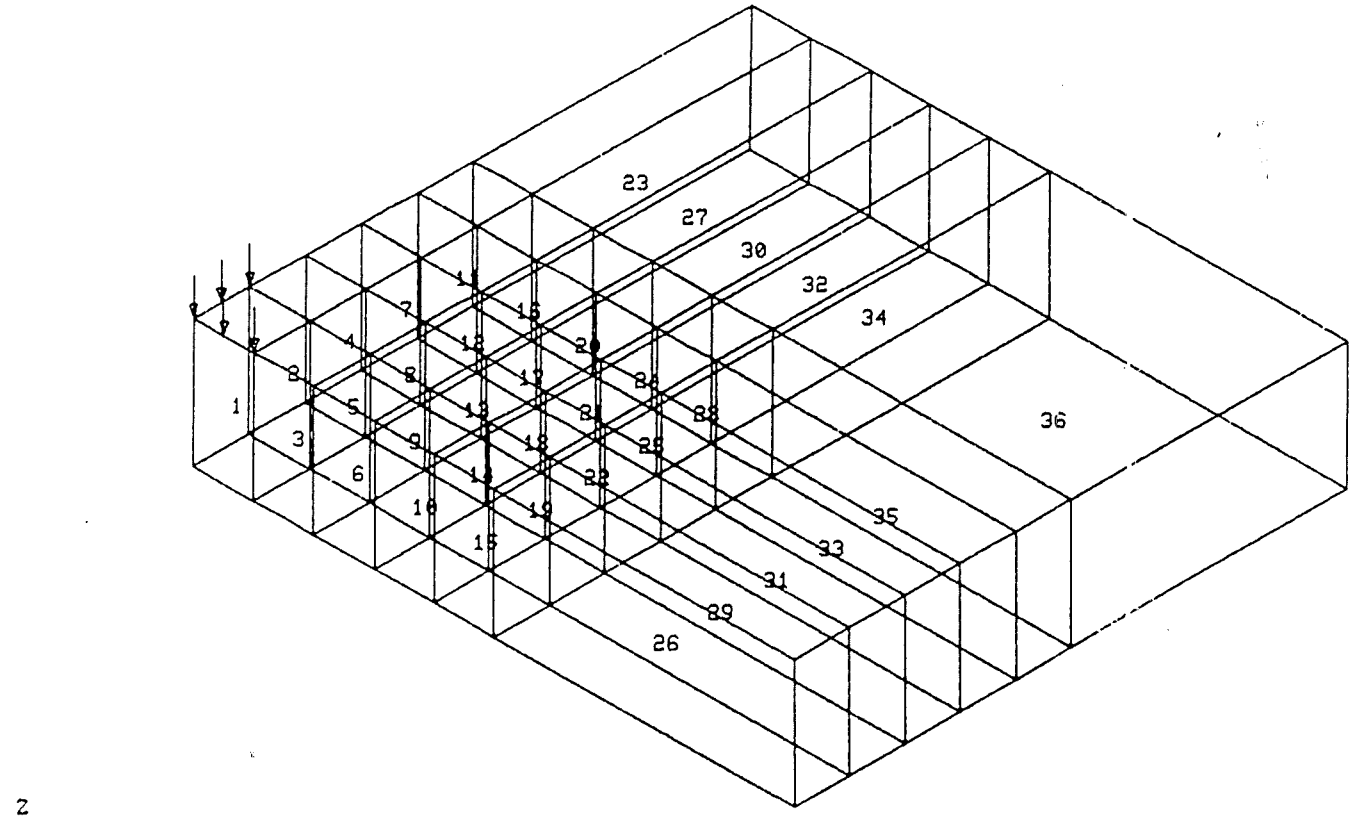

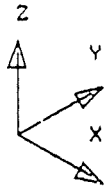

FIG. 5.3 MODEL OF 1/4 OF THE SLAB SHOWING LOAD APPLICATION

ORTHO V.P. 1.0000 -1.000 1.0000

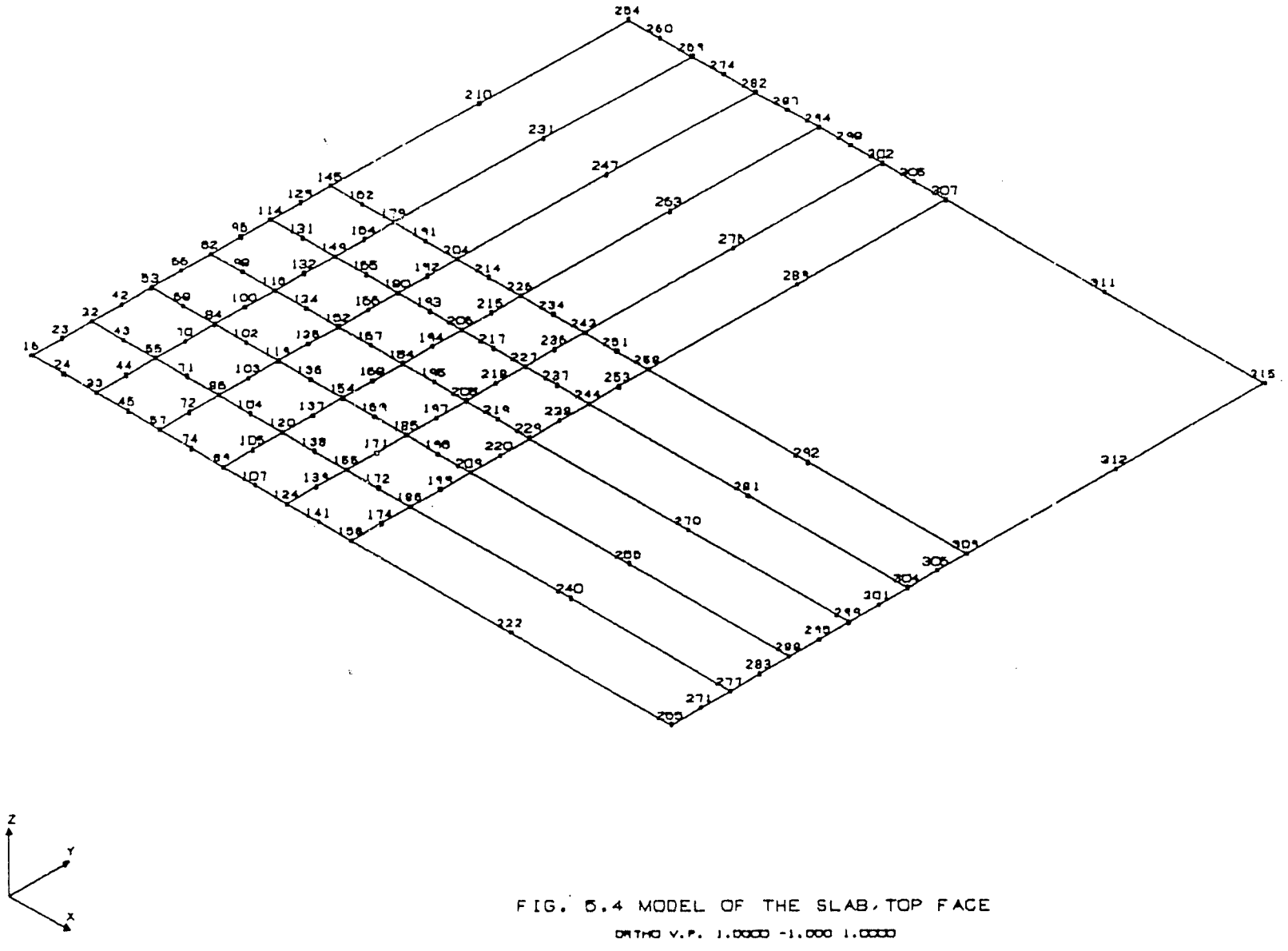

FIG. 5.4 MODEL OF THE SLAB, TOP FACE

ORTHO V.P. 1.0000 -1.000 1.0000

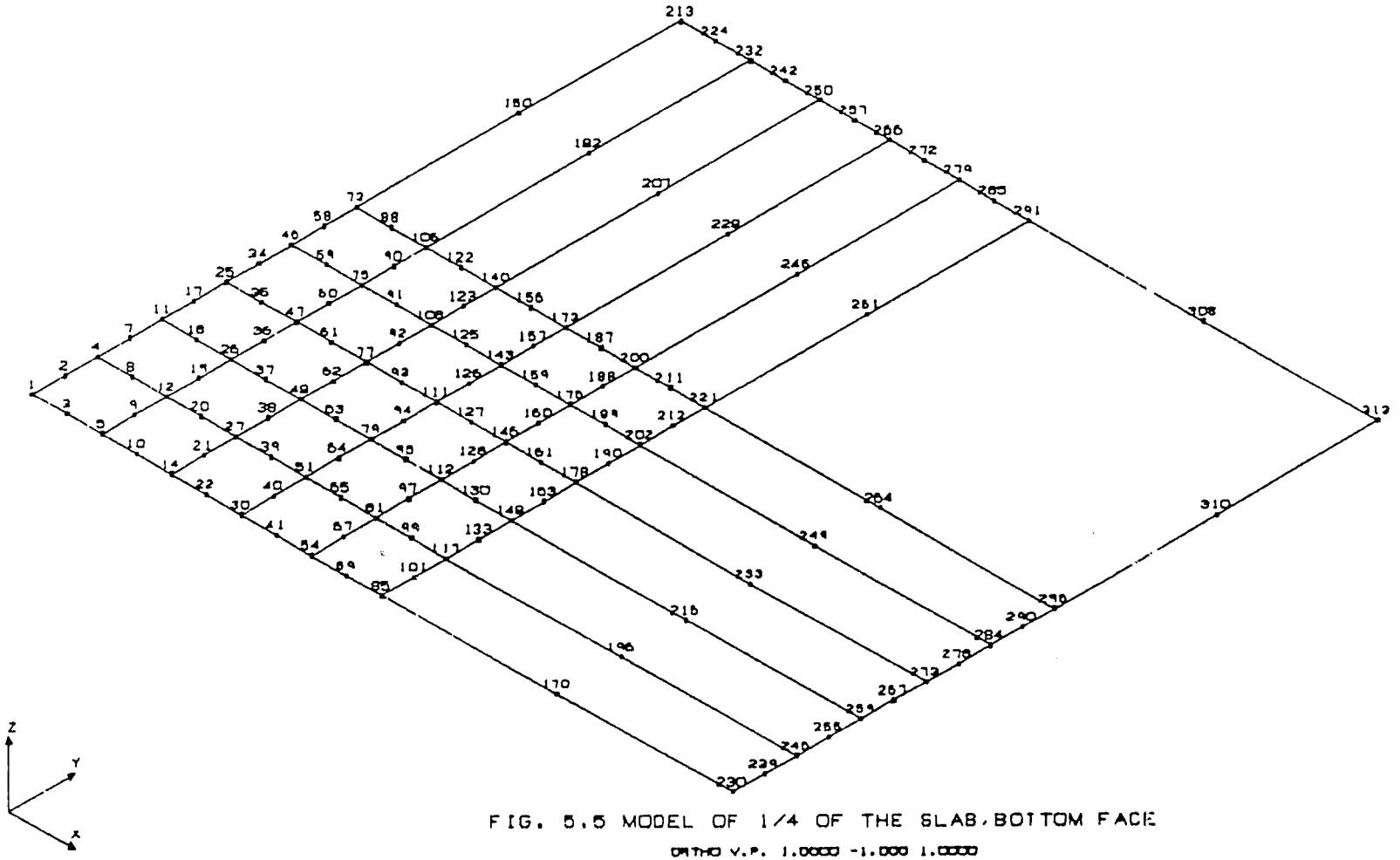

FIG. 5.5 MODEL OF 1/4 OF THE SLAB, BOTTOM FACE

ORTHO V.P. 1.0000 -1.000 1.0000

CHAPTER 6

COMPUTER PROGRAMS-NONSAP AND MARC

6.1 Program description of NONSAP and Modification Procedures

NONSAP is a finite element program for static and dynamic, linear and non-linear analyses developed by Bathe, Wilson and Iding [194] of the University of California, Berkeley. The main two aims in using the NONSAP package are firstly, to provide an efficient solution of a variety of practical non-linear problems and secondly, to introduce a concrete cracking model needed for impact on reinforced concrete structures. this was not present in the original version.

Since NONSAP is an in-core solver, the program capacity is essentially determined by the total number of degrees of freedom in the system. All matrices are stored in compacted form. This gives a Maximised system capacity and solution efficiency but, for very large problems with moderate in-core allocation, the analysis will not be feasible.

Both Wilson-Theta and Newmark time integration schemes are available in NONSAP. The incremental solution scheme used corresponds to a modified Newton iteration. Both 8- or 20-noded three-dimensional isoparametric solid elements are available in the NONSAP element library. The maximum number of integration points in each element are 8 (2 x 2 x 2). In the impact analysis 20-noded isoparametric elements are used. Although there are quite a number of two-dimensional constitutive material models available in NONSAP for both linear and non-linear analyses, there exists only 2 types of models for three-dimensional elements - isotropic linear elastic and curve description models. A three-dimensional model, which adopts the Ottosen failure criterion for concrete together with the composite effect of reinforced concrete, has therefore been developed and linked to the main program in order to carry out the analysis. The flow charts are shown in Tables 6.1, 6.2, 6.3 & 6.3a.

NONSAP has been written to accept new material models not included in the material model, library, however the overlay subroutines must be supplied by the user. The overlay subroutine used is ELT3D4. In NONSAP non-linear analysis, stresses are calculated at the Gauss integration points. During program execution, subroutine ELT3D4 must perform the following functions:-

(1) Call from INTWA3

The working storage array, WA is initialized during the element information input phase. The working storage, which will be the same throughout the solution, has to be allocated in the input card.

(2) Call from STST3N

The subroutine STST3N will be called to calculate the element stresses and/or the element tangent material law.

Table 6.1 NONSAP Brief Layout

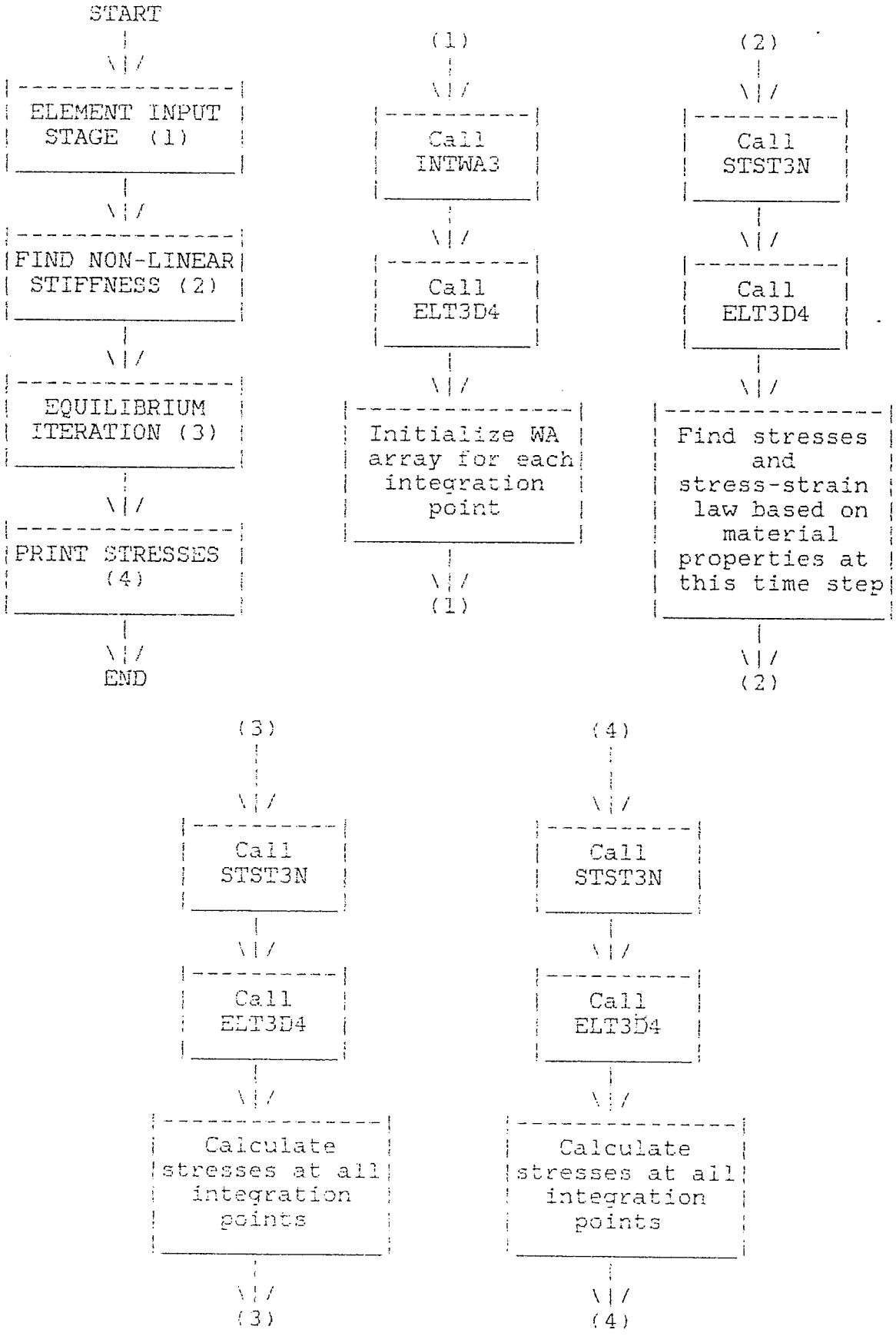

6.2 Three-dimensional Concrete Model - Main Subroutine (RCRK3D)

The overlay subroutine, ELT3D4 calls both subroutines, RCRK3D and IRCRK3D. Subroutine IRCRK3 initializes the working array, WA. The main operations of RCRK3D includes:-

1. Calculation of Young's modulus, yield stress and crushing strain of composite.

2. Testing regions for elastic, elasto-plastic, plastic and crushing.

3. Calculating and updating of stresses and stress-strain laws for elasticity, elasto-plasticity (flow rule) and plasticity.

4. Printing stresses and direction consines for cracks.

Subroutine CONMOD computes the Ottosen failure criterion of concrete behaviour based on the theory described in Section 2.3 - Failure Criterion in NONSAP. Subroutine RCMOD calculates the reinforced concrete material matrix based on the theory described in Section 2.4 - Reinforced Concrete Model for NONSAP. Subroutine CRACKD sets up the material matrices for cracked concrete based on the theory described in Section 2.5 - Concrete Cracking Model for NONSAP.

Some of the subroutines are listed in Appendix D. The operations for some of the subroutine are given in the following flowcharts:-

Table 6.2 - subroutine ELT3D4

Table 6.3 and 6.3a - subroutine RCRK3D

Table 6.2 Subroutine ELT3D4

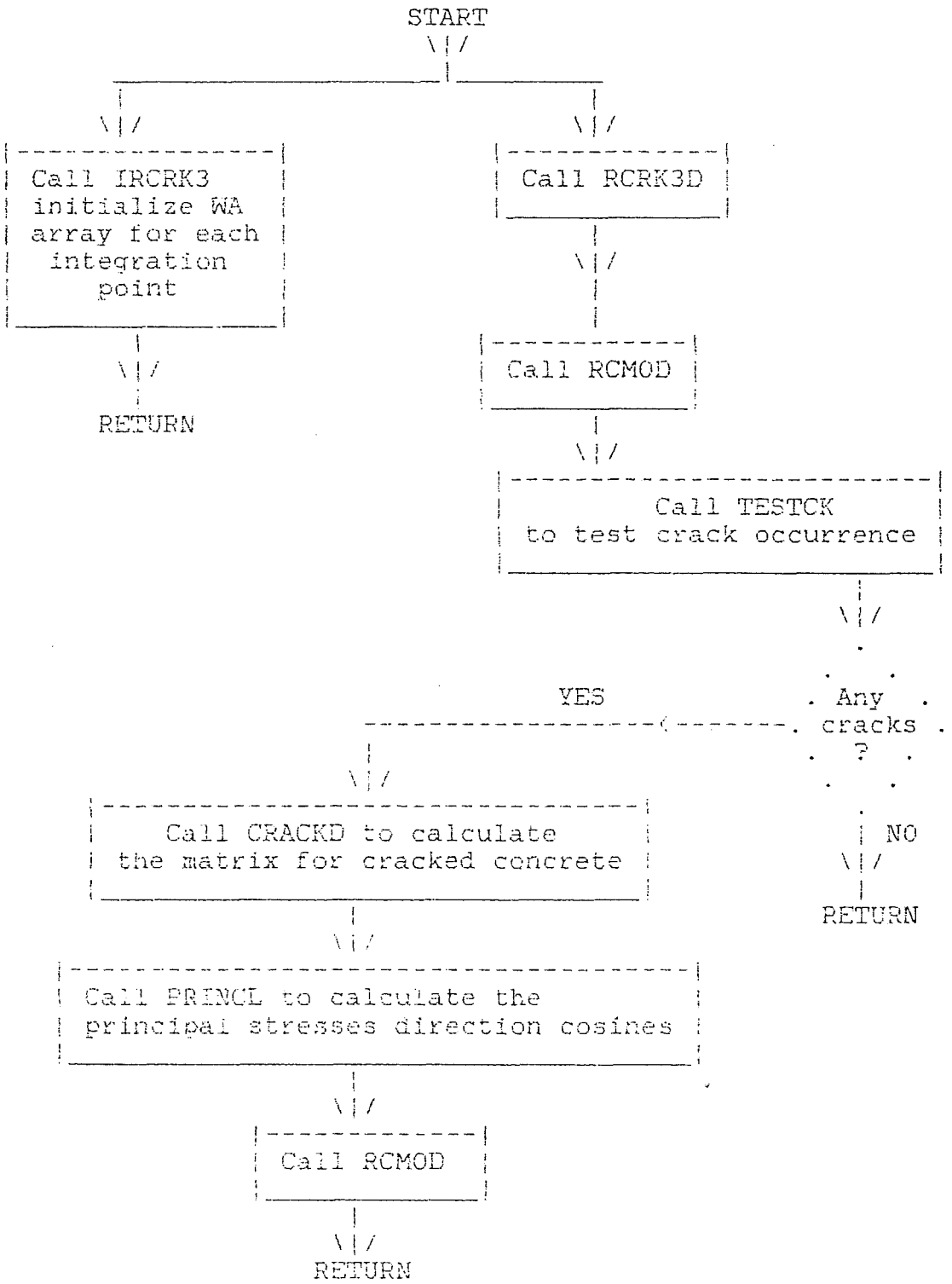

Table 6.3 Subroutine RCRK3D

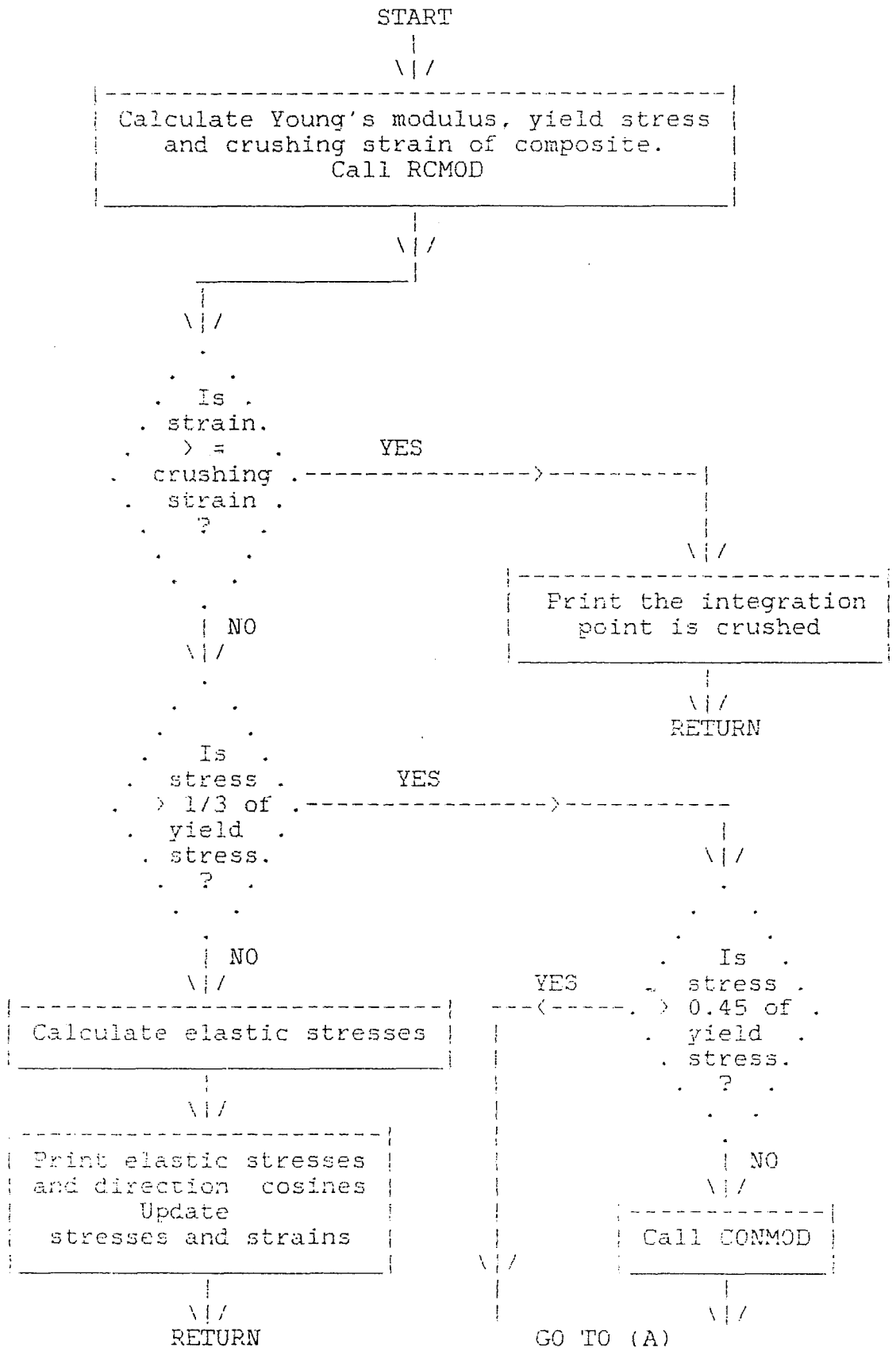

Table 6.3a Subroutine RCRK3D (Con't)

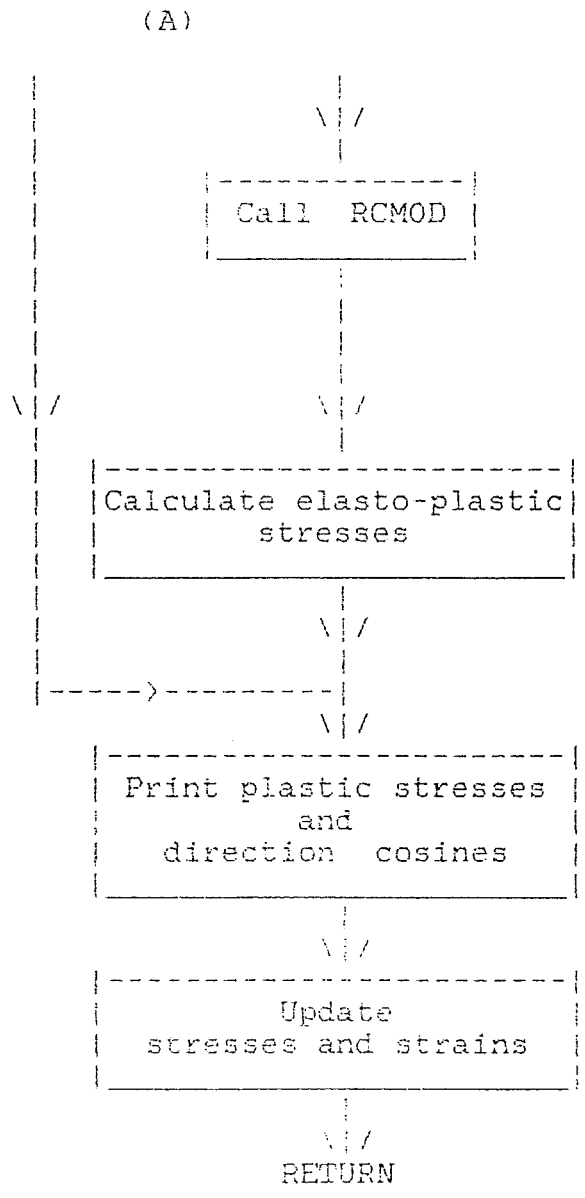

6.3 Program Description of MARC

Results from the well-known program MARC are included to compare with those obtained from the modified NONSAP. This process validates the modifications carried out in NONSAP by the author. Despite two different concrete failure criteria in NONSAP and MARC, the results from these two types of analysis, together with the experimental results, offer a comprehensive assessment of the response of reinforced concrete slabs subjected to impact loads.

MARC is a widely-used general purpose three-dimensional finite element package developed by MARC Analysis Research Corporation [198]. It can perform linear or non-linear stress analysis in both static and dynamic situations. It includes of a post-processor, MARC-PLOT, where the results are plotted in graphical form. MENTAT [199], a MARC interactive pre-processor, is used to generate meshes for the test models.

MARC has both in-core and out-of-core capabilities so that larger problems with moderate in-core allocation can also be solved. It also offers three integration methods (Newmark, Houbolt and Central Difference) - The Newmark method was chosen for the analysis. A number of three-dimensional solid elements are given in the MARC element library including heat transfer elements and elements for Mooney material formulation. In the current analysis, 20-noded, 27-Gaussian pointed (3 x 3 x 3) isoparametric brick elements were chosen.

As described in Section 2.6, Mohr-Coulomb failure criterion was used to represent the behaviour of concrete with Von Mises yield criterion representing the reinforcement behaviour in the body of the concrete element.

There are two user subroutines, REBAR and FORCDT, used in MARC analysis. Subroutine REBAR allows the user to input the reinforcement positions, areas and orientations. In this subroutine, the direction cosines of the tangent vector at each integration point are defined to indicate the axial orientation of the reinforcement at that integration point. It is sufficient enough to define the tangent components in the global system as the

normalisation is performed internally by the program. The position of the reinforcement is defined relatively to the thickness of the rebar element, which is the same thickness as the concrete element. The nominal area of the reinforcement is input by giving the relative area of the reinforcement to the concrete. For input, see Appendix E - Listing of MARC User Subroutines.

Subroutine FORCDT allows the user to input a time dependent load history in the MARC analysis. The nodes at which this load acts are specified in the input model card, FORCDT. The load-time function curve indicated in Fig. 4.10, is input in this subroutine by specifying the turning points of the curve. A straight line is assumed between two turning points. For input see Appendix G - Listing of MARC User Subroutines.

CHAPTER 7

ANALYSIS OF RESULTS

7.1 General Introduction

The results obtained from programs NONSAP and MARC on models B16 and B26 are given in this chapter. Results from NONSAP are compared with those from MARC. Both results are then compared with the experimental results provided by the UKAEA at Winfrith.

7.2 Modal Analysis

Five critical modes were obtained for both models using MARC. The mode shapes of B16 are listed in Figs. 7.1 to 7.5. The natural frequencies are tabulated as follows:-

Mode	Natural Frequency (rad/sec.)	
	Model B16	Model B26
1	1024.6	918.5
2	4452.8	4085.6
3	4943.3	4587.5
4	4943.3	5035.9
5	4959.3	5491.8

7.3 NONSAP Results

Fig. 7.5a shows the locations of displacement transducers in relation to the nodes of the model B16 and B26. Results from the computer output are expressed in graphical form which are listed as follows:-

Disp. Vs time from model B16 at nodes 119,204 and 247	(Fig. 7.6)
Disp. Vs time from model B16 at nodes 154,226 and 263	(Fig. 7.7)
Disp. Vs time from model B26 at nodes 204 and 247	(Fig. 7.8)
Disp. Vs time from model B26 at nodes 226 and 263	(Fig. 7.9)
Velocity Vs time from model B16 at nodes 119,204 and 247	(Fig. 7.10)
Velocity Vs time from model B16 at nodes 154,226 and 263	(Fig. 7.11)
Velocity Vs time from model B26 at nodes 204 and 247	(Fig. 7.12)
Velocity Vs time from model B26 at nodes 226 and 263	(Fig. 7.13)
Acc. Vs time from model B16 at nodes 119,204 and 247	(Fig. 7.14)
Acc. Vs time from model B16 at nodes 154,226 and 263	(Fig. 7.15)
Acc. Vs time from model B26 at nodes 204 and 247	(Fig. 7.16)
Acc. Vs time from model B26 at nodes 226 and 263	(Fig. 7.17)
Cracks on top face of the model B16	(Fig. 7.18)
Cracks on bottom face of the model B16	(Fig. 7.19)
Cracks and crushed areas of the model B16	(Fig. 7.20)
Cracks on top face of the model B26	(Fig. 7.21)
Cracks on bottom face of the model B26	(Fig. 7.22)
Cracks and crushed areas of the model B26	(Fig. 7.23)

7.4 MARC Results

The results of displacements, velocities and accelerations are plotted using the MARC post-processor, MARC-PLOT and the crack orientations from computer output are expressed in graphical forms. Some of these are given below:-

Disp. Vs time from model B16 at nodes 119,204 and 247 (Fig. 7.24)
Disp. Vs time from model B16 at nodes 154,226 and 263 (Fig. 7.25)
Disp. Vs time from model B26 at nodes 204 and 247 (Fig. 7.26)
Disp. Vs time from model B26 at nodes 226 and 263 (Fig. 7.27)
Velocity Vs time from model B16 at nodes 119,204 and 247 (Fig. 7.28)
Velocity Vs time from model B16 at nodes 154,226 and 263 (Fig. 7.29)
Velocity Vs time from model B26 at nodes 204 and 247 (Fig. 7.30)
Velocity Vs time from model B26 at nodes 226 and 263 (Fig. 7.31)
Acc. Vs time from model B16 at nodes 119,204 and 247 (Fig. 7.32)
Acc. Vs time from model B16 at nodes 154,226 and 263 (Fig. 7.33)
Acc. Vs time from model B26 at nodes 204 and 247 (Fig. 7.34)
Acc. Vs time from model B26 at nodes 226 and 263 (Fig. 7.35)
Cracks on top face from model B16 (Fig. 7.36)
Cracks on middle face from model B16 (Fig. 7.37)
Cracks on bottom face from model B16 (Fig. 7.38)
Cracks and crushed areas of the model B16 (Fig. 7.39)
Cracks on top face from model B26 (Fig. 7.40)
Cracks on middle face from model B26 (Fig. 7.41)
Cracks on bottom face from model B26 (Fig. 7.42)
Cracks and crushed areas of the model B16 (Fig. 7.43)

7.5 Comparison of NONSAP and MARC

Nodes 119,154,204,226,247 and 263 are chosen to output the displacements, velocities and accelerations because they are the nearest nodes to the locations of the displacement transducers of the experimental slabs. (See Fig. 7.5a). The maximum values of displacements, velocities and accelerations are summaried as follows:-

Model B16

	NONSAP			MARC		
	Disp. (mm)	Vel. (mm/s)	Acc. (mm/s^2)	Disp. (mm)	Vel. (mm/s)	Acc. (mm/s^2)
Nodes						
119	-4.15	1480.0	-920000.0	-5.60	1890.0	-1300000.0
154	-3.55	1340.0	-680000.0	-4.93	1666.7	-1080000.0
204	-2.90	1000.0	-240000.0	-4.05	1286.7	-802500.0
226	-2.65	690.0	120000.0	-3.68	1233.3	805000.0
247	-1.60	520.0	740000.0	-2.28	866.7	495000.0
263	-1.45	500.0	720000.0	-2.00	666.7	460000.0

Model B26

	NONSAP			MARC		
	Disp. (mm)	Vel. (mm/s)	Acc. (mm/s^2)	Disp. (mm)	Vel. (mm/s)	Acc. (mm/s^2)
Nodes						
204	-4.58	1485.0	780000.0	-5.90	2240.0	1016667.0
226	-4.10	1652.0	820000.0	-5.27	2240.0	1040000.0
247	-2.35	920.0	500000.0	-3.14	2356.0	1833333.0
263	-2.13	1400.0	510000.0	-2.08	2192.0	1070000.0

It can be seen from these results that MARC predicts higher values when compared to NONSAP. The differences are of the order of 25-35%. The peaks of displacements appear at about 0.006 second of total impact time in both NONSAP and MARC analyses. Zero velocities also appear at about this time for both analyses. There are two high peaks in each of the acceleration-time curves. In both the analyses, the first peak appears at about 0.001 second. The second peak appears at about 0.006 second in the MARC analysis but in NONSAP it appears at just before the value of 0.006 second.

The curves for model B16 have many similarities using both NONSAP and MARC analyses. However, for model B26, they appear to give slightly different results, especially towards the end of the analysis. In both analyses, before 0.006 second, velocities and accelerations graphs follow the same trend as for model B16. After

this time, NONSAP results still appear to follow the trend of model B16 but MARC results show slightly different behaviour. For model B26, in the NONSAP analysis, at the end of the impact, the nodes nearer to the impact zone have higher velocities and accelerations than those further away. In the MARC analysis, all the nodes very give close velocities at the end of the impact.It is also noticeable that in the MARC analysis towards the end of the impact time, the accelerations of nodes 226 and 204 drop considerably, while those of nodes 247 and 263 rise shapely.

From the output of cracks, it can be seen that the crushed zones produced by NONSAP analysis are greater than those produced by MARC analysis. Despite the fact that the MARC elements have more integration points with more cracks than the NONSAP analyses, it appears that more cracks have been found near the impact area using both analyses. Both analyses produced more cracks for model B26 than model B16. All the crack orientations tend to follow a similar pattern which is around 45 degree to the centre of the impact point.

7.6 Comparison of NONSAP, MARC and Experimental Results

Since the displacement transducers are located between nodes 119, 154, 204, 226, 247 and 263, interpolation was necessary to calculate the values of displacements from these nodes for comparison with those from transducers W1 and W3. The maximum values are summaried below:-

	B16 Maximum Displacement (mm)		
	NONSAP	MARC	Experimental
Location			
W1	-2.00	-2.61	-1.99 (average of W1,W2,W7,W8)
W3	-4.05	-5.32	< -4.0 (maximum values off graphs)

	B26 Maximum Displacement (mm)		
	NONSAP	MARC	Experimental
Location			
W1	-3.00	-3.92	-4.70 (average of W1,W2,W7,W8)

Reference is made to Figs. 7.44 to 7.50 for a comparative study of the two analyses. For model B16, NONSAP produces a very close set

of displacements to those obtained experimentally, while MARC produces higher displacements. For model B26, both NONSAP and MARC give lower displacements than those obtained from experiment but MARC give a closer value than NONSAP. For model B16 both MARC and NONSAP tend to produce more cracks than the experimental results. For model B26, both NONSAP and MARC produce close crack patterns to those obtained experimentally. Figs. 7.51 to 7.54 show the slabs after the experimental tests.

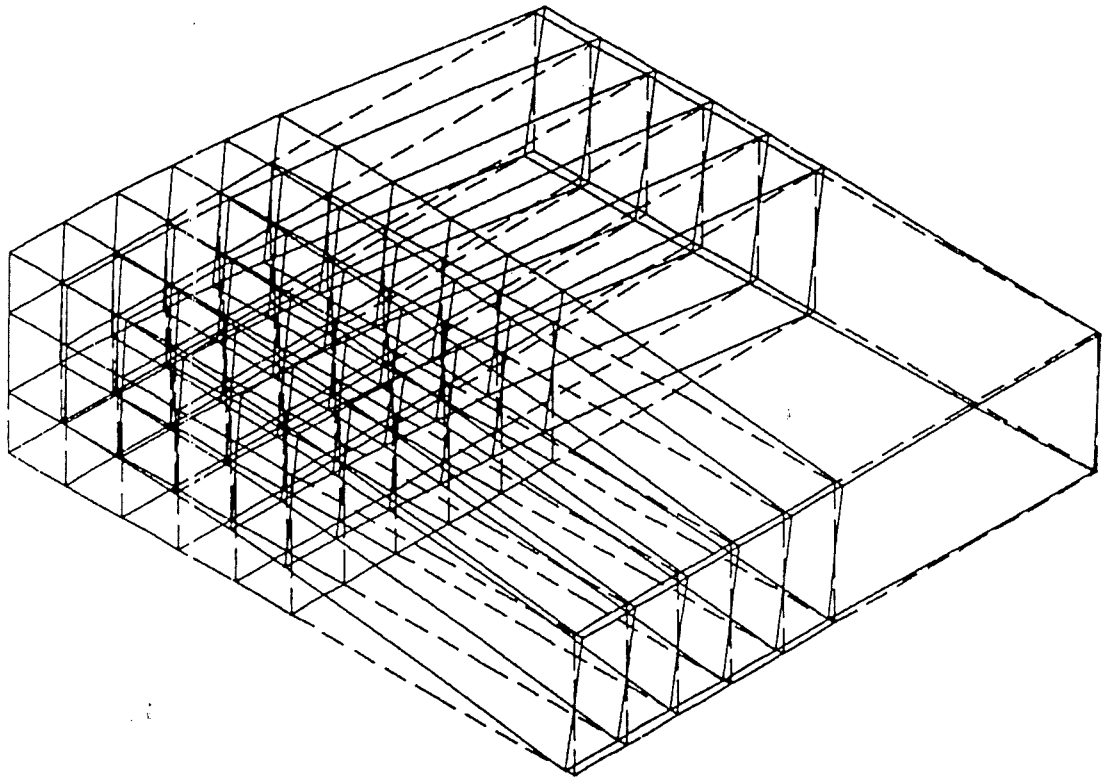

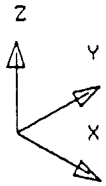

FIG 7.1 MODE 1 OF TARGET B16

DYN. MODE

ORTHO V.P. 1.0000 -1.000 1.0000

INCREM 0 SUBINC 2 TIME 0.0 FREQ 4.4528+3

MENTAT

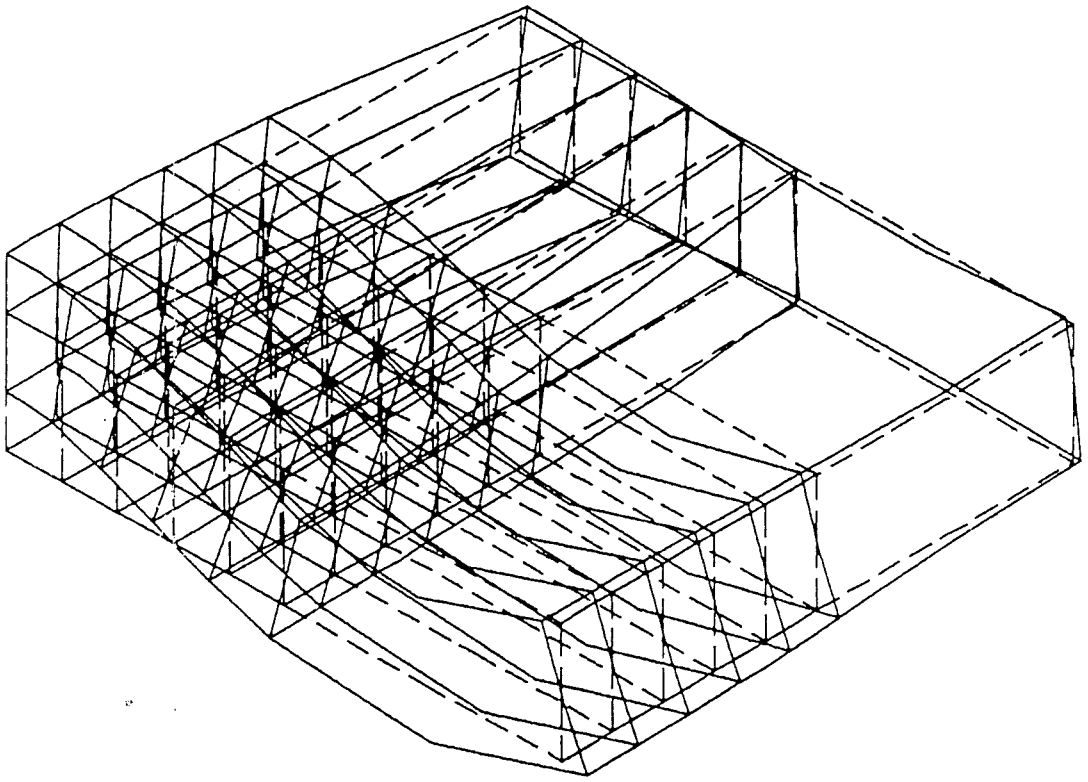

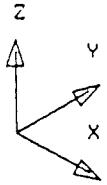

FIG. 7.2 MODE 2 OF TARGET B16

DYN. MODE

ORTHO V.P. 1.0000 -1.000 1.0000

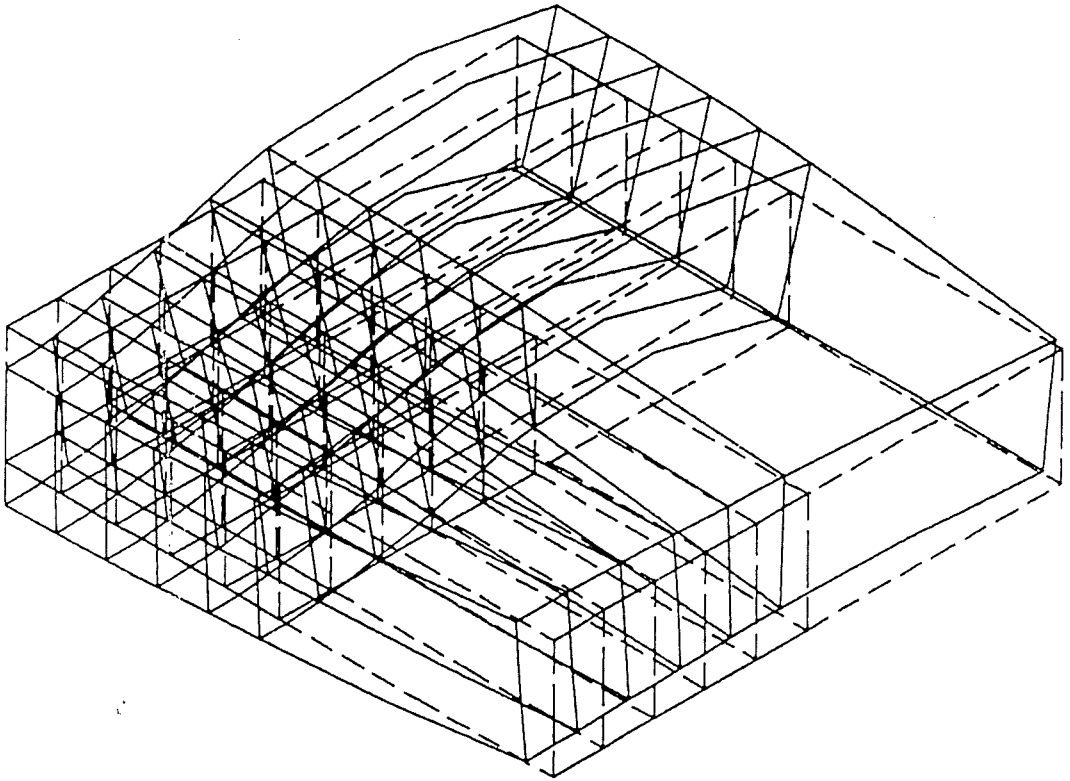

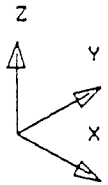

FIG. 7.3 MODE 3 OF TARGET B16

DYN. MODE

ORTHO V.P. 1.0000 -1.000 1.0000

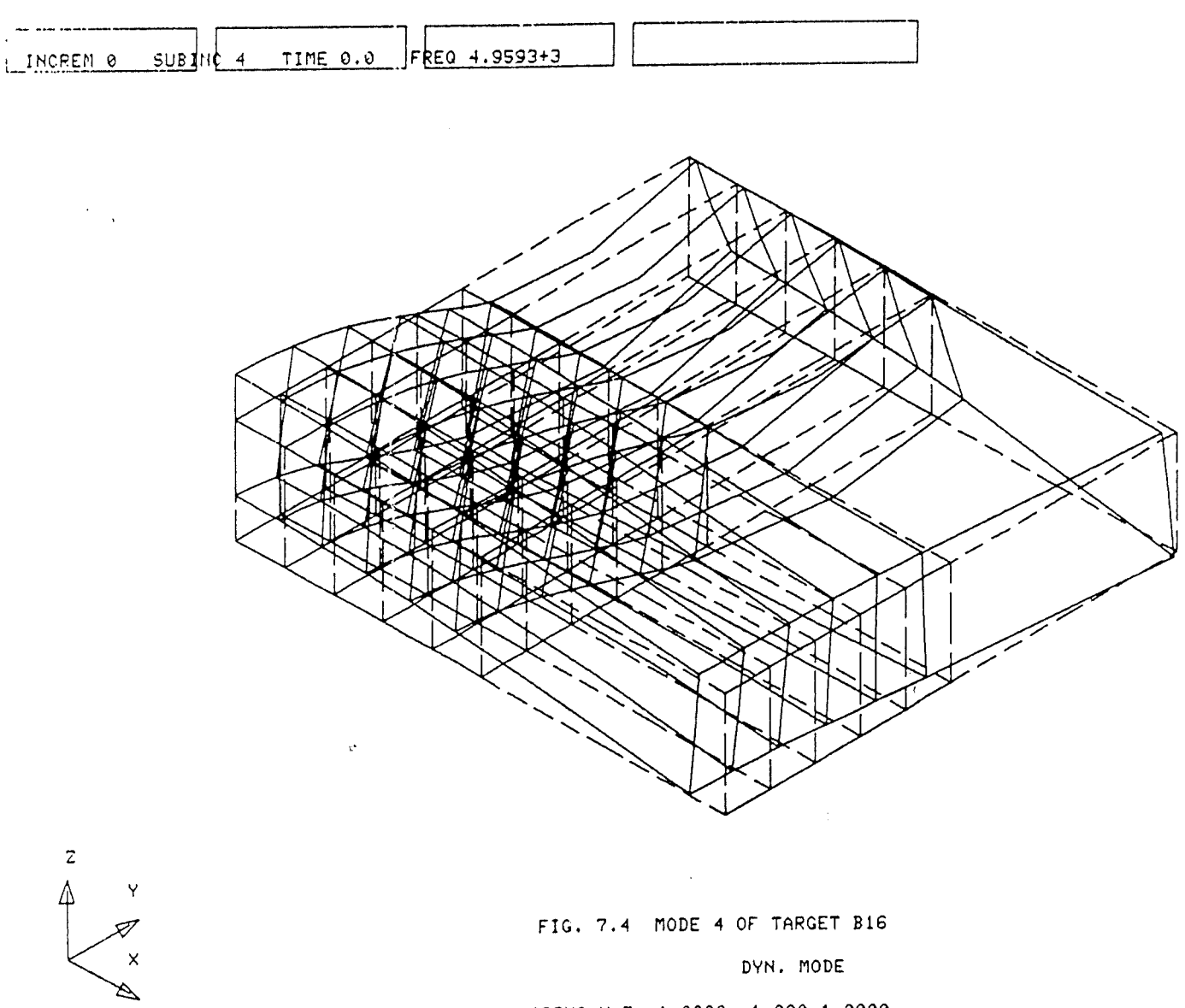

FIG. 7.4 MODE 4 OF TARGET B16

DYN. MODE

ORTHO V.P. 1.0000 -1.000 1.0000

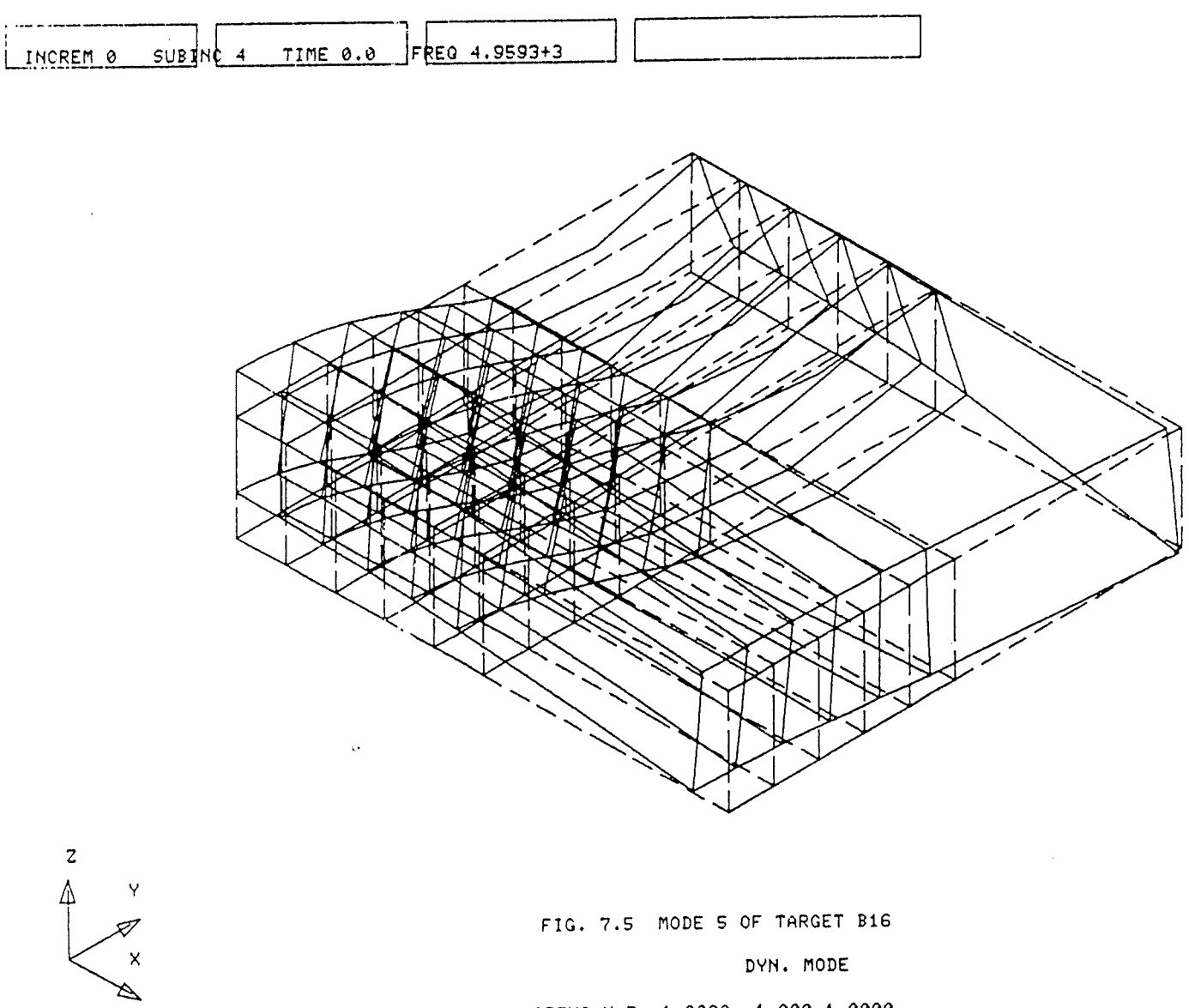

FIG. 7.5 MODE 5 OF TARGET B16

DYN. MODE

ORTHO U.P. 1.0000 -1.000 1.0000

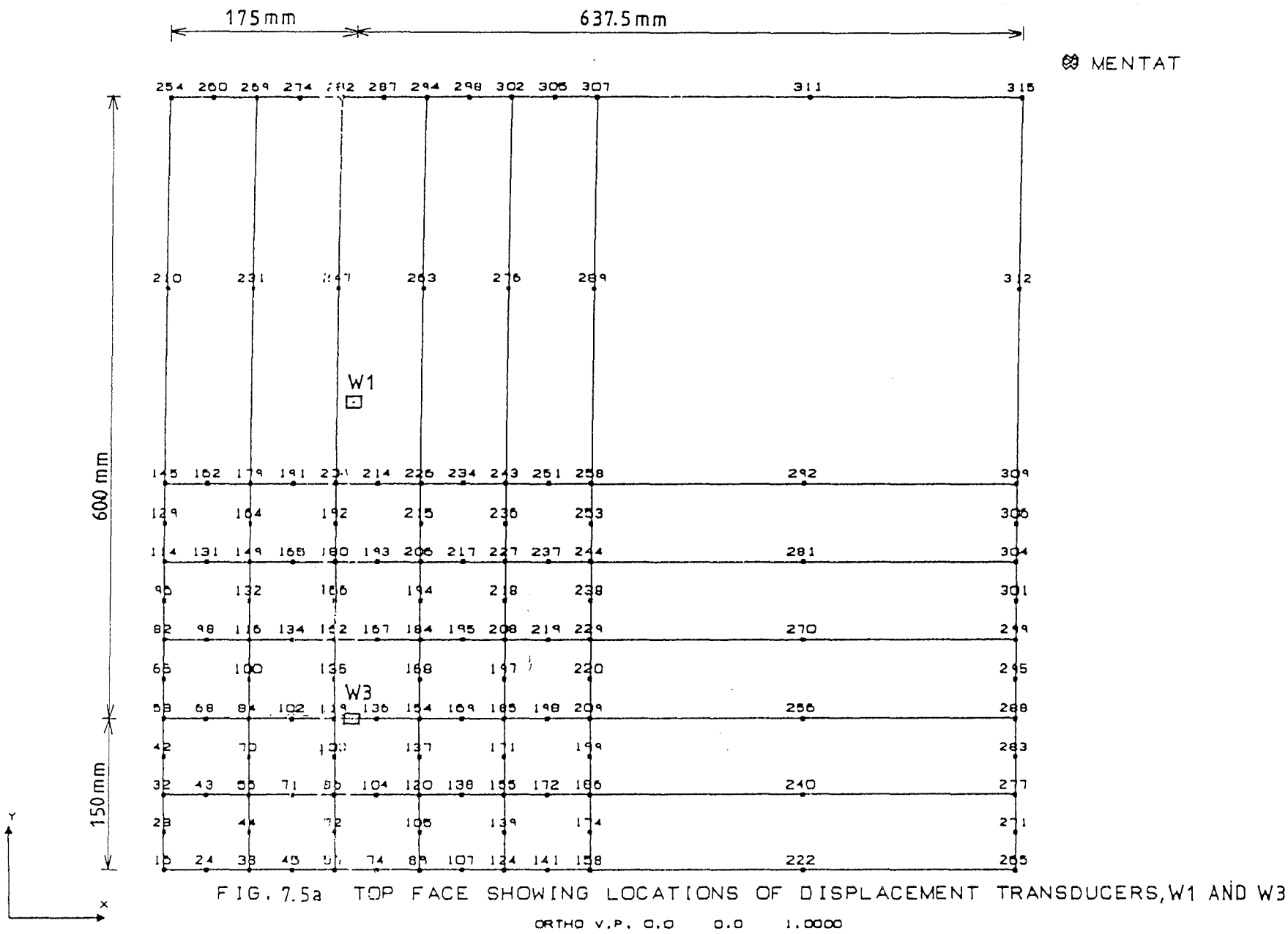

FIG. 7.5a TOP FACE SHOWING LOCATIONS OF DISPLACEMENT TRANSDUCERS, W1 AND W3

ORTHO V.P. 0.0 0.0 1.0000

Fig. 7.6

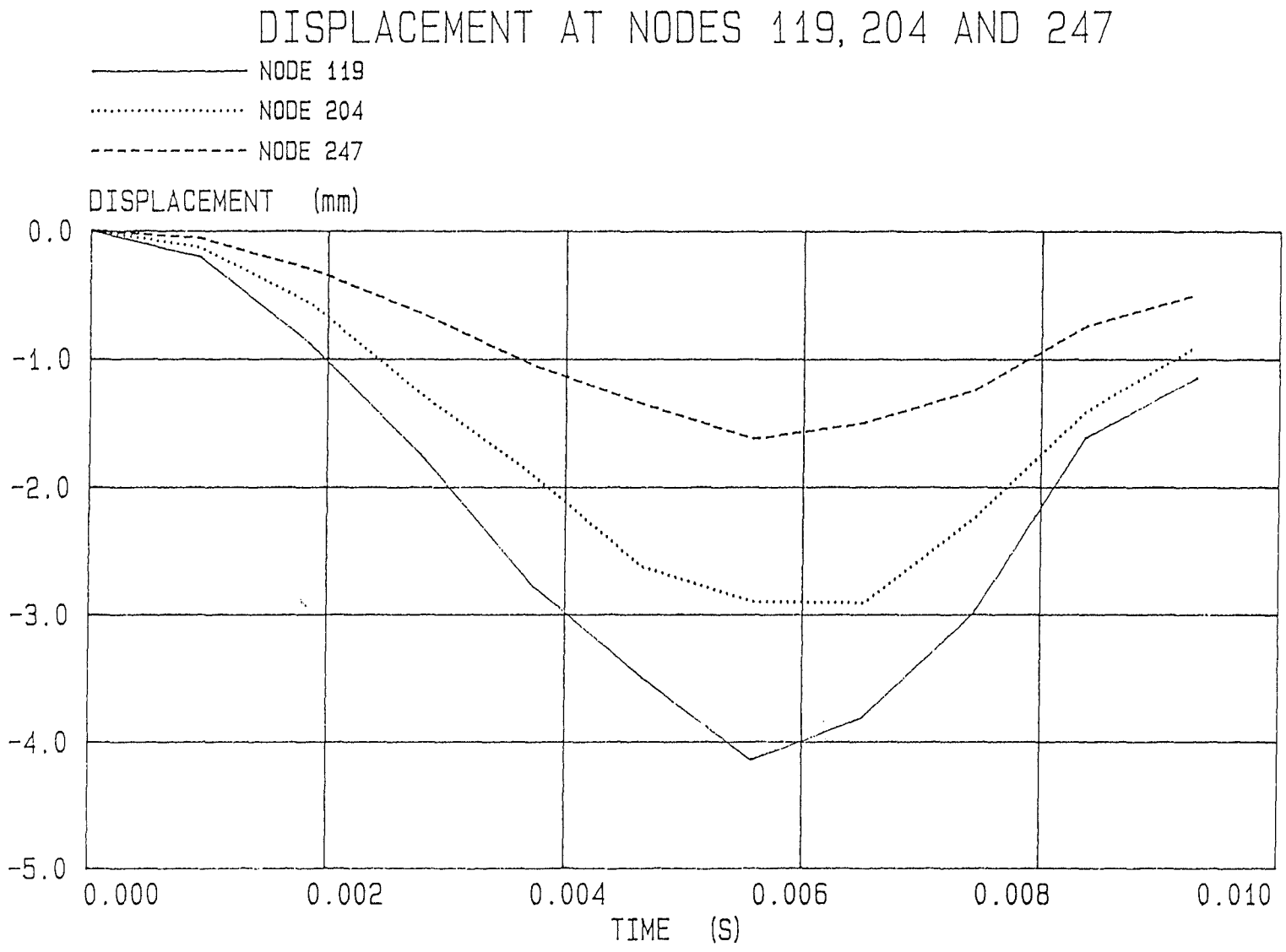
DISPLACEMENT AT NODES 119, 204 AND 247
NODE 119
NODE 204
NODE 247
DISPLACEMENT (mm)
0.0
-1.0
-2.0
-3.0
-4.0
-5.0
0.000
0.002
0.004
0.006
0.008
0.010
TIME (S)

NONB16 DISP
DISPLACEMENT AT Z-DIRECTION

Fig. 7.7

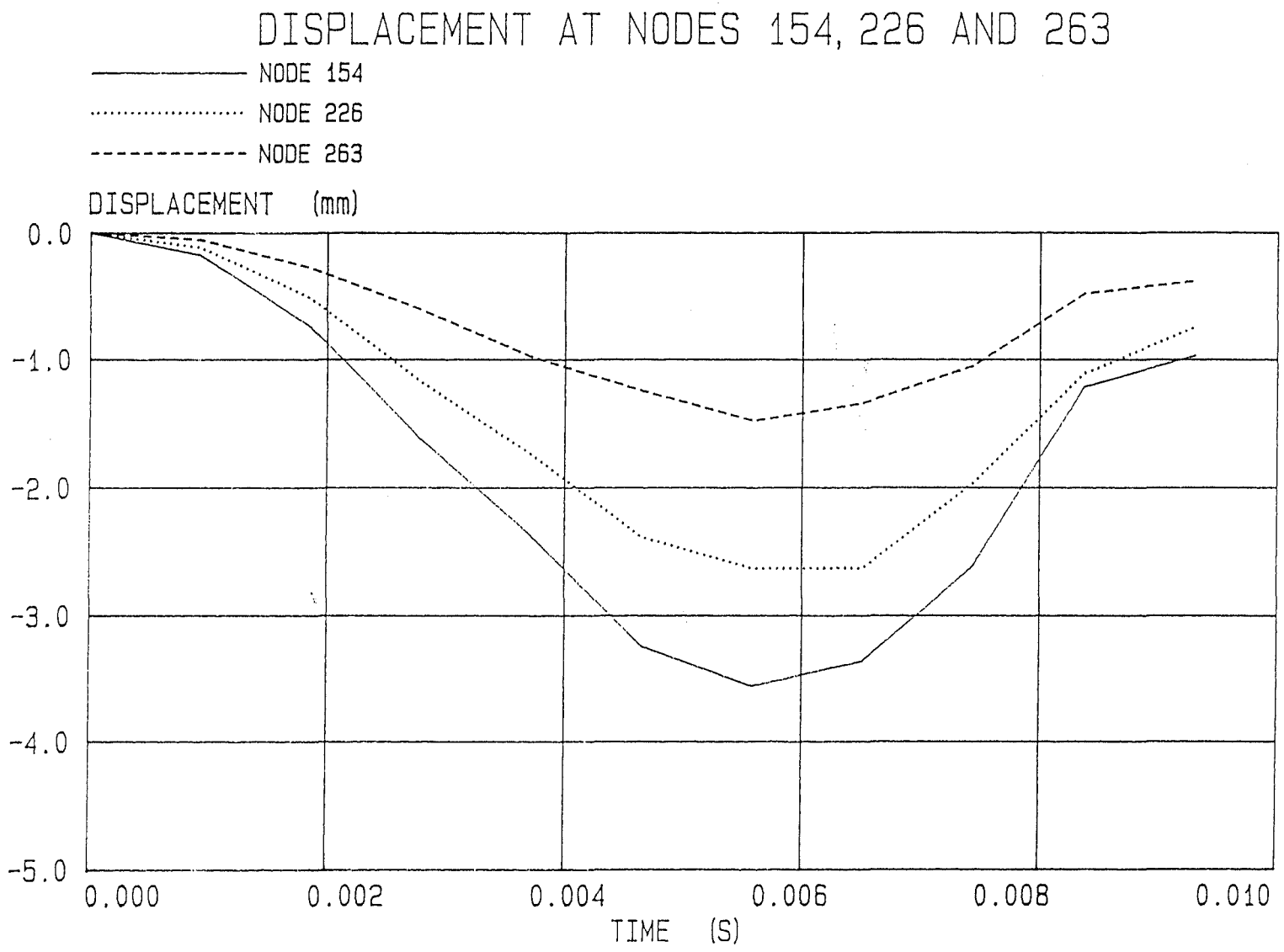

NONB26 DISP
DISPLACEMENT AT Z-DIRECTION

Fig. 7.8

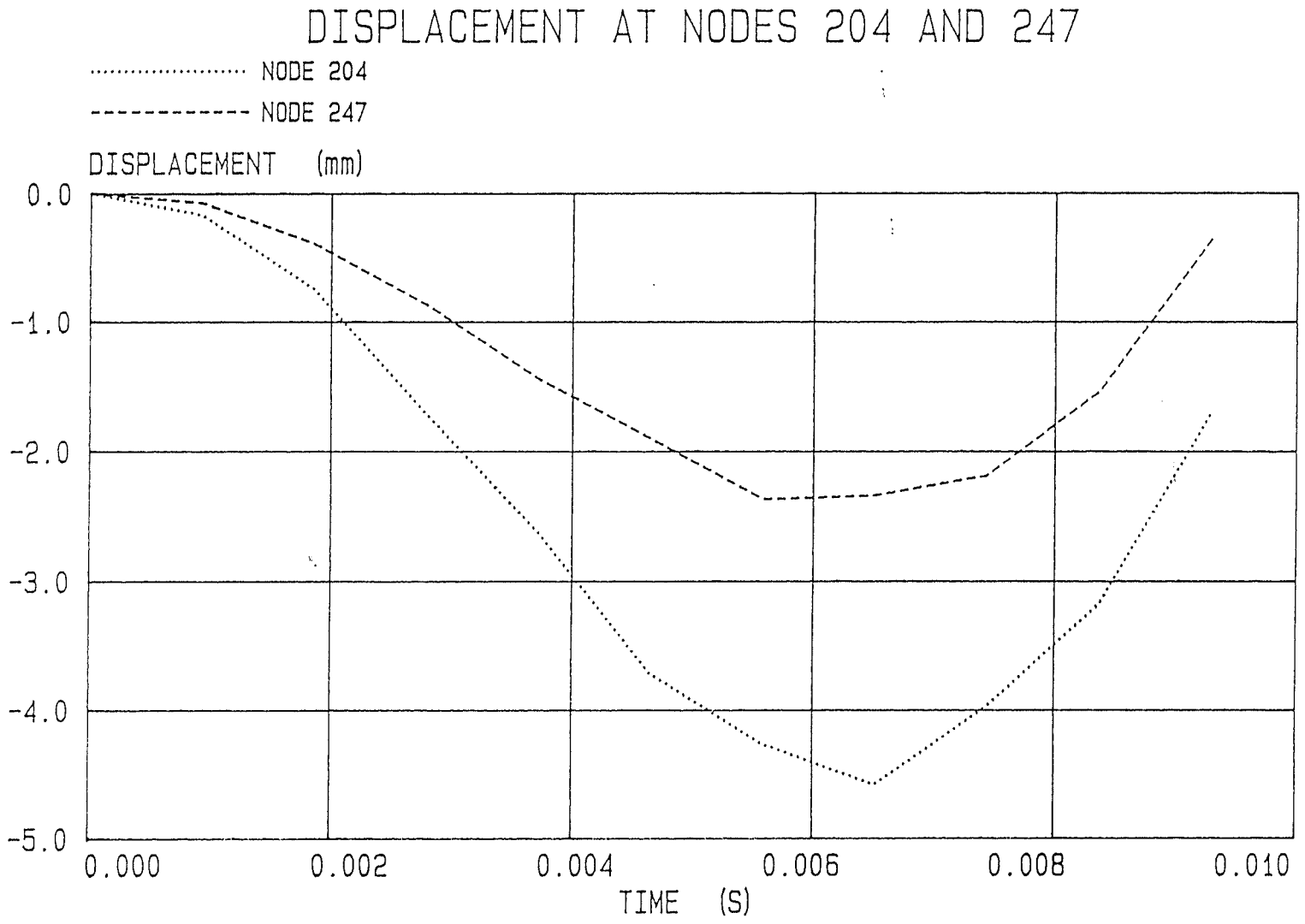

Fig. 7.9

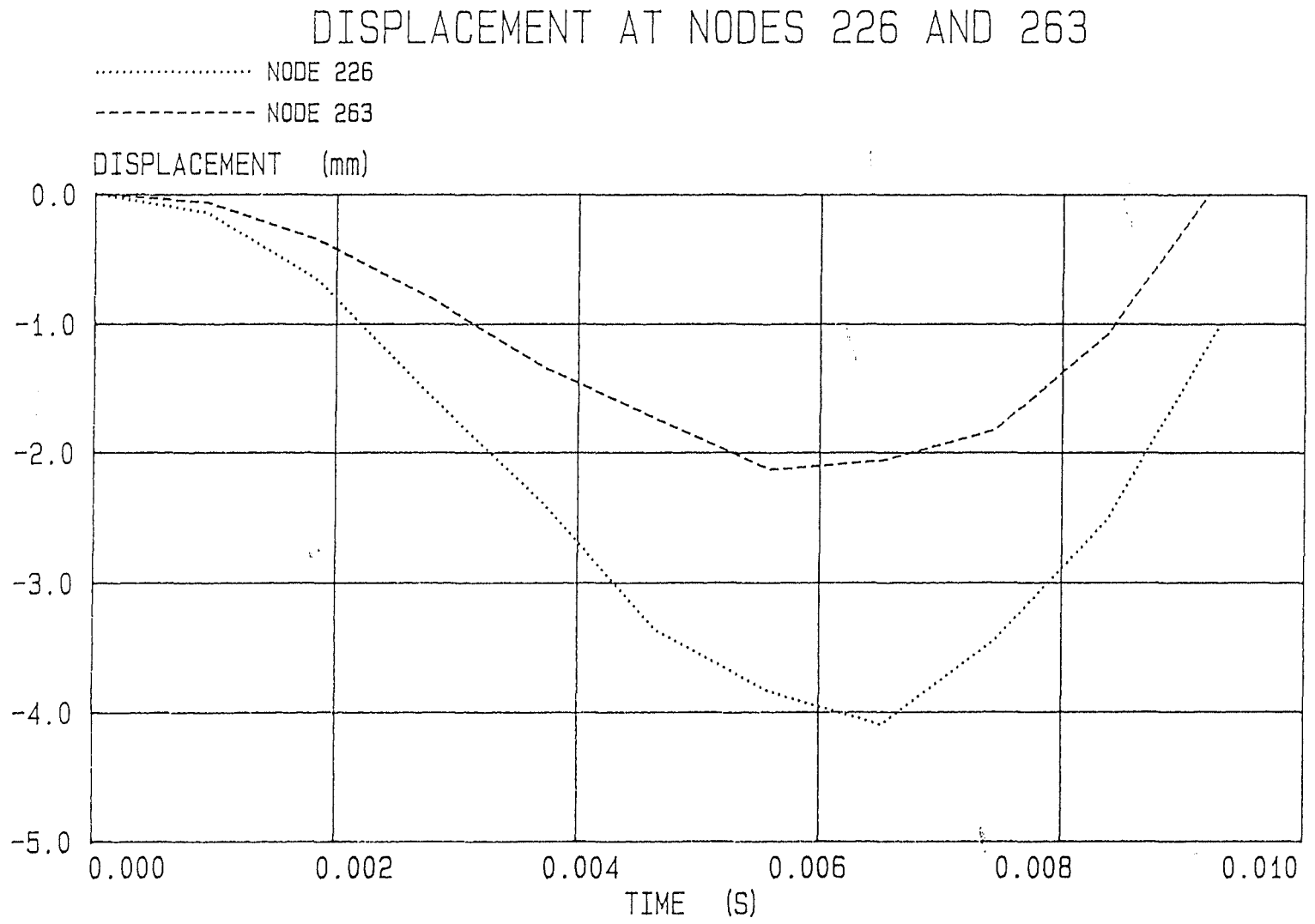
DISPLACEMENT AT NODES 226 AND 263
NODE 226
NODE 263
DISPLACEMENT (mm)
0.0
-1.0
-2.0
-3.0
-4.0
-5.0
0.000
0.002
0.004
0.006
0.008
0.010
TIME (S)

NONB16 VEL
VELOCITY AT Z-DIRECTION

Fig. 7.10

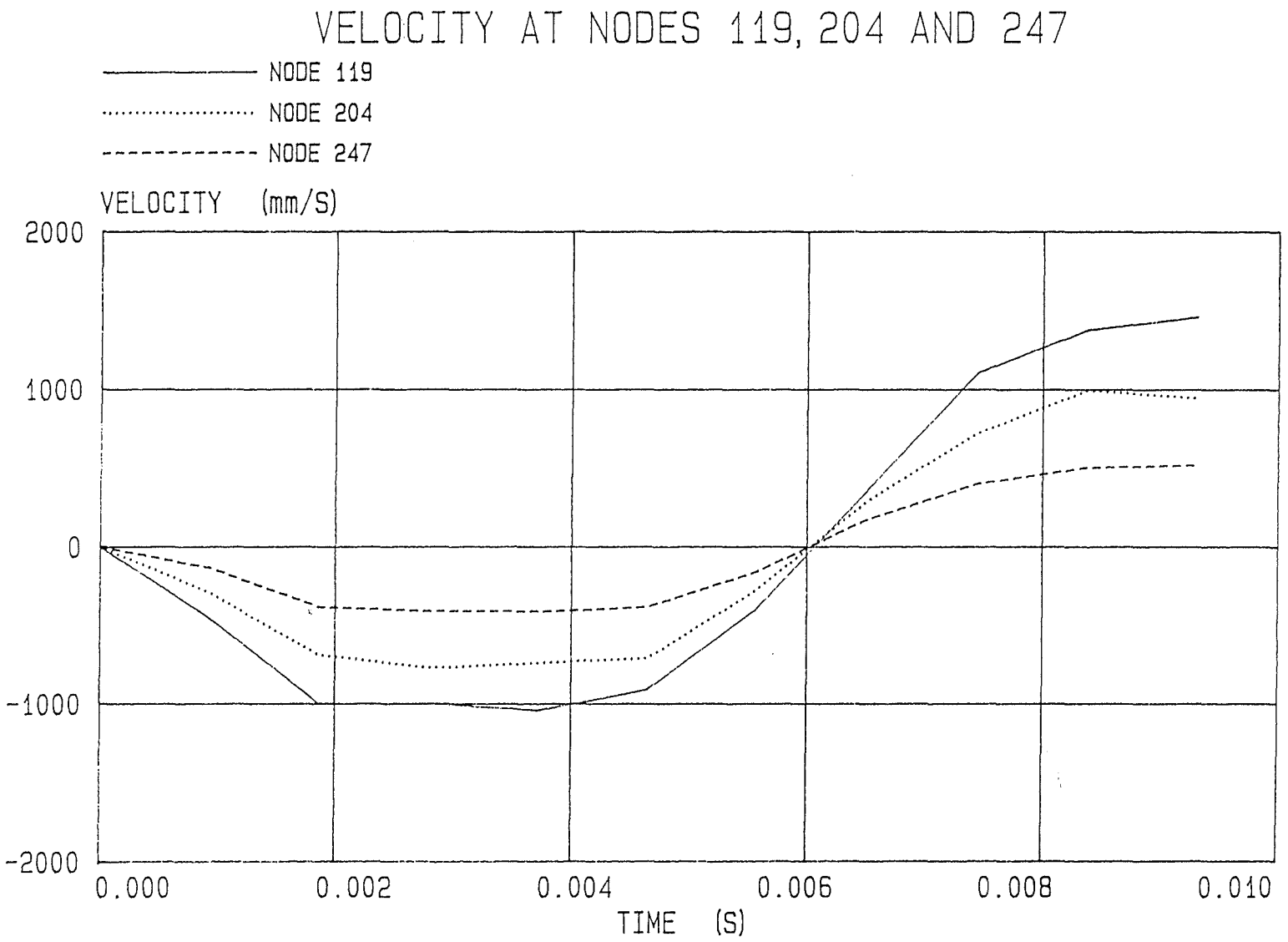

NONB16 VEL
VELOCITY AT Z-DIRECTION

Fig. 7.11

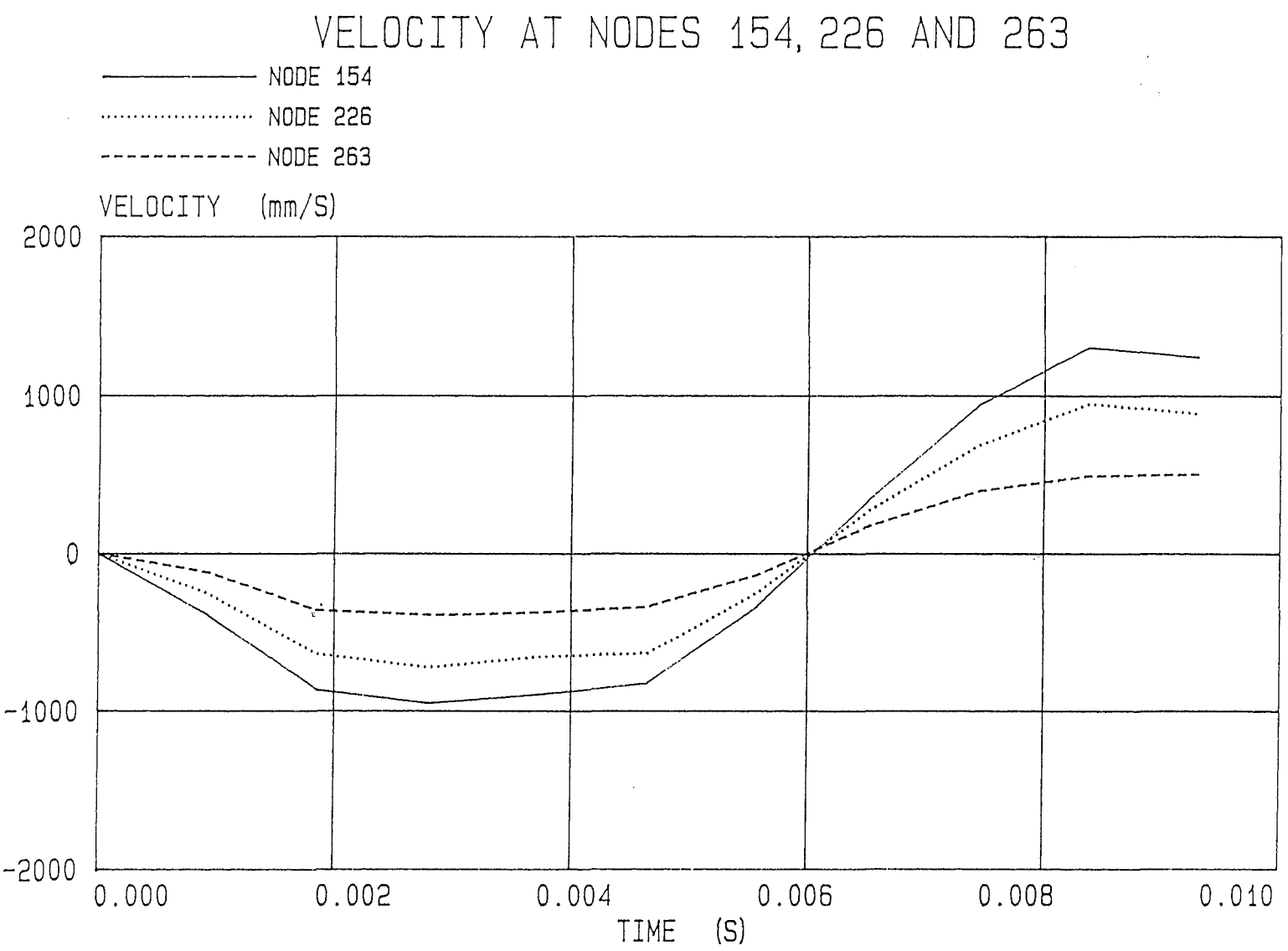

NONB26 VEL
VELOCITY AT Z-DIRECTION

Fig. 7.12

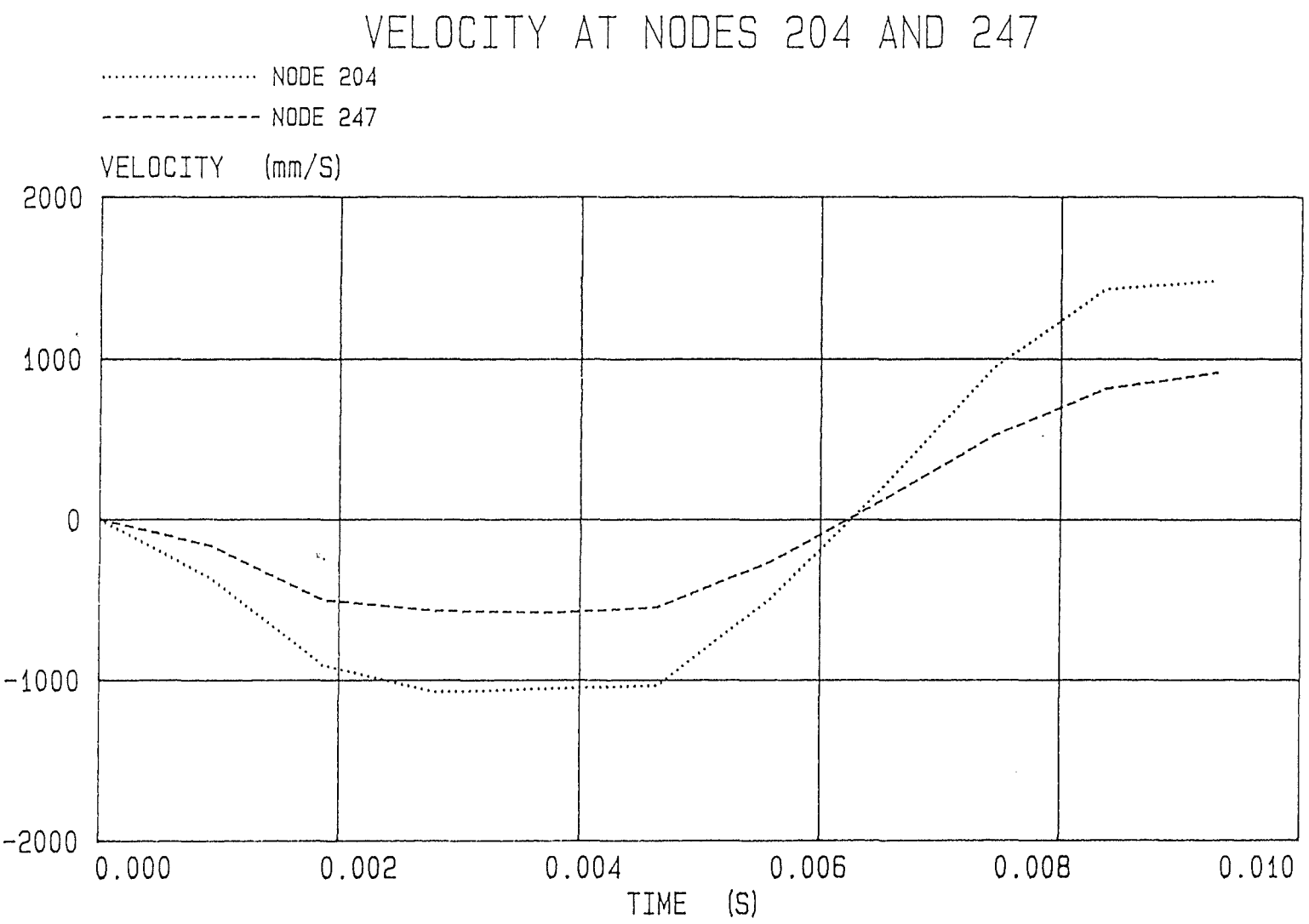

NONB26 VEL
VELOCITY AT Z-DIRECTION

Fig. 7.13

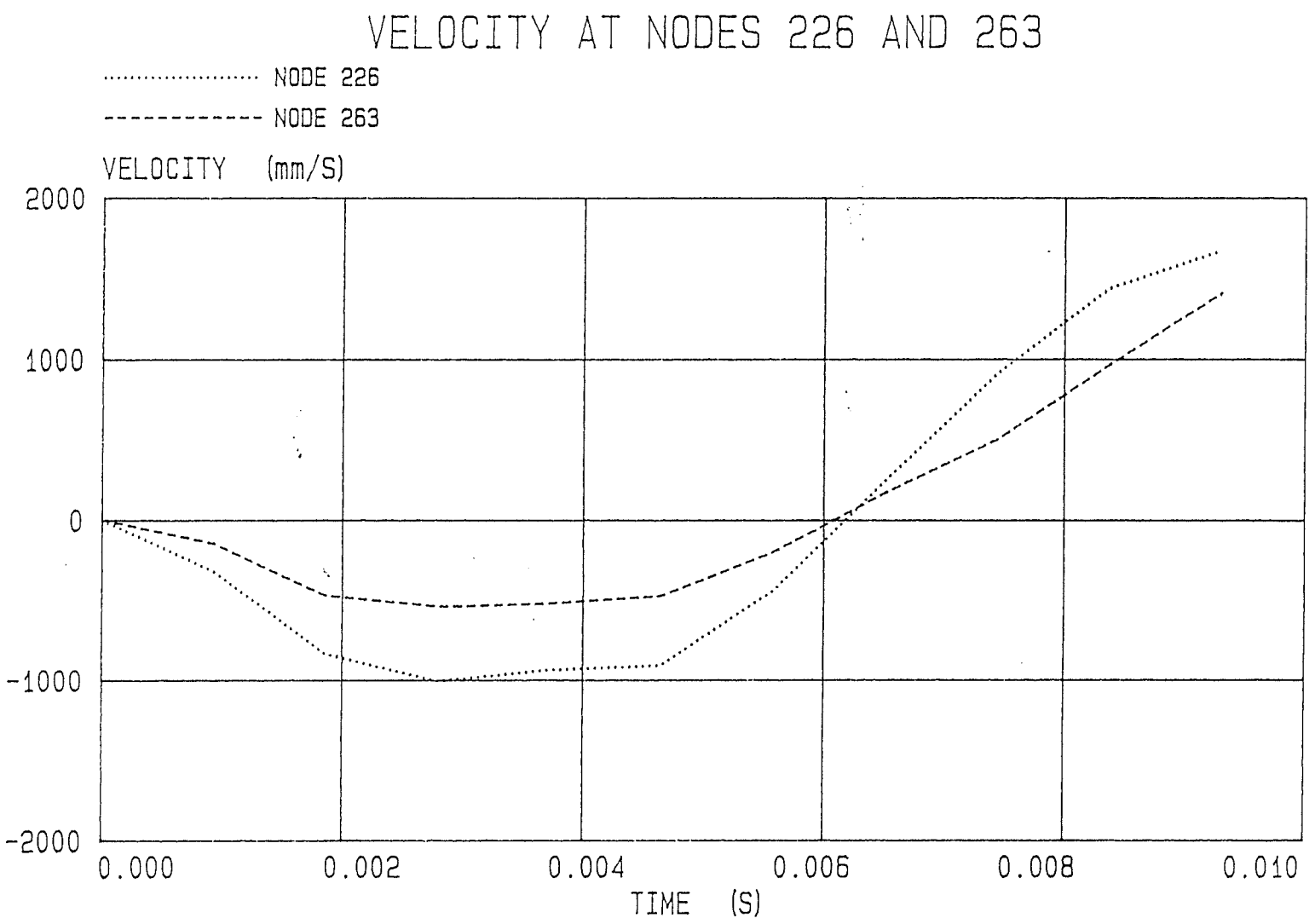

Fig. 7.14

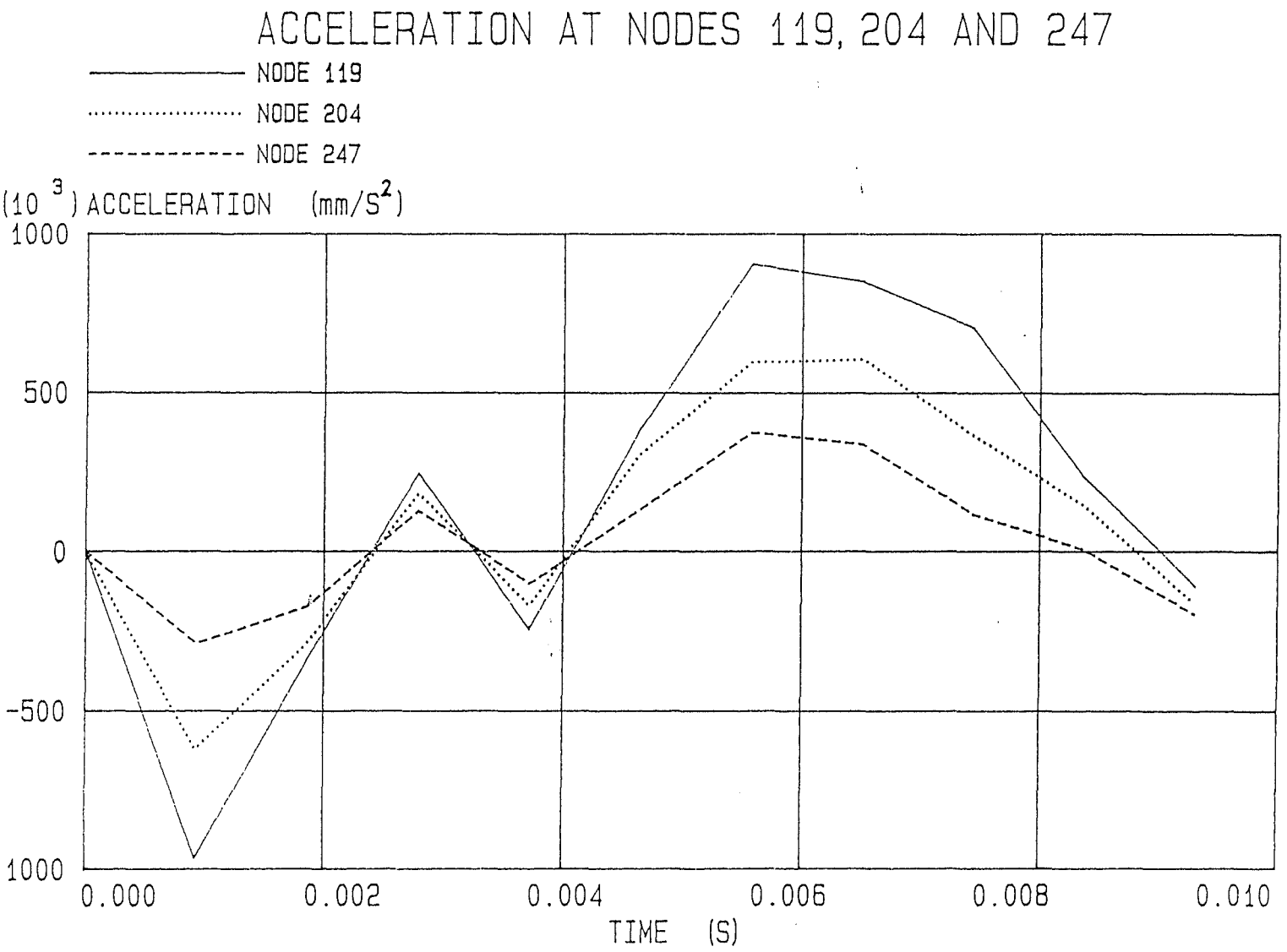
ACCELERATION AT NODES 119, 204 AND 247
NODE 119
NODE 204
NODE 247
(10 3) ACCELERATION (mm/S2)
1000
500
0
-500
1000
0.000
0.002
0.004
0.006
0.008
0.010
TIME (S)

NONB16 ACC
ACCELERATION AT Z-DIRECTION

Fig. 7.15

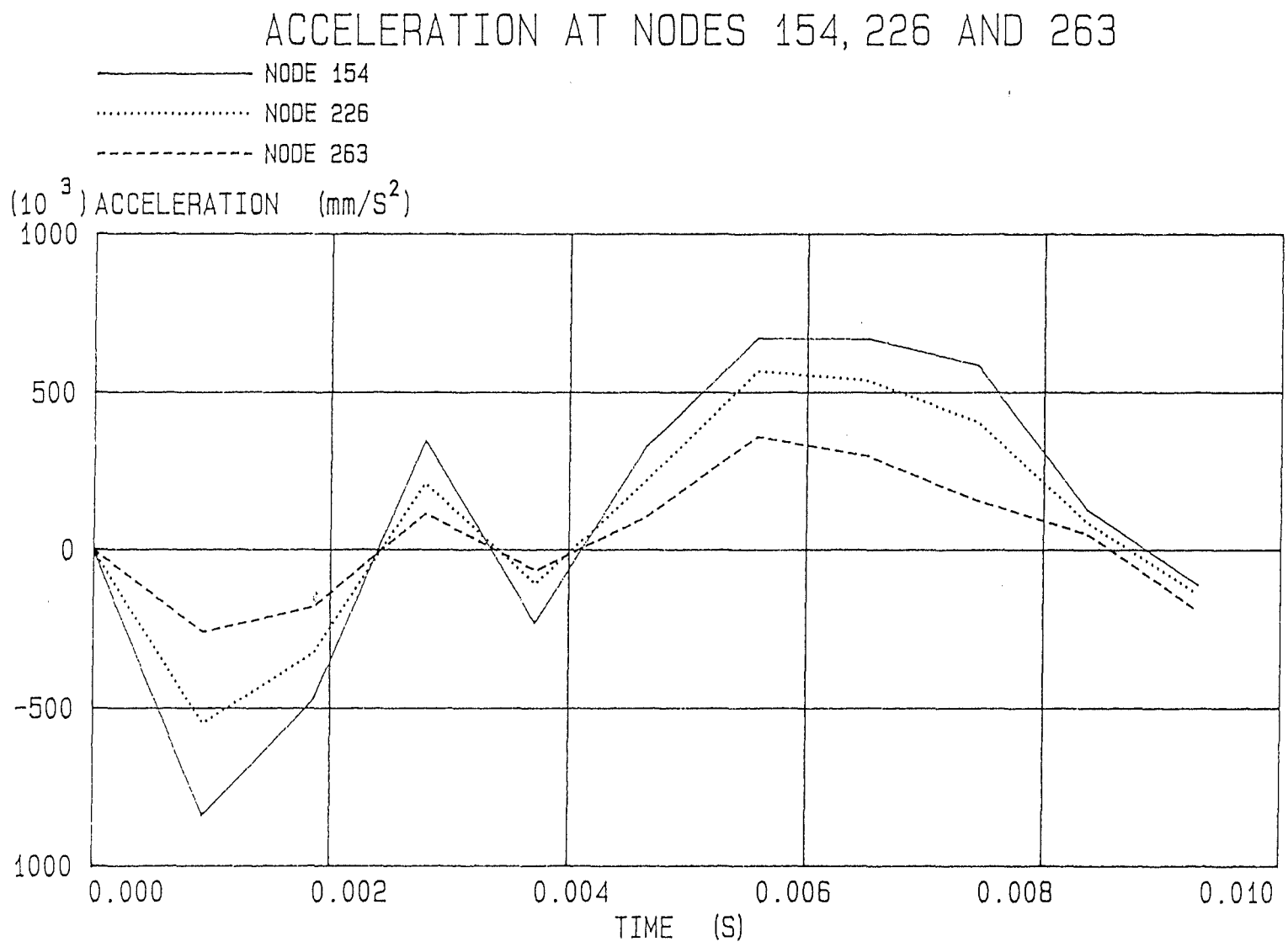

Fig. 7.16

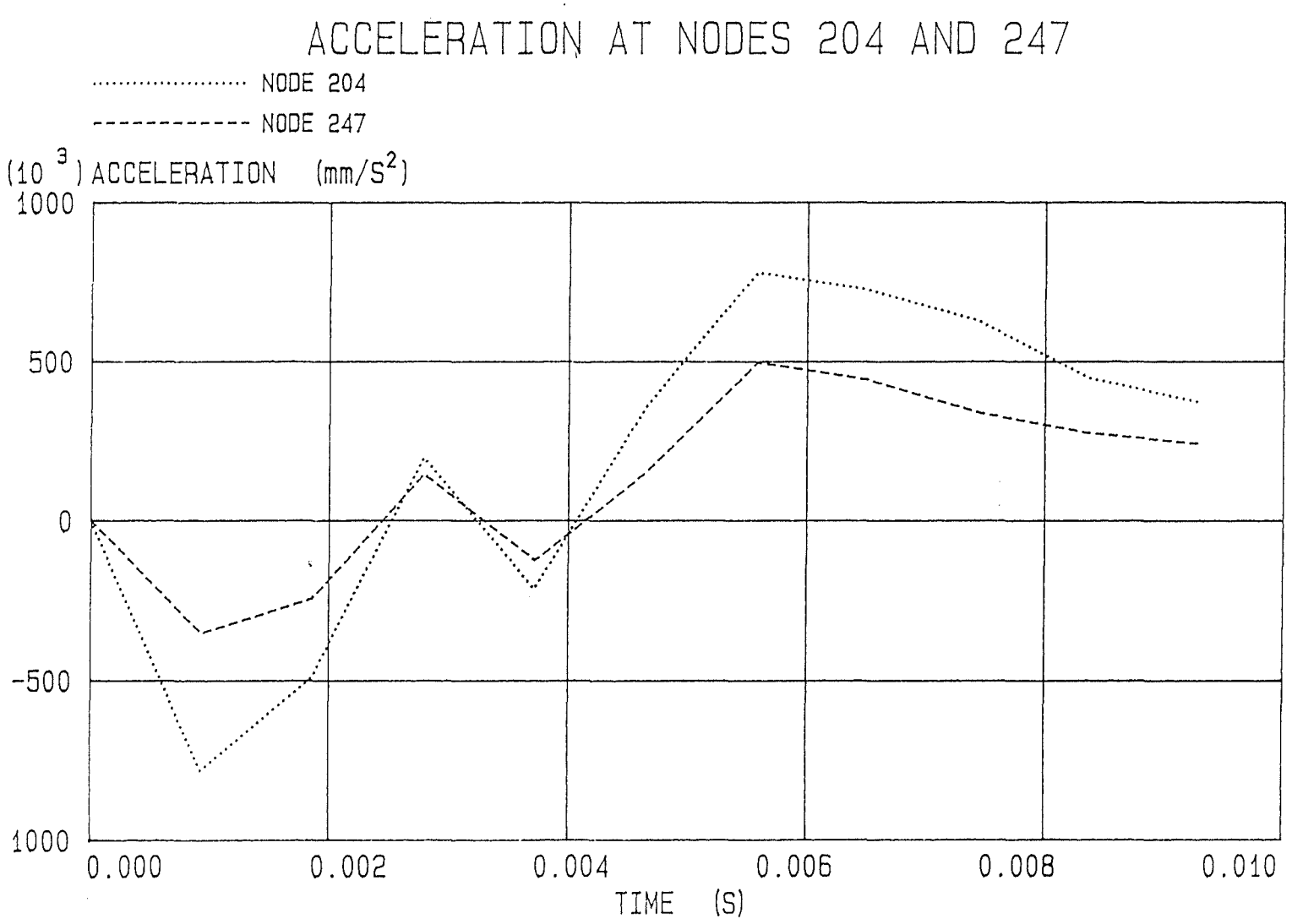
ACCELERATION AT NODES 204 AND 247
NODE 204
NODE 247
(10 3) ACCELERATION (mm/S2)
1000
500
0
-500
1000
0.000
0.002
0.004
0.006
0.008
0.010
TIME (S)

NONB26 ACC
ACCELERATION AT Z-DIRECTION

Fig. 7.17

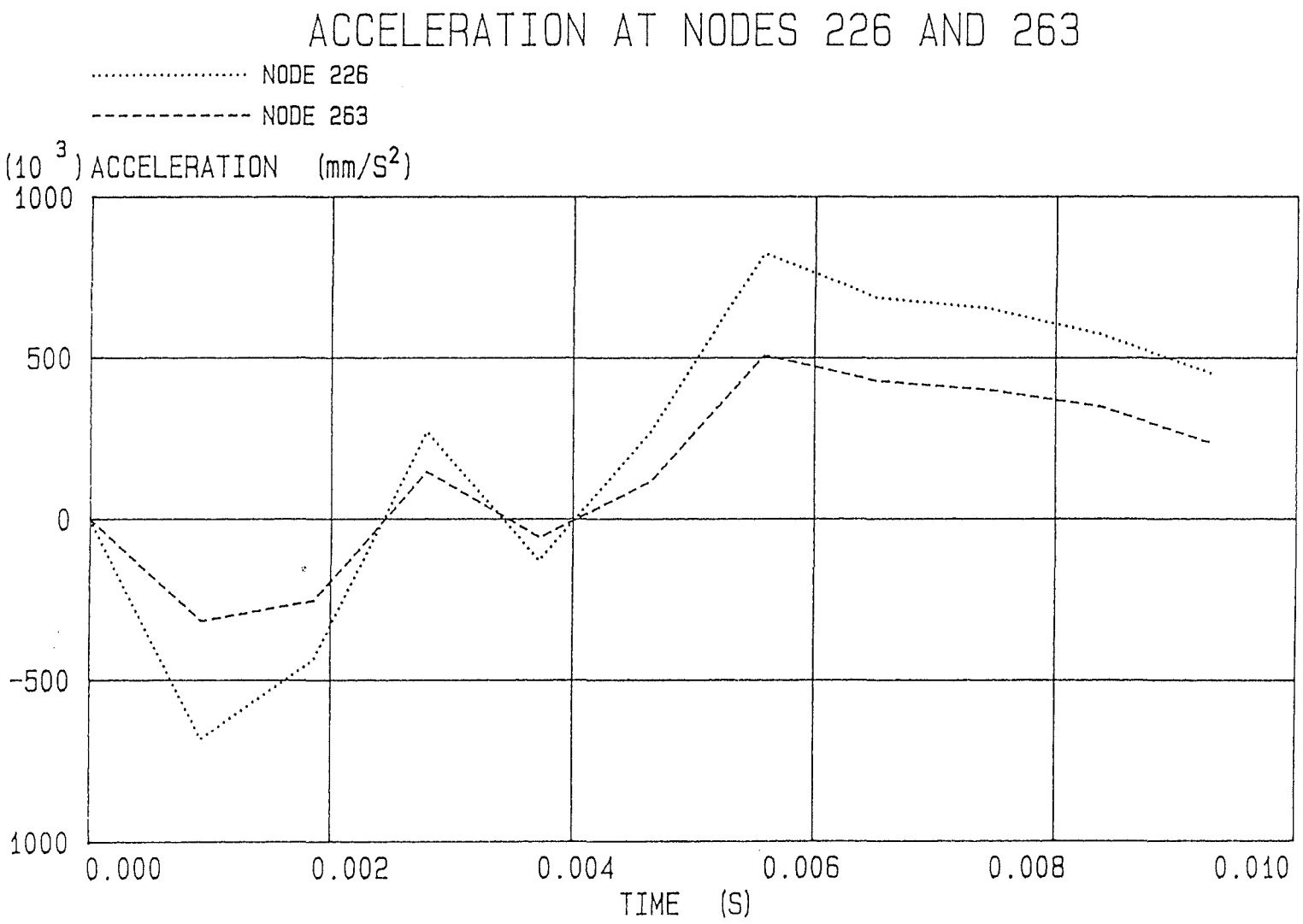

NONB16 (CKB16MDTF)
CRACKS AT TOP OF SLAB

Fig. 7.18

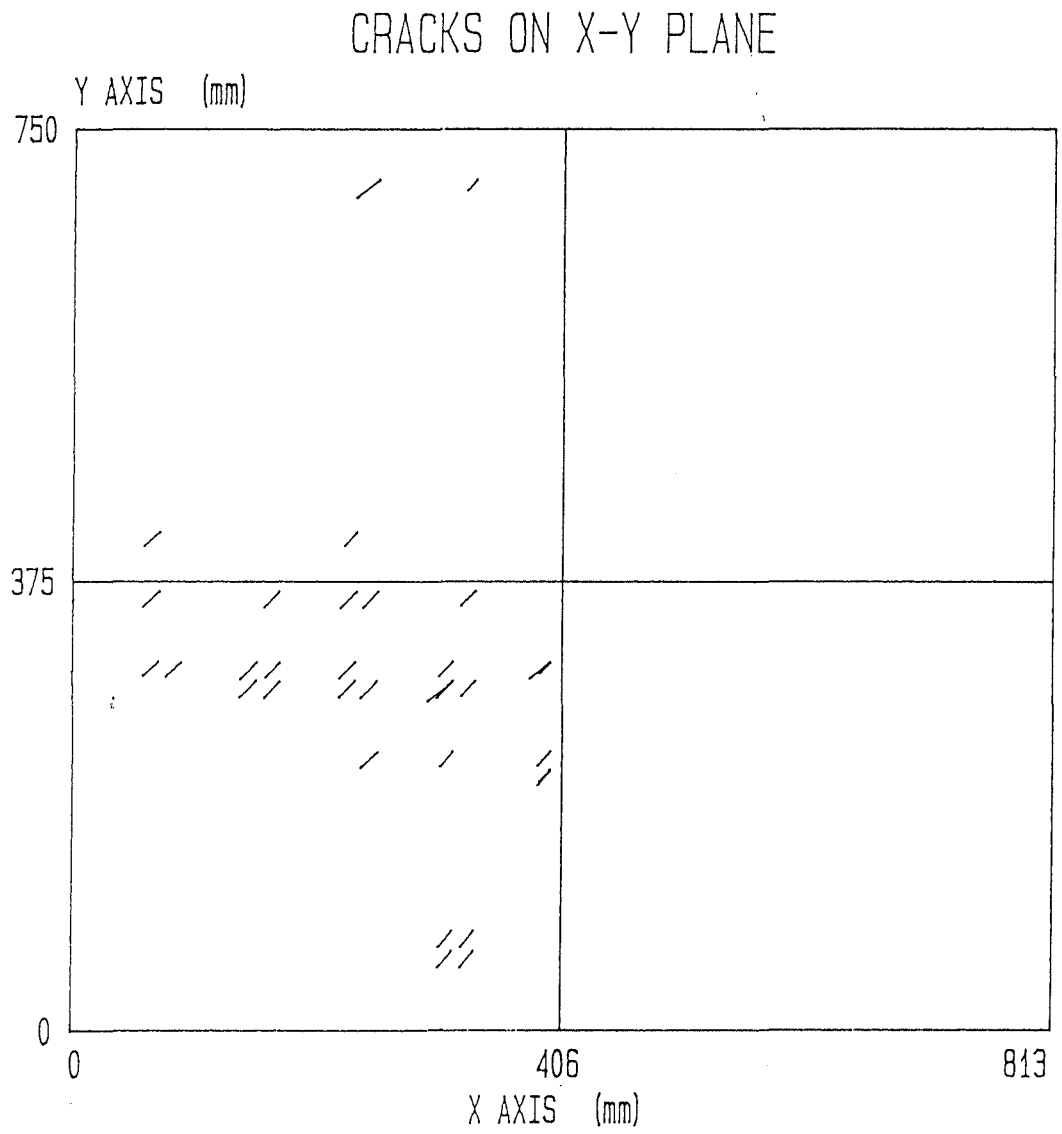

NONB16 (CKB16MDBF)
CRACKS AT BOTTOM OF SLAB

Fig. 7.19

ZENTECH CONSULTANTS

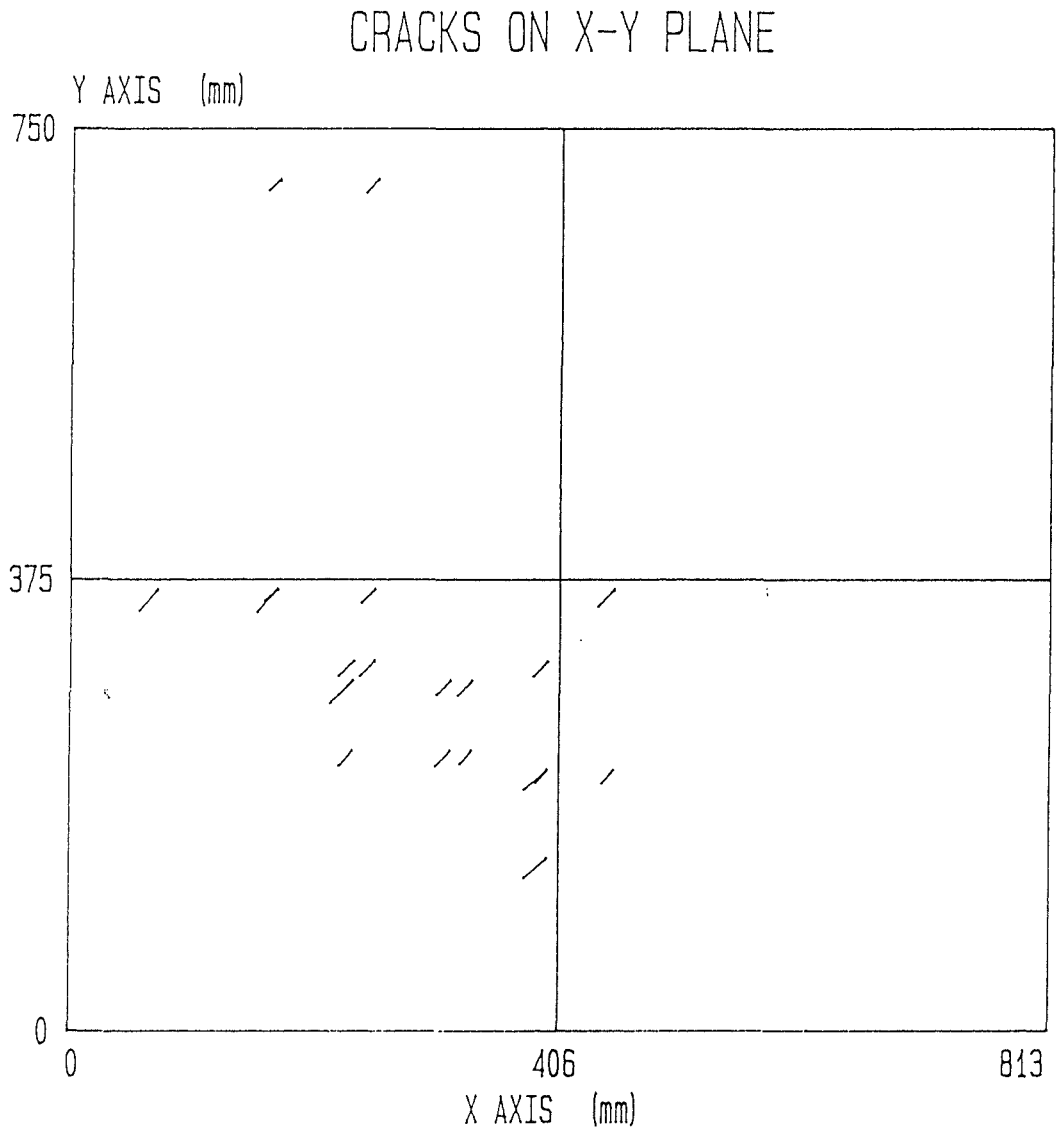

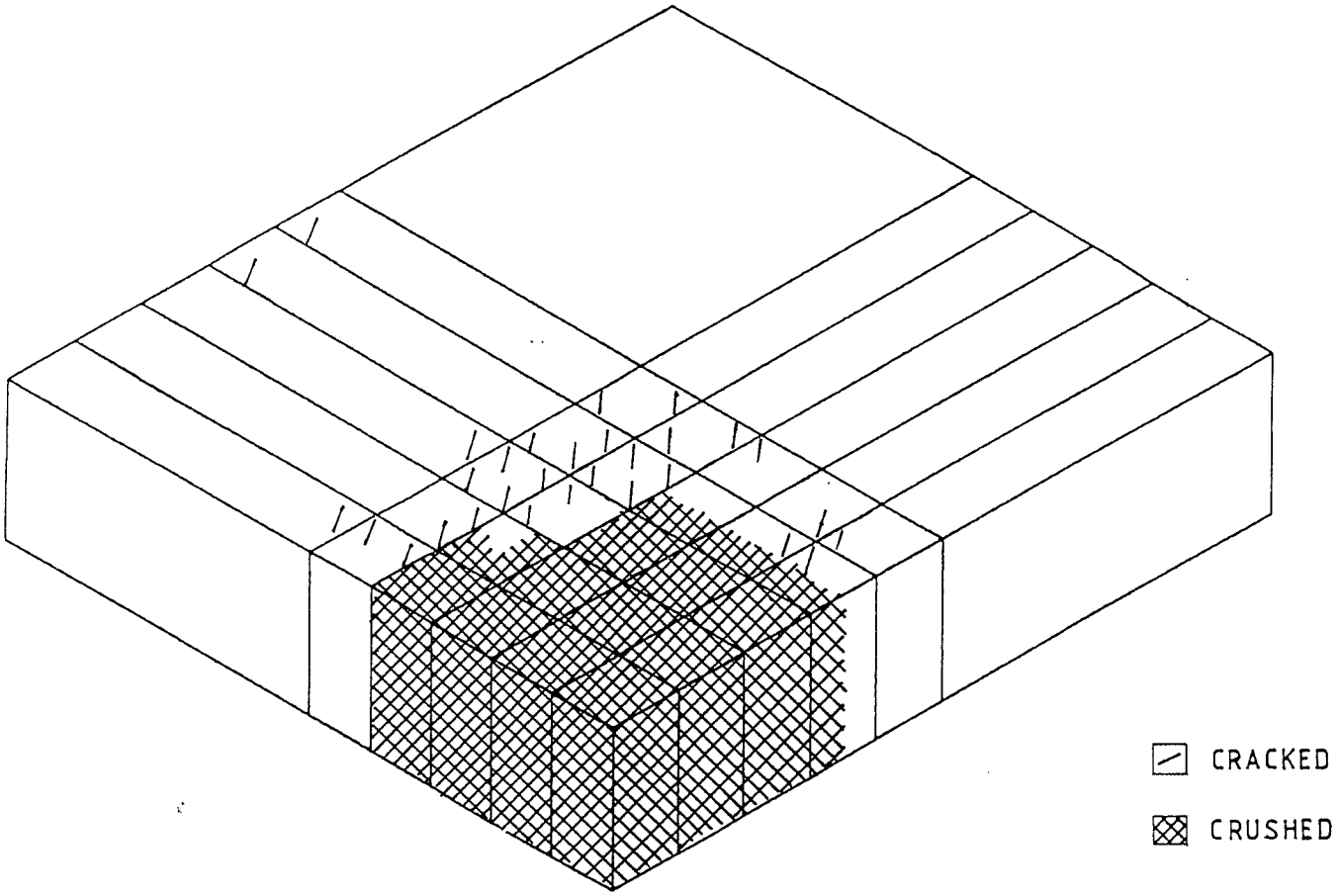

Fig. 7.20 CRACRED AND CRUSHED AREAS OF MODEL B16 FROM NONSAP ANALYSIS

NONB26 (CKB26MDTF)
CRACKS AT TOP OF SLAB

Fig. 7.21

ZENTECH CONSULTANTS

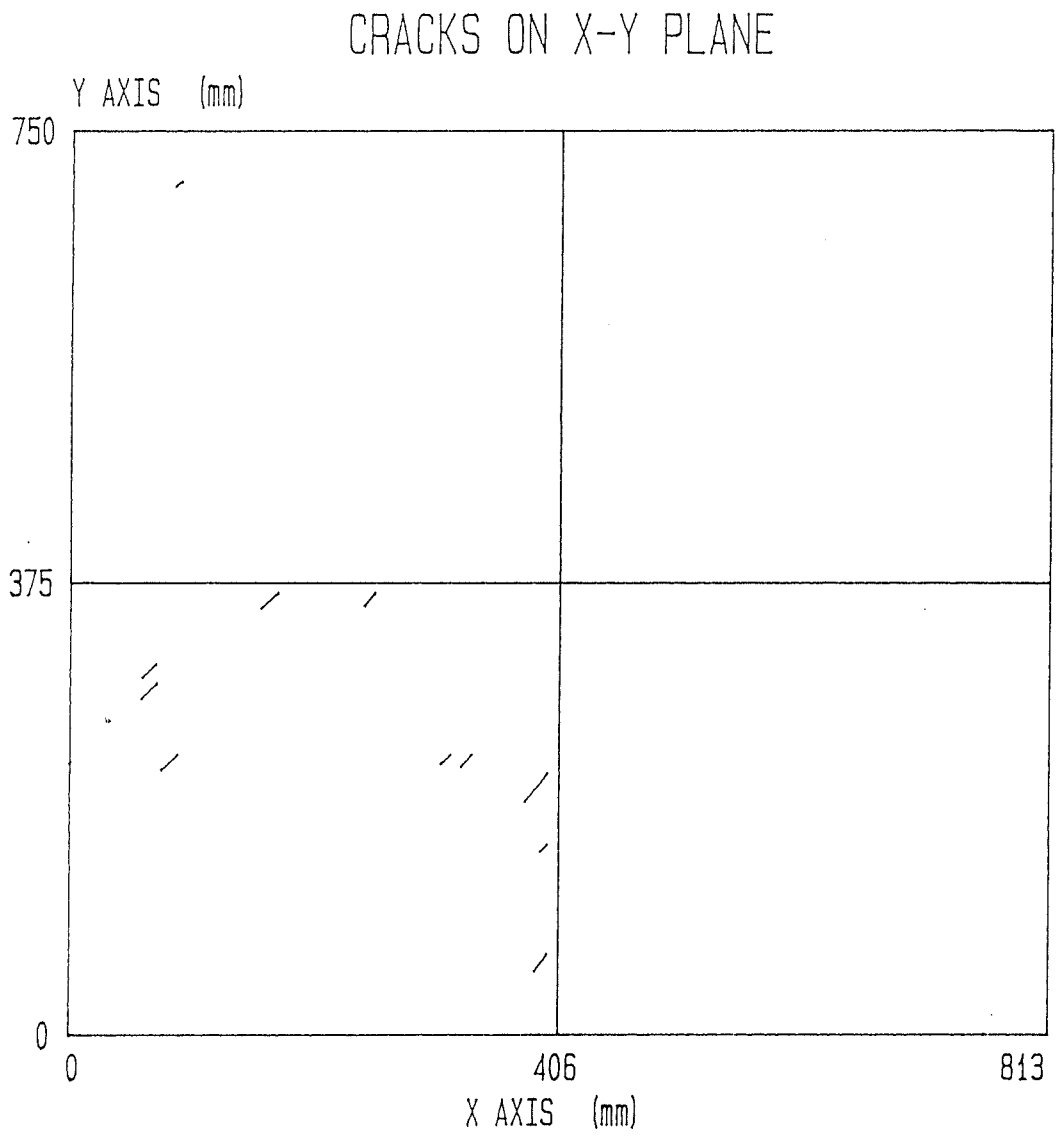

NONB26 (CKB26MDBF)
CRACKS AT BOTTOM OF SLAB

Fig. 7.22

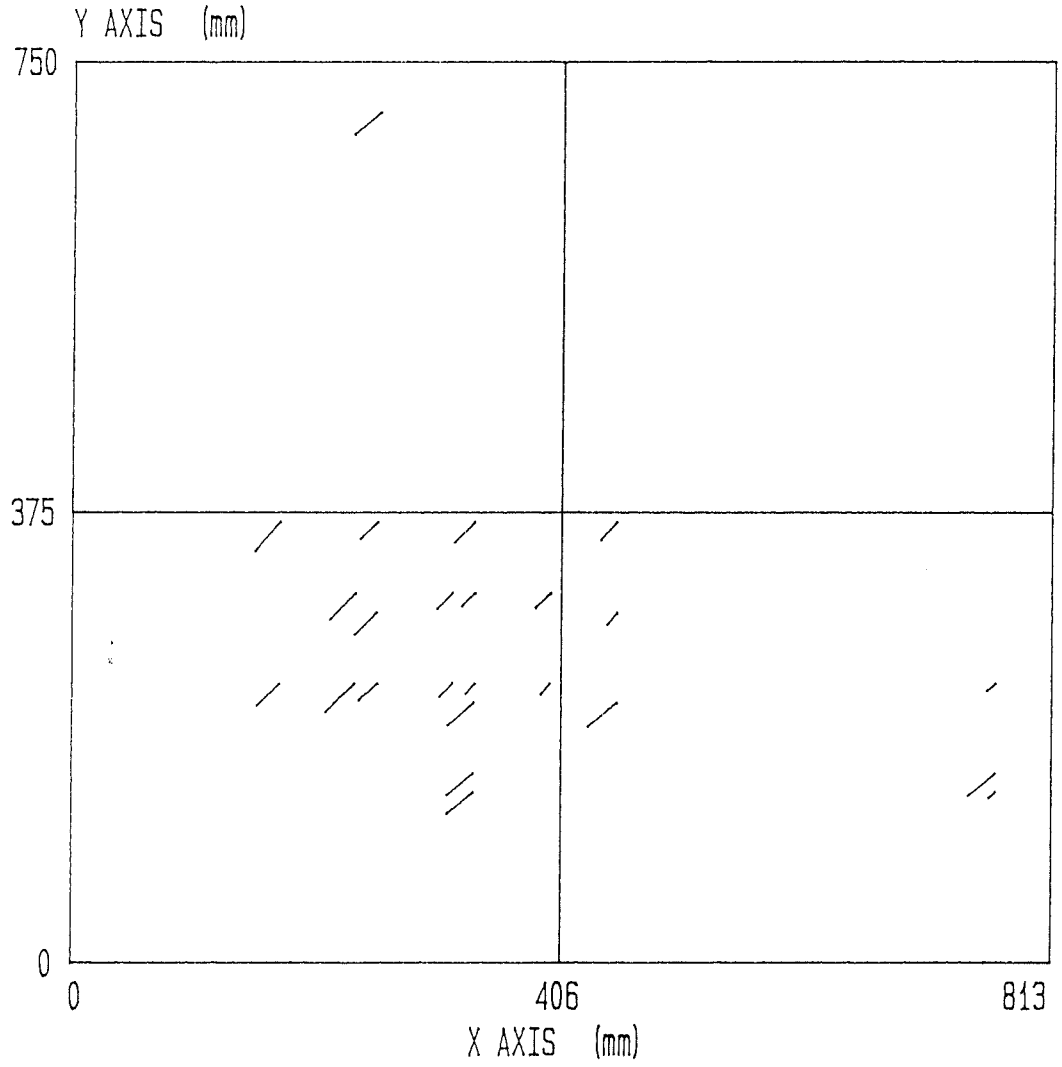

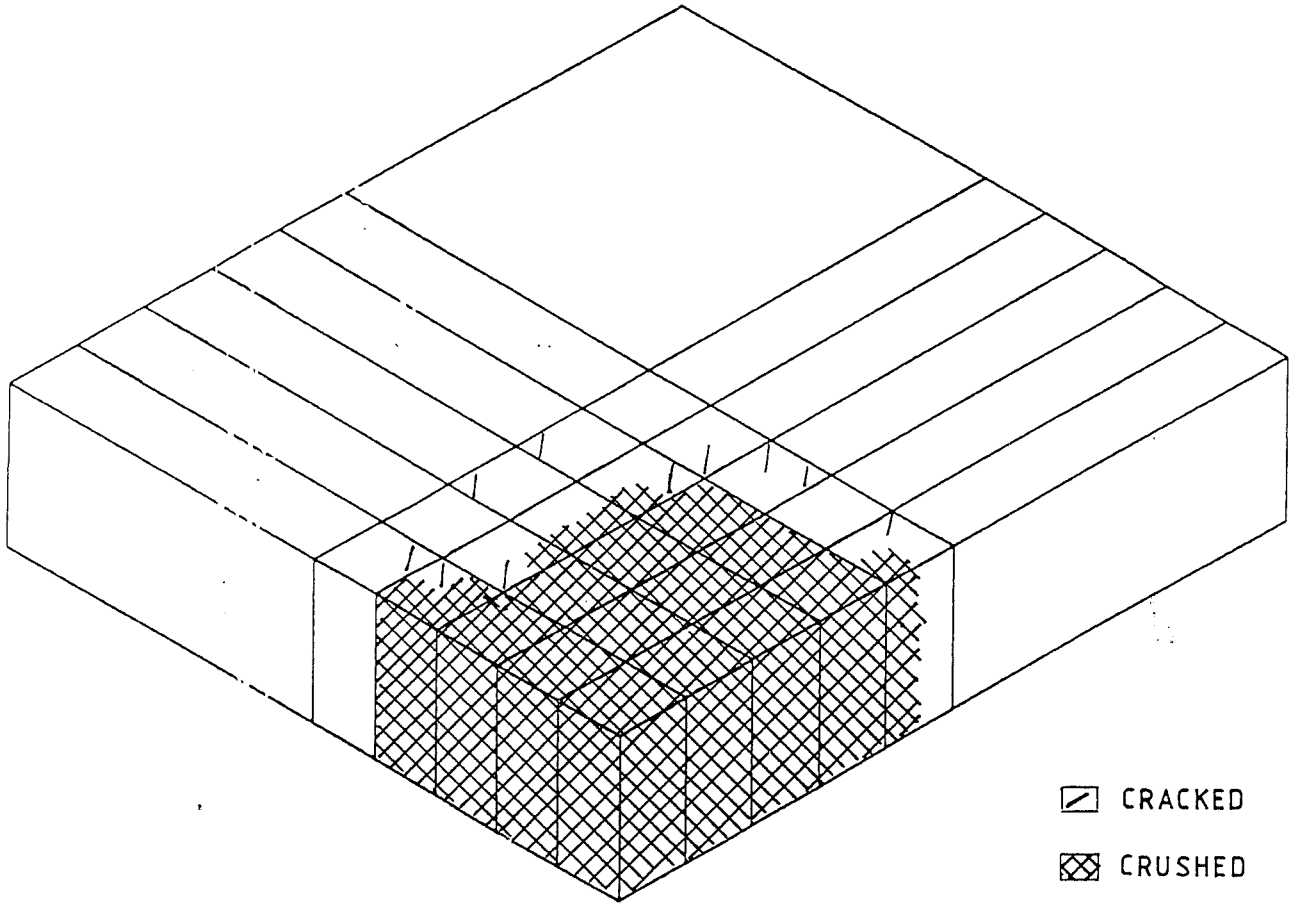

Fig. 7.23 CRACKED AND CRUSHED AREAS OF MODEL B26 FROM NONSAP ANALYSIS

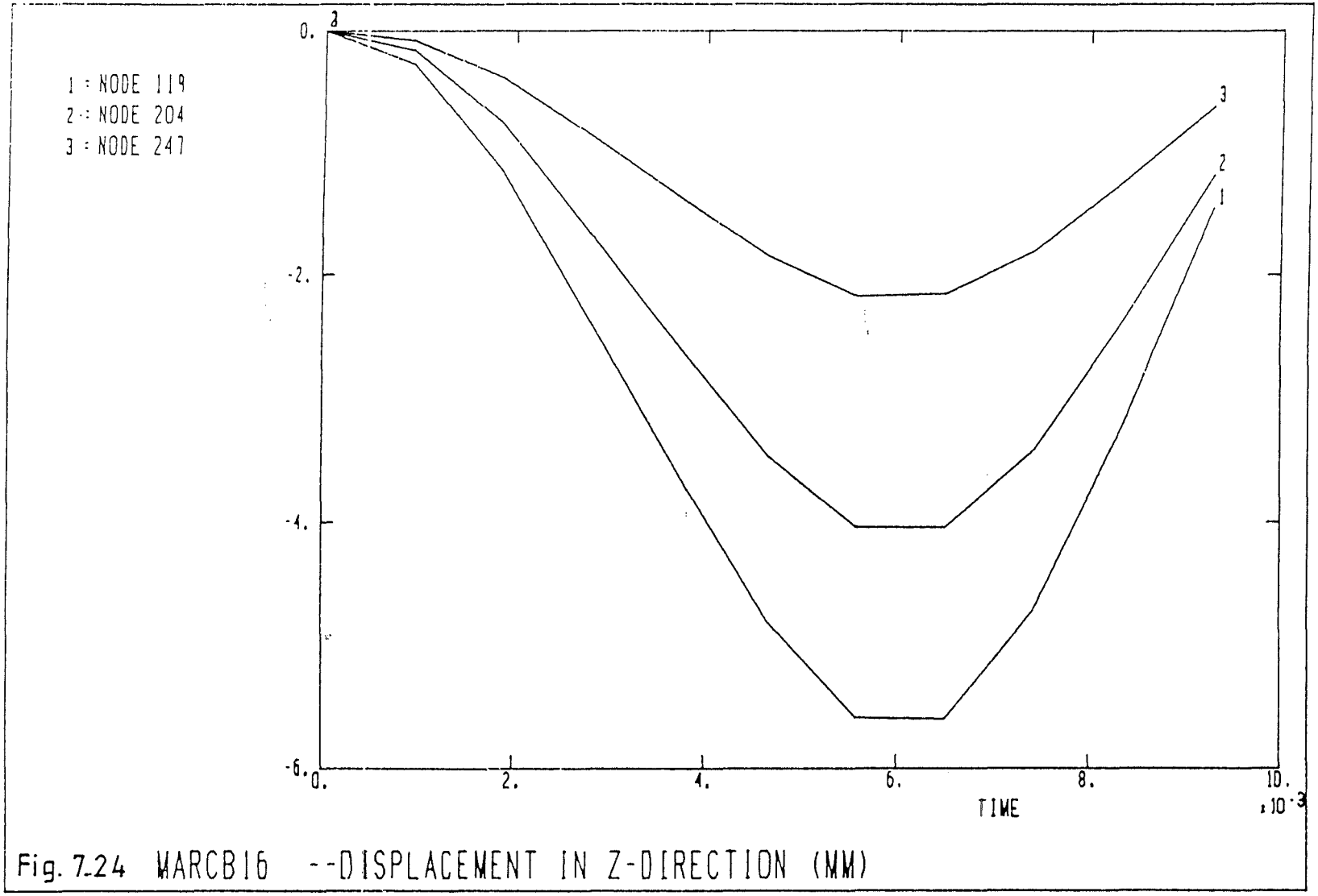

Fig. 7.24 MARCB16 --DISPLACEMENT IN Z-DIRECTION (MM)

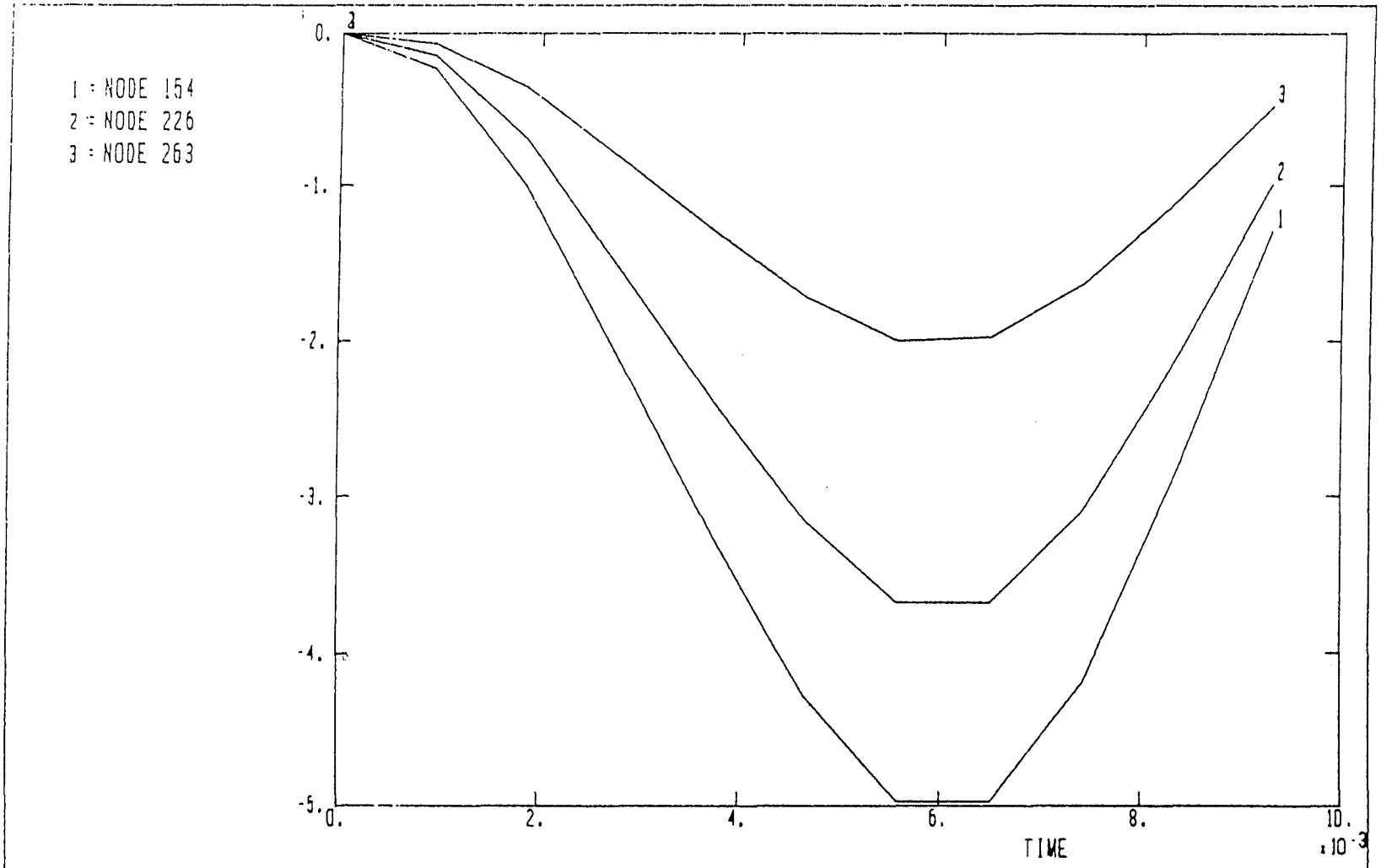

Fig. 7.25 MARCB16 --DISPLACEMENT IN Z-DIRECTION (MM)

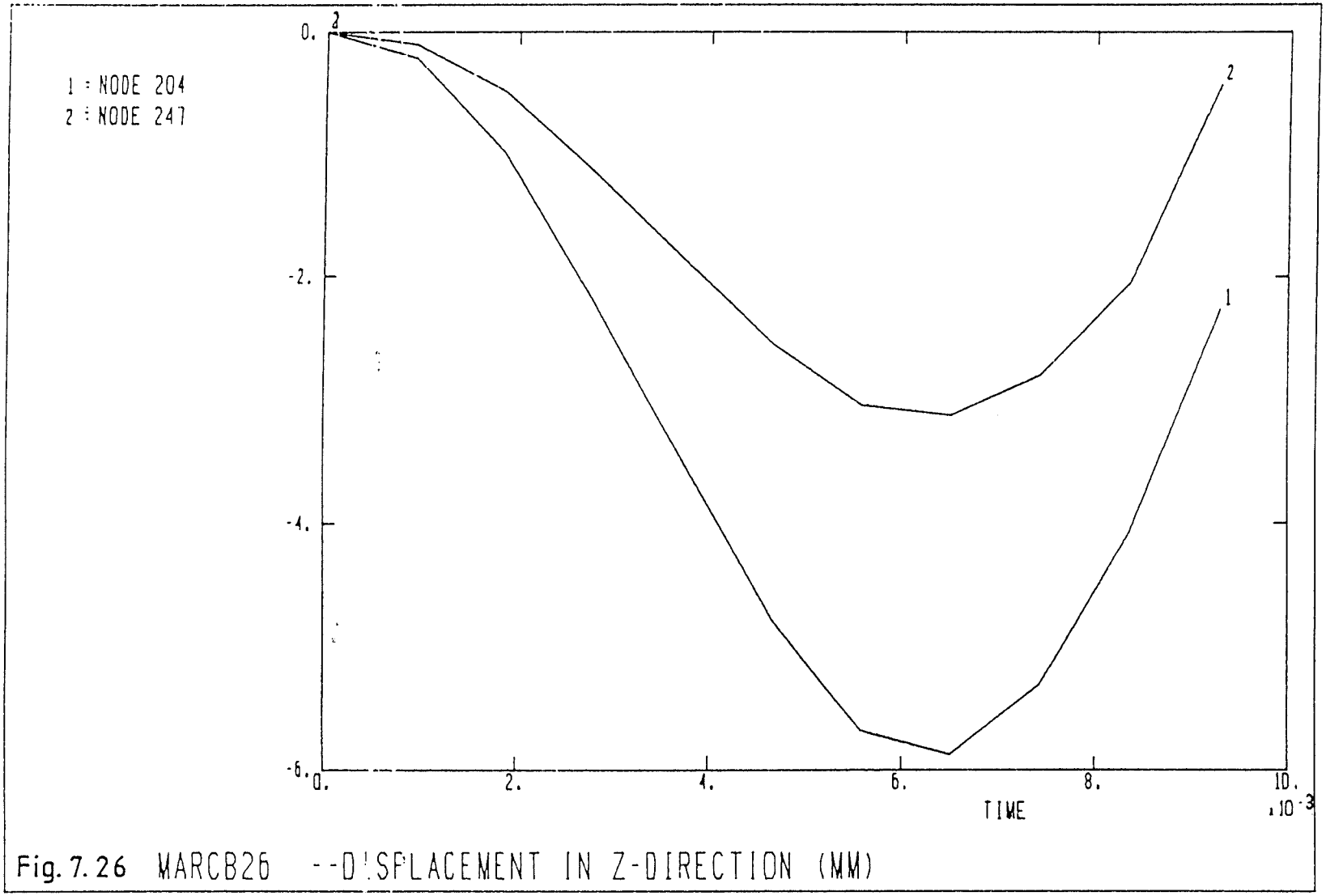

Fig. 7.26 MARCB26 --DISPLACEMENT IN Z-DIRECTION (MM)

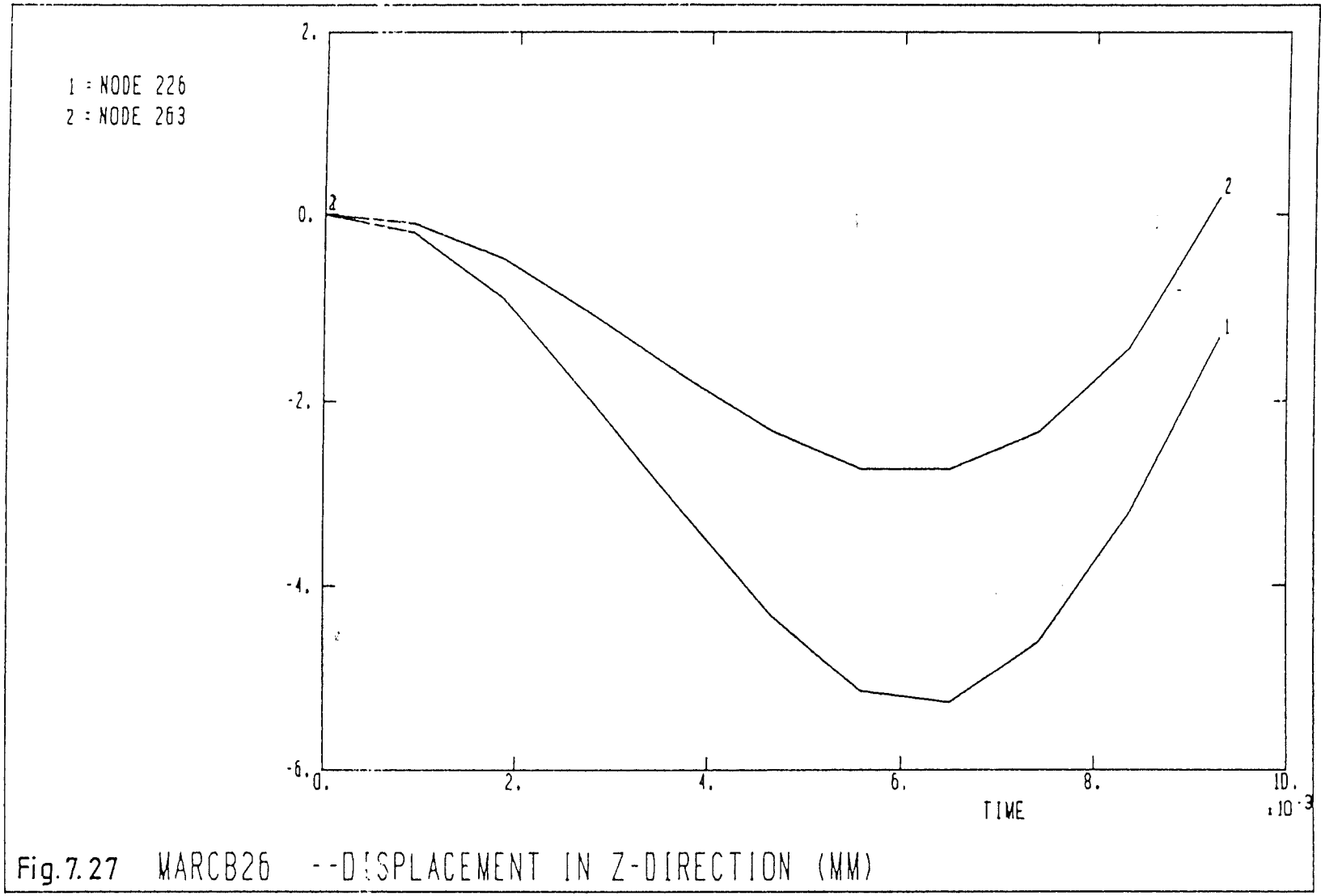

Fig. 7.27 MARCB26 --DISPLACEMENT IN Z-DIRECTION (MM)

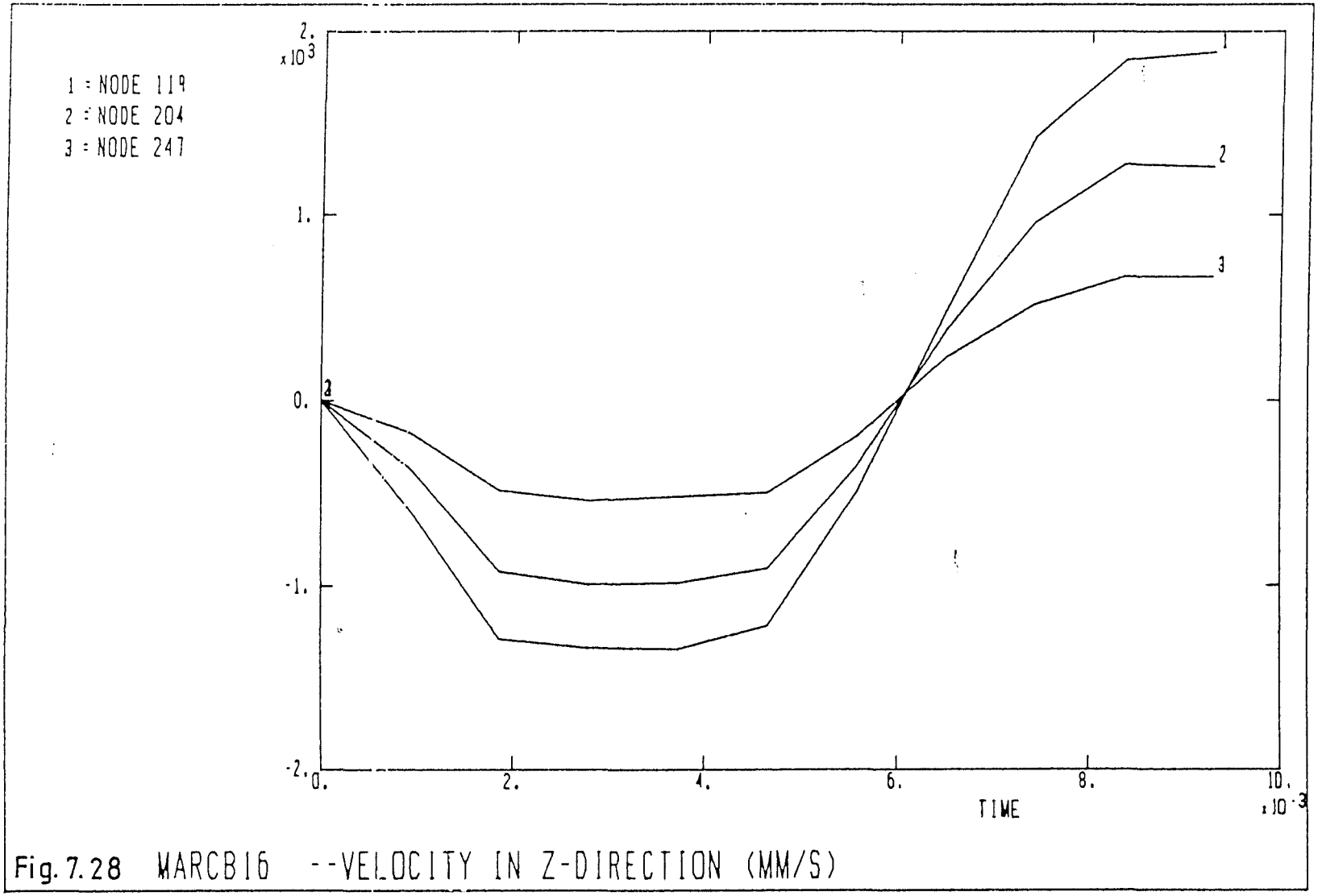

Fig. 7.28 MARCB16 --VELOCITY IN Z-DIRECTION (MM/S)

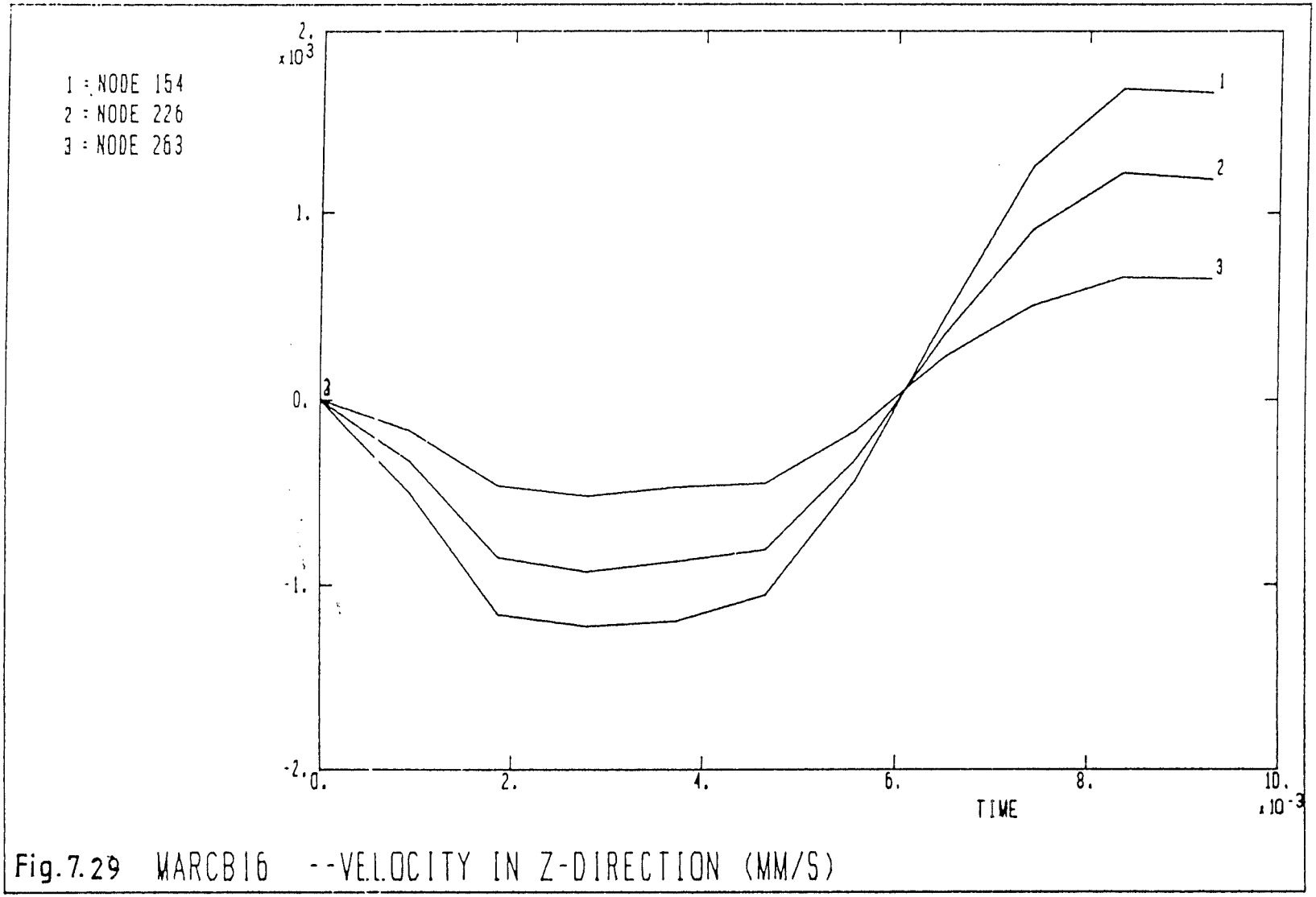

Fig.7.29 MARCB16 --VELOCITY IN Z-DIRECTION (MM/S)

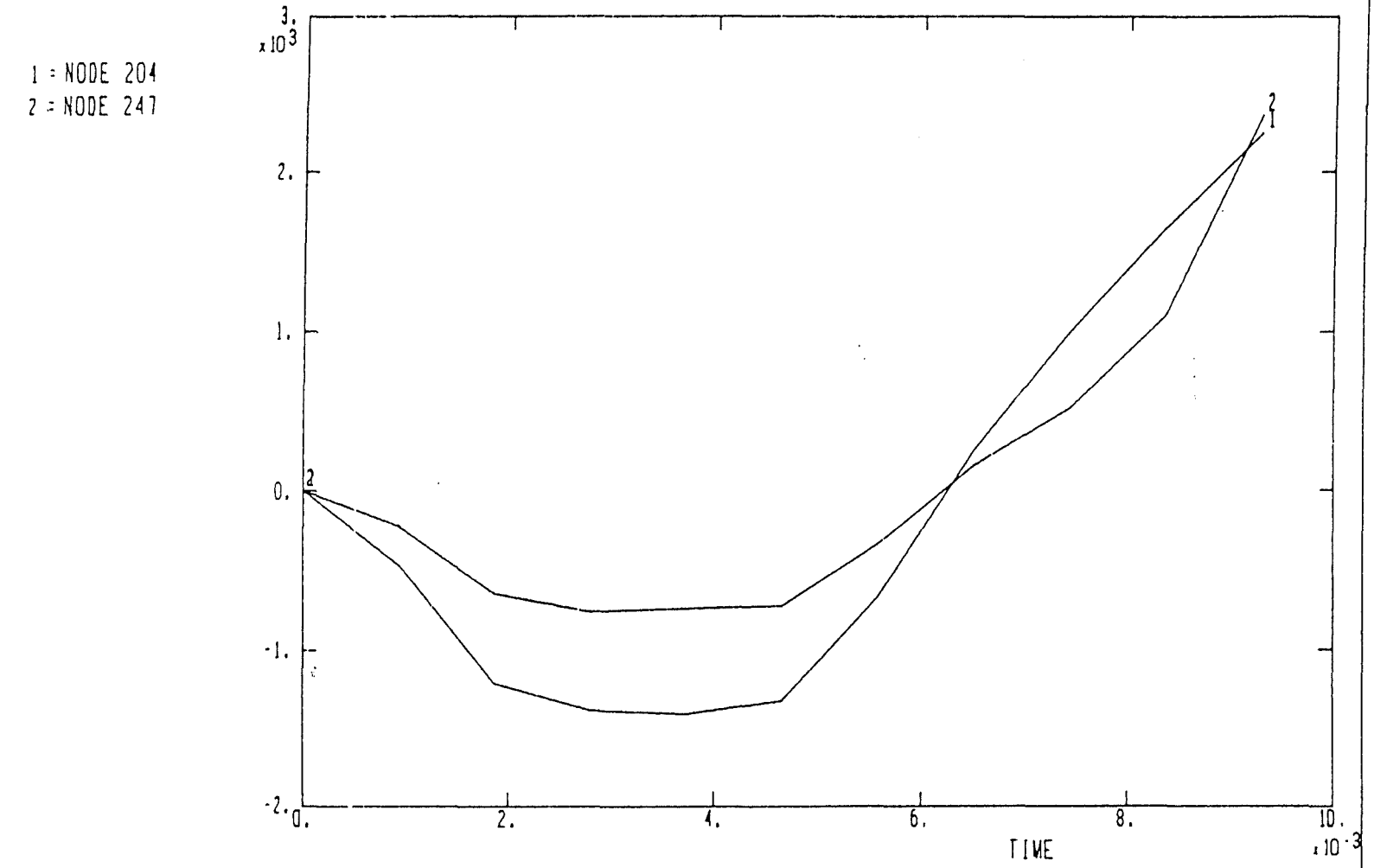

Fig. 7.30 MARCB26 --VELOCITY IN Z-DIRECTION (MM/S)

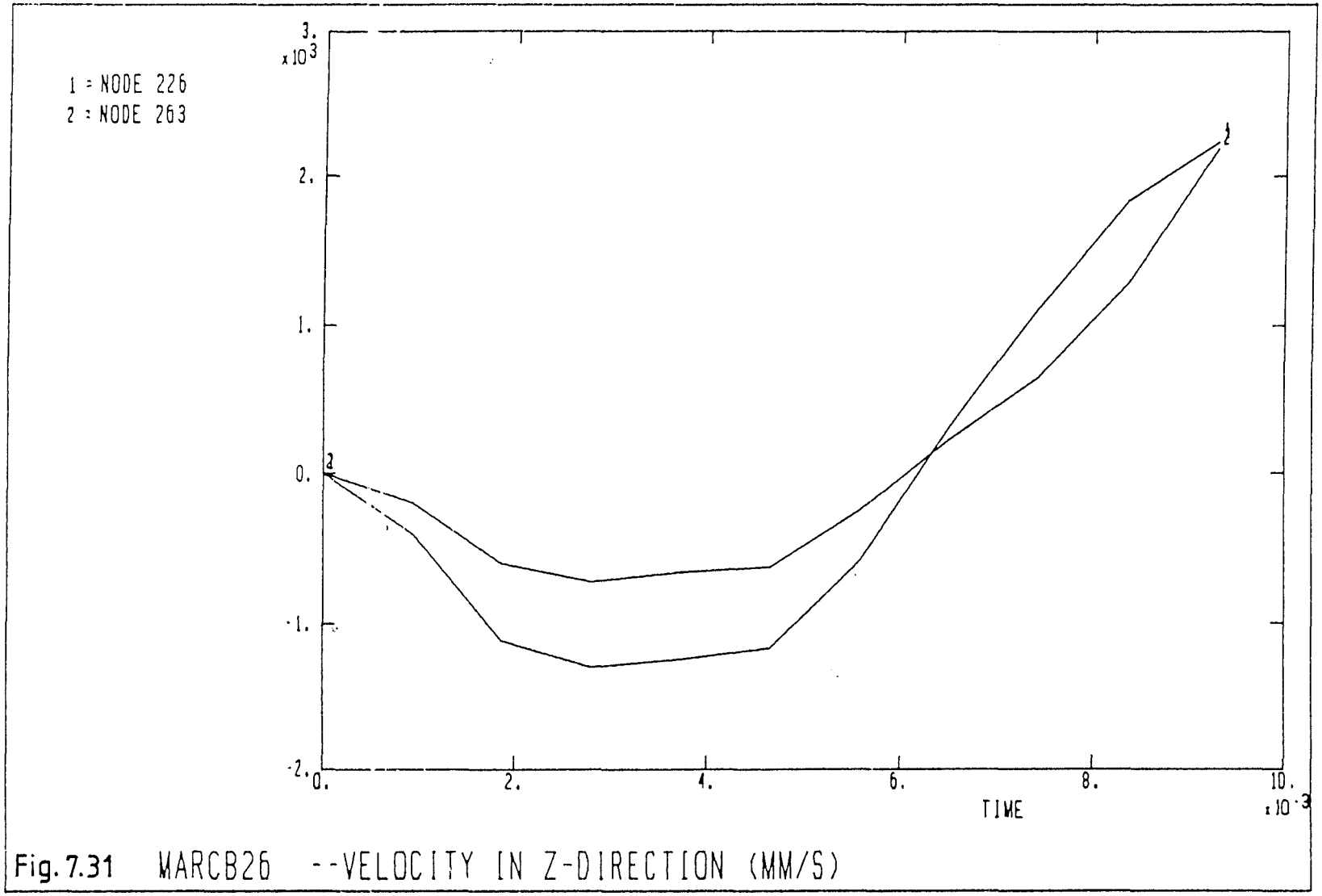

Fig. 7.31 MARCB26 --VELOCITY IN Z-DIRECTION (MM/S)

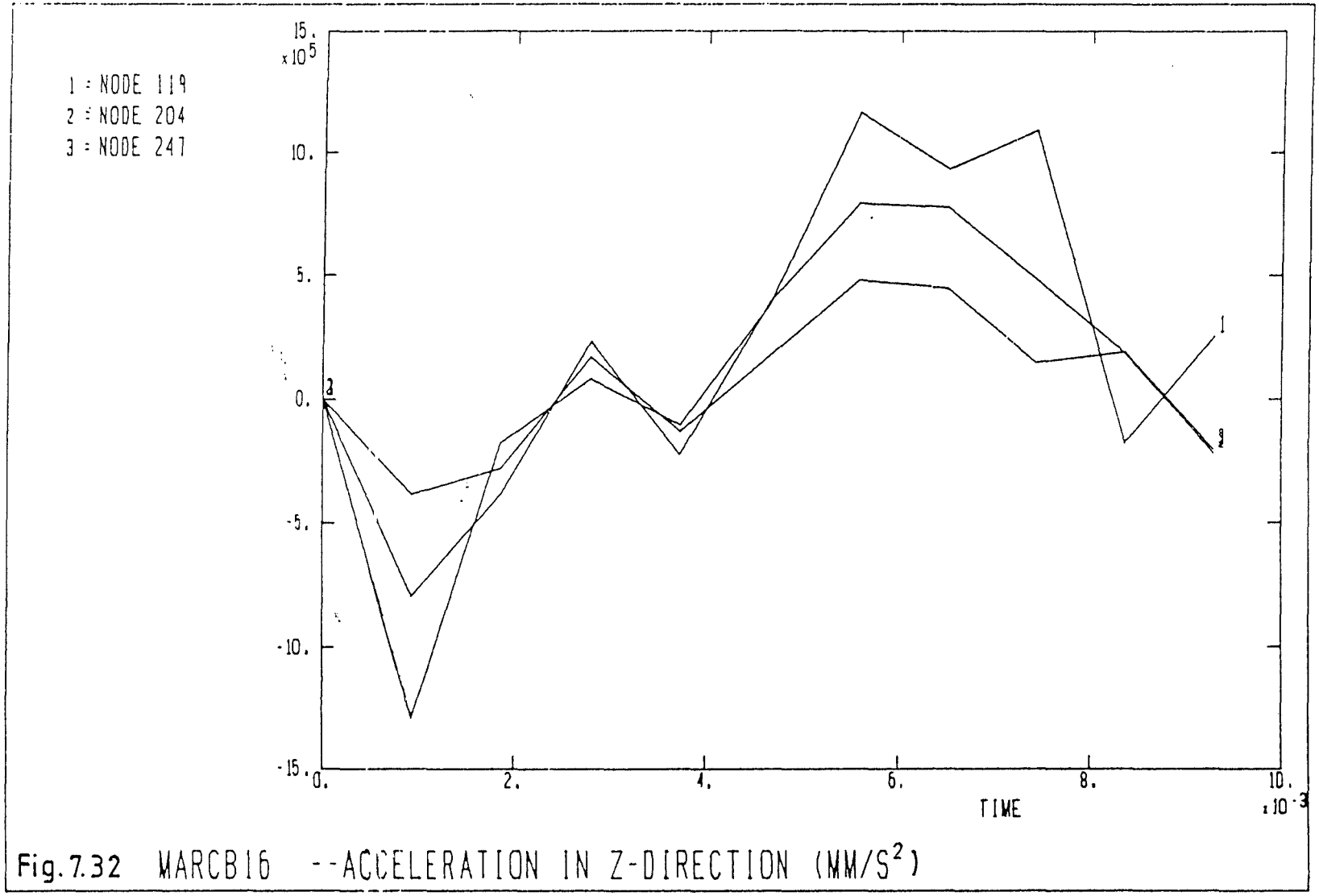

Fig. 7.32 MARCB16 --ACCELERATION IN Z-DIRECTION (MM/S^2)

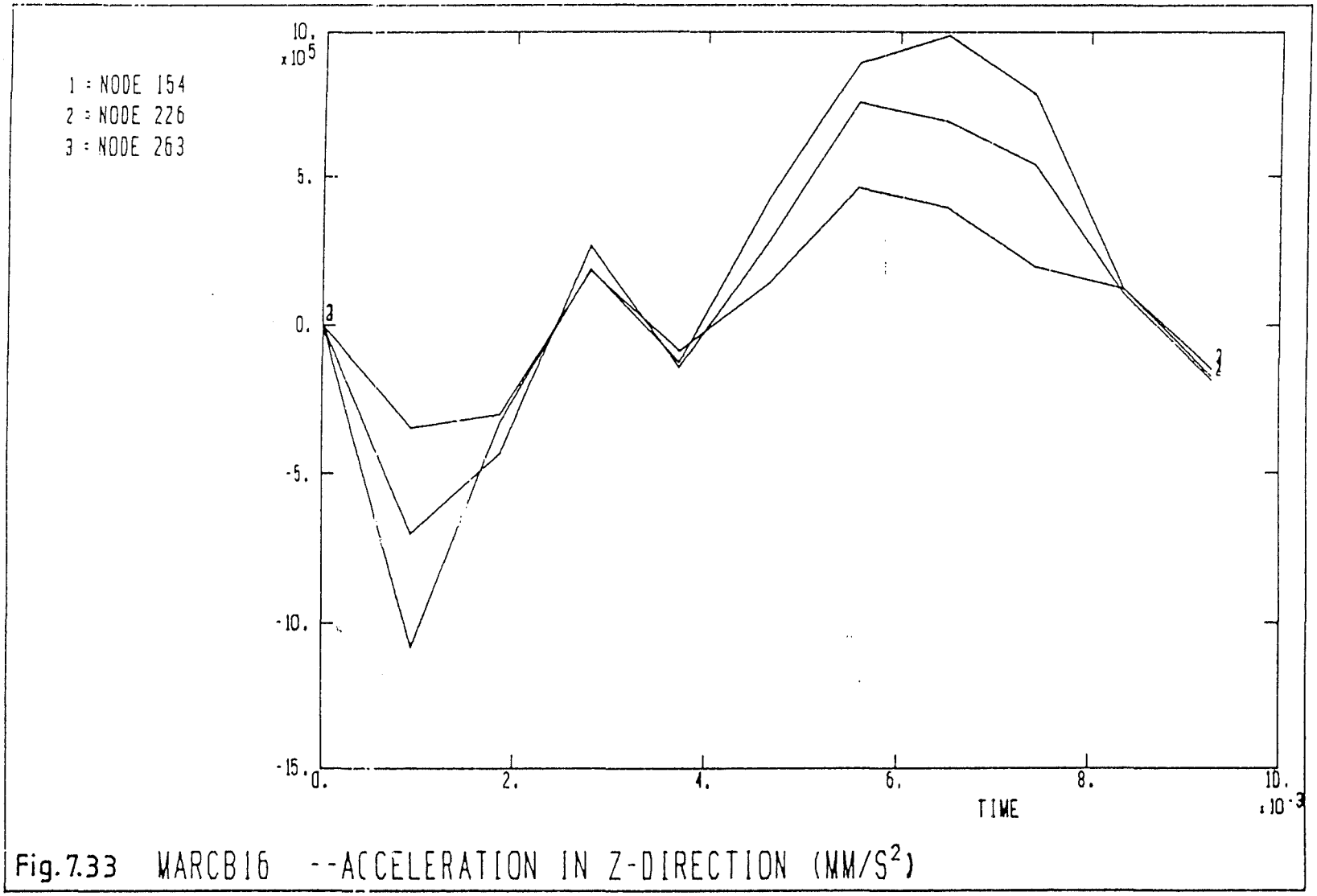

Fig. 7.33 MARCB16 --ACCELERATION IN Z-DIRECTION (MM/S^2)

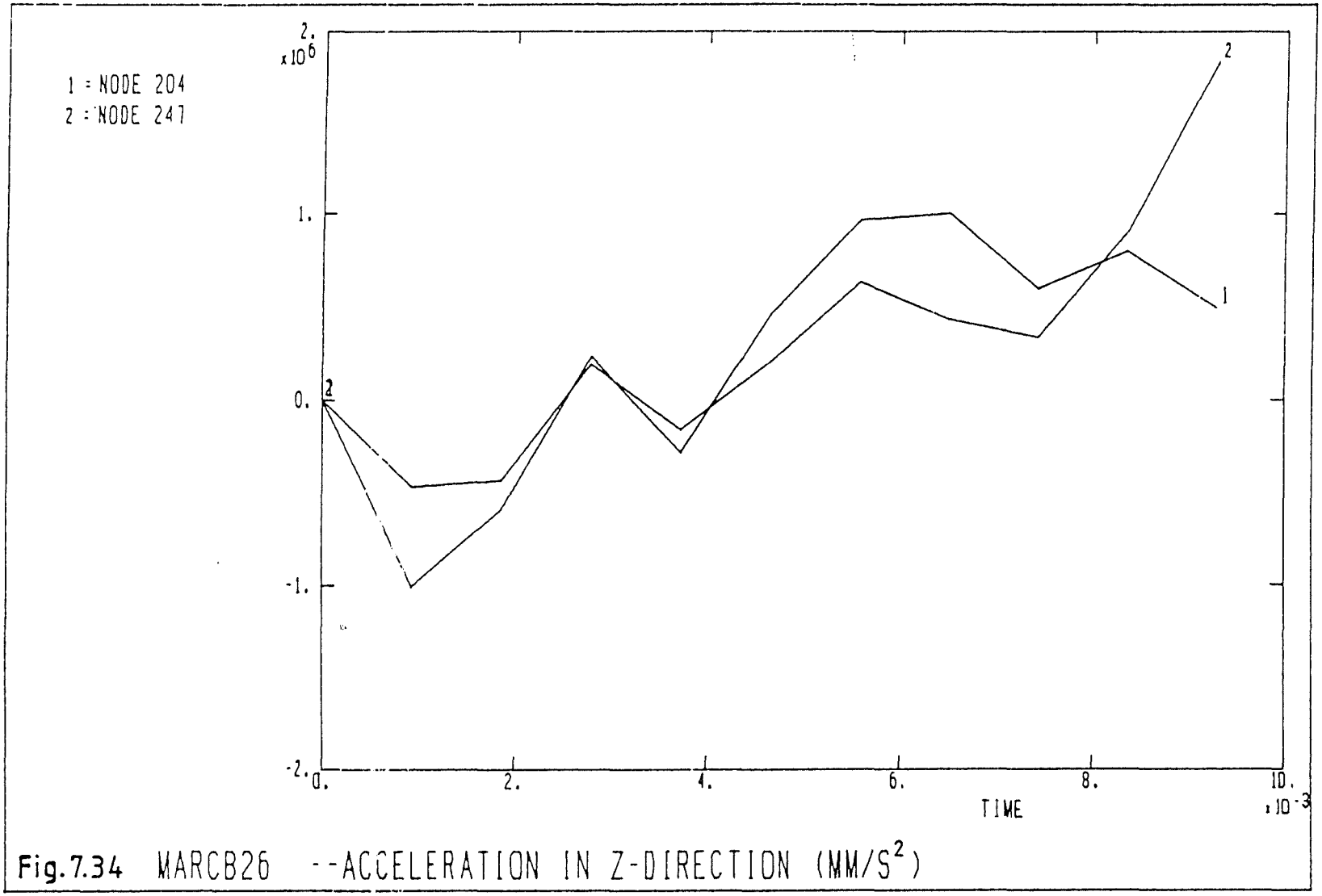

Fig.7.34 MARCB26 --ACCELERATION IN Z-DIRECTION (MM/S^2)

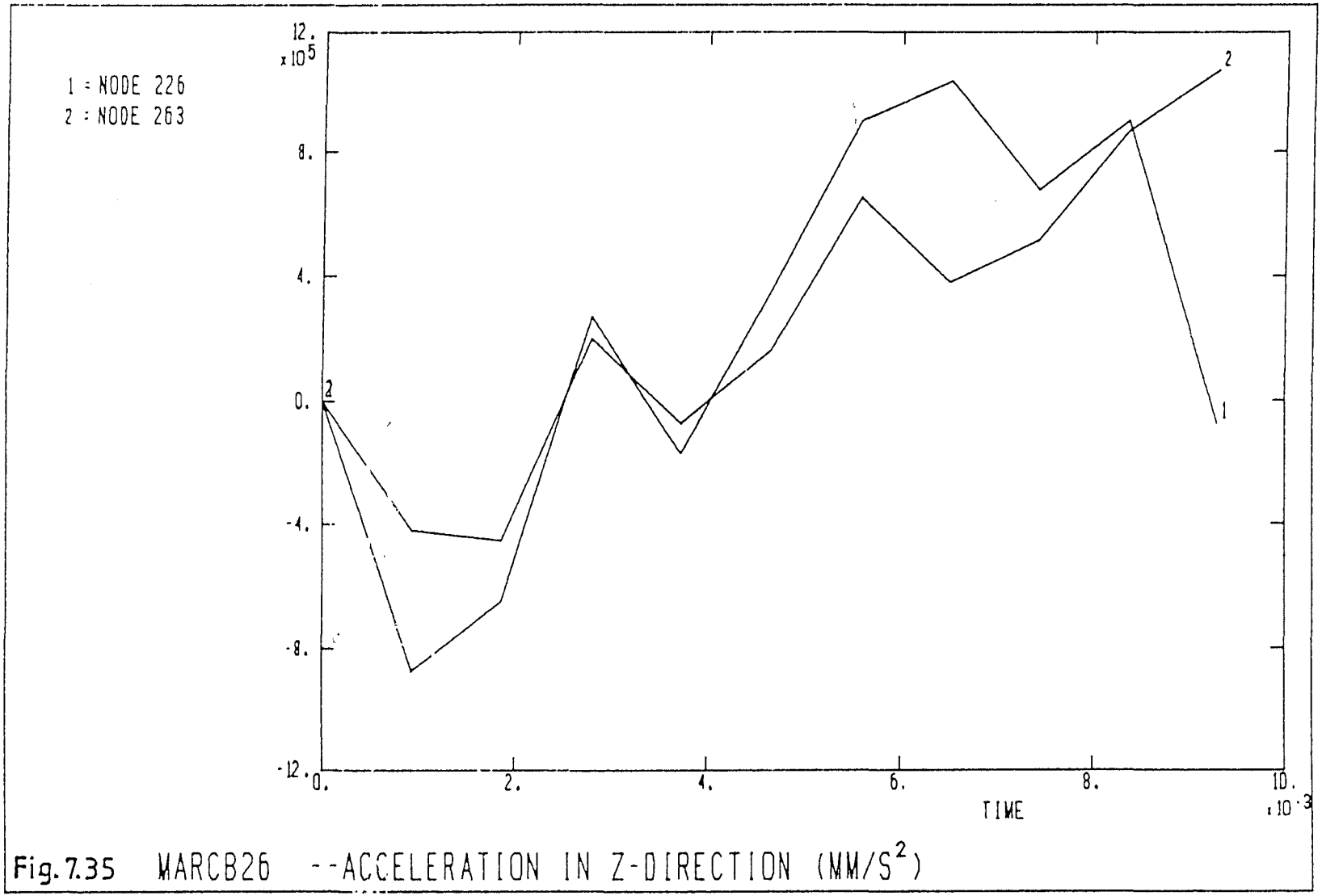

Fig. 7.35 MARCB26 --ACCELERATION IN Z-DIRECTION (MM/S^2)

MARCB16 (CKB16DTF)
CRACKS AT TOP OF SLAB

Fig.7.36

ZENTECH CONSULTANTS

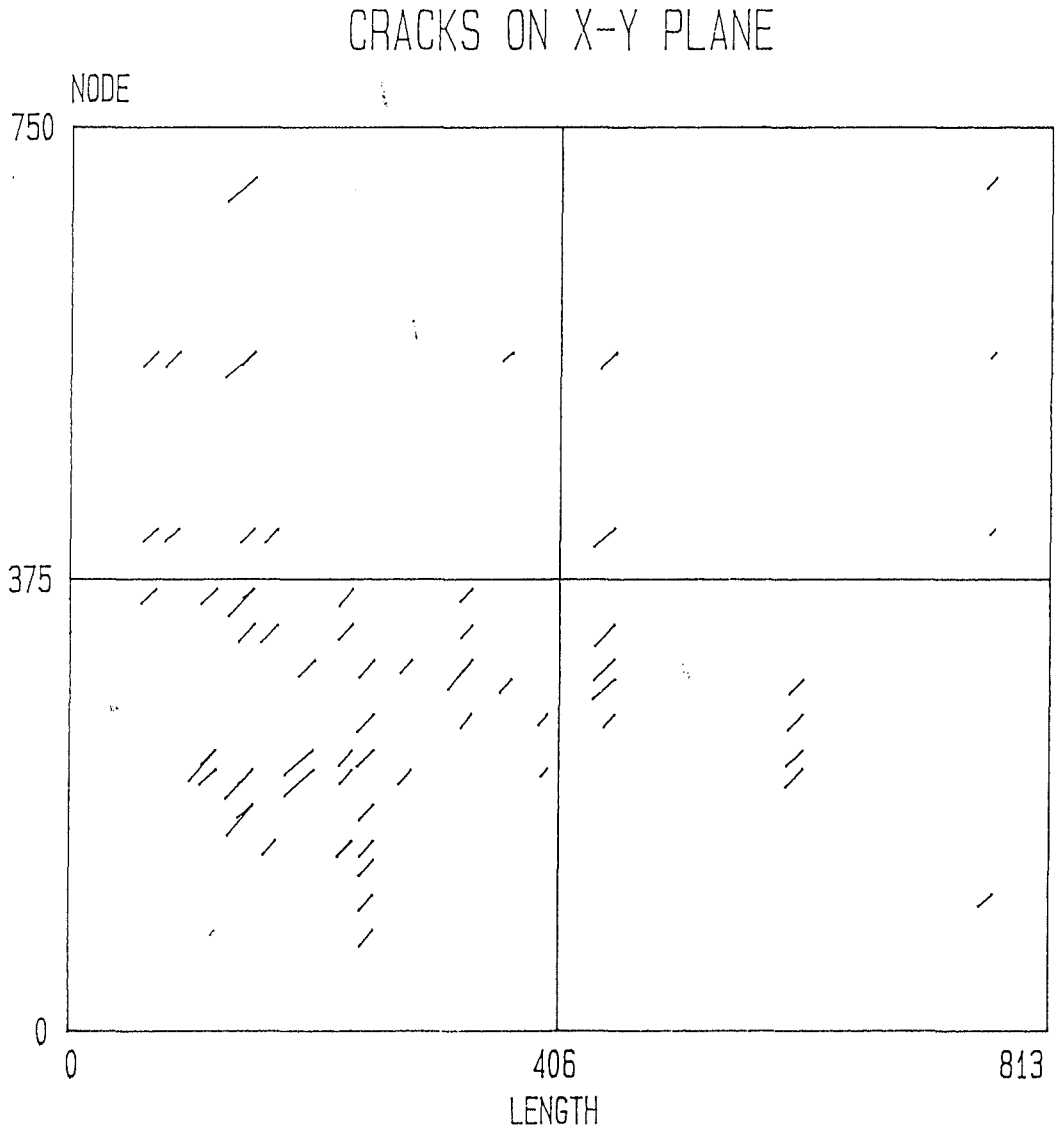

MARCB16 (CKB16DMF)
CRACKS AT MIDDLE OF SLAB

Fig. 7.37

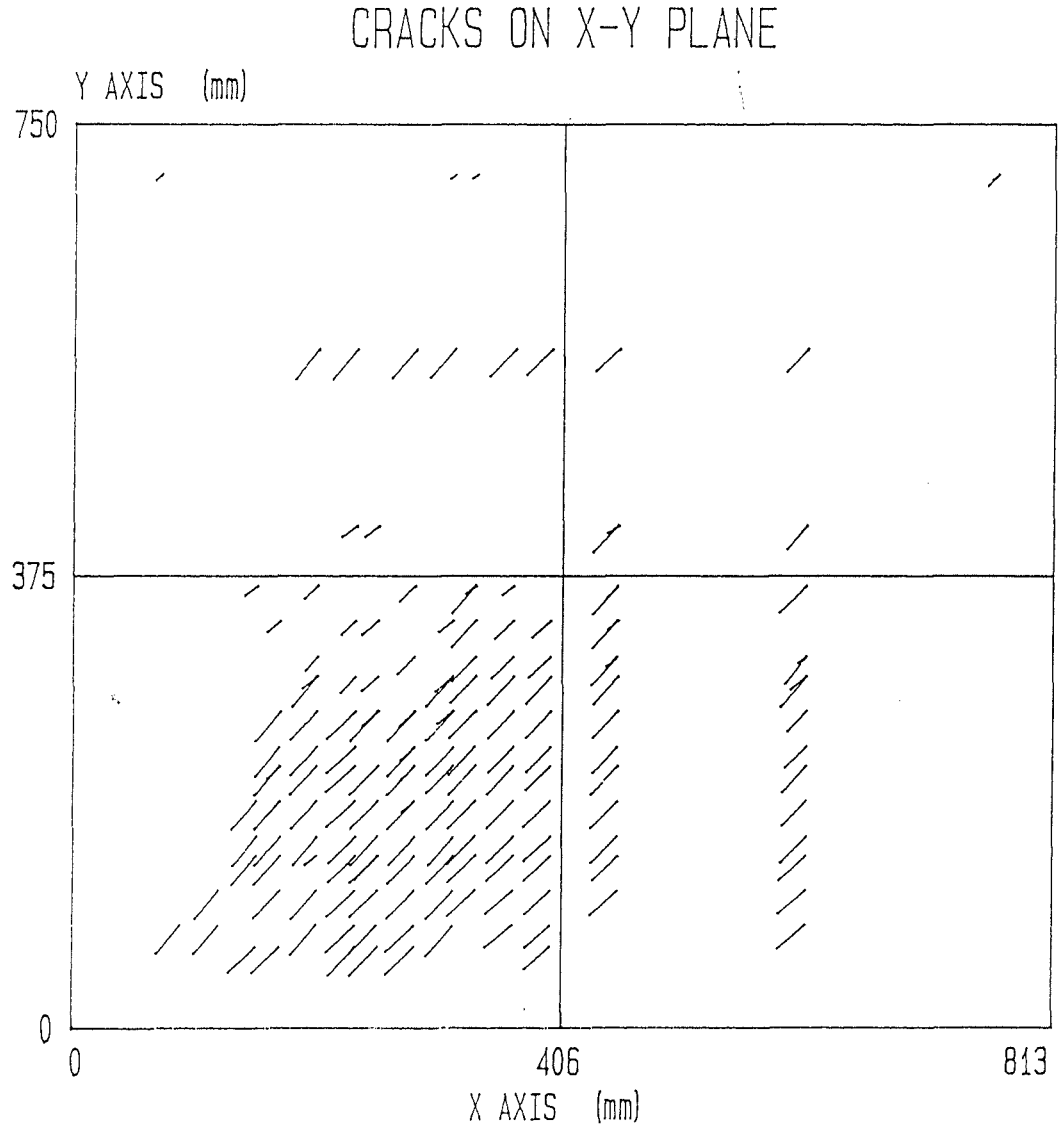

MARCB16 (CKB16DBF)
CRACKS AT BOTTOM OF SLAB

Fig. 7.38

ZENTECH CONSULTANTS

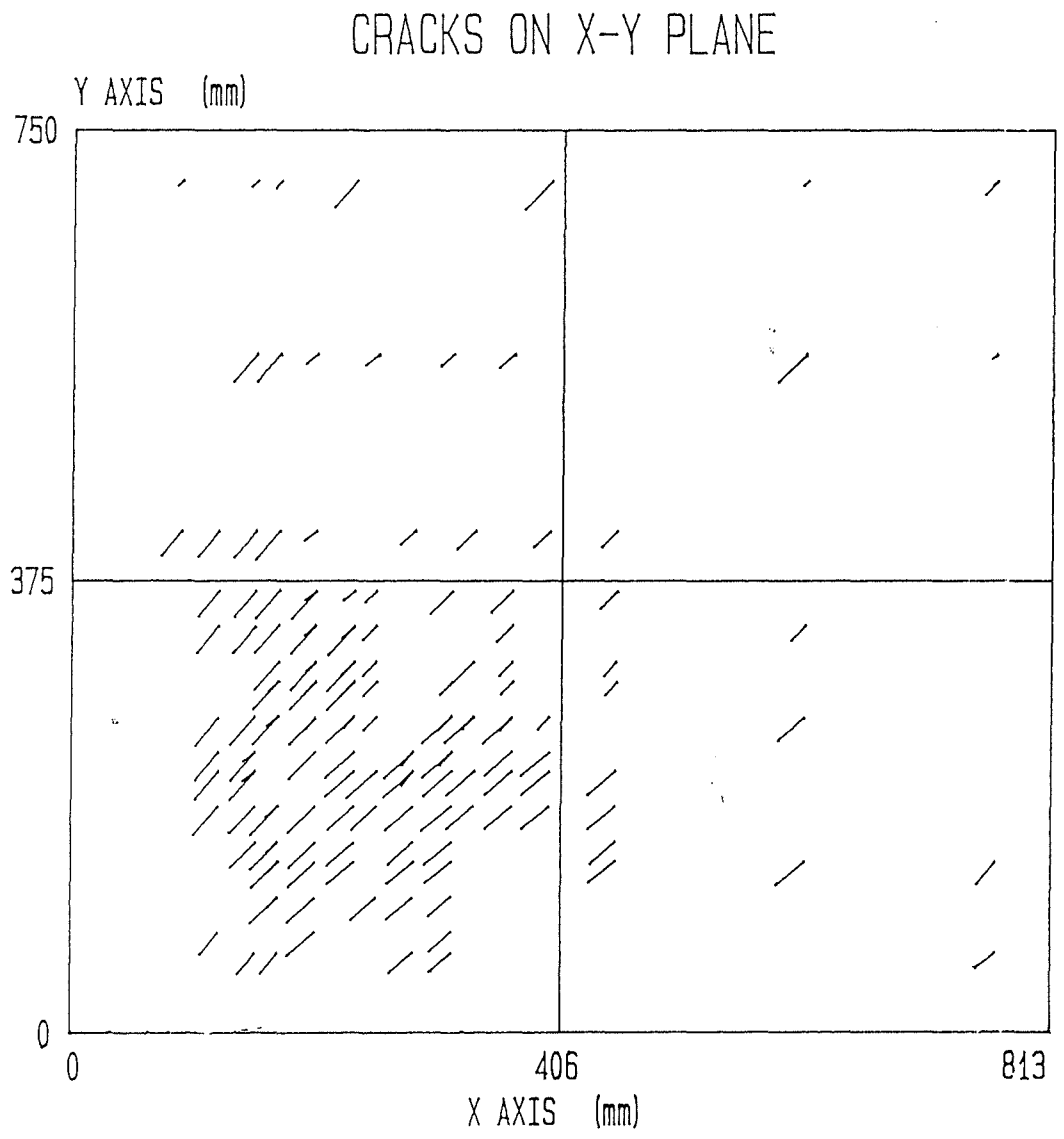

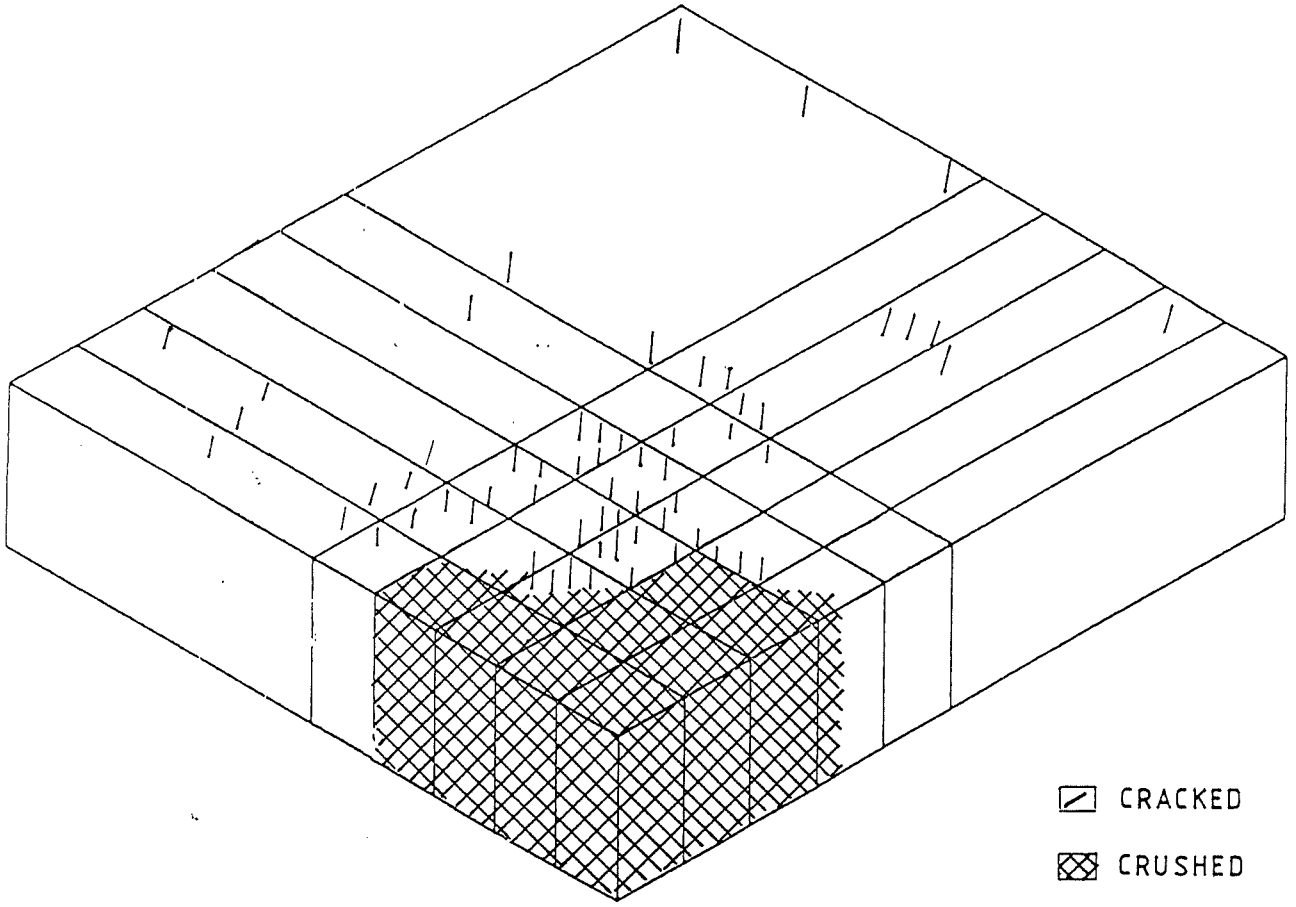

Fig. 7.39 CRACKED AND CRUSHED AREAS OF MODEL B16 FROM MARC ANALYSIS

MARCB26 (CKB26DTF)
CRACKS AT TOP OF SLAB

Fig.7.40

ZENTECH
CONSULTANTS

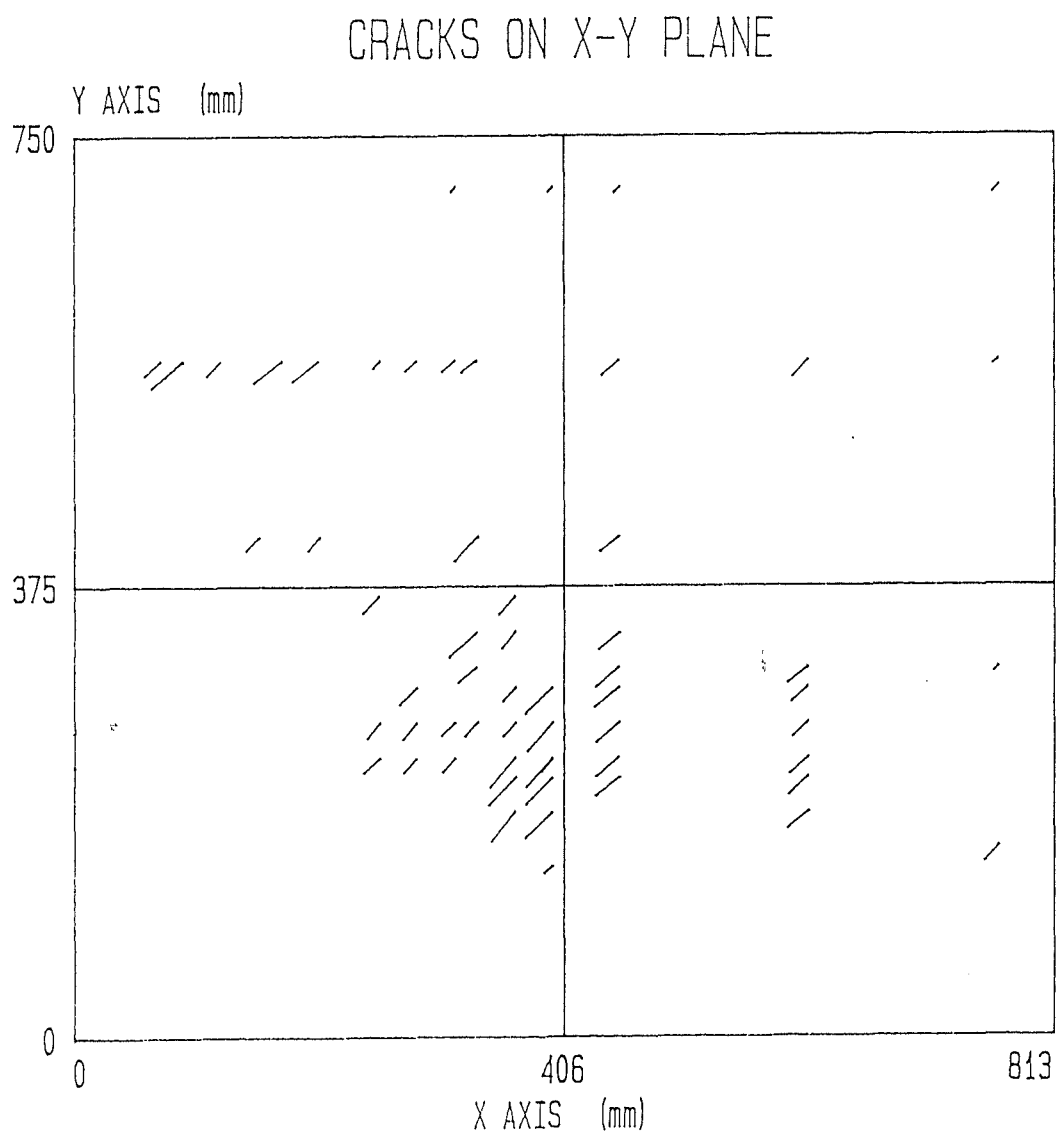

MARCB26 (CKB26DMF)
CRACK AT MIDDLE OF SLAB

Fig.7.41

ZENTECH CONSULTANTS

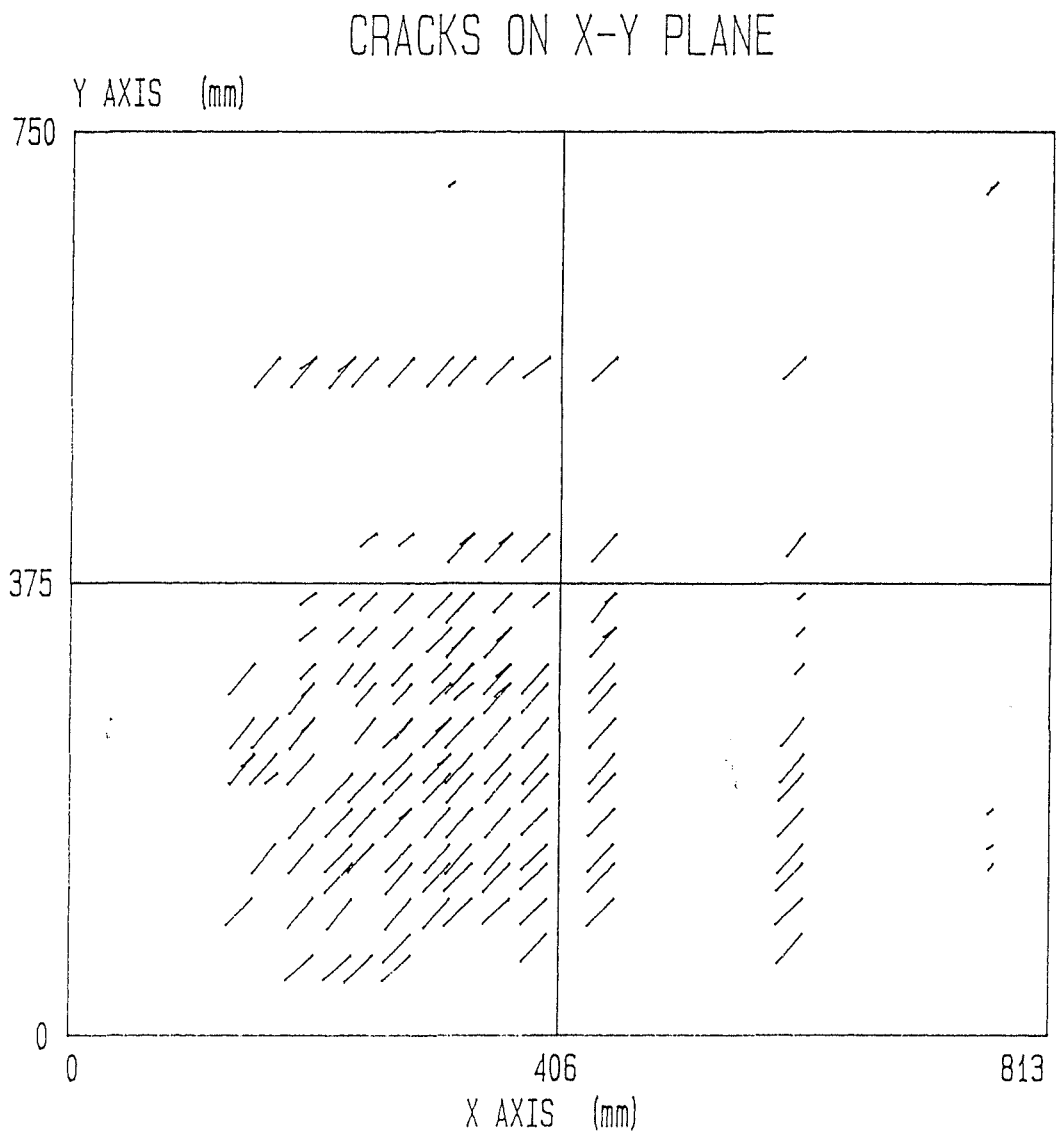

MARCB26 (CKB26DBF)
CRACKS AT BOTTOM OF SLAB

Fig.7.42

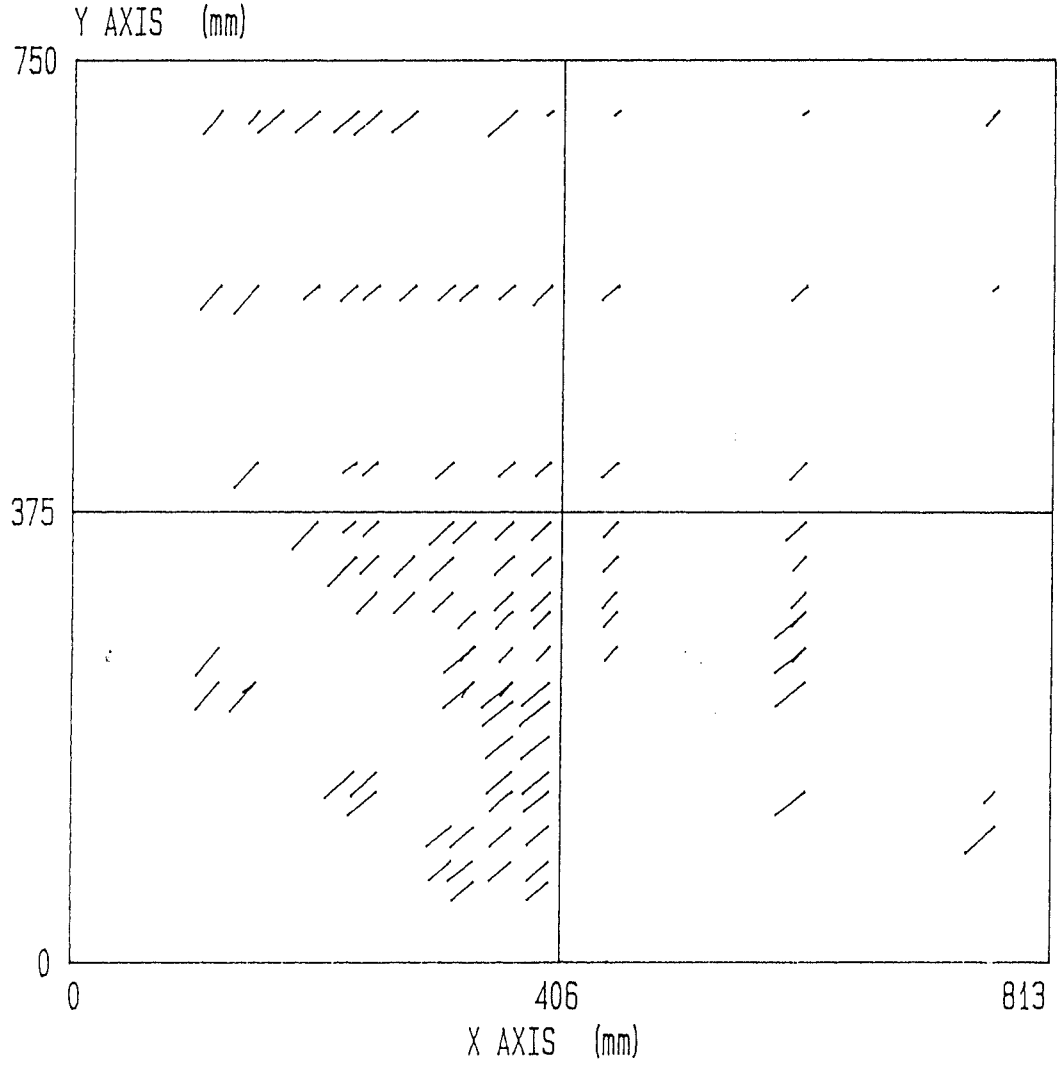

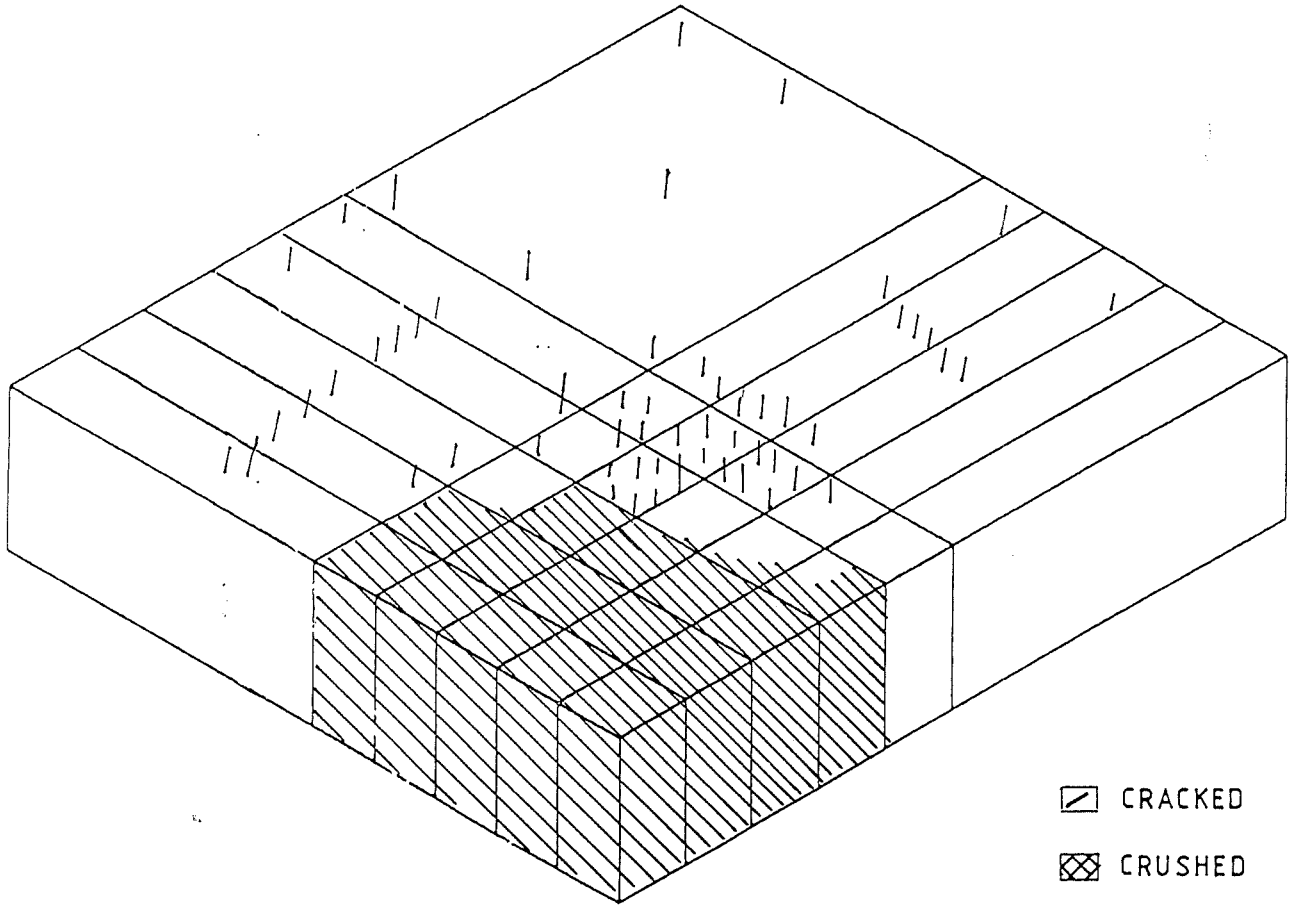

Fig. 7.43 CRACKED AND CRUSHED AREAS OF MODEL B26 FROM MARC ANALYSIS

NONB16 DISP
DISPLACEMENT AT Z-DIRECTION

Fig. 7.44

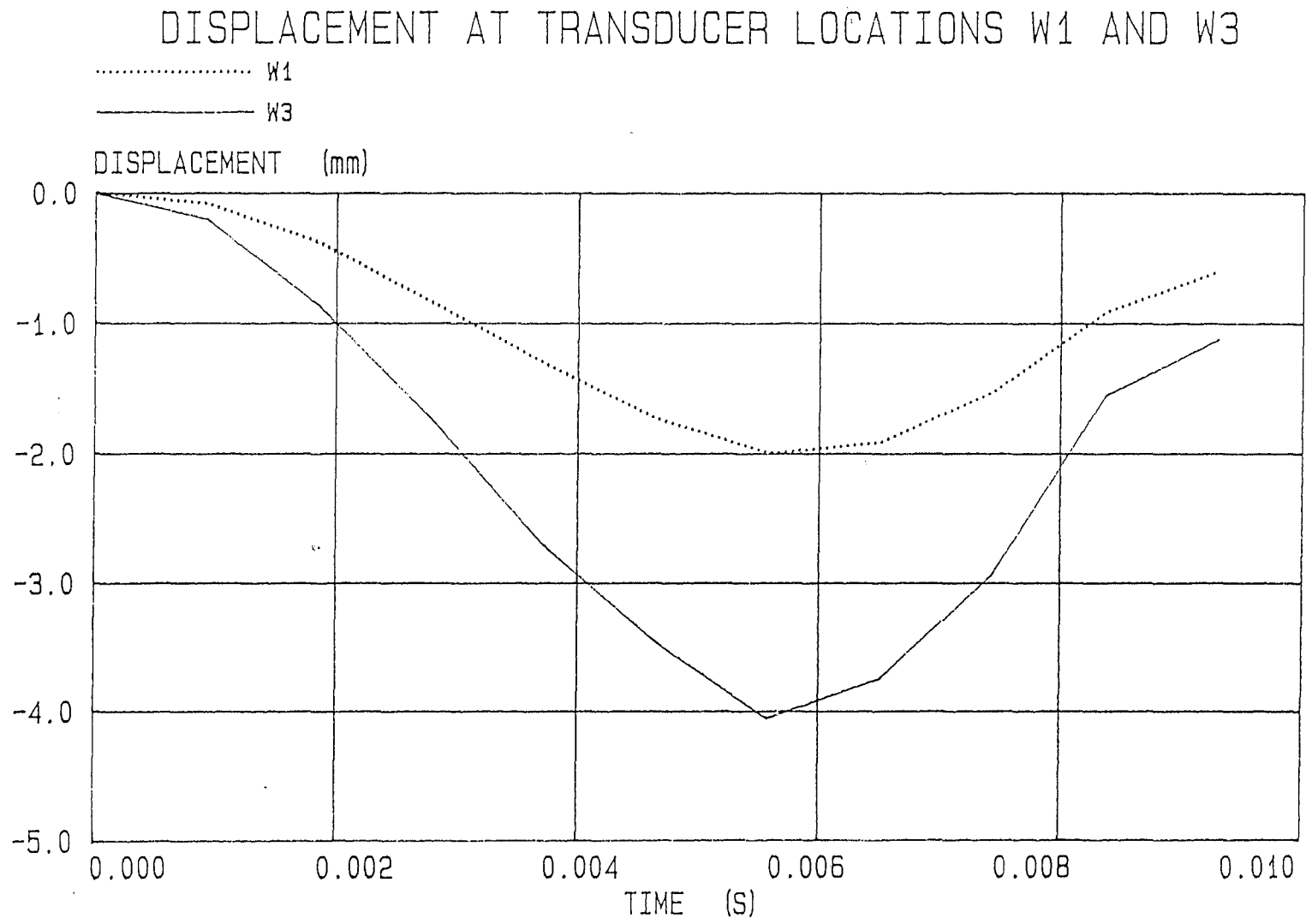

Fig. 7.45

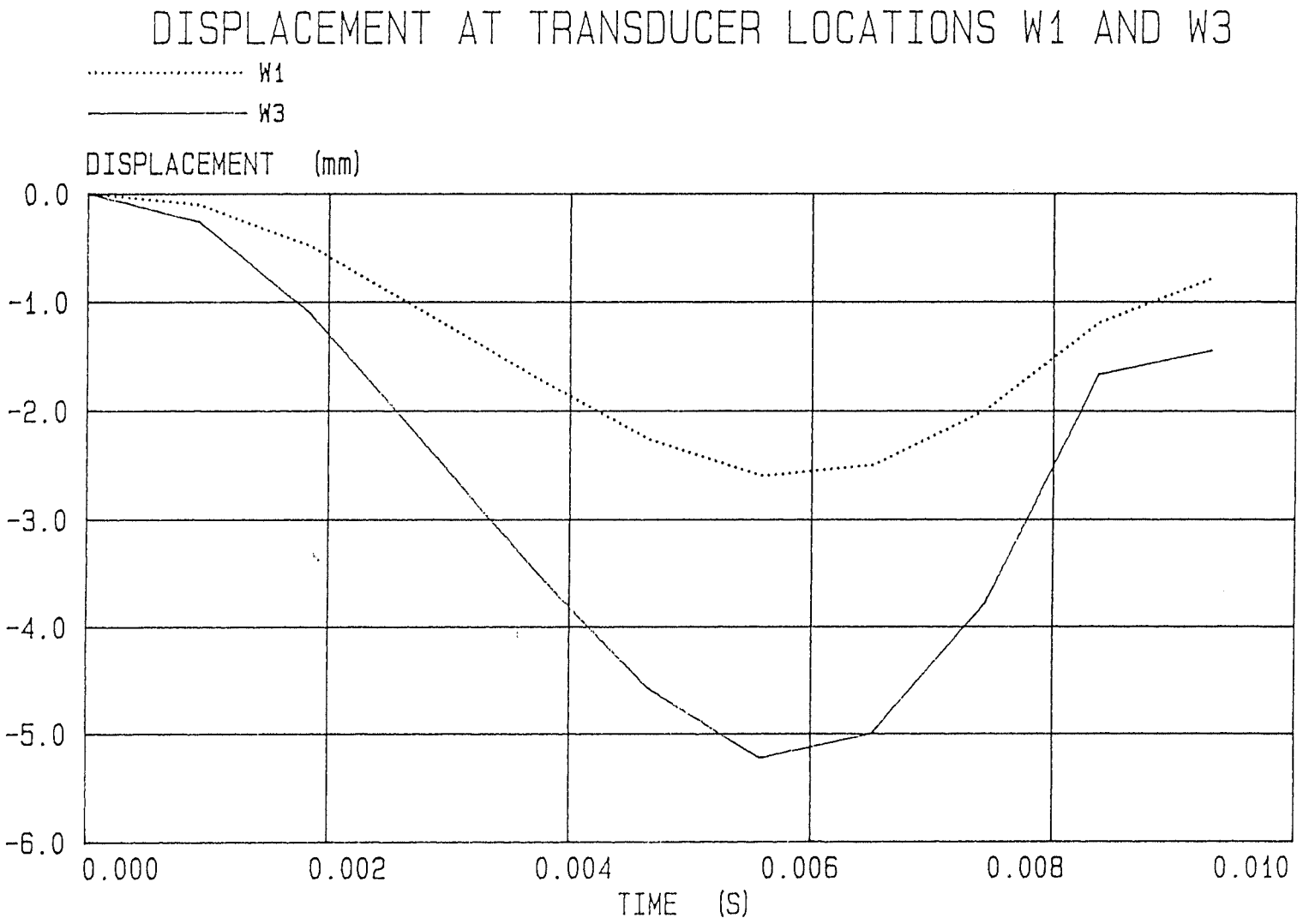
DISPLACEMENT AT TRANSDUCER LOCATIONS W1 AND W3
W1
W3
DISPLACEMENT (mm)
0.0
-1.0
-2.0
-3.0
-4.0
-5.0
-6.0
0.000
0.002
0.004
0.006
0.008
0.010
TIME (S)

NONB26 DISP
DISPLACEMENT AT Z-DIRECTION

Fig. 7.46

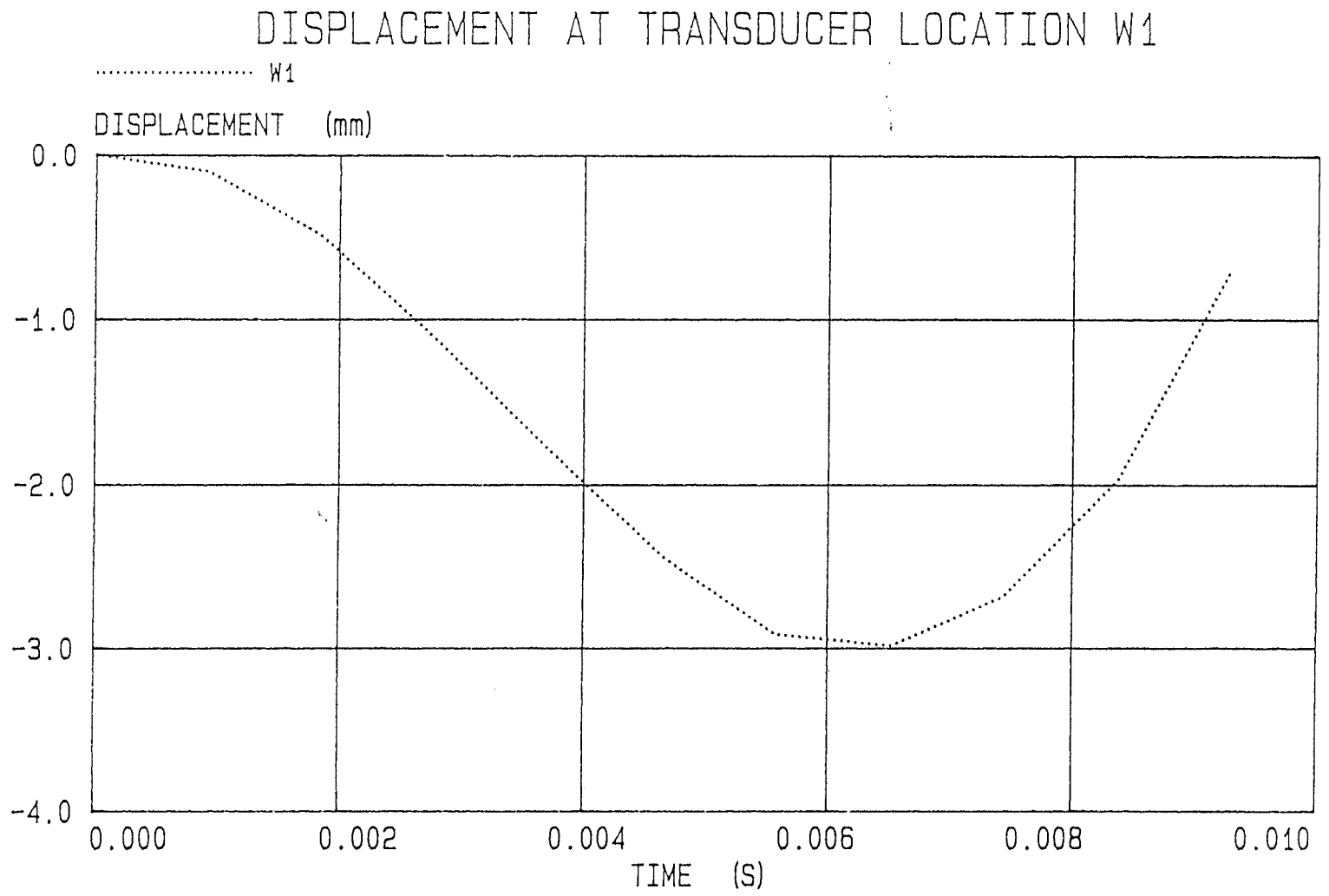

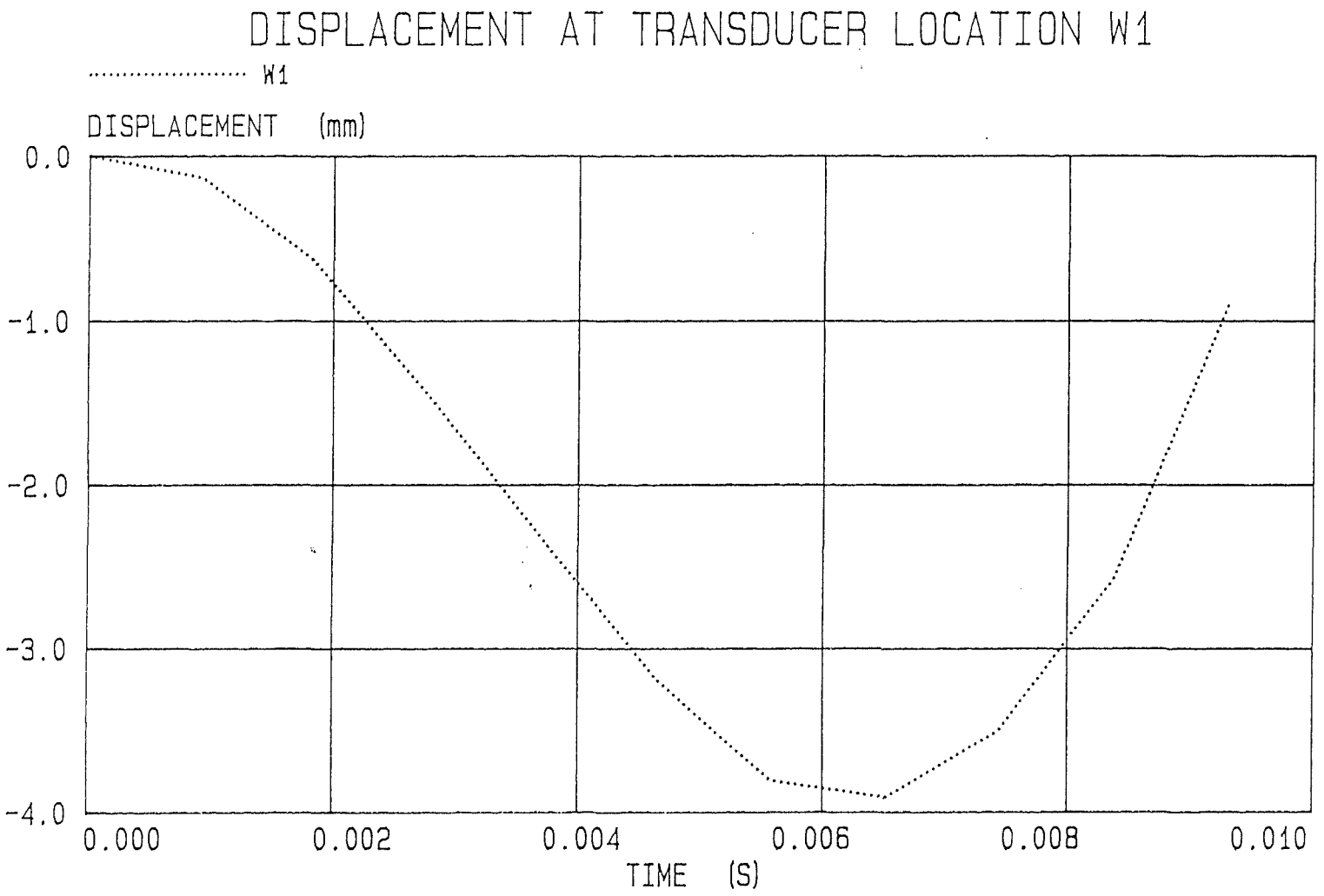
DISPLACEMENT AT TRANSDUCER LOCATION W1
W1
DISPLACEMENT (mm)
0.0
-1.0
-2.0
-3.0
-4.0
0.000
0.002
0.004
0.006
0.008
0.010
TIME (S)

RESULTS FROM NONSAP, MARC AND EXPERIMENT ON MODEL B16
DISPLACEMENT IN Z-DIRECTION

Fig. 7.48

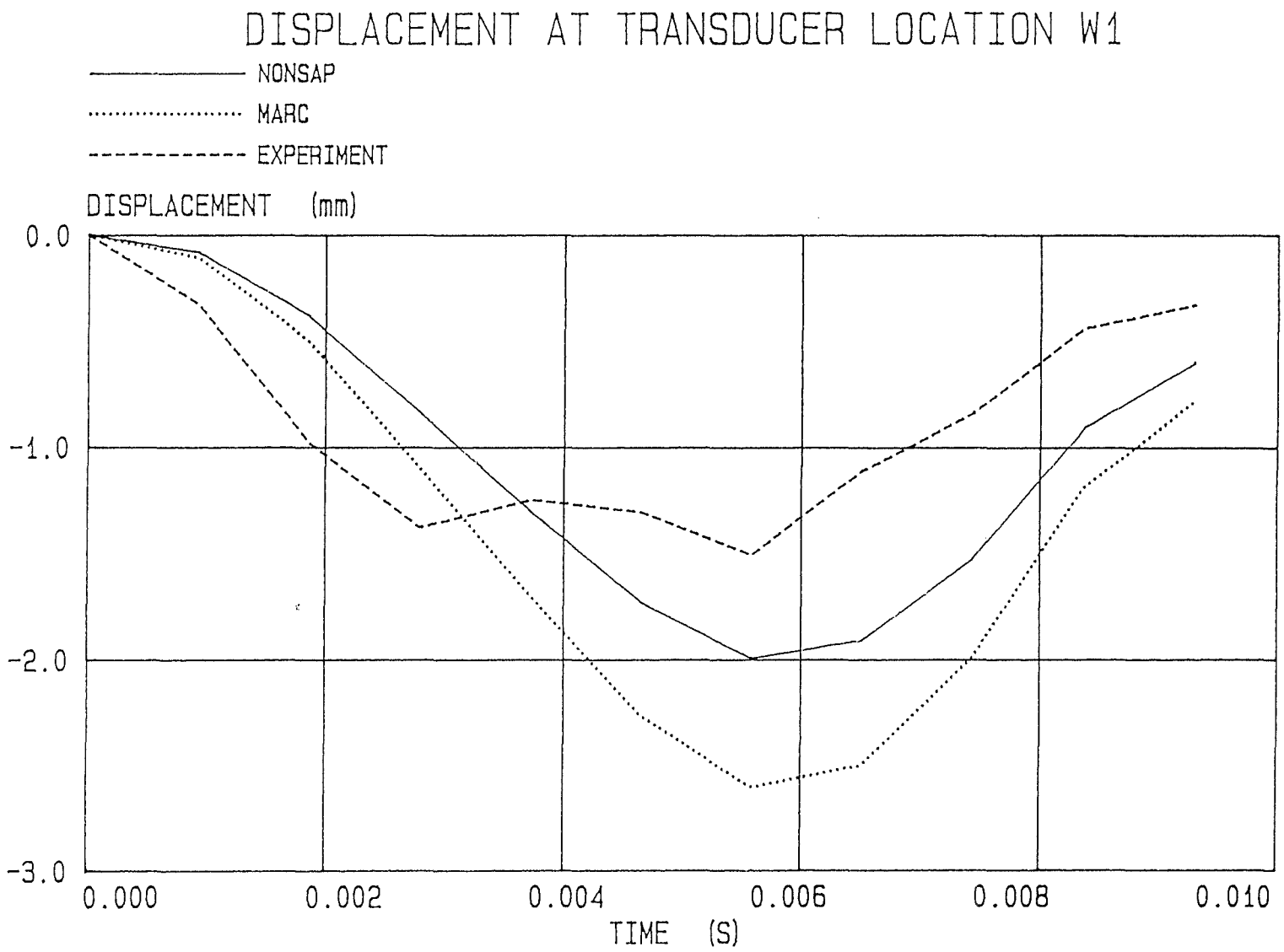

RESULTS FROM NONSAP, MARC AND EXPERIMENT ON MODEL B16
DISPLACEMENT IN Z-DIRECTION

Fig. 7.49

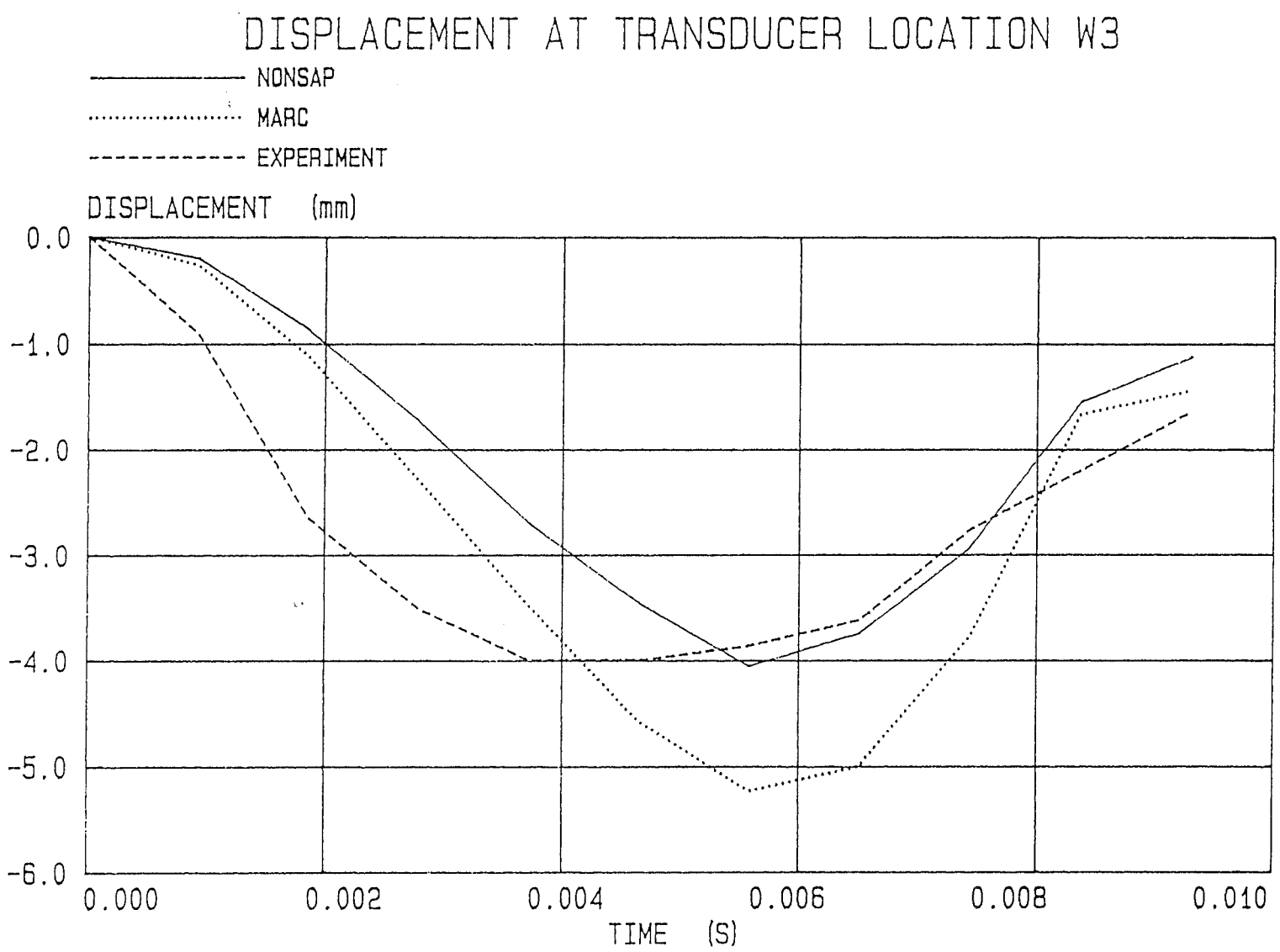

RESULTS FROM NONSAP, MARC AND EXPERIMENT ON MODEL B26
DISPLACEMENT IN Z-DIRECTION

Fig. 7.50

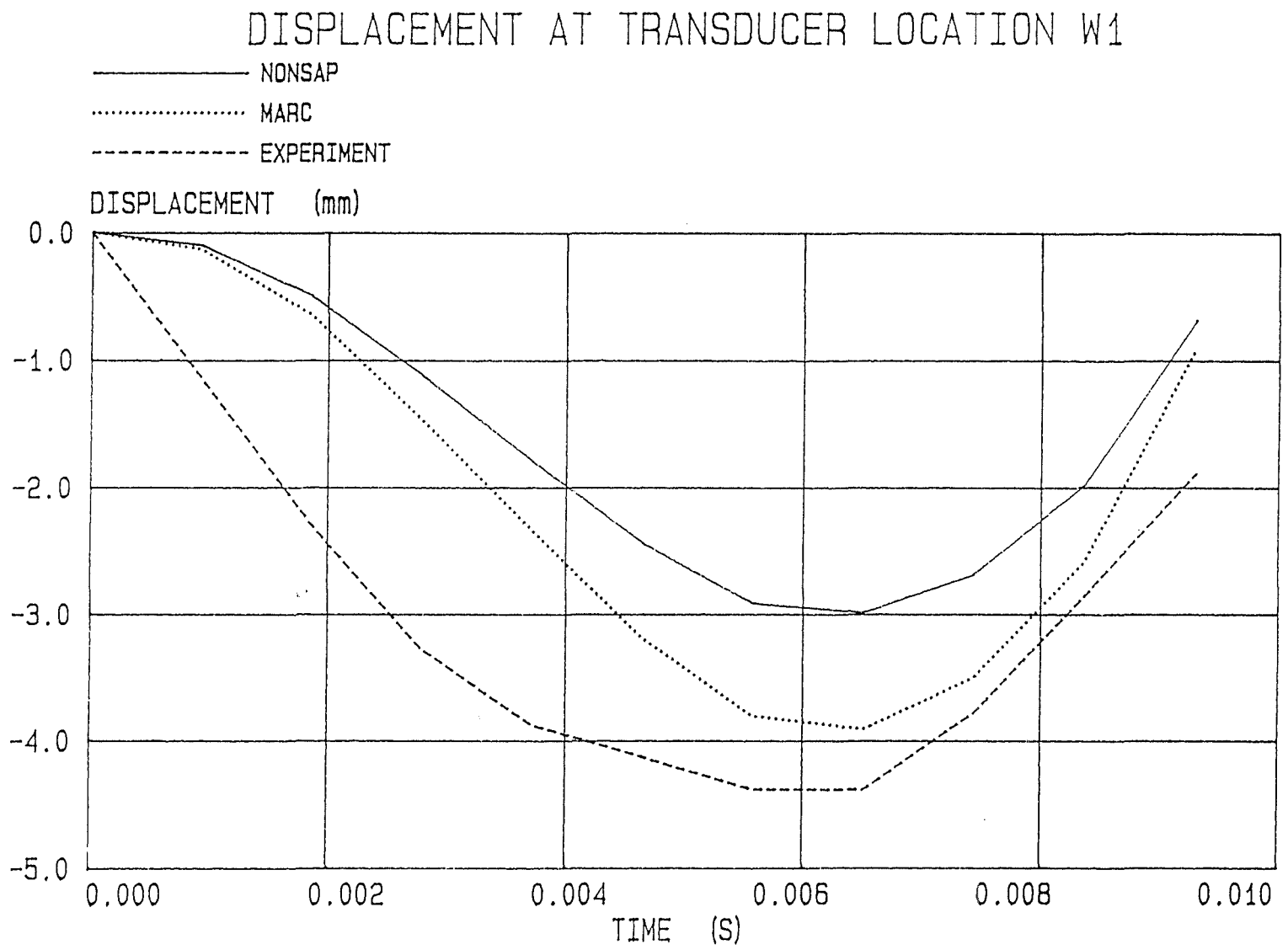

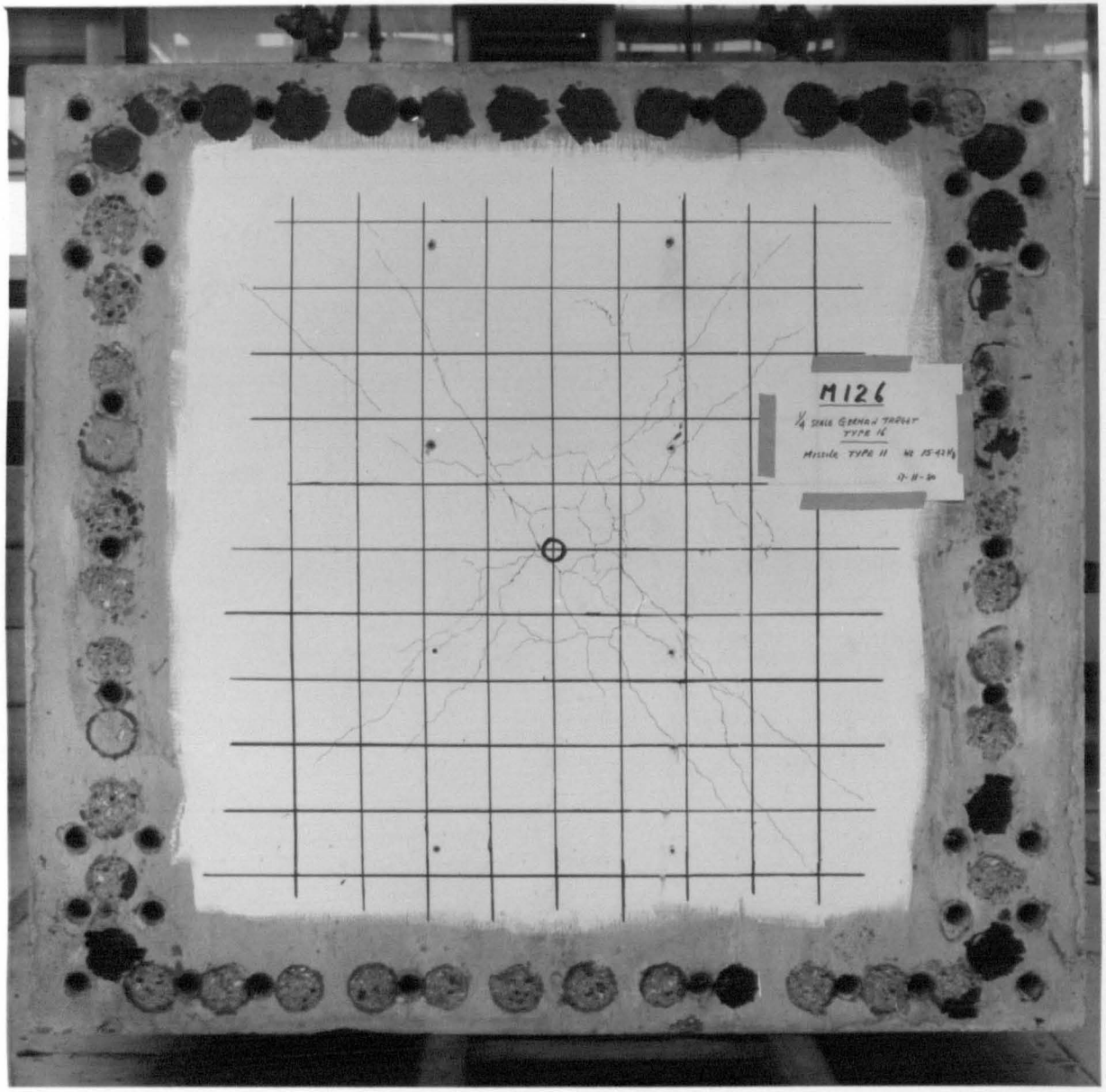

Fig. 7.51 BOTTOM FACE OF TARGET B16 AFTER IMPACT TEST

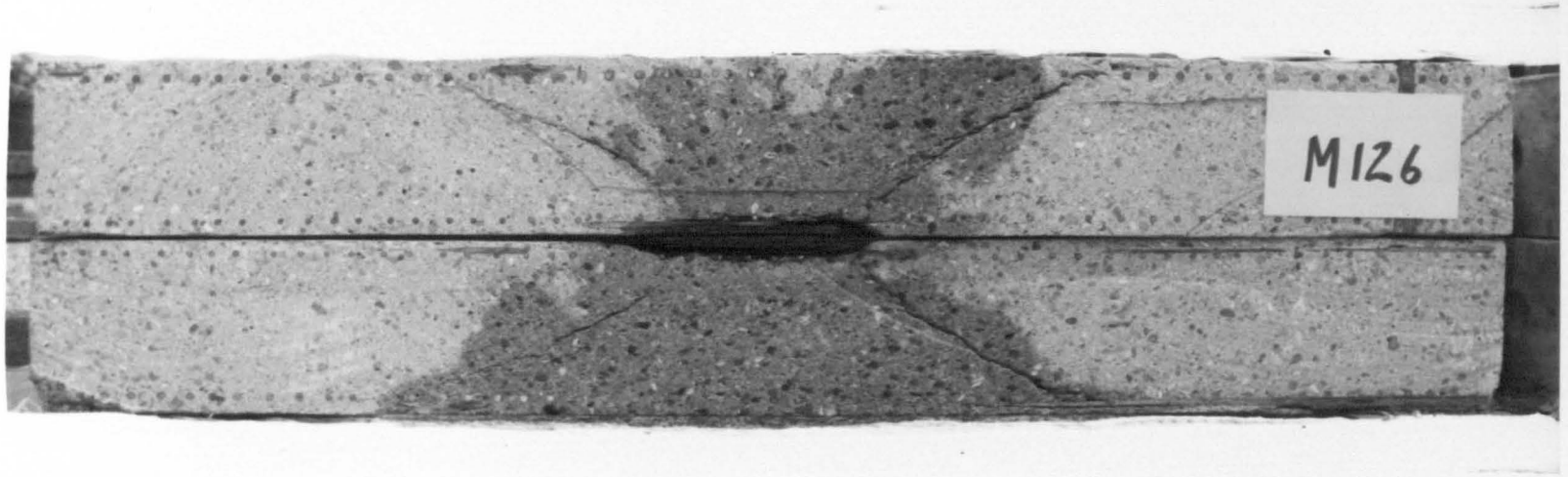

Fig. 7.52 CROSS SECTION THROUGH TARGET B16 AFTER IMPACT TEST

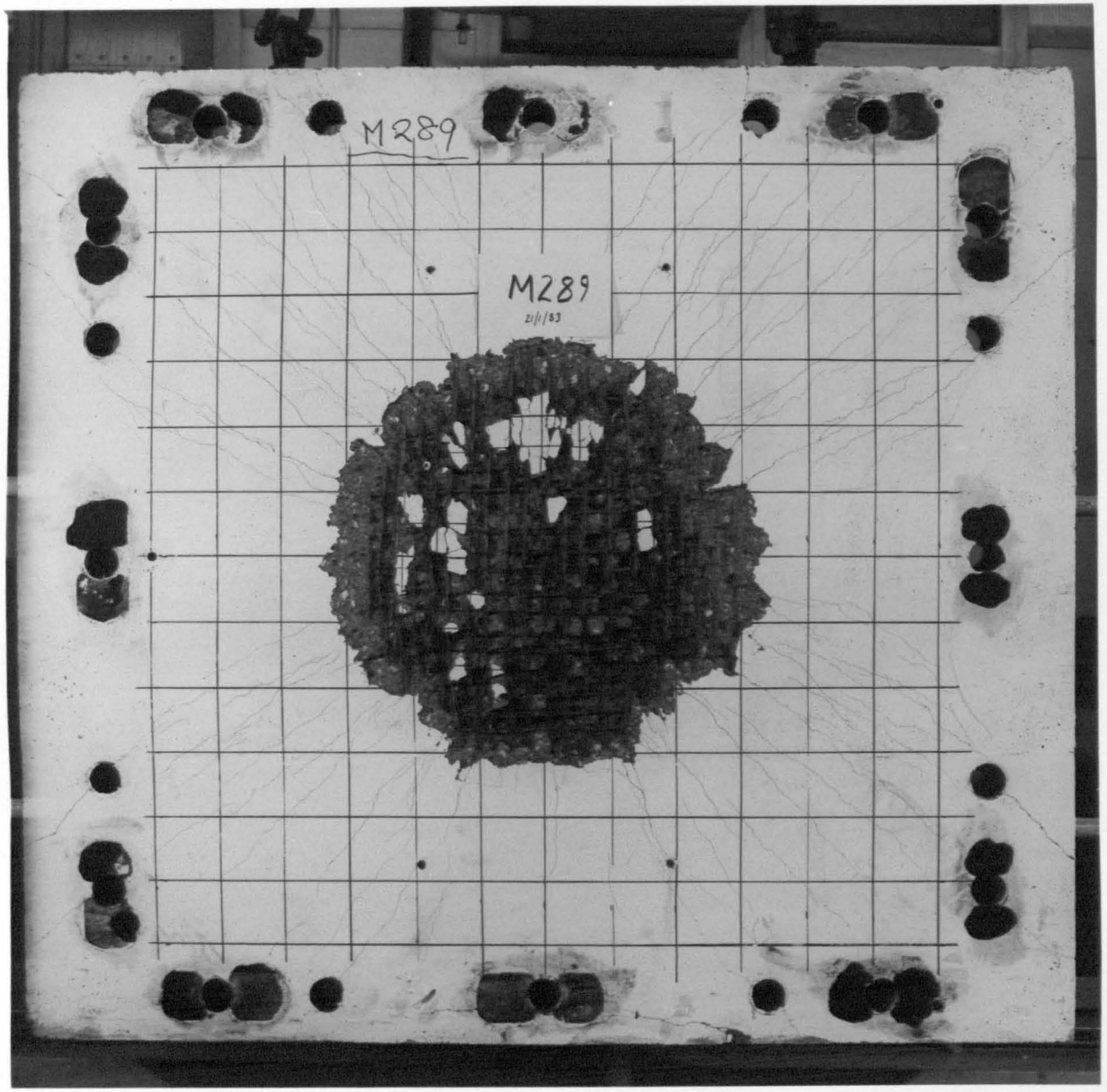

Fig. 7.53 BOTTOM FACE OF TARGET B26 AFTER IMPACT TEST

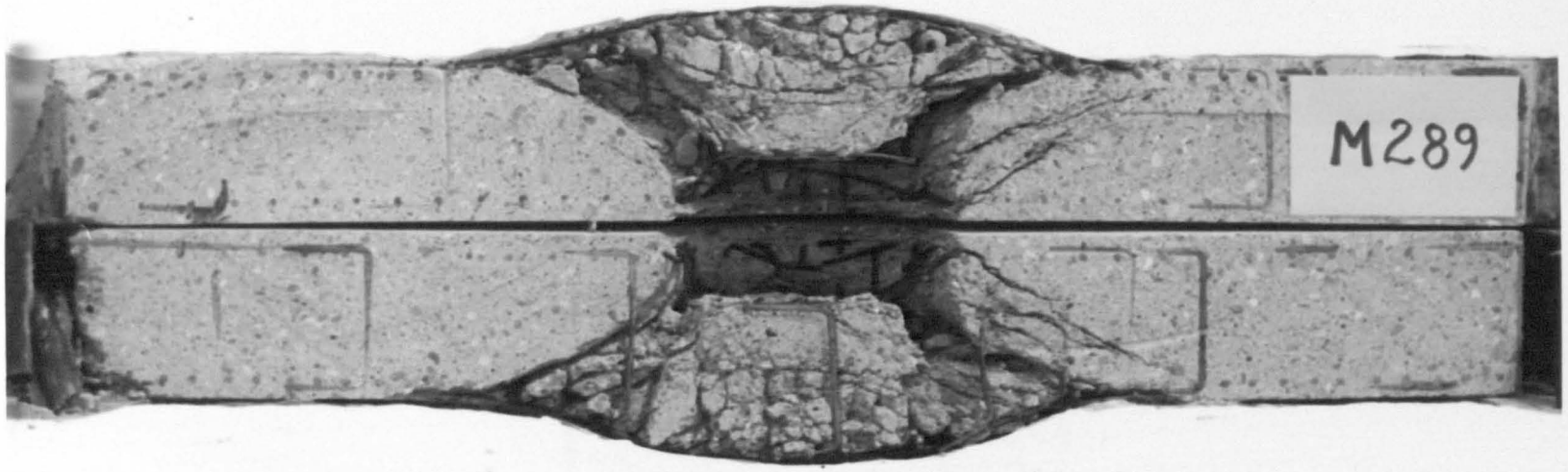

Fig. 7.54 CROSS SECTION THROUGH TARGET B26 AFTER IMPACT TEST

CHAPTER 8

CONCLUSIONS AND FUTURE RECOMMENDATIONS

8.1 Conclusions

Three-dimensional non-linear dynamic finite element programs, NONSAP and MARC were used to analyse the two reinforced concrete slabs (B16 and B26) subjected to impact of soft projectiles. The major results of this study are as follows:-

- The maximum displacements for model B16 calculated from NONSAP agree within 2% of those obtained experimentally while those calculated from MARC only agree within 25%. For model B26, those calculated from NONSAP and MARC agree within 37% and 17% respectively of those obtained experimentally.

- Both NONSAP and MARC produce crack patterns which show the typical shear plug failure similar to that produced experimentally, although both MARC and NONSAP produce more cracks than those obtained from the experiment on model B16. It is not always possible to closely monitor all cracks in an experiment.

- Higher displacements and more severe cracks were found causing damage to model B26.

- The maximum displacements appeared after about 0.006 seconds of the impact time.

- The crushed zones for B26 (Figs. 7.23 and 7.43)are greater than those for B16 (Figs. 7.20 and 7.39).

With reference to the mode shapes obtained by the analyses,it can be observed that higher frequencies occurred from the second mode onwards. It is these frequencies that had to be damped in the analyses.

Both analyses, MARC and NONSAP used different methods for dynamic

analysis and for concrete modelling. Slight variations in results are probably due to these effects. Some information was not available from the experiments to match up with that included in the two analyses. The layout of the reinforcement in the slabs was unconventional and some of the reinforcement could not easily be incorporated. The load-time function graph was accurately modelled in the analyses. The idealised version might have brought about some discrepancies compared with the experimental results. In general, the results from all three cases are in good agreement. The analytical methods used in this research can now be extended to examine more practical problems, including the impact of multi-role combat aircraft and military missiles on vital concrete installations.

8.2 Future Recommendations

In the current research, the number of elements for each model was limited to 36. In the future, it is recommended that more elements, especially in thickness, should be used to carry out further analysis and to achieve more sophisticated results. More load increments and an accelerated solution procedure would also be beneficial. The load application can be improved by applying distributed loads.

Despite the limitation, of the programs, the results show reasonable failure behaviours of reinforced concrete slabs subjected to soft missile impact. From the analyses, it can be seen that relatively less damage was found in the thicker model, B16. This shows that the thickness of the target is a very important parameter in preventing damage from missile impact. In future work this must be included as an additional parameter. Reinforcement (both bending and shear) also helps to prevent perforation and scabbing. Unfortunately this aspect could not be demonstrated in the experiments. The other major parameters affecting the damage criteria of the targets are missile and target stiffnesses, impacting velocities and angles of impact. All these areas are recommended for future testing using finite element analysis. The experimental test programmes should be reviewed, and the new UKAEA rig will provide better facilities for future testing.

REFERENCES

1. Broman R. Probabilistic analysis and design basis determination. Civil engineering and nuclear power, Vol. V, analysis of nuclear power plant structures for effects of impulse and impact loads, 1980.

2. Mchugh L., Seaman L. and Gupta Y. Scale-model test of turbine missile containment by reinforced concrete. U.S.A. 1983.

3. Takeda J. and Tachikawa H. Deformation of fracture of concrete subjected to dynamic loads. Proceedings of the international conference on mechanical behaviour of materials, Vol. IV, KYOTO, 1971.

4. Goldstein S., Berriaud C. and Labrot R. Experimental tests and calculation methods for missile crashing effects on a reactor containment. Paper J 5/6, SMIRT 3, 1975.

5. Spath W. Impact testing of materials. 1957.

6. Kameswara S. and Prasad S. Impact loads on beams on elastic foundations. Paper J 5/8, SMIRT 3, 1975.

7. Davis I. Studies of the response of reinforced concrete structures to short duration dynamic loads. Design for dynamic loading, Constructural Press, 1982.

8. Rezansoff T.,Jirsa J. and Breen J. Lap splicer in reinforced concrete under impact. Structural Division Journal of ASCE, Aug., 1981.

9. Suaris W. and Shah S. Properties of concrete subjected to impact. Structural Division Journal of ASCE, July, 1983.

10. Reinhardh H. Testing and monitoring technique for impact and impulsive loadings and introductory report of concrete structures under impact and impulseive loading. IBAM, June, 1982.

11. Brandes K. Behaviour of critical regions under soft missile impact and impulsive loading. IBAM, June, 1982.

12. Eibl J. Behaviour of critical regions under soft missile impact and impulsive loading. IBAM, June, 1982.

13. Hughes G. and Speirs D. An investigation of the beam impact problem. Technical report 546, C & CA, 1982.

14. Bate S. The effect of impact loading on prestressed and ordinary reinforced concrete beams. National building studies research paper 35, 1961.

15. Billing I. Structure concrete. London Macmillan and Co. LTD, 1960.

16. Watson A. and Ang T. Impact resistance of reinforced concrete structures. Design of dynamic loading, Construction Press, 1982.

17. Watson A. and Ang T. Impact response and post-impact residual strength of reinforced concrete structures. International conference and exposition of structural impact and crashworthiness, July, 1984.

18. Perry S. Brown I. Model prestressed slabs subjected to hard missile loading. Design for dynamic loading, Construction Press, 1982.

19. Perry S., Brown I. and Dinic G. Factors influencing the response of concrete slabs to impact. International conference and exposition of structural impact and crashworthiness, July, 1984.

20. Kufuor K. Perry S. Hard impact of shallow reinforced concrete domes. International conference and exposition of structural impact and crashworthiness, July, 1984.

21. Burgess W. and Campbell-Allen D. Impact resistance of reinforced concrete as a problem of containment. School of civil enginerring, The University of Sydney, Research report no. R251, 1974.

22. Stephenson A. Tornado-generated missiles full-scale testing. Proceedings of the symposium on tornadoes assessment of knowledgement and implication for man, Texas University, June, 1976.

23. Jankov Z., Turnahan J. and White M. Missile tests of quarter-scale reinforced concrete barriers. Proceedings of the symposium on tornadoes assessment of knowledgement and implication for man, June 1976.

24. Stephen A. and Silter G. Full-scale tornado-missile impact tests. Paper J 10/1, SMIRT 4, 1977.

25. Jonas W. and Rudiger E. Experimental and analytical research on the behaviour of reinforced concrete slabs subjected to impact loads. Paper J 7/6, SMIRT 4, 1977.

26. Beriaud C. et al. Local behaviour of reinforced concrete walls under hard missile impact. Paper J 7/9, SMIRT 4, 1977.

27. Gupta Y. and Seaman L. Local response of reinforced concrete to missile impacts. Paper J 10/4, SMIRT 4, 1977.

28. Barr P. et al. An experimental investigetion of scaling of reinforced concrete structures under impact loading. Design for dynamic loading, Construction press, 1982.

29. Barr P. et al. Experimental studies of the impact resistance of steel faced concrete composition. Paper J 8/4, SMIRT 7, 1983.

30. Barr P. et al. Studies of missile impact with reinforced concrete structures. Vol. 19, No. 3, Nuclear Energy, 1980.

31. Neilson A. Missile impact on metal structures. Vol. 19, No 3, Nuclear Energy, 1980.

32. Anderson W., Watson A. and Armstrong P. Fibre reinforced concrete for the protection of structures against high velocity impact. International conference and exposition of structural impact and crashworthiness, July, 1984.

33. Berriaud C. et al. Test and calculation of the local behaviour of concrete structures under missile impact. Paper J 7/1, SMIRT 5, 1979.

34. Brandes K., Limberger E. and Hertes J. Experimental investigation of reinforced concrete behaviour due to impact load. Paper J 7/3, SMIRT 5, 1979.

35. Sage E. and Pfeiffer A. Response of reinforced concrete targets to impacting soft missile. Paper J 8/4, SMIRT 5, 1979.

36. Jonas W. et al. Experimental investigations to determine the kinetic ultimate capacity of reinforced concrete slabs subject to deformable missiles. Paper J 8/4, SMIRT 5, 1979.

37. Dulac J. and Giraud J. Impact testing of reinforced concrete slabs. Paper J 7/1, SMIRT 6, 1981.

38. Chiba N. et al. Nonlinear dynamic analysis of steel plates subjected to missile impact. Paper J 7/4, SMIRT 6, 1981.

39. Ohte S. et al. The strength of steel plates subjected to missile impact. Paper J 7/10, SMIRT 6 1981.

40. Yamamoto S. et al. Nonlinear analysis of missile impact on steel plates. Paper J 7/3, SMIRT 7, 1983.

41. Woodfin R. and Sliter G. Modelling and contact of turbine missile concrete impact experiments. Paper J 8/1, SMIRT 6, 1981.

42. Woodfin R. and Sliter G. Results of full scale turbine missile concrete impact experiments. Paper J 8/2, SMIRT 6, 1981.

43. Rudiger E. and Riech H. Experimental and theoretical investigations on the impact of deformable missiles onto reinforced concrete slabs. Paper J 8/3, SMIRT 7, 1983.

44. Brandes K., Limberger E. and herter J. Strain rate dependent energy absorption capacity of reinforced concrete members under aircraft impact. Paper J 9/5, SMIRT 7, 1983.

45. Harrop J. and Abdul-Wahab H. The rigidity of perforated concrete slabs. Vol. 6, Nuclear Energy and Design, 1967.

46. Gueraud R. et al. Study of the perforation of reinforced concrete slabs by rigid missiles-general introduction and experimental study part I. Vol. 41, Nuclear Engineering and Design, 1977.

47. Figuet G. and Dacquet S. Study of the perforation of reinforced concrete slabs by rigid missiles-experimental study part II. Vol. 41, Nuclear Engineering and Design, 1977.

48. Goldstein S., Berriaud C. and Labrot R. Study of the perforation of reinforced concrete slabs by rigid missiles-experimental study part III. Vol. 41, Nuclear Engineering and Design, 1977.

49. Davidson I. and Bradbury J. The analysis of dynamically loaded non-linear structures. Vol. 45, Nuclear engineering and design, 1978.

50. Gupta Y. and Seamae L. Local response of reinforced concrete to missile impact. Vol. 45, Nuclear Engineering and Design, 1978.

51. Limberger E. A simple mode for predicting energy disspation of thin plates being perforated by hard missiles. Vol. 51, Nuclear Engineering and Design, 1979.

52. Stefanou G. An Investigation into the behaviour of perforated slabs for concrete reactor vessels under temperature and external load. Vol. 52, Nuclear Engineering and Design, 1979.

53. Bignon P. and Riera J. Verification of methods of analysis of soft missile impact problems. Vol 60, Nuclear Engineering and Design, 1980.

54. Albertini C. and Montagnani M. Contitutive laws of materials in dynamics-outline of a program of testing on small and large specimens for containment of extreme dynamic loading conditions. Vol. 68, Nuclear Engineering and Design, 1981.

55. Nachtsheim W. and Stangenberg F. Investigation of results of Meppen slab tests-comparison with parametric investigation. Vol. 75, Nuclear Engineering and Design, 1982.

56. Kussmaul K. The investigation of the tensile and notch impact bend test into an experimentally validated fracture mechanics concept. Vol. 72, Nuclear Engineering and Design, 1982.

57. Riera J. Basic concept and load characteristic in impact problem. IBAM, June, 1982.

58. Degen P. Perforation of reinforced concrete slabs by rigid missiles. Vol. 106, Structural Division Journal of ASCE, 1980.

59. Linderman R., Rotz J. and Yen G. Design of structures for missile impact. Topical Report BC-TOP-9A (Rev. 2) U.S.A., Sept., 1974.

60. Riera J. On the stress analysis of structures subjected to aircraft impact forces. Vol. 8, Nuclear Engineering and Design, 1968.

61. Yang H. and Godfrey D. Structural analysis of aircraft impact on a nuclear containment vessel and associated structures. Vol. 11, Nuclear Engineering and Design, 1970.

62. Hammel J. Impact loading on a spherical shell. Paper J 5/7, SMIRT 3, 1975.

63. Hammel J. Aircraft impact on a spherical shell. Vol. 37, Nuclear Engineering and Design, 1976.

64. Connor J. et al. Missile impact on reinforced concrete structures. Proceeding of second annual engineering mechanics division speciality conference. May, 1977.

65. Habip L. Characterization of structural design caused by extreme dynamic loads. Paper J 5/1, SMIIRT 3, 1975.

66. Florence A. Structural response of reinforced concrete slabs to impulsive loading. Paper J 7/8, SMIRT 4, 1977.

67. Ettouney M., Radini R. and Hsueh P. Analysis of the overall structural behaviour due to the impact of deformable missiles. Paper J 7/9, SMIRT 5, 1979.

68. Zimmermann Th. and Rodriguez C. Nonlinear analysis of reactor building for airplane impact loadings. Paper J 9/3, SMIRT 6, 1981.

69. McMahon P. et al. Structural response of reinforced concrete slabs to tornado missiles. Structural Division Journal of ASCE, 1979.

70. Labra J. Protective structures response to vehicle impact. Structural Division Journal of ASCE, 1979.

71. Ghaboussi J., Millavec W. and Jsenberg J. Reinforced concrete structures under impulsive loading. Structural Division Journal of ASCE, March, 1984.

72. Zerna W. and Stangenberg F. On the shock behaviour of reinforced concrete structural systems. IBAM, June, 1982.

73. Donglas R. and Bingham W. Strains and wave velocities in high velocity impact. Proceeding of second annual engineering mechanics division speciality conference, May, 1977.

74. Broman R. et al. Report of the ASCE committee on impactive and impulsive loads. Civil Engineering and Nuclear Power Vol. V, Sept., 1980.

75. Broman R. et al. Analysis and design for impact loads. Civil Engineering and Nuclear Power, Vol. V, Sept., 1980.

76. Rotz J. Evaluation of tornato missile impact effects on structures. Proceedings of the symposium on tornadoes assessment of knowledgement and implication for man, June 1976.

77. Bokor A. Partition of impact energy between local deformation and target response. Vol. 19, Nuclear Energy, 1980.

78. Jonker J. Dynamic response of a clamped/free hollow circular cylinder under travelling torsional impact loads. Vol. 67, Nuclear Engineering and Design, 1981.

79. Buyukozturk O. and Connor J. Nonlinear dynamic response of reinforced concrete under impulsive loading: research status and needs. Vol. 50, Nuclear Engineering and Design, 1978.

80. Broman R. et al. Analysis and design for impulsive loads. Civil Engineering and Nuclear Power, Vol V, Sept., 1980.

81. Chang W., Burdette E. and Barnett R. Missile penetration. Structural Division Journal of ASCE, May, 1976.

82. Chang W. Impact of solid missiles on concrete barriers. Structural Division Journal of ASCE, Feb., 1981.

83. Kar A. Barrier design for tornado generated missiles. Paper J 10/3, SMIRT 4, 1977.

84. Kar A. Local effects of tornado generated missiles. Structural Division Journal of ASCE, May, 1978.

85. Kar A. Projectile penetration into steel. Structural Division Journal of ASCE, Oct., 1979.

86. Kar A. Impactive effects of tornado missiles and aircrafts. Structural Division Journal of ASCE, Nov., 1979.

87. Kar A. Projectile penetration into buried structures. Structural Division Journal of ASCE, Jan., 1978.

88. Kar A. Impact load for tornado-generated missiles. Vol. 47, Nuclear Engineering and Design, 1978.

89. Kar A. Loading time history for tornado-generated missiles. Vol. 51, Nuclear Engineering and Design, 1979.

90. Sliter G. Assessment of empirical concrete impact formulae. Structural Division Journal of ASCE, May, 1980.

91. Haldar A. and Miller F. Penetration depth in concrete for non-deformable missiles. Vol. 71, Nuclear Engineering and Design, 1982.

92. Haldar A., Hatami M. and Miller F. Concrete structures: penetration depth estimation for concrete structures. Structural Division Journal of ASCE, Jan., 1983.

93. Haldar A., Hatami M. and Miller F. Penetration and spalling depth estimation for concrete structures. Paper J 7/2, SMIRT 7, 1983.

94. Berriaud C. et al. Local behaviour of reinforced concrete walls under missile impact. Vol. 45, Nuclear Engineering and Design, 1978.

95. Dubois J., Chedmail J. and Bianchini J. Numerical analysis of impact-penetration problems for nuclear reactor safety. Paper J 7/4, SMIRT 4, 1977.

96. Drittler K., Gruner P. and Krivy J. Calculation of forces arising from impacting projectiles upon yielding structures. Paper J 7/4, SMIRT 4, 1977.

97. Alderson M. et al. Reinforced concrete behaviour due to missile impact. Paper J 7/7, SMIRT 4, 1977.

98. Mcmahon P., Sen S. and Meyers B. Behaviour of reinforced concrete barriers subjected to the impact of turbine missiles. Paper J 7/6, SMIRT 5, 1979.

99. Stangenberg F. and Buttmann P. Impact testing of steel fibre reinforced concrete slabs with liner. Paper J 7/5, SMIRT 5, 1979.

100. Haldar A. Turbine missile- a critical review. Vol. 55, Nuclear Engineering and Design, 1979.

101. Haldar A. Impact loading- damage prediting equations. Paper J 8/4, SMIRT 6, 1981.

102. Davis I. Design and analysis of concrete structres under impact and impulsive loading. IBAM, June, 1982.

103. Healing J. Local effects of missile impact on protective barriers. Proceedings of the symposium on tornadoes assessment of knowledgement and implication for man, June 1976.

104. Tekeda J. Crashworthiness of concrete structures subjected to impact or explosion. International conference and exposition of structural impact and crashworthiness, July, 1984.

105. Zielinski A. Fracture of concrete under impact loading. International conference and exposition of structural impact and crashworthiness, July, 1984.

106. Zorn N. and Reinhardt H. Concrete structures under high intensity tensile waves. International conference and exposition of structural impact and crashworthiness, July, 1984.

107. Tulacz J. and Smith R. Assessment of missile generated by pressure component failure and its application to recent gas-cooled nuclear plant design. Vol. 19, No. 3, Nuclear Energy, 1980.

108. Nashtsheim W. and Stangenberg F. Impact of deformable missiles on reinforced concrete plates- comparisonal calculations of Meppens tests. Paper J 7/3, SMITH 6, 1981.

109. Nashtsheim W. and Stangenberg F. Slected results of Meppen slab tests- state of interpretion, comparison with computation investigation. Paper J 8/1, SMITH 7, 1983.

110. Davis I. Damaging effects from the impact of missiles against reinforced concrete structures. Vol. 19, No. 3, Nuclear Energy, 1980.

111. Kennedy R. A review of procedures for the analysis and design of concrete structures to resist missile impact effects. Vol. 37, Nuclear Engineering and Design, 1976.

112. Attalla I. Missile impact on reinforced concrete structures. Vol. 37, Nuclear Engineering and Design, 1976.

113. Hughes G. Hard missile impact on reinforced concrete. Vol. 77, Nuclear Engineering and Design, 1984.

114. Reynen J., Villafune E and Crutzen Y. Impulsive loading on concrete structures. Paper J 10/1, SMIRT 6, 1981.

115. Bangash Y. The limit state analysis of a prestressed concrete containment vessel for PWR. Paper J 3/8, SMIRT 7,1983.

116. Bangash Y. Containment vessel design and practice. Vol. 11, No. 2, Nuclear Energy, 1982.

117. Krulzik N. Analysis of aircraft impact problem. Avanced structural dynamics, Applied Science Publishers, 1980.

118. Barley and Davies Aircraft impact design for SGHWR containment. International conference on experience in the design, construction and operation of PCPV, Paper 128175, England, 1975.

119. Rice J. and Bahar L. Reaction-time relationship and structural design of reinforced concrete slabs and sheels for aircraft impact. Paper J 5/3, SMIRT 3, 1975.

120. Bahar Y. and Rice S. Simplied derivation of the reaction-time history in aircraft impact on a nuclear power plant. Vol. 49, Nuclear Engineering and Design, 1978.

121. Sharpe R., Ramil H. and Scunlan R. Analysis of aircraft impact on reactor building. Paper J 5/4, SMIRT 3, 1975.

122. Kamil H. et al. An overview of major aspects of the aircraft impact problem. Paper J 8/1, SMIRT 4, 1977.

123. Kamil H. et al. An overview of major aspects of the aircraft problem. Vol. 46, Nuclear Engineering and Design, 1978.

124. Schmidt R. et al. Structural design for aircraft impact loading. Paper J 8/2, SMIRT 4, 1977.

125. Kaiser A. et al. Local and global response of reactor buildings at the load case of aircraft impact. Paper J 8/3, SMIRT 4, 1977.

126. Fuzier J., Cheyrezy M. and Dufour C. Specific problems concerning aircraft impact on reactor comtainment vessels. Paper J 8/6, SMIRT 4, 1977.

127. Carlton D. and Bedi A. Theoretical study of aircraft impact on reactor containment structures. Paper J 8/7, SMIRT 4, 1977.

128. Kotulla B. and Hansson V. Analysis of the impact of aircraft crash on underground concrete ducts with protective slabs at reactor buildings. Paper J 8/8, SMIRT 4, 1977.

129. Danisch R. and Graubner U. Inelastic behaviour of reinforced concrete structures subjected to induced vibrations of aircraft impact or gas cloud explosion. Paper J 9/2, SMIRT 4, 1977.

130. Ree H. and Hock M. Analysis of the behaviour of a concrete structure due to airplane impact and the effect of the reinforcement. Paper J 9/5, SMIRT 5, 1979.

131. Lazzeri L., Olivieri M. and Travi S. On the analysis of the consequences of aircraft impact for the design of structures and components. Paper J 9/1, SMIRT 6, 1981.

132. Carlton D. and Bedi A. Theoretical study of aircraft impact on reactor containment structures. Vol. 45, Nuclear Engineering and Design, 1978.

133. Filho F., Coombs R. and Barreto L. Design of reinforced containment shell of a nuclear reactor for aircraft impact. Paper J 9/11, SMIRT 6, 1981.

134. Crutzen Y. and Reynen J. Disintegration of concrete shell structures under violent dynamic loadings conditions. Paper J 7/1, SMIRT 7, 1983.

135 Rebora B., Zimmermann Th. and Wolf J. Dynamic rapture analysis of reinforced concrete shells. Vol. 37, Nuclear Engineering and Design, 1976.

136. Puttonen J. The local deformations cauesd by aircraft impact on a containment building. Paper J 9/12, SMIRT 6, 1981.

137. Bauer J., Scharpf F. and Schwarz R. Analysis of reinforced concrete structures subjected to aircraft impact loading. Paper J 9/4, SMIRT 7, 1983.

138. Buchhardt F. et al. A nonlinear three-dimensional containment analysis for airplane impact. Paper J 9/6, SMIRT 7, 1983.

139. Marti J., Kalsi G. and Attalla I. Three-dimensional aircraft impact analysis. Paper J 9/7, SMIRT 7, 1983.

140. Thomson R. NASA Langley research center, USA research at NASA on crash dynamics. International conference and exposition of structural impact and crashworthiness, July, 1984.

141. Chelapati C., Kennedy R. and Wall I. Probabilistic assessment of air-craft hazard for Nuclear power plants. Vol. 19, Nuclear Engineering and Design, 1972.

142. Stangenberg F. Nonlinear dynamic analysis of reinforced concrete structures. Vol. 29, Nuclear Engineering and Design, 1974.

143. Drittler K. and Grunger P. Calculation of the total force acting upon a rigid wall by projectiles. Vol. 37, Nuclear Engineering and Design, 1976.

144. Drittler K. and Gruner P. The force resulting from impact of fast-flying military aircraft upon a rigid wall. Vol. 37, Nuclear Engineering and Design, 1976.

145. Degen P., Furrer H. and Jemielewski J. Structural analysis and design of a nuclear power plant building for aircraft effects. Vol. 37, Nuclear Engineering and Design, 1976.

146. Zerna W., Schnelleneach G. and Stangenberg F. Optimized reinforcement of nuclear power plant structures for aircraft impact forces. Vol. 37, Nuclear Engineering and Design, 1976.

147. Meder G. Dynamic response of a sdof elastic-plastic system subjected to aircraft impact pulses. Vol. 47, Nuclear Engineering and Design, 1982.

148. Schnellenbach G and Stangenberg F. Design of concrete containments for aircraft impact. Paper j 8/4, SMIRT 4, 1977.

149. Riera J. A critical reappraisal of nuclear power plant safety against accidentical aircraft impact. Vol. 57, Nuclear Engineering and Design, 1980.

150. Steveson J. Current summary of international extreme load design requirements for nuclear power plant facilities. Vol. 60, Nuclear Engineering and Design, 1980.

151. Hornyk K. Analytic modelliing of the impact of soft missiles on protective walls. Paper J 7/3, SMIRT 4, 1977.

152. Stoykovich M. Impact load time histories for viscoelastic missiles. Paper J 7/5, SMIRT 4, 1977.

153. Chiapetta R. and Costello J. Automobile impact forces on concrete walls. Paper J 8/8, SMIRT 6, 1981.

154. Porter W. Generation of missiles and destructive shock fronts and their consequences. Vol. 19, No. 3, Nuclear Energy, 1980.

155. McMahon P., Meyers B. and Buchert K. The behaviour of reinforced concrete barriers to the impact of tornado generated deformable missiles. Paper J 10/2, SMIRT 4, 1977.

156. Jones W. et al. Approxmate calculation of the impact of missiles onto reinforced concrete structures and comparison of test results. Paper J 8/6, SMIRT 5, 1979.

157. Hanagud S. and Bernard R. A penetration theory for axisymmetric projectiles. Paper J 7/10, SMIRT 4, 1977.

158. Brown M., Curtress N. and Jewett J. Local failure of reinforced concrete under missile impact loading. Paper J 8/7, SMIRT 5, 1979.

159. Jamet P. et al. Perforation of a concrete slab by a missile:- finfite element approach. Paper J 7/6, SMIRT 7, 1983.

160. Wittmann F. and Boulahdour T. Variability of resistance of concrete slabs under impact load. Paper J 7/2, SMIRT 6, 1981.

161. Stangenberg F. and Zerna W. Extreme load resistant design of nuclear power plant structures. Paper J 8/5, SMIRT 4, 1977.

162. Munday G. Initial velocities attained by plant generated missile. Vol. 19, No. 3, Nuclear Energy, 1980.

163. Yen G. Probability of a containment of turbine missile. Vol. 37, Nuclear Engineering and Design, 1976.

164. Twisdale L., Dunn W. and Davies T. Tornado missile transport analysis. Vol. 51, Nuclear Engineering and Design, 1979.

165. Goodman J. and Koch J. The probability of a tornado missile hitting a target. Vol. 75, Nuclear Engineering and Design, 1983.

166. Haldar A. and Hamieh H. Local effects of solid missiles on concrete structures. Structural Division Journal of ASCE, May, 1984.

167. Costello J., Simiu E. and Cordes M. Tornado borne missile speed. Structural Division Journal of ASCE, June, 1977.

168. Watwood Jr. V. The finite element method for prediction of crack behaviour. Vol. 11, Nuclear Engineering and Design, 1969.

169. Hopkirk R., Lympany S. and Marti J. Three-dimensional numerical preditions of impact effects. Vol. 19, No. 3, Nuclear Energy, 1980.

170. Bangash Y. The structural integrity analysis of concrete containment vessels under external impacts. Paper J 7/6, SMIRT 6, 1981.

171. Walter T. and Wolde-Tinsae A. Turbine missile perforation of reinforced concrete. Structural Division Journal of ASCE, Oct., 1984.

172. Silter G., Chu B. and Ravindra M. EPPI research on turbine missile effects in nuclear power plants. Paper J 8/5, SMIRT 7, 1983.

173. Kennedy K. et al. International seminar on probabilistic and extreme load design of nuclear plant facilities. Published by ASCE, Aug., 1977.

174. McGeorge R. and Swec Jr. L. Refined cracked concrete analysis of concrete containment structures subject to operational and enviromental loadings. Vol. 29, Nuclear Engineering and Design, 1974.

175. Abdul-Wahab H. and Harrop J. The rigidity of perforated plates with reinforced holes. Vol. 5, Nuclear Engineering and Design, 1967.

176. Gopalakrishna H. and Wolde-Tinsae A. Damage probability of turbine missile impact. Structural Division Journal of ASCE, Dec., 1984.

177. Romander C. and Sliter G. Model tests of turbine missile impact on reinforced concrete. Vol. 3, Nuclear Engineering and Design, 1984.

178. Twisdale L., Dunn W. and Frank R. Probabilitic methodology for turbine missile risk analysis. Vol. 3, Nuclear Engineering and Design, 1984.

179. Chadmail J., Krutzik N. and Dubois T. Equivalent loading due to airplane impact taking into account the non-linearities of impacted reinforced concrete buildings. Vol. 1, Nuclear Engineering and Design, 1985.

180. Miyamoto H. Integrity assessment of nuclear containment vesseles steels due to missile impact load. Vol. 2, Nuclear Engineering and Design, 1984.

181. Ohnuma H. Ito C. and Nomachi S. Dynamic response and local rupture of reinforced concrete beams and slabs under impact loading. Paper J, SMIRT 8, 1985.

182. Maurel M. et al. Three-dimensional dynamic analysis of a thick reinforced concrete slab subjected to the impact of a projectile. Paper J, SMIRT 8, 1985.

183. Cook R. Concepts and applications of finite element analysis. John Wiley and Sons, 1981.

184. Zienkiewicz O. The finite element method. McGraw-Hill book company (U. K.) limited, 1977.

185. Owen D. and Hinton E. Finite elements in plasticity theory and practice. Pineridge press limited, 1980.

186. Holand I. and Bell K. The finite element methods in stress analysis. Tapir, 1969.

187. Ottosen N. A failure criterion for concrete. Journal of The Engineering Mechanics Division, ASCE, Vol. 103, No. EM4, Aug., 1977.

188. Ottosen N. Constitutive model for short-time loading of concrete. Journal of The Engineering Mechanics Division, ASCE, Feb., 1979.

189. Chen W. Plasticity in reinforced concrete. McGraw-Hill book company, 1982.

190. Isenberg J. and Adham Analysis of orthotropic reinforced concrete structures. Journal of The Structural Division, ASCE, Dec., 1970.

191. Grootenboer. Finite element analysis of two-dimensional reinforced concrete sructures, taking account of nonlinear physical behaviour and the development of discrete cräcks, dissertation. Department of civil engineering, technical university Delft, 1979.

192. Konter A. Analysis of non-linear material behaviour using the MARC finite element system. Zoetermeer, Oct., 1985.

193. Schalkwijk R. and Konter A. Dynamic analysis with MARC. Zoetermeer, Oct., 1986.

194. Bathe, Wilson and Eding NONSAP-a structural analysis program for static and dynamic response of non-linear systems. College of engineering, University of California, Berkeley, California.

195. Bangash Y. the automated three-dimensional cracking analysis of prestressed concrete vessels. Paper H 3/2, SMIRT 6, 1981.

196. Bangash Y. Reactor pressure vessel design and practice. Progress in Nuclear Energy, Vol. 10, No. 1, Sept., 1981.

197. Ahmad M. Bond strength in prestressed reactor vessels, PhD thesis, Thames Ploytechnic, 1983.

198. MARC general purpose finite element program manual, volumes A, B, C and D. MARC analysis research corporation, California, U.S.A., 1974.

199. Heide and Zumsteg MENTAT, a system for finite element pre-and post-processing. California, U.S.A., 1986.

APPENDIX A

STRESS INVARIANTS AND CALCULATION OF OTTOSEN FAILURE CRITERION FOR NONSAP SUBROUTINE, CONMOD

The three invariants ($I_1, J_2, \text{Cos}3\theta$) of the stress tensor are expressed as:-

$$I_1 = \sigma_x + \sigma_y + \sigma_z \tag{A.1}$$

$$J_2 = \frac{1}{6}\left[(\sigma_x - \sigma_y)^2 + (\sigma_y - \sigma_z)^2 + (\sigma_z - \sigma_x)^2\right] + \sigma_{xy}^2 + \sigma_{yz}^2 + \sigma_{zx}^2 \tag{A.2}$$

$$J_3 = \sigma_x - \frac{I_1}{3}\left[\left(\sigma_y - \frac{I_1}{3}\right)\left(\sigma_z - \frac{I_1}{3}\right) - \sigma_{yz}^2\right] - \sigma_{xy}\left[\sigma_{xy}\left(\sigma_z - \frac{I_1}{3}\right) - \sigma_{zx}\,\sigma_{yz}\right] + \sigma_{zx}\left[\sigma_{xy}\,\sigma_{yz} - \sigma_{zx}\left(\sigma_y - \frac{I_1}{3}\right)\right] \tag{A.3}$$

$$\text{Cos}3\theta = \frac{3 \times 3^{1/2}}{2}\left(J_3\, J_2^{-3/2}\right)$$

From the failure criterion of Ottosen Model1, Equations (2.4), (2.7) and (2.8)

$$f(I_1, J_2, \text{Cos}3\theta) = \frac{A\,J_2}{fc^2} + \frac{La\,J_2^{1/2}}{fc} + \frac{B\,I_1}{fc} - 1 = 0$$

$$La = K_1\,\text{Cos}\left[\frac{1}{3}\,\text{Cos}^{-1}\left(K_2\,\text{Cos}3\theta\right)\right] \quad \text{for Cos}3\theta \ (> \text{or} =)\ 0$$

$$La = K_1\left[\text{Cos}\,\frac{\pi}{3} - \frac{1}{3}\,\text{Cos}^{-1}\left(-K_2\,\text{Cos}3\theta\right)\right] \quad \text{for Cos}3\theta < 0$$

For $\text{Cos}3\theta$ (> or =) 0

$$\frac{\text{La } J_2^{1/2}}{fc} = \frac{K_1 J_2^{1/2}}{fc} \text{Cos}\left[\frac{1}{3} \text{Cos}^{-1} (K_2 \text{Cos}3\theta)\right] \tag{A.4}$$

For $\text{Cos}3\theta$ < 0

$$\frac{\text{La } J_2^{1/2}}{fc} = \frac{K_1 J_2^{1/2}}{fc} \text{Cos}\left[\frac{\pi}{3} - \frac{1}{3} \text{Cos}^{-1} (-K_2 \text{Cos}3\theta)\right] \tag{A.5}$$

Now by partial differentiation

$$\frac{df}{d\sigma_{ij}} = \frac{df}{dI_1} \times \frac{dI_1}{d\sigma_{ij}} + \frac{df}{dJ_2} \times \frac{dJ_2}{d\sigma_{ij}} + \frac{df}{d\text{Cos}3\theta} \times \frac{d\text{Cos}3\theta}{d\sigma_{ij}} \tag{A.6}$$

where i = x,y,z

j = x,y,z

now

$$\frac{df}{dI_1} = \frac{B}{fc} \tag{A.7}$$

$$\frac{df}{dJ_2} = \frac{A}{fc^2} + \frac{\text{La}}{fc\ J_2^{1/2}}$$

For $\text{Cos}3\theta$ (> or =) 0

$$\frac{df}{d\text{Cos}3\theta} = \frac{K_1 K_2 J_2^{1/2}}{3fc} \times \frac{\text{Sin}\{[\text{Cos}^{-1} (K_2 \text{Cos}3\theta)]/3\}}{\text{Sin}[\text{Cos}^{-1} (K_2 \text{Cos}3\theta)]} \tag{A.8}$$

For Cos3 < 0

$$\frac{df}{d\text{Cos}3} = \frac{K_1 K_2 J_2^{1/2}}{3fc} \times \frac{\text{Sin}\left\{\pi/3 - 1/3 \left[\text{Cos}^{-1} (K_2 \text{Cos}3\theta)\right]\right\}}{\text{Sin}[\text{Cos}^{-1} (-K_2 \text{Cos}3\theta)]} \tag{A.9}$$

Now differentitating the invarians

$$\left[\frac{dI_1}{d\sigma_{ij}}\right]^T = [1,\ 1,\ 1,\ 0,\ 0,\ 0] \tag{A.10}$$

$$\left[\frac{dJ_2}{d\sigma_{ij}}\right]^T = \left[\frac{1}{3}(2\sigma_x - \sigma_y - \sigma_z),\ \frac{1}{3}(2\sigma_y - \sigma_x - \sigma_z),\ \frac{1}{3}(2\sigma_z - \sigma_x - \sigma_y),\ 2\sigma_{xy} + 2\sigma_{yz} + 2\sigma_{zx}\right] \tag{A.11}$$

$$\frac{dJ_3}{d\sigma_x} = \frac{1}{3}\left\{\left(\sigma_x - \frac{I_1}{3}\right)\left[-\left(\sigma_y - \frac{I_1}{3}\right) - \left(\sigma_z - \frac{I_1}{3}\right)\right] + 2\left(\sigma_y - \frac{I_1}{3}\right)\left(\sigma_z - \frac{I_1}{3}\right) - 2\sigma_{yz}^2 + \sigma_{xy}^2 + \sigma_{zx}^2\right\} \tag{A.12}$$

$$\frac{dJ_3}{d\sigma_y} = \frac{1}{3}\left\{\left(\sigma_y - \frac{I_1}{3}\right)\left[-\left(\sigma_x - \frac{I_1}{3}\right) - \left(\sigma_z - \frac{I_1}{3}\right)\right] + 2\left(\sigma_x - \frac{I_1}{3}\right)\left(\sigma_z - \frac{I_1}{3}\right) - 2\sigma_{zx}^2 + \sigma_{xy}^2 + \sigma_{yz}^2\right\} \tag{A.13}$$

$$\frac{dJ_3}{d\sigma_z} = \frac{1}{3}\left\{\left(\sigma_z - \frac{I_1}{3}\right)\left[-\left(\sigma_x - \frac{I_1}{3}\right) - \left(\sigma_y - \frac{I_1}{3}\right)\right] + 2\left(\sigma_x - \frac{I_1}{3}\right)\left(\sigma_y - \frac{I_1}{3}\right) - 2\sigma_{xy}^2 + \sigma_{yz}^2 + \sigma_{zx}^2\right\} \tag{A.14}$$

$$\frac{dJ_3}{d\sigma_{xy}} = -2\left(\sigma_z - \frac{I_1}{3}\right)\sigma_{xy} + 2\sigma_{yz}\sigma_{zx} \tag{A.15}$$

$$\frac{dJ_3}{d\sigma_{yz}} = -2\left(\sigma_x - \frac{I_1}{3}\right)\sigma_{yz} + 2\sigma_{xy}\sigma_{zx} \tag{A.16}$$

$$\frac{dJ_3}{d\sigma_{zx}} = -2\left(y - \frac{I_1}{3}\right)\sigma_{zx} + 2\sigma_{xy}\sigma_{yz} \tag{A.17}$$

So

$$\frac{dCos3\theta}{d\sigma_x} = \frac{3x3^{1/2}J_3}{2}\left[\frac{-3}{2}J_2^{-5/2}\ \frac{1}{3}(2\ \sigma_x - \sigma_y - \sigma_z)\right] + J_2^{-3/2}\ \frac{3x3^{1/2}}{2}\ \frac{dJ_3}{d\sigma_x}$$

$$= \frac{3x3^{1/2}}{2\ J_2^{3/2}}\left\{\left[\frac{-J_3}{2\ J_2^{1/2}}\ (2\ \sigma_x - \sigma_y - \sigma_z)\right] + \frac{dJ_3}{d\sigma_x}\right\} \qquad (A.18)$$

$$\frac{dCos3\theta}{d\sigma_y} = \frac{3x3^{1/2}}{2\ J_2^{3/2}}\left\{\left[\frac{-J_3}{2\ J_2^{1/2}}\ (2\ \sigma_y - \sigma_x - \sigma_z)\right] + \frac{dJ_3}{d\sigma_y}\right\} \qquad (A.19)$$

$$\frac{dCos3\theta}{d\sigma_z} = \frac{3x3^{1/2}}{2\ J_2^{3/2}}\left\{\left[\frac{-J_3}{2\ J_2^{1/2}}\ (2\ \sigma_z - \sigma_x - \sigma_y)\right] + \frac{dJ_3}{d\sigma_z}\right\} \qquad (A.20)$$

$$\frac{dCos3\theta}{d\sigma_{xy}} = \frac{3x3^{1/2}}{2\ J_2^{3/2}}\left[\frac{(-3\ J_3\ \sigma_{xy})}{J_2^{1/2}} + \frac{dJ_3}{d\sigma_{xy}}\right] \qquad (A.21)$$

$$\frac{dCos3\theta}{d\sigma_{yz}} = \frac{3x3^{1/2}}{2\ J_2^{3/2}}\left[\frac{(-3\ J_3\ \sigma_{yz})}{J_2^{1/2}} + \frac{dJ_3}{d\sigma_{yz}}\right] \qquad (A.22)$$

$$\frac{dCos3\theta}{d\sigma_{zx}} = \frac{3x3^{1/2}}{2\ J_2^{3/2}}\left[\frac{(-3\ J_3\ \sigma_{zx})}{J_2^{1/2}} + \frac{dJ_3}{d\sigma_{zx}}\right] \qquad (A.23)$$

APPENDIX B

CALCULATION OF NUMERICAL DAMPING FACTOR
AND INCREMENTAL TIME STEP FOR MARC

If ω is the frequency of the structure in radian per second
ts is the time step increment for Newmark integration
γ is the numerical damping coefficient

From the modal analysis of model B16, ω for mode 1 and 2 were found to be 1024.6 and 4452.8 rad/sec respectively.

Since

$$ts = \frac{1}{\omega}$$

mode 1

$$ts = 1/1024.6$$

$$= \underline{0.000976 \text{ second}}$$

mode 2

$$ts = 1 / 4452.8$$

$$= \underline{0.000225 \text{ second}}$$

If 5% of higher frequencies is to be damped out

mode 1

$$\gamma = \frac{0.05 \times 2\pi}{ts \times \omega}$$

$$= \frac{0.05 \times 2\pi}{0.000976 \times 1024.6}$$

$$= \underline{0.314}$$

mode 1

$$\gamma = \frac{0.05 \times 2\pi}{ts \times \omega}$$

$$= \frac{0.05 \times 2\pi}{0.000225 \times 4452.8}$$

$$= \underline{0.314}$$

APPENDIX C

CALCULATION OF CONSTANT FOR MOHR-COLUMB FAILURE CRITERION FOR MARC

If C is the cohesion

ϕ is the angle of friction

fc is the compressive strength of concrete and

η, ξ are cohesion constants

Assuming ϕ = 45 degree for concreete

From Equations 2.59 and 2.60 we have

$$\frac{3\eta}{(1 - 3\eta^2)^{1/2}} = \sin\phi$$

$$\Rightarrow \frac{3\eta}{(1 - 3\eta^2)^{1/2}} = \frac{1}{2^{1/2}}$$

$$\Rightarrow 18\eta^2 = 1 - 3\eta^2$$

$$\Rightarrow \eta = \underline{0.218}$$

For model B16

$$C = \frac{fc}{3\,(1 - 12\eta^2)^{1/2}}$$

$$\Rightarrow C = \frac{33.7}{3\,(1 - 12 \times 0.0475)^{1/2}}$$

$$\Rightarrow C = \underline{17.16}$$

and

$$\xi = \frac{\eta}{[3\,(3C^2 - \eta^2)]^{1/2}}$$

$$\Rightarrow \xi = \frac{0.218}{[3\,(3 \times 17.16^2 - 0.218^2)]^{1/2}}$$

$$\Rightarrow \xi = \underline{0.00424}$$

Similarly for model B26, C and ξ are found to be 18.84 and 0.00386 respectively.

APPENDIX D

LISTING OF NONSAP SUBROUTINES

```
CCCCCCCCCCCCCCCCCCCCCCCCCCCCCCCCCCCCCCCCCCCCCCCCCCCCCCCCCCCCCCCCCCCCCCCCCC
C                                                                     C
C     THE FOLLOWING SUBROUTINES HAVE BEEN DEVELOPED BY JOHNNY TANG    C
C     TO APPLY ELASTIC, ELASTO-PLASTIC AND PLASTIC BEHAVIOURS OF      C
C     REINFORCED CONCRETE WITH CRACKING IN THREE-DIMENSIONAL          C
C     SITUATION BASED ON OTTOSEN FAILURE CRITERION.                   C
C                                                                     C
CCCCCCCCCCCCCCCCCCCCCCCCCCCCCCCCCCCCCCCCCCCCCCCCCCCCCCCCCCCCCCCCCCCCCCCCCC
C
C
      SUBROUTINE ELT3D4
      IMPLICIT REAL*8(A-H,O-Z)
C
C . . . . . . . . . . . . . . . . . . . . . . . . . . . . . . . . . . .
C .                                                                   .
C .                 M O D E L    =    4                               .
C .                                                                   .
C .   REINFORCED CONCRETE MODEL WITH ELASTIC,ELASTO-PLASTIC & PLASTIC .
C .     WITH CRACRING                                                 .
C .   THIS OVERLAY CONTAINS ALL SUBROUTINES PERTAINING TO MODEL 3     .
C .                                                                   .
C . . . . . . . . . . . . . . . . . . . . . . . . . . . . . . . . . . .
C
C
      COMMON /EL/ IND,ICOUNT,NPAR(20),NUMEG,NEGL,NEGNL,IMASS,IDAMP,ISTAT
     1           ,NDOF,KLIN,IEIG,IMASSN,IDAMPN
      COMMON /DIMEL/ N101,N102,N103,N104,N105,N106,N107,N108,N109,N110,
     1               N111,N112,N113,N114,N120,N121,N122,N123,N124,N125
      COMMON /MTMD3D/  D(6,6),STRESS(6),STRAIN(6),IPT,NEL
      COMMON A(1)
      DIMENSION IA(1)
C
      EQUIVALENCE (NPAR(10),NINT), (NPAR(11),NINTZ), (NPAR(17),NCON)
      EQUIVALENCE (A,IA), (NPAR(18),NIDW)
C
C
C     FOR ADDRESSES N101,N102,N103,.... REFER TO PROGRAM THREDM
C
C
      IF (IND.NE.0) GO TO 100
C
C
C     I N I T I A L I Z E   W A   W O R K I N G   V E C T O R
C
C
      IDW = NIDW
      NPT=NINT*NINT*NINTZ
      NT=IDW*NPT
      NN=(NEL - 1)*NT
      CALL IRCRK3 (A(N112+NN),NPT,NIDW)
      RETURN
C
C
C     F I N D   S T R E S S - S T R A I N   L A W   A N D   S T R E S S
C
C
```

```
 100  IDW = NIDW
C     MATP=IA(N107 + NEL - 1)
      MATP=IA(2*N107+NEL-2)
      NM=N111 + (MATP-1)*NCON
      NPT=NINT*NINT*NINTZ
      NN=N112 + (NEL-1)*IDW*NPT + (IPT-1)*IDW
      CALL RCRK3D (A(NM),A(NN),A(NN+6))
      RETURN
      END
C
C
      SUBROUTINE IRCRK3 (WA,NPT,NIDW)
      IMPLICIT REAL*8(A-H,O-Z)
      DIMENSION WA(NIDW,1)
      DO 10 I = 1,NPT
      DO 10 J = 1,12
   10 WA(J,I) = 0.0
      RETURN
      END
C
C
      SUBROUTINE RCRK3D (PROP,SIG,EPS)
C
C     MATERIAL STIFFNESS MATRIES FOR CONCRETE AT ELASTIC AND
C     ELASTO-PLASTIC STAGES
C
C
C     IST         NO OF STRESS COMPONENTS (6)
C     ISR         NO OF STRAIN COMPONENTS (6)
C     SIG         TOTAL STRESSES AT TIME (T)
C     EPS         TOTAL STRAINS AT TIME (T)
C     DELSIG      INCREMENT IN STRESSES,ASSUMING ELASTIC BEHAVIOUR
C     DELEPS      INCREMENT IN STRAINS
C     PROP(1)     YOUNGS MODULUS OF CONCRETE
C     PROP(2)     YOUNGS MODULUS OF STEEL
C     PROP(3)     TENSILE STRENGTH OF CONCRETE
C     PROP(4)     COMPRESSIVE STRENGTH OF CONCRETE
C     PROP(5)     POISSONS RATIO OF COMPOSITE MATERIAL
C     PROP(6)     AREA OF CONCRETE IN X-DIRECTION
C     PROP(7)     AREA OF CONCRETE IN Y-DIRECTION
C     PROP(8)     AREA OF CONCRETE IN Z-DIRECTION
C     PROP(9)     AREA OF STEEL IN X-DIRECTION
C     PROP(10)    AREA OF STEEL IN Y-DIRECTION
C     PROP(11)    AREA OF STEEL IN Z-DIRECTION
C     PROP(12)    AGGREGATE INTERLOCKING FACTOR (0.0 TO 1.0)
C     PROP(13)    HARDENING PARAMETER A
C     PROP(14)    POISSIONS RATIO OF CONCRETE
C     PROP(15)    YIELD STRESS OF STEEL
C     PROP(16)    VOLUME FRACTION OF CONCRETE
C     PROP(17)    VOLUME FRACTION OF STEEL
C     IPEL = 1    ELASTIC
C     IPEL = 2    ELASTO-PLASTIC
C     IPEL = 3    PLASTIC
C
      IMPLICIT REAL*8(A-H,O-Z)
      COMMON /EL/ IND,ICOUNT,NPAR(20),NUMEG,NEGL,NEGNL,IMASS,IDAMP,
     @            ISTAT,NDOF,KLIN,IEIG,IMASSN,IDAMPN
      COMMON /MTMD3D/ D(6,6),STRESS(6),STRAIN(6),IPT,NEL
      COMMON /VAR/ NG,KPRI,MODEX,KSTEP,ITE,ITEMAX,IREF,IEQREF,INOCMD
      DIMENSION DF(6,6),FS(6,6),DFFT(6,6),FSTPOS(6,6),DFFTD(6,6),
```

```
     1          FTD(6,6),SIG(1),EPS(1),PROP(1),DEP(6,6),
     2          PS1(8),PS2(8),PS3(8),DC1(3),DC2(3),DC3(3),NCK(3),
     3          DELSIG(6),DELEPS(6),DS(6,6)
      YMCO = PROP(1)*PROP(16)+PROP(2)*PROP(17)
      YSTRC = PROP(4)/PROP(1)
      YSTRS = PROP(15)/PROP(2)
      YSTRCO = YSTRC*PROP(16)+YSTRS*PROP(17)
      YSIGCO = YSTRCO*YMCO
      USTRCO = 0.0035*PROP(16)+0.01*PROP(17)
      CALL RCMOD (PROP,DS,SIG,EPS,NCK,PS1,PS2,PS3,DC1,DC2,DC3)
      DO 5505 JJJL = 1,6
      IF (DABS(STRAIN(JJJL)) .LE. 1.0E-16) GOTO 5505
      ISIGN = STRAIN(JJJL)/DABS(STRAIN(JJJL))
      IF (DABS(STRAIN(JJJL)) .GE. USTRCO)
     @   STRAIN(JJJL) = USTRCO*ISIGN
 5505 CONTINUE
      DO 229 IIJK =1,6
  229 IF (DABS(STRAIN(IIJK)) .GE. USTRCO) GOTO 9999
      DO 333 II = 1,6
  333 IF (SIG(II) .LE. -YSIGCO/3.0) GOTO 300
       IPEL = 1
C
C     1. CALCULATION INCREMENTAL STRAINS
C
      DO 1010 ISIS = 1,6
 1010 DELEPS(ISIS) = 0.0
      DO 1120 IIS = 1,6
 1120 DELEPS(IIS) = STRAIN(IIS)-EPS(IIS)
C
C     2. CALCULATE STRAIN INCREMENTS,ASSUMING ELASTIC BEHAVIOUR
C
      DO 1110 IIID = 1,6
 1110 DELSIG(IIID) = 0.0
      DO 1220 IID = 1,6
      DO 1220 JJD = 1,6
 1220 DELSIG(IID) = DELSIG(IID)+D(IID,JJD)*DELEPS(JJD)
C
C     3. CALCULATE TOTAL STRESSES ASSUMING ELASTIC BEHAVIOUR
C
      DO 2222 IDD = 1,6
 2222 STRESS(IDD) = 0.0
      DO 1160 IIE = 1,6
 1160 STRESS(IIE) = SIG(IIE)+DELSIG(IIE)
      DO 5500 JJJ = 1,6
      IF (STRESS(JJJ) .LE. -0.45*YSIGCO) STRESS(JJJ) = -0.45*YSIGCO
 5500 CONTINUE
      DO 9333 IIT = 1,6
      IF (STRESS(IIT) .LE. -YSIGCO/3.0) GOTO 9999
 9333 CONTINUE
      CALL FLAGCK (NCK,PROP)
      IF (KPRI .NE. 0) GOTO 2140
      IF (IPT .NE. 1) GOTO 2120
      WRITE (6,4500)
      WRITE (0,4500)
      WRITE (6,4600) NEL
      WRITE (0,4600) NEL
 2120 WRITE (6,4700) IPT,(STRESS(I),I = 1,6)
      WRITE (0,4700) IPT,(STRESS(I),I = 1,6)
      IF (NCK(1) .EQ. 0 .AND. NCK(2) .EQ. 0 .AND. NCK(3) .EQ. 0)
     @    GOTO 1234
```

```
      CALL CONMOD (PROP,SIG,FS,FSTPOS)
      CALL RCMOD (PROP,DS,SIG,EPS,NCK,PS1,PS2,PS3,DC1,DC2,DC3)
      DO 3334 IDFF = 1,6
 3334 DF(IDFF,1) = 0.0
      DO 3000 IDF = 1,6
      DO 3000 JDF = 1,6
 3000 DF(IDF,1) = DF(IDF,1)+D(IDF,JDF)*FS(JDF,1)
      DO 3335 IDFFTT = 1,6
      DO 3335 JDFFTT = 1,6
 3335 DFFT(IDFFTT,JDFFTT) = 0.0
      DO 3100 IDFFT = 1,6
      DO 3100 JDFFT = 1,6
      DO 3100 KDFFT = 1,6
 3100 DFFT(IDFFT,JDFFT) = DFFT(IDFFT,JDFFT)+DF(IDFFT,KDFFT)*FSTPOS
     @                     (KDFFT,JDFFT)
      DO 3336 IDDD = 1,6
      DO 3336 JDDD = 1,6
 3336 DFFTD(IDDD,JDDD) = 0.0
      DO 3200 IDFFTD = 1,6
      DO 3200 JDFFTD = 1,6
      DO 3200 KDFFTD = 1,6
 3200 DFFTD(IDFFTD,JDFFTD) = DFFTD(IDFFTD,JDFFTD)+DFFT(IDFFTD,KDFFTD)*
     @                       D(KDFFTD,JDFFTD)
      DO 3337 IFTDD = 1,6
 3337 FTD(1,IFTDD) = 0.0
      DO 3300 IFTD = 1,6
      DO 3300 JFTD = 1,6
 3300 FTD(1,IFTD) = FTD(1,IFTD)+FSTPOS(1,JFTD)*D(JFTD,IFTD)
      FTDF = 0.0
      AFTDF = 0.0
      DO 3400 IFTDF = 1,6
      DO 3400 JFTDF = 1,6
      FTDF = FTDF+FTD(IFTDF,JFTDF)*FS(JFTDF,1)
 3400 AFTDF = PROP(13)+FTDF
      DO 3500 IDEP = 1,6
      DO 3500 JDEP = 1,6
 3500 DEP(IDEP,JDEP) = D(IDEP,JDEP)-DFFTD(IDEP,JDEP)/AFTDF
C
C     1. CALCULATION INCREMENTAL PLASTIC STRAINS
C
C
C     2. CALCULATE STRAIN INCREMENTS,PLASTIC BEHAVIOUR
C
C
C     3. CALCULATE TOTAL STRESSES PLASTIC BEHAVIOUR
C
      DO 3338 IDEPSS = 1,6
 3338 STRESS(IDEPSS) = 0.0
      DO 3520 IDEPS = 1,6
      DO 3520 JDEPS = 1,6
 3520 STRESS(IDEPS) = STRESS(IDEPS)+DEP(IDEPS,JDEPS)*
     @                (STRAIN(JDEPS)-EPS(JDEPS))
      DO 1166 IIE = 1,6
 1166 STRESS(IIEI) = STRESS(IIEI)+SIG(IIEI)
      CALL FLAGCK (NCK,PROP)
      DO 5502 JJJK = 1,6
      IF (STRESS(JJJK) .LE. -0.45*YSIGCO) STRESS(JJJK) = -0.45*YSIGCO
 5502 CONTINUE
      IF (ISTRES .GE. 1) GOTO 9999
 9999 DO 5666 IJJJ =1,6
```

```
      EPS(4) = STRAIN(4)
      EPS(5) = STRAIN(5)
      EPS(6) = STRAIN(6)
      RETURN
 4500 FORMAT (/
     1        8H ELEMENT,4X,6HOUTPUT,/ 2X,6HNUMBER,2X,8HLOCATION,7X,
     1        8HSIGMA-X1,7X,8HSIGMA-X2,7X,8HSIGMA-X3,8X,7HTAU-X12,
     2        8X,7HTAU-X13,8X,7HTAU-X23 / 1X)
 4600 FORMAT (I8)
 4650 FORMAT (13X,I5,' THIS POINT IS CRUSHED')
 4700 FORMAT (13X,I5,6E15.4)
  101 FORMAT (12X,'DIRECTION CONSINES AND CRACK DIRECTION')
  119 FORMAT (2X,9E14.6)
 2229 FORMAT (12X,'NCK(1) NCK(2) NCK(3)')
 3339 FORMAT (8X,3I8)
      END
C
C
      SUBROUTINE RCMOD (PROP,SIG,EPS,NCK,PS1,PS2,PS3,DC1,DC2,DC3)
C
C     ORTHOTROPIC VARIABLE-MODULUS MODEL FOR CONCRETE
C
      IMPLICIT REAL*8(A-H,O-Z)
      COMMON /MTMD3D/ D(6,6),STRESS(6),STRAIN(6),IPT,NEL
      DIMENSION E(3),G(3,3),DS(6,6),PROP(1),SIG(1),EPS(1),NCK(1),
     1          PS1(1),PS2(1),PS3(1),DC1(1),DC2(1),DC3(1)
      DO 222 II = 1,6
      DO 222 JJ = 1,6
  222 DS(II,JJ) = 0.0
      AA=(1.0-PROP(5))/(1.0+PROP(5))*(1.0-2.0*PROP(5))
      BB=PROP(5)/(1.0-PROP(5))
      E(1) = PROP(12)*PROP(1)*PROP(6)+PROP(2)*PROP(9)
      E(2) = PROP(12)*PROP(1)*PROP(7)+PROP(2)*PROP(10)
      E(3) = PROP(12)*PROP(1)*PROP(8)+PROP(2)*PROP(11)
      DO 7100 J=1,3
      DO 7100 K=1,3
 7100 G(J,K)=0.25*(AA*(E(J)+E(K)))-2.0*AA*BB*DSQRT(E(J)*E(K))
      DS(1,1)=AA*E(1)
      DS(1,2)=AA*BB*DSQRT(E(1)*E(2))
      DS(1,3)=AA*BB*DSQRT(E(1)*E(3))
      DS(2,1)=D(1,2)
      DS(2,2)=AA*E(2)
      DS(2,3)=BB*DSQRT(E(2)*E(3))
      DS(3,1)=D(1,3)
      DS(3,2)=D(2,3)
      DS(3,3)=AA*E(3)
      DS(4,4)=G(1,2)
      DS(5,5)=G(1,3)
      DS(6,6)=G(2,3)
      CALL TESTCK (PROP,SIG,EPS,NCK,PS1,PS2,PS3,DC1,DC2,DC3)
      DO 2220 III = 1,6
      DO 2220 JJJ = 1,6
 2220 D(III,JJJ) = DS(III,JJJ)
      RETURN
      END
C
C
      SUBROUTINE CONMOD (PROP,SIG,FS,FSTPOS)
C
C     OTTOSEN MODEL
```

```
C
      IMPLICIT REAL*8(A-H,O-Z)
      COMMON /MTMD3D/ DEP(6,6),STRESS(6),STRAIN(6),IPT,NEL
      DIMENSION PAR(3,5),FS(6,6),FSTPOS(6,6),PROP(1),SIG(1),
     @          DVI1DS(6),DVJ2DS(6),DVJ3DS(6),DVTHDS(6)
      OPEN (UNIT=5,FILE='PARAMETERS',STATUS='OLD')
      READ (5,*,END=3700)((PAR(IF,JF),JF=1,5),IF=1,3)
 3700 CLOSE (5)
      PK = PROP(3)/PROP(4)
      IP = 0
      JP = 0
      IF (PK .LE. 0.08) IP = 1
      IF (PK .EQ. 0.10) IP = 2
      IF (PK .GE. 0.12) IP = 3
      IF (PK .LT. 0.10) JP = 1
      IF (PK .GT. 0.10) JP = 2
      IF (IP .EQ. 0) GOTO 3800
      A = PAR(IP,2)
      B = PAR(IP,3)
      PK1 = PAR(IP,4)
      PK2 = PAR(IP,5)
      GOTO 3900
 3800 SUB1 = PK-PAR(JP,1)
      SUB2 = PAR(JP+1,1)-PAR(JP,1)
      A = SUB1*(PAR(JP+1,2)-PAR(JP,2))/SUB2+PAR(JP,2)
      B = SUB1*(PAR(JP+1,3)-PAR(JP,3))/SUB2+PAR(JP,3)
      PK1 = SUB1*(PAR(JP+1,4)-PAR(JP,4))/SUB2+PAR(JP,4)
      PK2 = SUB1*(PAR(JP+1,5)-PAR(JP,5))/SUB2+PAR(JP,5)
 3900 VARI1 = SIG(1)+SIG(2)+SIG(3)
      VARJ2 = 1.0/6.0*((SIG(1)-SIG(2))**2+(SIG(2)-SIG(3))**2+
     @        (SIG(3)-SIG(1))**2)+SIG(4)**2+SIG(5)**2+SIG(6)**2
      VARI13 = VARI1/3.0
      VI131 = SIG(1)-VARI13
      VI132 = SIG(2)-VARI13
      VI133 = SIG(3)-VARI13
      VARJ3 = VI131*(VI132*VI133-SIG(5)**2)-SIG(4)*(SIG(4)*VI133
     @        -SIG(6)*SIG(5))+SIG(6)*(SIG(4)*SIG(5)-SIG(6)*VI132)
      VAR3TH = 1.5*3.0**(0.5)*VARJ3/VARJ2**1.5
      IF (VAR3TH .GE. 0.0) GOTO 4000
      ALAM = 22.0/21.0-1.0/3.0*ACOS(-PK2*VAR3TH)
      TOTLAM = PK1*COS(ALAM)
      DFD3TH = PK1*PK2*VARJ2**0.5*SIN(ALAM)/(3.0*PROP(4)*
     @         SIN(ACOS(-PK2*VAR3TH)))
      GOTO 4100
 4000 ALAM = 1.0/3.0*ACOS(PK2*VAR3TH)
      TOTLAM = PK1*COS(ALAM)
      DFD3TH = PK1*PK2*VARJ2**0.5*SIN(ALAM)/(3.0*PROP(4)*
     @         SIN(ACOS(PK2*VAR3TH)))
 4100 DFDI1 = B/PROP(4)
      DFDJ2 = A/PROP(4)**2+TOTLAM/(PROP(4)*VARJ2**0.5)
      DVI1DS(1) = 1.0
      DVI1DS(2) = 1.0
      DVI1DS(3) = 1.0
      DVI1DS(4) = 0.0
      DVI1DS(5) = 0.0
      DVI1DS(6) = 0.0
      DVJ2DS(1) = 1.0/3.0*(2.0*SIG(1)-SIG(2)-SIG(3))
      DVJ2DS(2) = 1.0/3.0*(2.0*SIG(2)-SIG(1)-SIG(3))
      DVJ2DS(3) = 1.0/3.0*(2.0*SIG(3)-SIG(1)-SIG(2))
      DVJ2DS(4) = 2.0*SIG(4)
```

```
       DVJ2DS(5) = 2.0*SIG(5)
       DVJ2DS(6) = 2.0*SIG(6)
       DVJ3DS(1) = 1.0/3.0*(VI131*(-VI132-VI133))+2.0*VI132*VI131-
      @            2.0*SIG(5)**2+SIG(4)**2+SIG(6)**2
       DVJ3DS(2) = 1.0/3.0*(VI132*(-VI131-VI133))+2.0*VI131*VI133-
      @            2.0*SIG(6)**2+SIG(4)**2+SIG(5)**2
       DVJ3DS(3) = 1.0/3.0*(VI133*(-VI131-VI132))+2.0*VI131*VI132-
      @            2.0*SIG(4)**2+SIG(5)**2+SIG(6)**2
       DVJ3DS(4) = -2.0*VI133*SIG(4)+2.0*SIG(5)*SIG(6)
       DVJ3DS(5) = -2.0*VI131*SIG(5)+2.0*SIG(4)*SIG(6)
       DVJ3DS(6) = -2.0*VI132*SIG(6)+2.0*SIG(4)*SIG(5)
       CONVJ2 = 3.0*3.0**0.5/(2.0*VARJ2*1.2)
       VJ3J2 = VARJ3/VARJ2**0.5
       DVTHDS(1) = CONVJ2*(-0.5*VJ3J2*(2.0*SIG(1)-SIG(2)-SIG(3))+
      @            DVJ3DS(1))
       DVTHDS(2) = CONVJ2*(-0.5*VJ3J2*(2.0*SIG(2)-SIG(1)-SIG(3))+
      @            DVJ3DS(2))
       DVTHDS(3) = CONVJ2*(-0.5*VJ3J2*(2.0*SIG(3)-SIG(1)-SIG(2))+
      @            DVJ3DS(3))
       DVTHDS(4) = CONVJ2*(-3.0*VJ3J2*SIG(4)+DVJ3DS(4))
       DVTHDS(5) = CONVJ2*(-3.0*VJ3J2*SIG(5)+DVJ3DS(5))
       DVTHDS(6) = CONVJ2*(-3.0*VJ3J2*SIG(6)+DVJ3DS(6))
       DO 4200 IS = 1,6
       FS(IS,1) = DFDI1*DVI1DS(IS)+DFDJ2*DVJ2DS(IS)+
      @           DFD3TH*DVTHDS(IS)
  4200 FSTPOS(1,IS) = FS(IS,1)
       RETURN
       END
 C
 C
 C
 C
       SUBROUTINE FLAGCK (NCK,PROP)
       IMPLICIT REAL*8 (A-H,O-Z)
       COMMON /MTMD3D/ D(6,6),STRESS(6),STRAIN(6),IPT,NEL
       DIMENSION NCK(1),PROP(1)
       NCK(1) = 0
       NCK(2) = 0
       NCK(3) = 0
       DO 1000 II = 1,3
       IF (STRESS(II) .GE. PROP(3)) NCK(II) = 1
  1000 CONTINUE
       RETURN
       END
C
C
       SUBROUTINE CRACKD (PROP,NCK,SIG,EPS,PS1,PS2,PS3,DC1,DC2,DC3)
       IMPLICIT REAL*8(A-H,O-Z)
C
C      SET UP MATERIAL MATRICES FOR CRACKED CONCRETE
C
```

```
      COMMON /MTMD3D/ D(6,6),STRESS(6),STRAIN(6),IPT,NEL
      DIMENSION DD(6,6),PROP(1),NCK(1),SIG(1),EPS(1),
     @          PS1(1),PS2(1),PS3(1),DC1(1),DC2(1),DC3(1)
      CALL PRINCL (IPT,STRESS,PS1,PS2,PS3,DC1,DC2,DC3)
      CALL RCMOD (PROP,DS,SIG,EPS,NCK,PS1,PS2,PS3,DC1,DC2,DC3)
      DO 222 I = 1,6
      DO 222 J = 1,6
  222 DD(I,J) = 0.0
      JJJ = 1
      LL = 0
      IF (NCK(1).EQ.1) LL = 1
      IF (NCK(2).EQ.1) LL = 2
      IF (NCK(3).EQ.1) LL = 3
      IF (NCK(1).EQ.1.AND.NCK(2).EQ.1) LL = 4
      IF (NCK(2).EQ.1.AND.NCK(3).EQ.1) LL = 5
      IF (NCK(1).EQ.1.AND.NCK(3).EQ.1) LL = 6
      IF (NCK(1).EQ.1.AND.NCK(2).EQ.1.AND.NCK(3).EQ.1) LL = 7
      IF (LL.EQ.7) GOTO 99
      IF (JJJ.EQ.0) GOTO 200
      IF (LL.EQ.0) GOTO 999
      GOTO (113,114,115,116,117,118),LL
C
C     ONLY ONE DIRECTION CRACKED
C
  113 CONTINUE
C
C     CRACK IN DIRECTION 1
C
      DD(1,1) = 0.0
      DD(1,2) = 0.0
      DD(1,3) = 0.0
      DD(2,1) = 0.0
      DD(2,2) = D(2,2)-D(1,2)*D(1,2)/D(1,1)
      DD(2,3) = D(2,3)-D(1,3)*D(1,2)/D(1,1)
      DD(3,1) = 0.0
      DD(3,2) = DD(2,3)
      DD(3,3) = D(3,3)-D(1,3)*D(1,3)/D(1,1)
      DD(4,4) = PROP(12)*D(4,4)
      DD(5,5) = D(5,5)
      DD(6,6) = PROP(12)*D(6,6)
      GOTO 121
  114 CONTINUE
C
C     CRACK IN DIRECTIOR 2
C
      DD(1,1) = D(1,1)-D(2,1)*D(2,1)/D(2,2)
      DD(1,2) = 0.0
      DD(1,3) = D(1,3)-D(1,2)*D(2,3)/D(2,2)
      DD(2,1) = 0.0
      DD(2,2) = 0.0
      DD(2,3) = 0.0
      DD(3,1) = DD(1,3)
      DD(3,2) = 0.0
      DD(3,3) = D(3,3)-D(2,3)*D(2,3)/D(2,2)
      DD(4,4) = PROP(12)*D(4,4)
      DD(5,5) = PROP(12)*D(5,5)
      DD(6,6) = D(6,6)
      GOTO 121
```

```
  115 CONTINUE
C
C     CRACK IN DIRECTION 3
C
      DD(1,1) = D(1,1)-D(1,3)*D(1,3)/D(3,3)
      DD(1,2) = D(1,2)-D(1,3)*D(2,3)/D(3,3)
      DD(1,3) = 0.0
      DD(2,1) = DD(1,2)
      DD(2,2) = D(2,2)-D(2,3)*D(2,3)/D(3,3)
      DD(2,3) = 0.0
      DD(3,1) = 0.0
      DD(3,2) = 0.0
      DD(3,3) = 0.0
      DD(4,4) = D(4,4)
      DD(5,5) = D(5,5)*PROP(12)
      DD(6,6) = D(6,6)*PROP(12)
      GOTO 121
  116 CONTINUE
C
C     CRACKS IN TWO DIRECTIONS
C
C     CRACKES IN DIRECTIONS 1 & 2
C
      DENOM = D(1,1)*D(2,2)-D(1,2)*D(2,1)
      DD(1,1) = 0.0
      DD(1,2) = 0.0
      DD(1,3) = 0.0
      DD(2,1) = 0.0
      DD(2,2) = 0.0
      DD(2,3) = 0.0
      DD(3,1) = 0.0
      DD(3,2) = 0.0
      DD(3,3) = D(3,3)
     1          -D(3,1)*(D(2,2)*D(1,3)-D(1,2)*D(2,3))/DENOM
     2          -D(3,2)*(D(1,1)*D(2,3)-D(2,1)*D(3,1))/DENOM
      DD(4,4) = PROP(12)*D(4,4)
      DD(5,5) = PROP(12)*D(5,5)
      DD(6,6) = PROP(12)*D(6,6)
      GOTO 121
  117 CONTINUE
C
C     CRACKS IN DIRECTIONS 3 & 2
C
      DENOM = D(2,2)*D(3,3)-D(2,3)*D(3,2)
      DD(1,1) = D(1,1)
     1          -D(1,2)*(D(3,3)*D(2,1)-D(3,1)*D(2,3))/DENOM
     2          -D(1,3)*(D(2,2)*D(3,1)-D(2,1)*D(3,2))/DENOM
      DD(1,2) = 0.0
      DD(1,3) = 0.0
      DD(2,1) = 0.0
      DD(2,2) = 0.0
      DD(2,3) = 0.0
      DD(3,1) = 0.0
      DD(3,2) = 0.0
      DD(3,3) = 0.0
      DD(4,4) = PROP(12)*D(4,4)
      DD(5,5) = PROP(12)*D(5,6)
      DD(6,6) = PROP(12)*D(6,6)
      GOTO 121
  118 CONTINUE
```

```
C
C     CRACKS IN DIRECTION 1 & 3
C
      DENOM = D(1,1)*D(3,3)-D(3,1)*D(1,3)
      DD(1,1) = 0.0
      DD(1,2) = 0.0
      DD(1,3) = 0.0
      DD(2,1) = 0.0
      DD(2,2) = D(2,2)
     1          -D(2,1)*(D(3,3)*D(1,2)-D(3,2)*D(1,3))/DENOM
     2          -D(2,3)*(D(1,1)*D(3,2)-D(3,1)*D(1,2))/DENOM
      DD(2,3) = 0.0
      DD(3,1) = 0.0
      DD(3,2) = 0.0
      DD(3,3) = 0.0
      DD(4,4) = PROP(12)*D(4,4)
      DD(5,5) = PROP(12)*D(5,5)
      DD(6,6) = PROP(12)*D(6,6)
  121 CONTINUE
      GOTO 99
  200 CONTINUE
      IF (LL .EQ. 0) GOTO 999
      GOTO (1,2,3,4,5,6),LL
    1 CONTINUE
      DD(2,2) = D(2,2)
      DD(2,3) = D(2,3)
      DD(3,2) = DD(2,3)
      DD(3,3) = D(3,3)
      DD(4,4) = PROP(12)*D(4,4)
      DD(5,5) = PROP(12)*D(5,5)
      DD(6,6) = PROP(12)*D(6,6)
      GOTO 99
    2 CONTINUE
      DD(1,1) = D(1,1)
      DD(1,3) = D(2,3)
      DD(3,1) = DD(1,3)
      DD(3,3) = D(3,3)
      DD(4,4) = PROP(12)*D(4,4)
      DD(5,5) = PROP(12)*D(5,5)
      DD(6,6) = D(6,6)
      GOTO 99
    3 CONTINUE
      DD(1,1) = D(1,1)
      DD(2,2) = D(2,2)
      DD(1,2) = D(1,2)
      DD(3,3) = D(3,3)
      DD(2,1) = DD(1,2)
      DD(4,4) = D(4,4)
      DD(5,5) = PROP(12)*D(5,5)
      DD(6,6) = PROP(12)*D(6,6)
      GOTO 99
    4 CONTINUE
      DD(3,3) = D(3,3)
      DD(4,4) = PROP(12)*D(4,4)
      DD(5,5) = PROP(12)*D(5,5)
      DD(6,6) = PROP(12)*D(6,6)
      GOTO 99
    5 CONTINUE
      DD(1,1) = D(1,1)
      DD(4,4) = PROP(12)*D(4,4)
```

```
      DD(5,5) = PROP(12)*D(5,5)
      DD(6,6) = PROP(12)*D(6,6)
      GOTO 99
    6 CONTINUE
      DD(2,2) = D(2,2)
      DD(4,4) = D(4,4)
      DD(5,5) = D(5,5)
      DD(6,6) = D(6,6)
   99 CONTINUE
C
C     CRACKS IN ALL THREE DIRECTIONS
C     TRANSFER DD TO D
C
      DO 101 J = 1,6
      DO 101 K = 1,6
      D(J,K) = DD(J,K)
  101 CONTINUE
  999 CONTINUE
      RETURN
      END
C
```

APPENDIX E

LISTING OF MARC SUBROUTINES

```
CCC   SUBROUTINE FOR MARCB16.DAT
      SUBROUTINE REBAR (M,NN,T,PR,TR,A)
C
C     M      ELEMENT NUMBER
C     NN     INTEGRATION POINT NUMBER
C     T      NOMINAL SIZE IN 'THICKNESS' DIRECTION
C     PR     RELATIVE POSITION OF REINFORCEMENT LAYER WITH RESPECT TO T
C     TR     EQUIVALENT THICKNESS OF REINFORCEMENT
C     A      DIRECTION COSINES OF THE REINFORCEMENT
C     KC     LAYER NUMBER
C
      COMMON/JOHNNY/ IFLAG,KC
      DIMENSION A(3)
      IF (NN .GT. 36) KC = 5
      IF (NN .GT. 27) KC = 4
      IF (NN .GT. 18) KC = 3
      IF (NN .GT. 9) KC = 2
      IF (NN .LE. 9) KC = 1
      IF (IFLAG .NE. 1) WRITE (6,600)
      IFLAG = 1
      GOTO (100,200,300,400,500) , KC
CCC   Y6.25@31 C/C BOT
  100 T = 175.0
      PR = 10.625
      TR = 0.962
      A(1) = 1.0
      A(2) = 0.0
      A(3) = 0.0
      RETURN
CCC   Y6.25@31 C/C BOT
  200 T = 175.0
      PR = 16.875
      TR = 0.962
      A(1) = 0.0
      A(2) = 1.0
      A(3) = 0.0
      RETURN
CCC   Y4.5@65 C/C  SHEAR
  300 T = 175.0
      PR = 20.0
      TR = 0.235
      A(1) = 0.0
      A(2) = 0.0
      A(3) = 1.0
      RETURN
CCC   Y4.5@31 C/C TOP
  400 T = 175.0
      PR = 160.75
      TR = 0.499
      A(1) = 0.0
      A(2) = 1.0
      A(3) = 0.0
      RETURN
CCC   Y4.5@31 C/C TOP
  500 T = 175.0
      PR = 165.25
      TR = 0.499
      A(1) = 1.0
      A(2) = 0.0
      A(3) = 0.0
  600 FORMAT ('          SUBROUTINE REBAR IS USED')
      RETURN
      END
```

```
CCC   SUBROUTINE FOR MARCB26.DAT
      SUBROUTINE REBAR (M,NN,T,PR,TR,A)
C
C     M     ELEMENT NUMBER
C     NN    INTEGRATION POINT NUMBER
C     T     NOMINAL SIZE IN 'THICKNESS' DIRECTION
C     PR    RELATIVE POSITION OF REINFORCEMENT LAYER WITH RESPECT TO T
C     TR    EQUIVALENT THICKNESS OF REINFORCEMENT
C     A     DIRECTION COSINES OF THE REINFORCEMENT
C     KC    LAYER NUMBER
C
      COMMON/JOHNNY/ IFLAG,KC
      DIMENSION A(3)
      IF (NN .GT. 36) KC = 5
      IF (NN .GT. 27) KC = 4
      IF (NN .GT. 18) KC = 3
      IF (NN .GT. 9) KC = 2
      IF (NN .LE. 9) KC = 1
      IF (IFLAG .NE. 1) WRITE (6,600)
      IFLAG = 1
      GOTO (100,200,300,400,500) , KC
CCC   Y6.25@28 C/C BOT
  100 T = 150.0
      PR = 12.125
      TR = 1.057
      A(1) = 1.0
      A(2) = 0.0
      A(3) = 0.0
      RETURN
CCC   Y6.25@28 C/C BOT
  200 T = 150.0
      PR = 18.375
      TR = 1.057
      A(1) = 0.0
      A(2) = 1.0
      A(3) = 0.0
      RETURN
CCC   Y5.0@62 C/C SHEAR
  300 T = 150.0
      PR = 21.5
      TR = 0.302
      A(1) = 0.0
      A(2) = 0.0
      A(3) = 1.0
      RETURN
CCC   Y4.5@37 C/C TOP
  400 T = 150.0
      PR = 134.25
      TR = 0.414
      A(1) = 0.0
      A(2) = 1.0
      A(3) = 0.0
      RETURN
CCC   Y4.5@31 C/C TOP
  500 T = 150.0
      PR = 138.75
      TR = 0.414
      A(1) = 1.0
      A(2) = 0.0
      A(3) = 0.0
  600 FORMAT ('          SUBROUTINE REBAR IS USED')
      RETURN
      END
C
```

```
      SUBROUTINE FOR BOTH MARCB16.DAT AND MARCB26
      SUBROUTINE FORCDT (U,V,A,DP,DU,TIME,DTIME,NDEG,NODE,UG,
     1                   XORD,NCRD,IACFLG,INC)
C     U       ARRAY OF TOTAL DISPLACEMENTS AT THIS NODE
C     V       ARRAY OF TOTAL VELOCITIES AT THIS NODE
C     A       ARRAY OF TOTAL ACCELERATIONS AT THIS NODE
C     DP      ARRAY OF INCREMENTAL POINT LOADS AT THIS LOAD
C     DU      ARRAY OF INCREMENTAL DISPLACEMENTS OR TOTAL ACCELERATIONS
C             AT THIS LOAD
C     TIME    TOTAL TIME AT BEGINNING OF INCREMENT
C     DTIME   INCREMENT OF TIME
C     NDEG    NUMBER OF DEGREE OF FREEDOM
C     NODE    GLOBAL NODE NUMBER
C     UG      ARRAY OF TOTAL DISPLACEMENTS IN THE GLOBAL SYSTEM
C     XORD    ARRAY OF ORIGINAL NODAL COORDINATES
C     NCRD    NUMBER OF COORDINATES PER NODE
C     INC     INCREMENT NUMBER
      COMMON /JOHNNY1/ IFLAG1
      DIMENSION U(NDEG),V(NODE),A(NDEG),DP(NDEG),DU(NDEG),UG(1),XORD(1)
      IF (TIME .GE. 0.00315 .AND. (TIME-DTIME) .GE. 0.00315)
     1    DP(3) = ((0.0093-TIME)*3.85E6+1.13E4)*-1.0
     2            -((0.0093-TIME+DTIME)*3.85E6+1.13E4)*-1.0
      IF (TIME .GE. 0.00315 .AND. (TIME-DTIME) .LT. 0.00315)
     1    DP(3) = ((0.0093-TIME)*3.85E6+1.13E4)*-1.0
     2            -((0.00315-TIME+DTIME)*1.5E6+2.0E4)*-1.0
      IF (TIME .GE. 0.00015 .AND. TIME .LT. 0.00315
     1    .AND. (TIME-DTIME) .GE. 0.00015)
     2    DP(3) = ((0.00315-TIME)*1.5E6+2.0E4)*-1.0
     3            -((0.00315-TIME+DTIME)*1.5E6+2.0E4)*-1.0
      IF (TIME .GE. 0.00015 .AND. TIME .LT. 0.00315
     1    .AND. (TIME-DTIME) .LT. 0.00015)
     2    DP(3) = ((0.00315-TIME)*1.5E6+2.0E4)*-1.0
     3            -(TIME-DTIME)*-1.633333E8
      IF (TIME .LT. 0.00015)
     1    DP(3) = TIME*-1.633333E8
     2            -(TIME-DTIME)*-1.633333E8
      IF (IFLAG1 .NE. 1) WRITE (53,4000)
      IFLAG1 = 1
      WRITE (53,5000) INC,DTIME,TIME,DP(3)
      WRITE (54,5000) INC,DTIME,TIME,DP(3)
      CLOSE (54)
 4000 FORMAT ('  INC     DTIME          TIME          DP(3)',/)
 5000 FORMAT (I5,'    ',E10.4,'    ',E10.4,'   ',E10.4)
      RETURN
      END
C
```